Enhanced strain-based fatigue methodology for high strength aluminum alloys

Attilio Arcari

Dissertation submitted to the Faculty of the
Virginia Polytechnic Institute and State University
in partial fulfillment of the requirements for the degree of

Doctor of Philosophy

in

Engineering Mechanics

Norman E. Dowling, Chair

Mark S. Cramer

Scott L. Hendricks

Abby W. Morgan

Surot Thangjitham

January 29th 2010

Blacksburg, VA

Keywords: Aluminum alloys, fatigue, strain-based approach, mean stress, relaxation, variable amplitude loading

Abstract

Enhanced strain-based fatigue methodology for high strength aluminum alloys

Attilio Arcari

The design of any mechanical components requires an understanding of the general statical, dynamical and environmental conditions where the components will be operating to give satisfactory results in terms of performance and endurance. The premature failure of any components is undesirable and potentially catastrophic, therefore predictions on performances and endurances of components to proceed with repair or substitution is vital to the stability of the structure where the component is inserted.

Improvements to a strain based approach to fatigue were obtained in this study, studying the effects of mean stresses on fatigue life and investigating cyclic mean stress relaxation of two aluminum alloys, 7075-T6511 and 7249-T76511, used in structural aircraft applications. The two aluminum alloys were tested and their fatigue behavior characterized. The project, entirely funded by NAVAIR, Naval Air Systems Command, and jointly coordinated with TDA, Technical Data Analysis Inc., was aimed to obtain fatigue data for both aluminum alloys, with particular interest in 7249 alloy because of its enhanced corrosion resistance, and to give guidelines for improving the performances of FAMS, Fatigue Analysis of Metallic Structures, a life prediction software from the point of view of both mean stress effects and mean stress relaxation.

The sensitivity of engineering materials to mean stresses is of high relevance in a strain based fatigue approach. The performance of the most common models used to calculate mean stress correction factors was studied for the two aluminum alloys 7075 and 7249 to give guidelines in the use of those for life predictions. Not only mean stresses have a high influence on fatigue life, but they are also subjected to transient cyclic behaviors. The following study considered both an empirical approach and a plasticity theory approach to simulate and include these transient effects in life calculations. Results will give valid directions to a successful modification of FAMS like any other life calculation software to include in the picture transient phenomena.

Acknowledgments

I want to thank my family for all their support, from the first day I arrived in Blacksburg until the day of my final defense. This would not have been possible without their continuous presence, help and example. Thanks to my mother, Mariarosa, because her love for knowledge opened my mind to multiple interests, to my father, Bruno, because his strong perseverance and calm taught me how to approach any problems, and to my sister, Ilaria, because she showed me to never give up my dreams. A special thanks to my grandparents, their infinite strength, care and love is the foundation of any of my accomplishments. Thanks to Nonna Anna, Nonno Angelo, and Nonna Memi. Thanks to my Nonno Nenè, whose presence is greatly missed by all of us. Thanks to all the rest of my family for all the great times we spent together and the special moments that I had every time I went back to my beloved home town, Mantova. Thanks to American Mom and Dad, Nancy and Gary Rooker, for all their help and love in these years.

I want to thank and remember my friend Elena Goffredi, who died in October of 2002 when she was only 18. Her memory helped me from the first days of my college studies in all the difficult moments and her presence is always strongly perceived inside me.

I thank all my friends from Mantova, for the happy moments we had together in these years and for keeping in touch even if far apart. I want to thank my friend Matteo, "Teo", from Cremona, for always keeping in touch in these years and for the great times we had in Cremona and Milano Marittima. I also thank the Italian friends in Blacksburg, for the great times that we shared and for all our fruitful exchange of opinions, points of view and experiences. Thanks to all of my friends in Blacksburg and a special thanks to Lisa Pryor for her help with the writing and to Dr. Kaushik Das, for being a great friend and roommate.

I want to thank my advisor, Dr. Norman E. Dowling, for his help in all the phases of the PhD process. He represents both a professional guide and an example to me. His passion for the subjects of this research, for science and knowledge in general, strongly influenced and stimulated my desire of accomplish always more with this research and in my professional life. This would never have been possible without his precious teachings, and without his guide and support.

I also would like to express my gratitude to the U.S. Naval Air Systems Command, Patuxent River, MD, for financial support, and especially to Nam D. Phan and Trung T. Nguyen of NAVAIR Structures for technical direction. I also thank Pamela F. Bowen of Integrated Systems Solutions, Inc., California, MD, for performing the project administration. A special thanks is addressed to Technical Data Analysis, Inc., Falls Church, VA, for their collaboration in the project work, and in particular to Nagaraja Iyyer and Subhasis Sarkar for their help in planning and supervising the activity. Institutional support was provided by the Engineering Science and Mechanics Department, and by the Materials Science and Engineering Department, Virginia Tech, Blacksburg, VA. I feel especially indebted to staff engineer Marshal McCord of the ESM Department, who aided with the laboratory work.

Table of contents

Abstract…….…….....ii

Acknowledgements……iii

Table of contents……...……...…v

List of Figures……...…viii

List of Tables……...…….xv

1. Introduction……...…1
   1.1. Fatigue of Engineering metals…….....1
   1.2. Monotonic and Cyclic response……..…….....3
   1.3. The strain-life curve……...……...…7
   1.4. Damage calculation……...…9
   1.5. Cycle Counting in Variable Amplitude Loading…….…..10
   1.6. Application to Notched members……...…….……..11
   1.7. Application to biased states of stress or strain……...……14
      1.7.1 The effects of Mean Stresses…….14
      1.7.2. Mean Stress Relaxation in cyclic loading……..18
   1.8. Problem Statement and Objectives...…….……19

2. Literature Review……...……22
   2.1. Considerations for variable amplitude loading……..22
   2.2. Mean Stress models and Performance……..……25
   2.3. Mean Stress and Residual Stress Relaxation Models...…….……29
   2.4. Introduction to Plasticity Models…….……..32
   2.5. An example of use of plasticity models for mean stress relaxation...……40

3. Experimental Methods……...…41
   3.1. Materials characterization and use…….41
   3.2. Tensile Properties of 7075 and 7249……..……...……42
   3.3. Specimen Design and Laboratory Equipment…….……..….44
   3.4. Test design…….49
      3.4.1. Constant Amplitude Loading Zero Mean……..49
      3.4.2. Pre-strain effects…….……..51
      3.4.3. Constant Amplitude Loading Non-Zero Mean…….....53
      3.4.4. Variable Amplitude Loading…….…55

4. Stress-strain, stress-life and strain-life fitting……58
   4.1. Representative Test Results……..……58

4.2. Cyclic stress-strain curve fit……61
4.2.1. Elastic modulus, yield strength and Plastic Strain calculation from data……62
4.2.2. Cyclic Stress-Strain Curve Fits……64
4.3. Stress-Life Curve Fit……65
4.4. Strain-Life Curve Fit……70
4.5. Mean stress models comparison……76
4.5.1. Stress-Life comparisons……77
4.5.2. Amplitude-Mean Plots……81
4.5.3. Stress Deviation Analysis……83

5. Mean Stress Relaxation in Constant Amplitude Loading……88
5.1. Representative test results……88
5.2. The Landgraf Model……90
5.2.1. Preliminary fitting on 7475……90
5.2.2. Preliminary fitting on 7075-T6511 and 7249-T76511……91
5.3. The non linear Maxwell model……96
5.3.1. Preliminary fitting on 7075-T6511 and 7249-T76511……96
5.4. Improved Landgraf model fitting ……102
5.4.1. Compressive mean stress relaxation……102
5.4.2 The mean stress offset……105
5.4.3. Fitting 7075 and 7249 relaxation data……106

6. Mean Stress Relaxation in Variable Amplitude Loading……111
6.1. Representative test results……111
6.2. Tentative application of Landgraf model to variable amplitude loading……116
6.2.1. Landgraf approach to variable amplitude loading……116
6.2.2. Simulations……118
6.3. The Wetzel model……121
6.3.1. The stress-strain curve……121
6.3.2. The relaxation constant M_r……123
6.3.3. Improvements to the Wetzel model……128
6.3.4. The Wetzel table approach……130
6.3.5. Simulations……133
6.4. The Jiang model……139
6.4.1. Route to the Jiang model……139
6.4.2. Adaptation of the Jiang model and Monte Carlo Analysis……144
6.4.2.1. Simplifications to the Jiang model……145
6.4.2.2. c(i)'s and r(i)'s for the Jiang model……145
6.4.2.3. Monte Carlo Analysis and the χ(i)'s constants……148
6.4.2.4. Results from Monte Carlo Analysis……149
6.4.3. Optimization of χ's constants for Jiang……150
6.4.4. Simulations……152

7. Variable amplitude loading life calculation……...……..157
7.1. Influence of mean stress relaxation on fatigue life analysis in a strain-based approach ……..……..……157
7.2. Improvements with the Wetzel and Jiang model…….....164

8. Discussion and Conclusions……..…..…….172
8.1 7075 and 7249 Aluminum alloys……...……172
8.2 Mean Stress Models……...……176
8.3 Mean Stress Relaxation……..……178
8.3.1 Constant amplitude loading and the Landgraf model……..…178
8.3.2 Mean stress relaxation in variable amplitude loading……..…180
8.3.2.1 The Landgraf Model……180
8.3.2.2 The Wetzel Model……181
8.3.2.3 The Jiang Model……..182
8.4 Life calculation……..……183

References……185

Appendix A: Fatigue data tables……..……191

Appendix B: Constant amplitude loading stress-strain curves……196

Appendix C: Variable amplitude loading stress-strain curves…….……..…..…202

Appendix D: Variable amplitude loading simulation results with Wetzel and Jiang model…….....……..……...……..216

List of Figures

Figure 1-1. Monotonic stress-strain response of aluminum alloy 7075-T6511…….4

Figure 1-2. Cyclic behavior of metallic materials with formation of a hysteresis loop; cyclic yield points in tension and compression are shown, along with elastic modulus. Adapted from Dowling [3]……..4

Figure 1-3. Example of stress-plastic strain fit to obtain constants for Ramberg-Osgood equation……..6

Figure 1-4. Comparison of monotonic and cyclic Ramberg-Osgood fitted behavior for 7075-T6511 aluminum alloy and A36 steel……...7

Figure 1-5. Representation of strain-life curve with formulation shown in Eq. 1.3……..8

Figure 1-6. Example of application of Rain Flow counting method, with indicated points in the loading history where memory effects occur adapted from Ref. [10]……...11

Figure 1-7. Schematic representation of variation of k_f, fatigue stress concentration factor……...12

Figure 1-8. Graphical representation of the Goodman model and the two Morrow models……...16

Figure 1-9. Graphical representation of SWT model and Walker for different values of γ……17

Figure 1-10. Example of mean stress relaxation in constant amplitude loading for a strain amplitude of 0.95% and 0.2%.....18

Figure 2-1. Loading patterns with same number of cycles and amplitudes of cycles, but causing different damage due to sequence effects…….23

Figure 2-2. Pre-strain control signal and stress-strain response for 7075-T6511……24

Figure 2-3. Incremental step test performed on 7075-T6511 aluminum and fitting of the stress-strain relationship.....25

Figure 2-4. Mean stress relaxation in an axial test of 7075-T6511 aluminum alloy. The sample was cycled at a strain amplitude of 0.0072 about a mean strain of 0.0108……..29

Figure 2-5. Spring and nonlinear dashpot model…….32

Figure 2-6. Simulation of random loading pattern with Wetzel model and constants fitted to 7075-T6511 aluminum……..39

Figure 3-1. Tensile specimen geometry with c= 0.5, h=1.75, w_1=0.25, d=0.125 , b=0.331 , g=2.00 , w_2=0.5 , L= 6.42……43

Figure 3-2. Projection of the extrusion from which all test specimens are taken; dimensions in inches…….45

Figure 3-3. Test specimen geometries; dimensions in inches……..46

Figure 3-4. Variations in the controlled strain amplitude and mean, and the resulting mean stress, during an early test……49

Figure 3-5 and Table 3-2. Graphical representation of the points in the plan for the first part of the research on 7075-T6511 and 7249-T76511……50

Figure 3-6. Pre-strain effects on strain-life curve of 7075-T6511……...53

Figure 3-7. Strain controlled loading profiles for tests on Variable Amplitude loading, Types A, B, C, and D... ….57

Figure 4-1. Stain control and stress response for test 75LT-4, the strain amplitude is 1.8% and the test is completely reversed……59

Figure 4-2. Stress-strain response from low cycle fatigue strain controlled test on 7075-T6511 aluminum……...59

Figure 4-3. Stain control and stress response for test 75RT-3, the strain amplitude is 0.2% and the test is completely reversed……60

Figure 4-4. Stress-strain response from high cycle fatigue strain controlled test on 7075-T6511 aluminum…….60

Figure 4-5. Stress-strain response from low cycle fatigue strain controlled test on 7075-T6511 aluminum……..61

Figure 4-6. Hysteresis loop of low cycle fatigue test on 7075-T6511; data points for calculation of plastic strain amplitude are shown……63

Figure 4-7. Initial loading in a low cycle fatigue test on 7075-T6511; the initial part of the curve used to calculate the elastic modulus is shown, along with the 0.2% offset line to calculate yield stress……...63

Figure 4-8. Cyclic stress-strain curves for the two alloys……64

Figure 4-9. Stress amplitude versus plastic strain amplitude data and the fitting of Eq. 1.1……...65

Figure 4-10. Strain-life curve fitted with 0-mean data only and scattered mean stress data points……66

Figure 4-11. Unsuccessful attempt to fit the Walker equation to the non-zero mean stress data points obtained experimentally……...67

Figure 4-12. Stress-life data and fits for the two alloys. The fitted lines are based on the Walker mean stress equation at intermediate and long lives, and a separate fit is employed at short lives. ……69

Figure 4-13. Fitted strain-life curve for 7075-T6511 with data point from tensile test and without data point from tensile test……..72

Figure 4-14. Fitted plastic strain-life curve for 7075-T6511 with data point from tensile test and without data point from tensile test……72

Figure 4-15. Plastic strain amplitude versus Walker equivalent life and the fitting of Eq. 1.7……...74

Figure 4-16. Strain amplitude versus Walker equivalent life for the two alloys. ……...75

Figure 4-17. Cyclic stress-strain curves with points located corresponding to the strain-life transition strain ε_{ai} and the mean stress relaxation transition ε_{a12}. The 0.2% offset cyclic yield strength is also shown for comparison. …76

Figure 4-18. Equivalent completely reversed stress amplitude versus life correlations for the Goodman equation. …….79

Figure 4-19. Equivalent completely reversed stress amplitude versus life correlations for the Morrow fracture strength equation……..……79

Figure 4-20. Equivalent completely reversed stress amplitude versus life correlations for the Morrow intercept equation. Note that it is necessary to use two decades for the stress scale to accommodate the large deviations from the zero-mean-stress line……..80

Figure 4-21. Equivalent completely reversed stress amplitude versus life correlations for the Smith-Watson-Topper equation…….80

Figure 4-22. Normalized stress amplitude-mean plots for the two alloys……..82

Figure 4-23. SWT and Walker amplitude-mean plots for the two alloys……...83

Figure 5-1. Strain control and stress response of mean stress relaxation test on 7075-T6511 aluminum alloy……..86

Figure 5-2. Stress-strain response and mean stress relaxation response of 7075-T6511 aluminum to strain controlled mean stress relaxation tests in Figure 5-1……..…87

Figure 5-3. Strain control and stress response of mean stress relaxation test on 7075-T6511 aluminum alloy……..87

Figure 5-4. Stress-strain response and mean stress relaxation response of 7075-T6511 aluminum to strain controlled mean stress relaxation tests in Figure 5-3…….88

Figure 5-5. Mean stress relaxation curves for preliminary tests on 7475-T651…….89

Figure 5-6. Linear fitting of relaxation exponents of the Landgraf formulation and strain amplitudes……..89

Figure 5-7. Mean stress relaxation tests on 7475-T651 aluminum alloys and Landgraf model curves……...91

Figure 5-8. Relaxation exponent versus strain amplitude data for 7075-T6511 aluminum, with lines from the multiple regression constants also shown…….93

Figure 5-9. Relaxation exponent versus strain amplitude data for 7249-T76511 aluminum, with lines from the multiple regression constants also shown……93

Figure 5-10. Experimental curves and Landgraf model curves for mean stress relaxation tests on 7075-T6511 and 7249-T76511…….95

Figure 5-11. Correlation of with $\sigma_{max,i}$ for 7075-T6511 aluminum……...97

Figure 5-12. Experimental curves and Maxwell model curves for mean stress relaxation tests on 7075-T6511 and 7249-T76511…….99

Figure 5-13. Summary of mean stress relaxation curves for 7075-T6511 and 7249-T76511……...104

Figure 5-14. Empirical stress offset σ_b as a function of strain amplitude, as used in modeling……108

Figure 5-15. Mean stress relaxation and offset modeling for high strain amplitudes in the two alloys……...109

Figure 5-16. Mean stress relaxation and offset modeling for low strain amplitudes in the two alloys……109

Figure 5-17. Relaxation exponent versus strain amplitude for the two alloys……...110

Figure 6-1. Type A variable amplitude loading test for 7075-T6511. Test number is B75-54 and show are the strain control (a), the stress response (b), the stress-strain response (c) and mean stress relaxation (d)……..112

Figure 6-2. Comparison of mean stress relaxation for 0.9% strain hysteresis loop in constant and variable amplitude loading conditions……...113

Figure 6-3. Type B variable amplitude loading test for 7075-T6511. Test number is B75-28 and the stress-strain response (a) and mean stress relaxation (b) are shown……..113

Figure 6-4. Type C variable amplitude loading test for 7075-T6511. Test number B75-26, and the stress-strain response (a) and mean stress relaxation are shown (b)……...114

Figure 6-5. Service type of variable amplitude loading test for 7075-T6511……115

Figure 6-6. Example of Landgraf application to variable amplitude loading: a new hardening exponent for the Ramberg-Osgood relation is calculated with the use of $\Delta\sigma_r$……...117

Figure 6-7. Possible ending points of the loading segment with new n_r', calculated with the Landgraf relation….118

Figure 6-8. Constant amplitude loading simulation with Wetzel model, corresponding to 75NLB-1, test 2 Table 5.5 for 7075……..118

Figure 6-9. Constant amplitude loading simulation with Landgraf model, corresponding to 75NLB-3, test 12 Table 5.5 for 7075…….119

Figure 6-10. Type A variable amplitude loading simulation with Landgraf model, corresponding to test B75-54 for 7075. The mean stress relaxation response is shown……..120

Figure 6-11. Type C variable amplitude loading simulation with Landgraf model, corresponding to test B75-26 for 7075. The mean stress relaxation response is shown……..120

Figure 6-12. Spectrum variable amplitude loading simulation with Wetzel, corresponding to test NAV1-75-15 for 7075. The mean stress relaxation response is shown……..120

Figure 6-13. Stress-strain segments of the Wetzel model for 7075-T6511 (a) and 7249-T76511 (b)……...122

Figure 6-14. Simulation residuals for constants amplitude loading test plotted versus the value of Wetzel relaxation constant M_r……..124

Figure 6-15. Simulations of constant amplitude loading relaxation tests with Wetzel model and averaged M_r for 7075……125

Figure 6-16. Simulations of constant amplitude loading relaxation tests with Wetzel model and weighted averaged M_r for 7075……127

Figure 6-17. Simulations of constant amplitude loading relaxation tests with Wetzel model and optimum M_r for ε_a = 0.95% for 7075……127

Figure 6-18. Simulations of variable amplitude loading relaxation tests with Wetzel model and averaged M_r for 7075……128

Figure 6-19. Correlation between M_r and ε_a for 7075 and 7249 in constant amplitude tests……129

Figure 6-20. Visualization of $\Delta\sigma_r$ in a constant amplitude loading simulation with the Wetzel model for 7075……130

Figure 6-21. Scheme of constant amplitude loading relaxation tests to create a relaxation table for the Wetzel model……...132

Figure 6-22. Graphical representation of the relaxation table for the Wetzel model……133

Figure 6-23. Constant amplitude loading simulation with Wetzel model, corresponding to 75NLB-1, test 2 Table 5.5 for 7075 and to 49LC-3, test 2 Table 5.6 for 7249. The mean stress relaxation response is shown……...134

Figure 6-24. Constant amplitude loading simulation with Wetzel model, corresponding to 75NLB-3, test 12 Table 5.5 for 7075 and to 49LC-5, test 11 Table 5.6 for 7249. The mean stress relaxation response is shown……...135

Figure 6-25. Constant amplitude loading simulation with Wetzel model, corresponding to B75-47, test (a) Table 5.5 for 7075 and to B49-27, test (a) Table 5.6 for 7249. The mean stress relaxation response is shown……...135

Figure 6-26. Constant amplitude loading simulation with Wetzel model, corresponding to B75-38, test (f) Table 5.5 for 7075 and to B49-53, test (e) Table 5.6 for 7249. The mean stress relaxation response is shown……135

Figure 6-27. Type A variable amplitude loading simulation with Wetzel, corresponding to test B75-54 for 7075 and B49-60 for 7249……...137

Figure 6-28. Type C variable amplitude loading simulation with Wetzel, corresponding to test B75-26 for 7075 and B49-44 for 7249……...138

Figure 6-29. Type C variable amplitude loading simulation with Wetzel, corresponding to test B75-49 for 7075 and B49-41 for 7249……138

Figure 6-30. Spectrum variable amplitude loading simulation with Wetzel, corresponding to test NAV1-75-15 for 7075 and NAV1-49-1 for 7249……138

Figure 6-31. Comparison of Ramberg-Osgood fitted stress-strain curve for 7075 with the stable stress-strain response of A-F models with one and two back stresses……....140

Figure 6-32. Simulation of a constant amplitude loading test and a Type A variable amplitude loading with a A-F model with one back stress for 7075……141

Figure 6-33. Simulation of a constant amplitude loading and a Type A variable amplitude loading with a A-F model with two back stresses for 7075……141

Figure 6-34. Simulation of a constant amplitude loading and a Type A variable amplitude loading with the Jiang model with constants obtained from fitting 7075 data……...143

Figure 6-35. Simulation of a constant amplitude loading and a Type A variable amplitude loading with the Döring model with constants obtained from fitting 7075 data.……. ……143

Figure 6-36. Incremental step test data for 7075 and 7249……146

Figure 6-37. Ramberg-Osgood fitted curve and Jiang stress-strain curve for 7075 and 7249……...146

Figure 6-38. Partial Correlation Coefficient and Partial Rank Correlation Coefficients between constants $\chi_{(i)}$'s of the Jiang model and the simulation residuals for 55000 simulations of 11 variable amplitude loading patterns…...150

Figure 6-39. Constant amplitude loading simulation with Jiang model, corresponding to 75NLB-1, test 2 Table 5.5 for 7075 and to 49LC-3, test 2 Table 5.6 for 7249. The mean stress relaxation response is shown…….…...153

Figure 6-40. Constant amplitude loading simulation with Jiang model, corresponding to B75-47, test (a) Table 5.3 for 7075 and to B49-27, test (a) Table 5.3 for 7249. ……153

Figure 6-41. Type A variable amplitude loading simulation with Jiang, corresponding to test B75-54 for 7075 and B49-60 for 7249. ……153

Figure 6-42. Type C variable amplitude loading simulation with Jiang, corresponding to test B75-26 for 7075 and B49-44 for 7249. ……...154

Figure 6-43. Type C variable amplitude loading simulation with Jiang, corresponding to test B75-49 for 7075 and B49-41 for 7249. ……154

Figure 6-44. Type B variable amplitude loading simulation with Jiang, corresponding to test B75-28 for 7075 and B49-56 for 7249. ……154

Figure 6-45. Spectrum variable amplitude loading simulation with Jiang, corresponding to test NAV1-75-15 for 7075 and NAV1-49-1 for 7249. ……155

Figure 6-46. Comparison of a low cycle fatigue hysteresis loop in variable amplitude loading, Test data and Jiang model simulations, and in constant amplitude loading simulations with the Jiang model…….156

Figure 7-1: Schematic representation of cycle counting applied to a simple constant amplitude loading for test 75LB-6……158

Figure 7-2: Schematic representation of cycle counting applied to a 2-Levels variable amplitude loading for test B75-54…….……161

Figure 7-3. Performance of mean stress relaxation models in life calculation for 7075-T6511; the filled squares are the experimental lives…….165

Figure 7-4. Performance of mean stress relaxation models in life calculation for 7249-T76511; the filled squares are the experimental lives…….166

Figure 7-5. Percentage difference between predicting models and experimental life for 7075-T6511; the models used are a standard strain-based approach and the improved version developed in this study, with the use of the Wetzel model or the Jiang model……169

Figure 7-6. Percentage difference between predicting models and experimental life for 7249-T76511; the models used are a standard strain-based approach and the improved version developed in this study, with the use of the Wetzel model or the Jiang model……....170

Figure 8-1. Comparison of stable cyclic stress-strain behavior for 7075-T6511 and 7249-T76511……173

Figure 8-2. Comparison of stress-life Walker fit for 7075-T6511 and 7249-T76511……...174

Figure 8-3. Comparison of plastic strain-life fit for 7075-T6511 and 7249-T76511……174

Figure 8-4. Comparison of strain-life fit for 7075-T6511 and 7249-T76511……175

Figure 8-5. Area comparison of Goodman, Morrow fracture and intercept, and SWT mean stress models for 7075-T6511. ……177

Figure 8-6. Area comparison of Goddman, Morrow fracture and intercept, and SWT mean stress models for 7249-T76511……177

Figure 8-7. Comparison of Landgraf model behavior for 7075-T6511 and 7249-T76511……179

List of Tables

Table 3-1. Tensile properties from tests run at Virginia Tech……..44

Table 3-2. Graphical representation of the points in the plan for the first part of the research on 7075-T6511 and 7249-T76511……..50

Table 3-3. Constant amplitude zero-mean tests with pre-strain……52

Table 3-4. Non zero mean strain controlled test plan for both aluminum alloys……..55

Table 4-1. Cyclic Stress-Strain and Strain-Life Constants……...68

Table 4-2. Values of Stress Deviations for Mean Stress Equations……..85

Table 5-1. Fitting constants for the Landgraf formulation……90

Table 5-2. Test details for 7475-T651 alloy……..91

Table 5-3. Landgraf model fitting constants for 7075-T6511 and 7249-T76511 aluminum……94

Table 5-4. Nonlinear Maxwell model fitting constants for 7075-T6511 and 7249-T76511 aluminum……...98

Table 5-5. Test details for 7075-T6511 alloy……..100

Table 5-6. Test details for 7249-T76511 alloy……101

Table 5-7. Names of mean stress relaxation tests and identifiers on plots……..103

Table 5-8. Points Identifying Empirical Mean Stress Offsets ……108

Table 5-9. Mean Stress Relaxation Constants for the Landgraf Model with a Stress Offset…..110

Table 6-1. Summary of fitted constants for improved version of Wetzel model……128

Table 6-2. Exemplified relaxation table for the Wetzel model……...131

Table 6-3. Jiang model parameters $c_{(i)}$'s from fitted stress-strain curve……147

Table 6-4. Jiang model parameters $r_{(i)}$'s from fitted stress-strain curve……147

Table 6-5. Optimized values of $\chi^{(i)}$'s for 7075 and 7249; the values are used in simulations……...151

Table 7-1: Analysis of constant amplitude loading for test 75LB-6……...159

Table 7-2: Life calculation analysis with standard method of constant amplitude loading for test 75LB-6…….159

Table 7-3: Analysis of constant amplitude loading for test 49LB……..……159

Table 7-4: Life calculation analysis with standard method of constant amplitude loading for test 49LB……159

Table 7-5: Life calculation analysis with "relaxed" mean stress values of constant amplitude loading for test 75LB-6……160

Table 7-6: Life calculation analysis with "relaxed" mean stress values of constant amplitude loading for test 49LB……...160

Table 7-7: Analysis of Type A variable amplitude loading for test B75-54..……161

Table 7-8: Life calculation analysis of Type A variable amplitude loading with standard method for test B75-54.……161

Table 7-9: Analysis of Type A variable amplitude loading for test B49-60.…….162

Table 7-10: Life calculation analysis of Type A variable amplitude loading with standard method for test B49-60..…….162

Table 7-11: Life calculation analysis with "relaxed" mean stress values of constant amplitude loading for test B75-54……162

Table 7-12: Life calculation analysis with "relaxed" mean stress values of constant amplitude loading for test B49-60……163

Tables 7-13: Test numbers and test names of variable amplitude loading relaxation tests in Figure 7-3..…… 166.

Tables 7-14: Test numbers and test names of variable amplitude loading relaxation tests in Figure 7-4..……. ……167

Chapter 1
Introduction

1.1 Fatigue of Engineering metals

The awareness of fatigue failure of structures in engineering started around the mid-1800's with a number of failures, mainly in railway and bridge components [1]. Observations of failure after repeated application of stress beyond the ultimate limit of the material gave the idea of a material becoming more "tired", weakened by the continuous low level solicitation. This gave birth to the concept of fatigue [2]. Successive studies and testing by Wohler in Germany, with the application of repeated loading to mainly railway axles, opened the field to a more systematic investigation of fatigue properties of materials. His experimental work gave foundation to the stress-based approach with the use of S-N curves. Wohler also started the investigation of the role of mean stresses in the fatigue process. These are still frequent subjects of debate and potentially the most critical part of the theory of fatigue [3].

As engineering advanced with material science in the study of new alloys and potentially better performing metals, the need of a solid theory to asses fatigue and fracture mechanisms became more apparent. The challenges faced during World War II and the flights of the first jet propelled airplanes shortly after the end of the war, increased the attention on the fatigue and fracture mechanics problems. Many factors in the 1950s and 1960s laid the basis for the current notch strain fatigue analysis. These include the introduction by Irwin of the stress intensity factor concept K_I, the studies on low cycle fatigue and attention to a plastic deformation-life relationship by Topper and Morrow, and finally the cycle counting method introduced by Matsuishi and Endo [1].

All these studies led to the development of three points of view that can be used to approach the problem of fatigue. The first, the stress-based approach, is based on the stress applied to the material. Then next is based on the deformation applied to the material, the strain-based approach. Finally, the fractures mechanics approach is based on the consequence that the loadings have on the growth of the cracks in the material.

The stress-based approach relates fatigue life with nominal stress, defined as the average stress acting on the material. It is visually represented by a Stress-Life (S-N) curve, describing the way life changes with stress. In case of notches and mean stress effects, stresses are calculated through elastic stress analysis and correction factors obtained by empirical formulas. Limiting factors in the stress-based approach are the effects on fatigue life due to local yielding and plastic deformations at notches, and the inadequacy of life predictions in presence of mean stresses at short lives [3].

The strain-based approach focuses the attention on the plastic deformations caused by loading and relates the local stresses and strains with the life of the material., These stresses and strains are often calculated with empirical formulas such as Neuber's rule and a relation between stress and strain like the Ramberg-Osgood relationship. The strain based approach in life predictions has many advantages over the stress based approach; this is especially true in cases of localized yielding with the presence of notches. The strain based approach is also a more rational approach in managing mean stresses [3].

The principles of linear elastic fracture mechanics approach can be applied to the study of cracked configurations to obtain solutions to the stress function and expressions of stress intensity factors at notches [4]. Life in fracture mechanics is studied through crack growth: the material is initially considered as free from flaws, then after a certain number of cycles N, small cracks will initiate. Depending on the severity of the loading and geometric conditions, those cracks will grow at a different rate, until they reach a threshold value called critical crack length, causing unstable growth and possibly failure of the component under investigation.

Each one of these methods can be applied to a fatigue problem. The choice can be derived from economical, computational and design standards, but possibly also personal discretion of the engineers. The strain based approach is particularly successful in modeling fatigue life of critical components subjected to local yielding at stress raisers. It does not require a great computational effort or a large number of material constants or assumptions to obtain accurate predictions when dealing with most engineering metals.

This study will focus on the strain-based fatigue approach. It will propose solutions and guidelines to improve its effectiveness when dealing with mean stresses and mean stress

relaxation. The materials tested will be two aluminum alloys, 7075-T6511 and 7249-T76511, with attention on the latter one, a fairly new alloy with improved corrosion resistance.

In a strain based approach to fatigue, a material must be characterized in terms of its stress-strain response and its strain-life response. The characterization is performed following ASTM standard requirements in the design of specimens and in meeting the specifics of the equipment. These methods are applicable to a large number of structural metals with a relatively low number of tests needed [5].

1.2 Monotonic and Cyclic response

An understanding of the elastic and inelastic responses of engineering metals is required before approaching a fatigue problem. The monotonic and cyclic responses of those metals can be significantly different and need to be modeled accurately.

When subjected to increased deformation, most engineering metals initially show a linear region where the stress in the material is proportional to the strain applied to the material. In this region, every deformation is recoverable upon removal of the force applied. The behavior is usually referred as elastic behavior, and the strain applied is referred as elastic strain, ε_{ea}. When a certain level of deformation is reached, called the yield point, a part of the total deformation, ε_a, applied to the material becomes not recoverable, and it is usually referred to as plastic strain, ε_{pa}.

A tension test for 7075 is shown in Figure 1-1. The elastic portion and the yield point are clearly recognizable; for this material the yield is around 0.6% strain.

The range of elastic moduli for structural metals is wide, depending on the class of materials. It typically goes from 200 GPa for steels to 70 GPa for aluminum alloys [3]. The profile of the plastic part of the deformation can change dramatically for different classes of metals. In the same way, the ductility and strength may vary significantly. The monotonic loading shown is typical for the 7th series of aluminum alloy, showing high strength and good ductility.

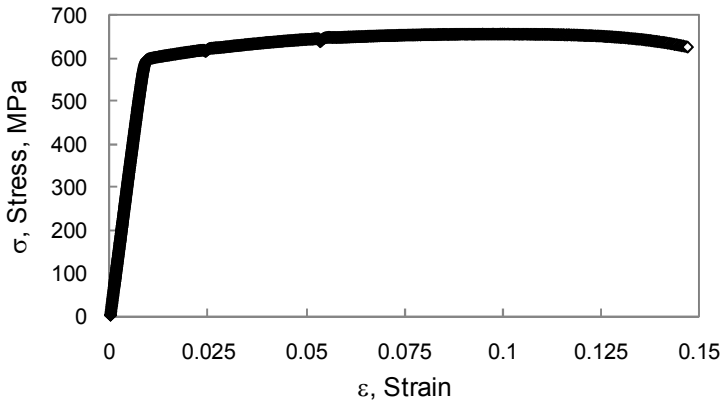

Figure 1-1. Monotonic stress-strain response of aluminum alloy 7075-T6511.

When subjected to cyclic deformations, materials respond by forming a characteristic curve called hysteresis loop. This loop consists of two branches, one corresponding to the loading phase and one to the unloading phase of the cycle. Both branches have a linear region and a cyclic yield point, so that the loop is closed.

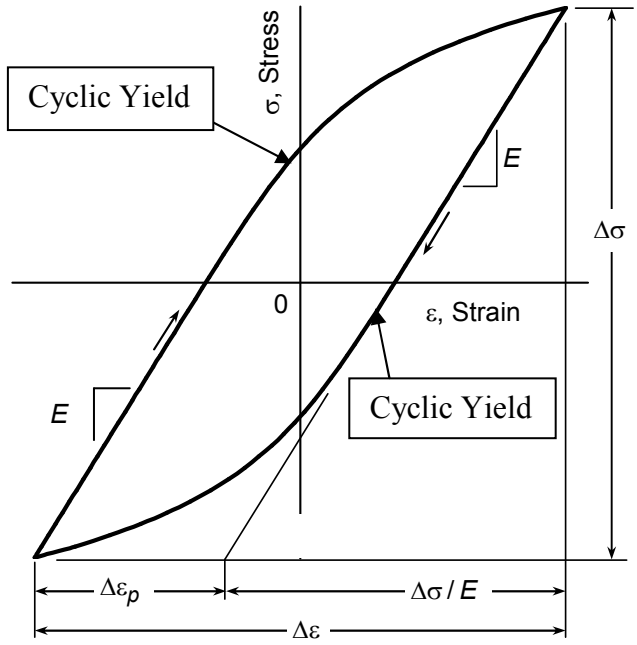

Figure 1-2. Cyclic behavior of metallic materials with formation of a hysteresis loop; cyclic yield points in tension and compression are shown, along with elastic modulus. Adapted from Dowling [3].

The linear region is considered to have a constant slope, equal to the elastic modulus of the material. The deformation range is divided in elastic deformation, $\Delta\varepsilon_e$ or $\Delta\sigma/E$, and plastic deformation, $\Delta\varepsilon_p$; the range of stress obtained is called $\Delta\sigma$. When referring to stress or strain amplitude, ε_a and σ_a it is usually referring to half of the ranges just described. A representation is shown in Figure 1-2.

The first goal in a strain-based approach to fatigue is the characterization of the cyclic stress-strain curve of the material. Standard procedures require several completely reversed tests, $\sigma_{min}/\sigma_{max} = -1$, run at different strain amplitudes to obtain hysteresis loops. Analysis of these loops is used to find the corresponding stress amplitude and to fit the values to a stress-strain equation. The Ramberg-Osgood equation, a linear-power hardening rule, is generally employed:

$$\varepsilon_a = \frac{\sigma_a}{E} + \left(\frac{\sigma_a}{H'}\right)^{\frac{1}{n'}} \qquad (1.1)$$

Where σ_a is the stress amplitude, E is the elastic modulus, and H' and n' are fitted constants [6]. The stress amplitude from different hysteresis loops is fitted to plastic strain amplitude in a log-log plot to obtain values for H' and n'. The elastic modulus can be taken to be a single value from the average of the elastic moduli from the initial monotonic loading of each test.

In Figure 1-3, the stress-plastic strain fit for 7075 are shown. The same results will be shown in Chapter 4, but as a general reference, it is observable that when the plastic strains are too small, a lot of noise is shown. Therefore, some of the points are left out of the fit as they do not represent useful information.

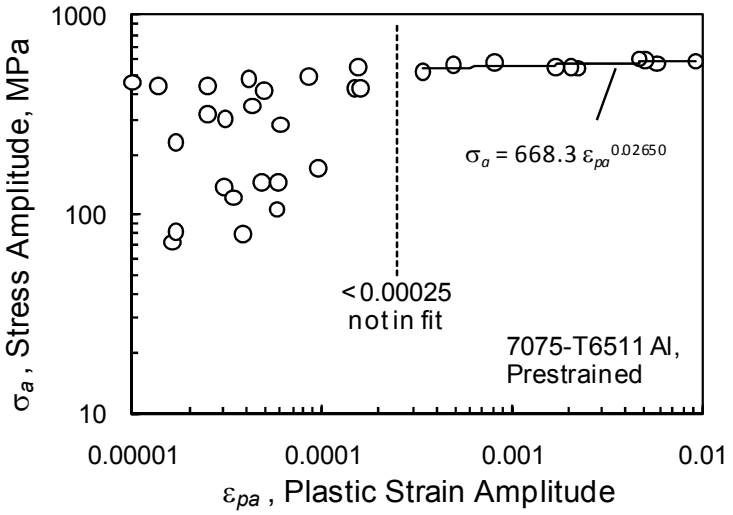

Figure 1-3. Example of stress-plastic strain fit to obtain constants for Ramberg-Osgood equation.

The area inside an hysteresis loop as the one shown in Figure 1-2 is the energy per unit volume stored in the material due to the cyclic deformation applied. The integral of the area inside the hysteresis loop obtained with the application of the Ramberg-Osgood formulation of stress-strain is [7]:

$$\left(\frac{1-n'}{1+n'}\right)\Delta\sigma\Delta\varepsilon_p = \frac{\mathrm{J}}{\mathrm{m}^3} \qquad (1.2)$$

where J is the units of energy, i.e. Joule. Some of this energy is translated into internal structure changes, other into heat [8].

For some materials the cyclic stress-strain response can differ significantly from the monotonic response, like A36 steel or 4140 steel or Ti-4Al-6V. For some others, the differences can be more limited, like the materials in the current study, 7075-T6511 and 7249-T76511 Al. In Figure 1-4 the monotonic and the fitted Ramberg-Osgood cyclic response of A36 steel and 7075-T6511 aluminum are shown.

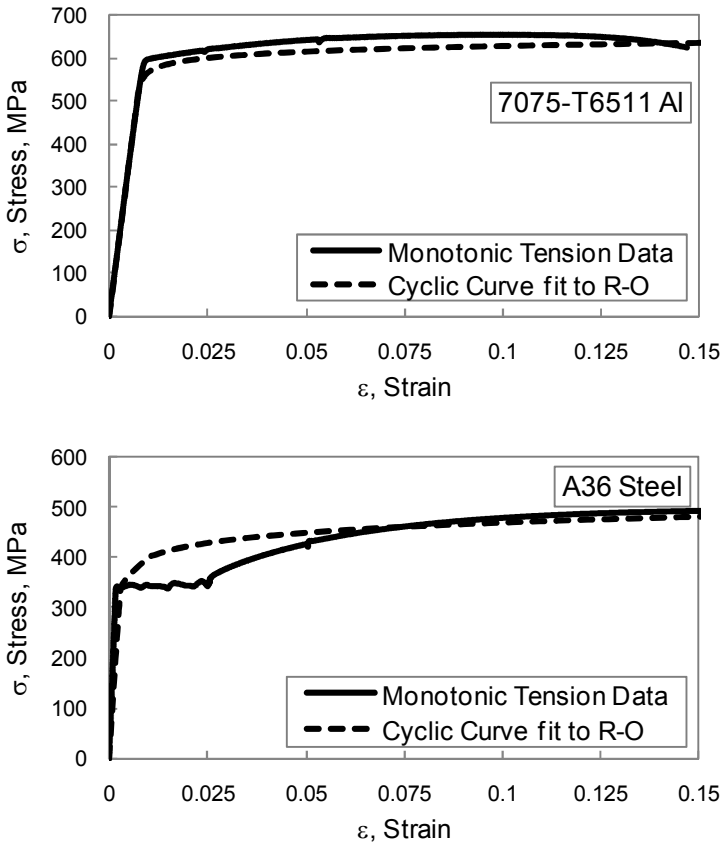

Figure 1-4. Comparison of monotonic and cyclic Ramberg-Osgood fitted behavior for 7075-T6511 aluminum alloy and A36 steel.

The Ramberg-Osgood equation can be applied with success to stress-strain analysis of notched members in combination with Neuber's rule.

1.3 The strain-life curve

In the strain-based approach to fatigue, the fatigue life of the material is related to the strain applied to it; completely reversed tests are run at different strain amplitudes, and the life to failure is used to fit the strain-life curve. A representation of the strain-life curve is shown in Figure 1-5.

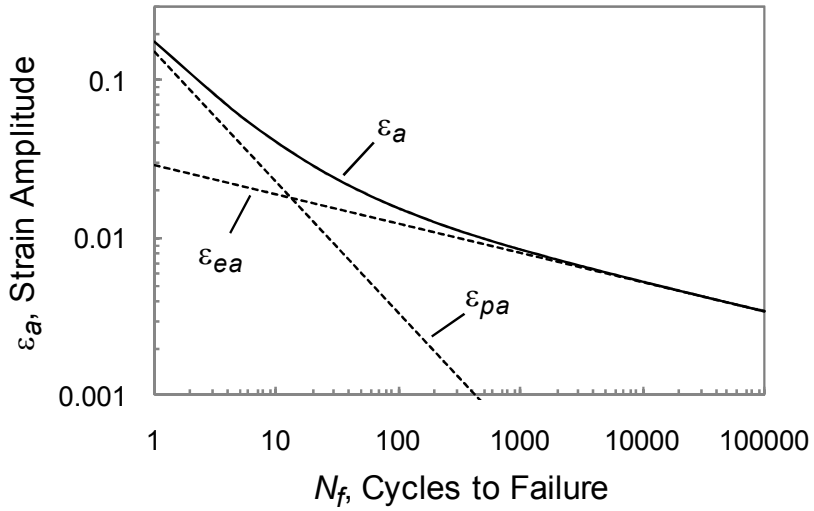

Figure 1-5. Representation of strain-life curve with formulation shown in Eq. 1.3.

The most common form of a strain-life curve is a double linear relationship in a log-log plot [8]. The elastic strain amplitude, ε_{ea}, and the plastic strain amplitude, ε_{pa}, are fitted to life to failure, N_f, separately. Both fitted curves are lines in a log-log scale:

$$\varepsilon_a = \frac{\sigma_f^{'}}{E}\left(2N_f\right)^b + \varepsilon_f^{'}\left(2N_f\right)^c \qquad (1.3)$$

Where σ_f', ε_f', b and c are the fitting constants, as firstly introduced by Morrow [1].

The strain-life curve, as formulated above, shows two regions of behavior: one plastically dominated and one elastically dominated. These are called respectively, low cycle fatigue and high cycle fatigue. The difference in life is related to the different deformation applied to the material causing different times and modes of crack nucleation and propagation. In low cycle fatigue, cracks of relatively large size are nucleated early in life, and the high level of deformation is responsible for the growth of the crack, taking most of the total part of the life. In high cycle fatigue, the nucleation of a crack of significant size takes a much higher percentage of the life, and the growth of this crack to the critical size is relatively fast as occupying a small

fraction of the total life [9]. The critical size is the ultimate size that causes fracture upon successive loading cycles.

Other relationship can be used to represent material behavior in some cases. Depending on the type of material, the elastic part of the curve might deviate from linear behavior, asymptotically following a fatigue limit. In other cases, the plastic part might be better described by two linear segments. In addition, more refined fitting techniques can be applied when convenient to modify the curve for mean stress effects. This basic form for the strain-life curve will be used in the current study, and modifications will be applied and justified when necessary.

1.4 Damage calculation

The theoretical damage for each hysteresis loop is the reciprocal of the number of cycles to failure that the material can withstand when repeatedly loaded at the same amplitude. This is true when a fracture is considered to be corresponding to a damage value of 1.

To account for the contribution of each cycle in a loading history, a damage summation rule must be taken into account. A summation rule can be linear or non linear, and the choice depends on the level of confidence that can be placed in the rule of summation. It is generally common to use a linear rule in the form of Palmgren-Miner:

$$N_f = \sum \frac{N_j}{N_{jf}} \qquad (1.4)$$

Where N_j is the number of cycles performed at a certain strain level and N_{jf} is the number of cycles to failure for the material at the same strain level.

Although ignoring history effects might seem to omit useful data, it has been proven that in most cases a linear damage rule has shown satisfactory results [10] [11]. Non linear damage rules could also be applied to the problem in this study, but it is beyond the scope of this research to investigate history effects and the use of a non-linear damage rule, therefore the Palmgren-Miner rule will be employed.

1.5 Cycle Counting in Variable Amplitude Loading

Constant amplitude loading tests, i.e. tests where the amplitude of each segment of loading is constant throughout the test, are used to characterize the stress-strain and strain-life. These tests will also be shown to characterize mean stress behavior of materials in a strain-based approach to fatigue, but service loadings are mostly constituted by loading segments of variable amplitude.

One of the difficulties when dealing with a fatigue problem is the counting of the hysteresis loops when the loading history is formed by variable amplitude loading segments. The application of the strain-based fatigue approach needs the analysis of the points when each cycle is closed to account for damage, i.e. to record in the linear summation the damage due to the specific hysteresis loop [12].

Memory effects are visible at the loading points in the cyclic response of the material where a loading segment from a hysteresis loop intersects and continues on the path traced by another loading segment in the same direction. This occurs typically for smaller loops inside a larger hysteresis loop, and memory effects determine the closure of those loops.

Counting rules have been developed so that, from a loading history, it is possible to recognize memory effects acting during cyclic deformation of the material, and where hysteresis loops are closed. Some of those which agreed with the experimental data and are sometimes used in life calculations are Peak counting, Mean Crossing Peak, Level crossing, Range counting, and the Rain Flow counting method. However, all but the last can be highly inaccurate in certain situations. The Rain Flow counting method, developed by Prof. Endo and his colleagues in 1968, is then the most reliable and quickly applicable method when dealing with variable amplitude loading [13].

The name of the method derives from the fact that each peak in the loading history is considered as a source of rain drops. Then closed loops are calculated depending on the way the water falls from peak to peak, imagining the load history with time axis in the vertical direction as shown in Figure 1-6.

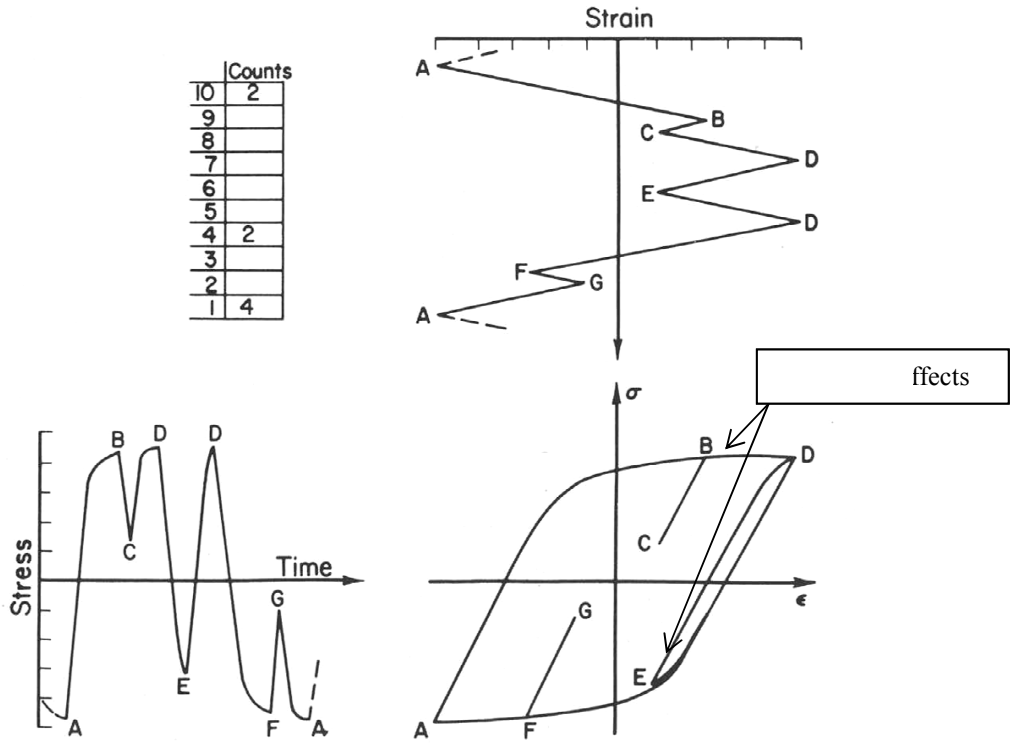

Figure 1-6. Example of application of Rain Flow counting method, with indicated points in the loading history where memory effects occur adapted from Ref. [10].

This method immediately showed good agreement with test data and higher improvements with respect to the previous ones. For variable amplitude loading histories and complicated histories, it was shown by Dowling to be the most accurate method in comparative results for 2024-T4 Aluminum [14].

Widely accepted as the most accurate method to describe material behavior in variable amplitude loading cases, it will be used in the current investigation for life calculations, and it is implemented in the computer program FAMS [15].

1.6 Application to Notched members

Holes, fillets, grooves and keyways are frequently necessary in design, but these geometries act as stress raisers, locally increasing the severity of the stress nominally applied to the components that they are part of. The success of the strain-based approach is also due to its application to notched members, most of the time the highly critical components in any structure. The strain based approach can be applied to a stress-strain condition at the stress raisers or notches of structural components if a stress-strain analysis is successfully performed on the element.

Geometrical stress analysis of notched members is aimed to find the value of k_t, a stress concentration factor that has to be used to obtain the local values of stress and strain. In fatigue analysis, a fatigue notch factor, k_f, is frequently employed due to several local effects. One of those effects, fundamental when considering ductile metals at intermediate and short lives, is called reversed yielding. This phenomenon is due to localized yielding at the notch: in fact, if the loading is mainly elastic, k_t and k_f tend to be equivalent, depending the amount of plastic deformation, the deviation of k_t from k_f gets larger until k_f reaches a stable value of 1. The dependence of k_f from the amount of plastic deformation involved is sometimes referred to a cycles to failure dependence [16], as shown in Figure 1-7.

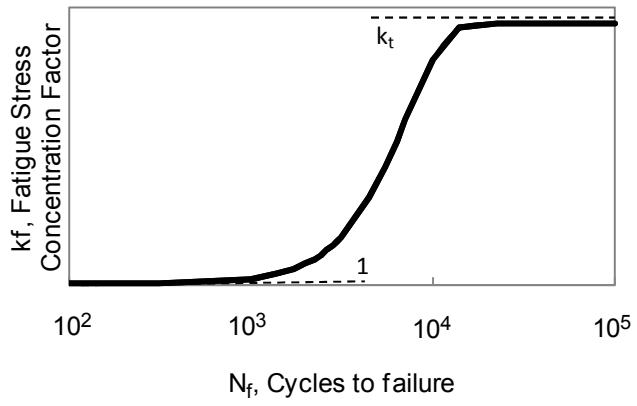

Figure 1-7. Schematic representation of variation of k_f, fatigue stress concentration factor.

Another effect is due to geometrical constraints, as a small notch radius can cause significant differences between k_t and k_f. Some other effects involve the slope of the distribution of the stress at the notch, called stress gradient: the process zone size, weakest link and crack growth effects. The first states that the difference in k_t and k_f may be due to a different effective stress at the notch in a fatigue test, creating discrepancy between life of smooth and notched elements. The second theorizes that a potential damage initiation site, the weakest link, is statistically more likely to be found in a smooth specimen than in the small region at the notch. The third effect introduces the crack growth concept in the notch problem, considering that a crack will start fairly soon in a notched member and grow into a low stress region, while this would not happen in a smooth member. This can cause the k_t to differ significantly from k_f.

The stress based approach requires the use of empirical formulas relating the values of k_t and the values of k_f for different loading conditions. The strain-based approach seems to handle this difficult situation in a more rational way, introducing a relationship between stresses and strains locally. The relationship is empirical, and it is convenient to use it for a number of applications unless the accuracy of the solution requires the use of a finite element analysis. The equation used more frequently is Neuber's rule:

$$\sigma\varepsilon = \frac{(k_t S)^2}{E} \qquad (1.5)$$

Where σ and ε are stress and strain at the notch, k_t is the stress concentration factor of the notch, S is the nominal stress applied to the component and E is the elastic modulus. Neuber's rule simply states that the product of stress and strain at the notch is constant, and this product can be found from the nominal stress S, stress concentration factor k_t, and elastic modulus.

Given a certain nominal loading history, it is possible to obtain the local stress and strain response at the notch using Neuber's rule. Then the hysteresis loops can be drawn with the given local history with the use of a cycle counting rule. The application of Neuber's rule confirms the relationship between k_t and k_f that had to be used in a stress-based approach to approximate the

response at the notch, implicitly showing the more intimate understanding of the local problem of the strain-based approach.

1.7 Application to biased states of stress or strain

When a material or a notched member is cycled following a loading biased with respect to zero, a mean stress is developed in the material. The presence of a mean stress in the loading pattern can change the number of cycles to failure, with respect to the unbiased situation. Mean stresses have to be taken into account when dealing with life calculation, but mean stress sensitivity for different materials is highly variable, and mean stress effects cannot be easily modeled.

1.7.1 The effects of Mean Stresses

A good number of empirical formulas were developed in more than a century of mean stress effects studies. In fact, significantly different results can be obtained in the application of one or the other, with practically no certified standard or agreements in the scientific community. The empirical formulas are meant to change the stress amplitude, in the case of a stress based approach, or the strain amplitude, for a strain based approach, of the tests loaded at a certain mean level so that a completely reversed equivalent strain amplitude is found to have the same number of cycles to failure.

If the general form of those models, in a stress based approach, is visualized as a function of stress amplitude and mean stress as in:

$$\sigma_{ar} = f(\sigma_a, \sigma_m) \qquad (1.6)$$

where σ_{ar} is the equivalent completely reversed stress amplitude; then the strain-life curve is modified in the following way:

$$\varepsilon_a = \frac{\sigma_f'}{E}(2N^*)^b + \varepsilon_f'(2N^*)^c \qquad (1.7)$$

$$\text{with} \quad N^* = N_f\left(\frac{\sigma_a}{f(\sigma_a, \sigma_m)}\right)^{1/b}$$

The importance of the function f, chosen to represent the effect on life due to the presence of a tensile or compressive mean stresses, becomes clear. In a mainly empirical effort to fit experimental data, many methods have been shown to be successful and the correspondent models used in life calculations. Some of the most recognized mean stress models are shown in the following paragraphs.

Goodman [17] developed with success and obtained good consensus on one of the functions to calculate the completely reversed stress amplitude around 1919 in a study on different types of steels, using as material constant the ultimate strength σ_u. The formula was then later modified by Smith [18] and written in its actual form:

$$\sigma_{ar} = \frac{\sigma_a}{1 - \frac{\sigma_m}{\sigma_u}} \qquad (1.8)$$

Morrow [19] proposed the same type of formula to calculate completely reversed stress amplitude, but instead of using the ultimate strength, he substituted it with the true fracture strength of the material [20], changing the formula into:

$$\sigma_{ar} = \frac{\sigma_a}{1 - \frac{\sigma_m}{\tilde{\sigma}_{fB}}} \qquad (1.9)$$

As a second alternative, Morrow proposed also to change the true fracture strength with the material constant σ_f' from the stress-life curve:

$$\sigma_{ar} = \frac{\sigma_a}{1 - \frac{\sigma_m}{\sigma'_f}} \qquad (1.10)$$

These first three models are usually visualized on a σ_a / σ_{ar} vs σ_m graph, where each of them represents a straight line, as shown in Figure 1-8.

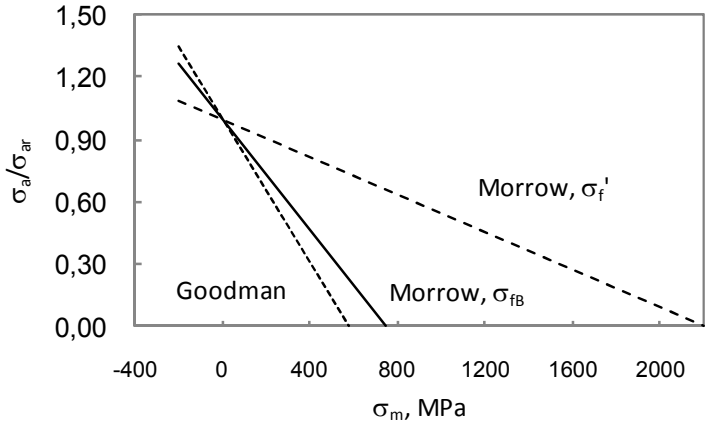

Figure 1-8. Graphical representation of the Goodman model and the two Morrow models.

Smith, Watson and Topper [21] with cumulative work, experimentally verified the good agreement of mean stress data and life to failure with a different type of equation that does not use a material constant:

$$\sigma_{ar} = \sqrt{\sigma_{\max}\sigma_a} \qquad (1.11)$$

or

$$\sigma_{ar} = \sigma_{\max}\sqrt{\frac{1 - R}{2}} \qquad (1.12)$$

Another experimental formula was obtained by Walker [22], and it is similar in its form to the SWT:

$$\sigma_{ar} = {\sigma_{\max}}^{1-\gamma}{\sigma_a}^{\gamma} \qquad (1.13)$$

or

$$\sigma_{ar} = \sigma_{\max}\left(\frac{1-\mathrm{R}}{2}\right)^{\gamma} \qquad (1.14)$$

Walker's solution requires data fitting to obtain the material constant γ, and when γ is 0.5 the solution coincides with SWT. The SWT and Walker can be visualized on a mean-amplitude graph, with mean normalized by σ_{ar}, as shown in Figure 1-9.

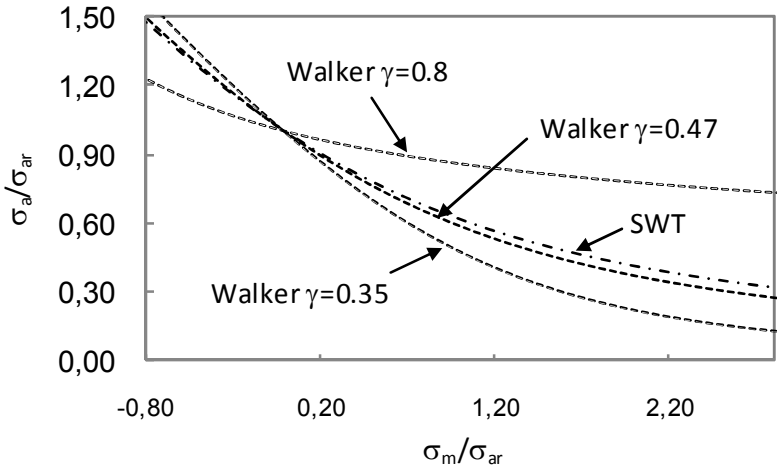

Figure 1-9. Graphical representation of SWT model and Walker for different values of γ.

Mean stress models are significantly different from one another, and their performance is also not known a priori for a given material. Continuous research is required to characterize for which classes of materials some forms may be more suitable, and also to give at least the possibility of knowing which models are appropriate for the different classes of metals.

1.7.2
Mean Stress Relaxation in cyclic loading

The problem of mean stresses in fatigue is exacerbated by the instability of mean stresses during cyclic loading. When a cyclic biased deformation is applied in the material, mean stresses tend to relax to a stable value. The rate of relaxation, the amount of relaxation, and the stable values are all dependent on the loading conditions.

Similarly to what is observed statically for some materials at certain environmental conditions, a constant state of deformation is managed interiorly by the material with structural rearrangements responsible for a decrease in stress. This is observed to occur statically, as in a standard relaxation test, or cyclically as in the case of this study. The physical mechanisms behind cyclic relaxation are not as clear as the ones shown to happen for static relaxation. In most of materials loaded cyclically, it happens at room temperature, whereas specific conditions of temperature are frequently needed for static creep and relaxation for most structural metals.

An example of two different relaxation curves from test data is reported in Figure 1-10.

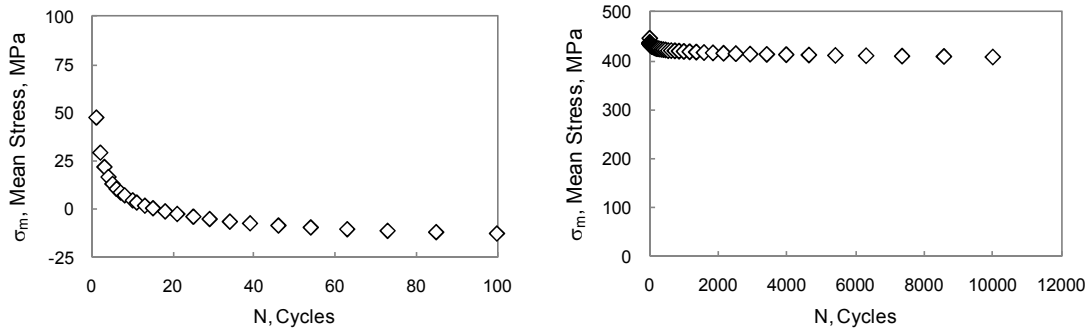

Figure 1-10. Example of mean stress relaxation in constant amplitude loading for a strain amplitude of 0.95% and 0.2%.

In the first test, a constant amplitude test with a strain amplitude of approximately 1% strain, mean stress starts at a lower tensile value, decreases until crossing zero, and stabilizes to a small compressive value. In the second test, a constant amplitude test with a strain amplitude of approximately 0.2%, the high tensile mean stresses decrease to a lower tensile value.

Both relaxation curves can effectively change the life predictions when one mean stress correction model is used, and a difference in life up to a factor of 2 can be easily obtained.

Mean stresses are also subjected to relaxation during service; it is therefore necessary to observe experimentally this phenomenon under variable amplitude loading.

The degree of difficulty of the problem is high and requires further investigation since fatigue life calculations are frequently carried out without considering relaxation effects with over conservative predictions. In notched members, both cyclic mean stress relaxation and cyclic creep are observed to occur during service life, where cyclic creep is a similar transient phenomenon involving the increase in mean strain for a force controlled test, recalling a static creep test. The advance in understanding of the type of mechanisms leading to those temporary deviations from stable behavior is of great importance. This is especially true for cases where the stress-strain analysis is a key element in the survival of the structure.

1.8 Problem Statement and Objectives

The cost of the fracture of materials in the United States has a great impact on the rate of growth of the country in terms of large expenses for conservative design, inspections, reduced service time, and replacements to match safety factors and prevent possible catastrophic failures. This high cost limits the possibilities of investment, especially for aircraft companies, motor vehicle companies, residential and non-residential construction companies, and contributes to the difficulties recently experienced in these business sectors [23].

A study in 1983 estimated a cost of $119 billion due to cracking, deformation, and concurrent damage phenomena, not considering wear and corrosion; cracking due to fatigue, represents 80% of this expense. The development of reliable methods for fatigue life prediction in engineering is therefore of great importance.

The strain based fatigue approach is extensively used in many engineering applications involving fatigue and life predictions, especially when dealing with structurally critical components where plastic deformations may occur during life [3]. The relative simplicity of the method in analyzing complicated stress-strain problems in critical locations and the improvements that this method introduced in the analyses of local stresses and strains, are two of the reasons why the strain-

based method is extensively used in industry. Computational times are also of interest when dealing with fatigue life calculations; software based on the strain-based method and the rain flow counting for variable amplitude loading showed to be fast and easy to handle for most of users [15].

Nonetheless, several difficulties are encountered in life predictions, especially when introducing mean stress effects. As shown in the introduction and literature review, the attention to this topic in the field is high, because the erroneous handling of mean stresses in fatigue life can lead to unacceptably high levels of conservatism or to potentially dangerous non conservative predictions. In both cases the cost of keeping structures functional is increased by a considerable amount, and especially in economically critical times, this possibly means a slower rate of development in many scientific fields.

Mean stresses, being responsible for one of the biggest uncertainties in life calculations, are also subjected to transient phenomena: in a state of biased deformation, mean stresses tend to relax to a stable value, different from the initial value theorized by a standard stress-strain approach. At stress raisers also mean stresses tend to relax, in a combined relaxation and ratcheting behavior, both stresses and strains reach a stable value different from the one calculated with an analysis excluding transient effects.

Valid fatigue data on materials frequently used in aircraft structures was needed by the sponsor of this project NAVAIR, Naval Air System Command, and information on the possibility of including some of the transient effects in fatigue life calculations was also desired. A life calculation software, FAMS [15], developed by TDA, Technical Data Analysis, conjugate coordinator of the project, is the target of advances in fatigue calculations that could be obtained with the data analyzed in this study.

The materials of interest are two 7th series high strength aluminum alloys, 7075-T6511 and 7249-T76511; special interest was given to the latter, because it is an improvement with respect to corrosion resistance of the well known and more extensively studied 7075.

Effects of environmental conditions effects have to be taken into account when dealing with material performance; temperature, pH, composition of atmosphere, and the presence of other materials in the same environment, can drastically lower the fatigue life. Metals are

particularly subjected to corrosion when inserted in aggressive environments. The concurrent action of service loading damage and corrosion damage risk shorten fatigue life drastically. New structural compositions and new heat treatments to enhance corrosion resistance are continuously investigated, but frequently a micro structural change for a material possibly means also a different mechanical behavior. This is the main reason why 7075 structural components substituted with corrosion resistant 7249 could have different mechanical behaviors that interfere with the correct structural response of those components. This study will also give a response to this question by collecting fatigue data for both alloys.

The main goals of the current research are the characterization of the two materials provided by NAVAIR in terms of tension properties, cyclic stress-strain properties, and strain-life curve characteristics. An extensive study regarding mean stress effects will be conducted to evaluate mean stress models shown in literature, and to suggest a convenient approach in life predictions when dealing with loadings biased with respect to zero. Cyclic mean stress relaxation will be investigated in constant amplitude loading to have a deeper insight of the relaxation phenomena occurring during life. The last part of the experimental work of the current research will regard the observation of cyclic mean stress relaxation in variable amplitude loading conditions for both aluminum alloys. The modeling of the stress-strain response, including this transient effect, will be the last part of the data analysis and effects on fatigue life of the improved method will be evaluated.

Finally guidelines for the modifications of FAMS will be suggested in terms of implementation of mean stress models, use of mean stress models for life calculations, and implementation of new stress-strain models including the effects of mean stress relaxation.

Chapter 2
Literature review

The strain-based approach to fatigue is extensively used in life calculations for critical parts of structures in aeronautics, automotive, biomechanics and civil engineering applications. As previously discussed, it is a convenient method to deal with problems of local yielding at notches, and in general when dealing with high plastic deformations [6].

Although the application of this method is successful in giving accurate life estimates, frequently those predictions are quite conservative. Mean stress effects and mean stress relaxation are causes of errors in life predictions which typically lead to excessively conservative results.

An overview of the interest of the scientific community in the strain-based method and its improvements in solving fatigue life calculation problems is presented in the literature review of this chapter. Also, a more detailed exploration of mean stresses and cyclic mean stress relaxation, the two main issues of this research, will be included.

2.1 Considerations for variable amplitude loading

The strain-based fatigue approach has limitations when applied to variable amplitude loading conditions. The first source of inaccuracy is the Palmgren-Miner rule; several studies have been performed on the consequences of fatigue calculations with the Palmgren-Miner rule and sequence effects [24], [10], [25], [11], [26]. In one of those studies, Dowling and colleagues quantified the error for block effects and random sequences. Depending on the difference between the levels and on the way they are arranged in the history, the deviation can be relatively consistent or untraceable. For example, if two levels are considered, as in Figure 2-1, the highest deviation from linear summation is observed when the highest level is at the beginning of the history. This phenomenon is mainly due to the fact that the damage introduced by the severe loadings is enough to enhance the effects of the smaller successive cycles. For high cycle fatigue, most of the life is spent in nucleating a micro crack, while in low cycle fatigue, most is spent in

growing the micro crack. The different span of the two main phases in fatigue is a cause of interference of small and large cycles in variable amplitude loading.

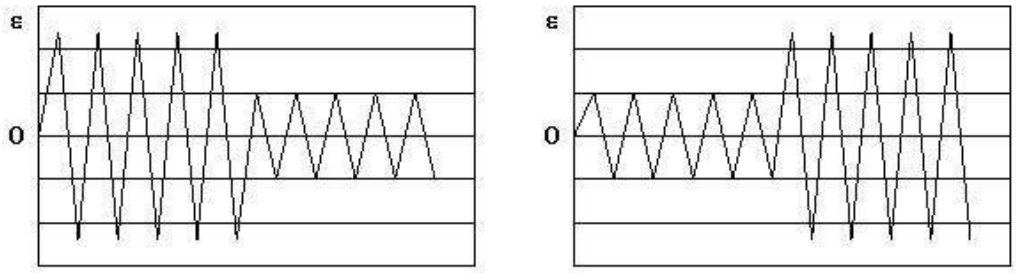

Figure 2-1. Loading patterns with same number of cycles and amplitudes of cycles, but causing different damage due to sequence effects.

It is not an emphasis of this study to evaluate the ways to overcome the difficulty in the application of the Palmgrim-Miner rule, but to give guidelines to deal with complex variable amplitude loading problems and to analyze the effects of mean stresses and mean stress relaxation in life calculation. Nonetheless, one way to overcome this difficulty is proposed and used in this study: at the beginning of any tests the material is pre-strained for five cycles at a high deformation level (1.2% strain) and cycled 10 times at progressively decreasing strain levels until a state of zero strain, zero stress is reached. This type of loading is shown in Figure 2-2. Micro cracks or precursors of these are initiated in the pre-strain process, artificially lowering the strain-life curve in high cycle fatigue region and including, at least in part, sequence effects in the strain life curve [27], [28], [29].

Furthermore, when dealing with a variable amplitude loading pattern, plastic deformations in the material can be different depending on the loading sequence. In a stress-strain analysis, this means a change in their mutual relationship and a deviation from the standard Ramberg-Osgood formulation, reducing the accuracy of local stress-strain calculations and fatigue life predictions. It was shown in several studies that if H' and n' from the Ramberg-Osgood relationship, Eq. 1.1, were calculated with constant amplitude tests, then during a non-constant amplitude test, the actual plastic strains at low stresses were larger than what was predicted [14], [25], [30], [9]. It was suggested [14] that a way to obtain material constants,

taking into account the variations due to non-constant amplitude loadings, is to run an incremental step test, a loading pattern constituted by the product of a sine wave and a triangular wave [10], [31], [32]. Instead of calculating *H'* and *n'* from hysteresis loops run at constant amplitude, those material constants could be fitted to hysteresis loops obtained with a single incremental step test. The stress-strain response to an incremental step test on 7075-T6511 is shown in Figure 2-3.

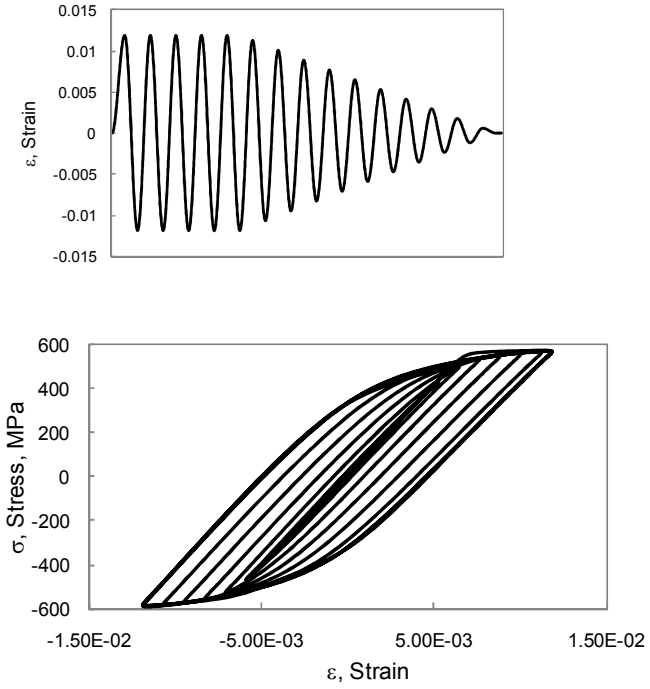

Figure 2-2. Pre-strain control signal and stress-strain response for 7075-T6511.

The differences for aluminum alloys are not extreme and similar values of H' and n' are usually obtained. Nonetheless, incremental step tests are going to be included in the variable amplitude loading plan of the current study.

During analysis on service loadings, the rain flow counting method is usually applied to obtain the amplitude of the closed hysteresis loops and the effects of memory in the loading. Even if it is a fast counting method, often service loadings are simplified, to avoid including an excessive number of small elastic hysteresis loops, sometimes composing the largest part of the

loading. Instead, the focus is on the effects of bigger loops involving more noticeable plastic deformations. The limit strain amplitude, under which no damage is counted, can be decided a priori before fatigue analysis, and eventually modified for successive calculations in case of unsatisfactory results.

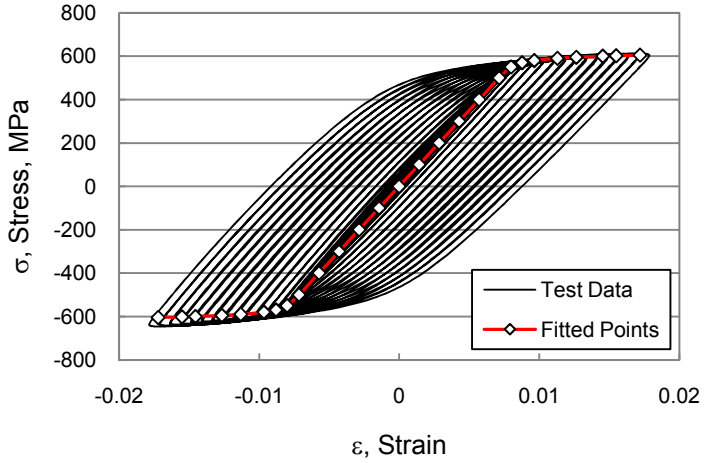

Figure 2-3. Incremental step test performed on 7075-T6511 aluminum and fitting of the stress-strain relationship.

The variable amplitude loading patterns in this study usually involve a significant amount of plastic deformation, mainly because of the particular interest in relaxation phenomena, highly enhanced in the plastic regime.

2.2 Mean Stress models and Performance

Many life calculation softwares still have the possibility to exclude the use of a mean stress correction methods, due to the difficulty in interpreting the results, even though predictions will generally be highly conservative. A good number of studies in literature are aimed at improving the understanding of mean stress models [33] and clarifying their performance.

A complete summary of the methods currently used to handle mean stresses is presented in a study by Wehner and Fatemi [34], and more recently by Dowling and Thangjitham [35]. The latter is a wider overview of the methods for fatigue analysis, the stress-based, strain-based and fracture mechanics approach. It focuses on the mean stress methods for both stress and strain

approach and shows fitting results for AISI 4340 steel and 2024-T3 alumiunum with all the mean stress models shown in Chapter 1.

When applying mean stress methods, every stress amplitude-mean stress situation is solved with the introduction of an equivalent zero mean stress amplitude, where the stress-based approach is considered for simplicity of formulation. The stress versus fatigue life relationship for the material, viewed as the elastic part of the strain-life relationship when using a strain-based approach, multiplied by the elastic modulus, is transformed accordingly as shown:

$$\sigma_{ar} = \sigma'_f \left(2N_f\right)^b \qquad (2.1)$$

where σ_{ar} is called equivalent completely reversed stress, i.e. the stress amplitude at zero mean corresponding to a stress amplitude σ_a, applied at a mean stress σ_m.

In the stress based approach, the relationships to obtain equivalent stress amplitude involve a ratio of an applied nominal stress to a material property in the case of Goodman and Morrow models; fitting results will be affected by the uncertainty in defining an applied stress from a nominal stress in the case of notched members [36]. The application of the mean stress models in the strain based approach is not affected by the same deficit, due to different handling of local stress-strain conditions at the notch. The solution of the local stress-strain problem with Neuber's rule overcomes the difficulties in defining a local stress, σ, from a nominal stress, S, and also in defining a local mean stress, σ_m, from a nominal mean stress, S_m.

The representative results shown for 4340 steel by Dowling and Thangjtham suggest that the use of the Goodman model leads to highly conservative life predictions, that the Morrow model is able to fit experimental data satisfactorily in both its formulations, and that SWT gives intermediate results. In the case of aluminum alloys the trends are similar, with the exception of the Morrow model where σ'_f fits the mean stress data poorly. The main reason is that σ'_f highly deviates from $\tilde{\sigma}_{fB}$, causing a higher scatter in the mean vs amplitude plot. The Walker method is suggested as a good model to use for both materials if a high amount of experimental data is available and fitting procedures to obtain γ give reasonable correlation.

The application of mean stress models to a large number of experimental data, mainly for steels and aluminum alloys, has been shown by Dowling et al. [37], [38]. All the data are reduced with the models previously described, Goodman, Morrow, SWT and Walker, and for each material and method a performance value is calculated:

$$s_z = \sqrt{\frac{\sum_{i=1}^{n} z_i^2}{n-1}} \qquad (2.2)$$

where z_i is the stress difference of each point in the σ_{ar} vs N_f (stress-life) plot from the line curve representing the mean stress model. The Eq. 2.1 line is the same for all models as it represents zero mean behavior. It is the σ_{ar} that differ for the various models. This quantity, called stress deviation, represents the scatter of the σ_{ar} defined by each model around the zero mean stress in a σ_{ar} vs N_f plot. The lower the stress deviation, the better the model is able to reduce mean stress data and the more significant are the constants obtained fitting the σ_{ar} vs N_f relationship, Eq. 2.1.

The use of a performance quantity for mean stress models can help in the quick individuation of the most performing method for a particular material. It will be used in the current study also for the mean stress analysis.

Among all the mean stress models considered here, only the Walker method needs a fitted constant obtained from mean stress analysis. The Goodman and Morrow models use material constants, not necessarily obtainable with mean stress data. The same study [38] also shows a detailed explanation on how to fit the Walker equation and obtain the constant γ:

$$\sigma_{ar} = AN_f^b = \sigma_{\max}\left(\frac{1-R}{2}\right)^{\gamma} \qquad (2.3)$$

$$\text{where } N_f = \left[\sigma_{\max}\left(\frac{1-R}{2}\right)^{\gamma}\frac{1}{A}\right]^{1/b}, \quad \text{and} \quad \sigma_f' = A/2^b$$

Starting from the general form for the Walker model and taking the logarithm of both sides of the N_f equation is shown, the following form is obtained:

$$\log N_f = \frac{1}{b}\log \sigma_{\max} + \frac{\gamma}{b}\log\left(\frac{1-R}{2}\right) - \frac{1}{b}\log A \quad , \text{ where } \sigma_f' = A/2^b \qquad (2.4)$$

A multiple linear regression can be performed to obtain the value of γ by using all the N_f values from the mean stress tests, the R ratios, and the maximum stresses, σ_{max}. The need of fitting mean stress data for a satisfactory application of the Walker method is a possible disadvantage if experimental data are not available.

The study revealed that the Goodman model is in most cases not accurate in describing mean stress effects, with s_z values ranging from typically 0.2 for steels and 0.3 for aluminum alloys. The Goodman model is excessively conservative for tensile mean stresses and dangerously non conservative for compressive mean stresses. The use of the Goodman model is therefore not suggested.

The Morrow model in the form employing the true fracture strength, $\tilde{\sigma}_{fB}$, shows general better agreement with experimental data for steels particularly and reasonably good agreement for aluminum alloys, values of s_z go from 0.11 in steels to 0.15 in aluminum.

The use of Morrow with σ_f' is debatable. From one point of view, the scatter for steels is acceptable and in the range of the model with $\tilde{\sigma}_{fB}$, but the performance for aluminum alloys is poor. The main reason is the fitting of low cycle fatigue tests data to obtain σ_f' for aluminum alloys, shows a large deviation from linear behavior from what it is usually obtained for steels, and a clear divergence of the value of σ_f' with respect to $\tilde{\sigma}_{fB}$. This gives large scatter and poor performance, therefore suggesting avoiding the use of the model when dealing with mean stress effects for aluminum alloys.

The SWT method is generally successful in fitting data for both classes of materials, performing similarly to the Morrow method for steels, but improving significantly the

performance for aluminum alloys. The use of this method is suggested by the authors, also taking into account the simplicity of the model and the lack of need for other material constants.

The Walker method is by far the most successful in fitting experimental data, mainly because the constant γ is directly obtained from the mean stress analysis. The agreement with data is superior to any of the other models, with values of s_z typically around 0.07 for steels and 0.09 for aluminum alloys.

The same analysis will be performed in the current study on 7075-T6511 and 7249-T76511 to include some of the results obtained in the never ending discussion about mean stress models and give important guidelines to the sponsor of the current project when dealing with these two alloys or materials showing similar characteristics.

2.3 Mean Stress and Residual Stress Relaxation Models

As previously introduced, mean stress relaxation is a cyclic, transient phenomenon occurring in engineering materials when subjected to cyclic biased deformations. It consists in the gradual shifting of the mean stress, as shown in Figure 2-4 , from an initial value to a different stable value.

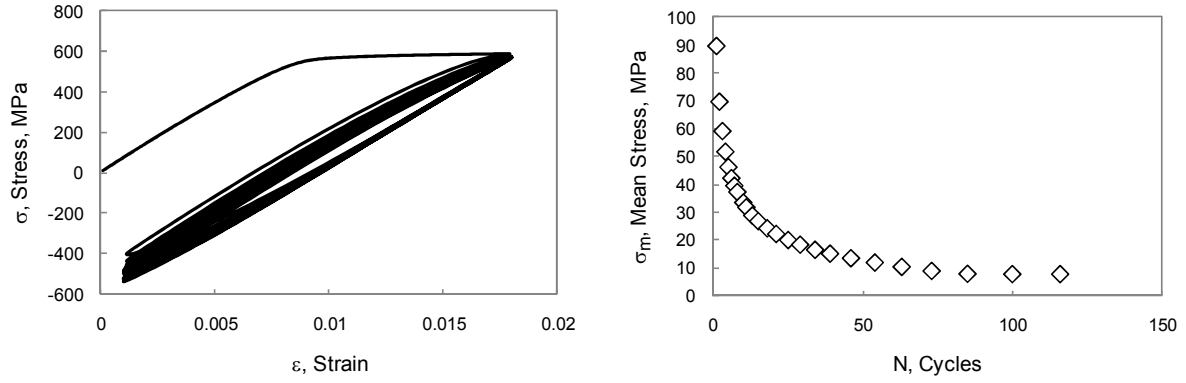

Figure 2-4. Mean stress relaxation in an axial test of 7075-T6511 aluminum alloy. The sample was cycled at a strain amplitude of 0.0072 about a mean strain of 0.0108.

Even though the phenomenon is transient, life can be altered significantly, especially in materials with high sensitivity to mean stresses. In addition, when mean stress models are

applied in fatigue analysis, mean stress relaxation, added to the uncertainty in the application of the mean stress models and to the errors given by their experimental nature, degrades the reliability of life predictions.

An early attempt to model cyclic mean stress relaxation for steel was reported by Morrow and Sinclair in 1958 [39]. Their theory was based on the concept that the amount of relaxation that occurs is dependent on the plastic deformation involved. The mean stress was expressed as a nonlinear function of cycle number, stress amplitude, the material's cyclic yield stress and strain, as well as its strain hardening exponent.

Other methods and models have been developed to study the related problem of residual stress relaxation. (Residual stresses are internal stresses that are present even under zero applied loading, so that they alter the local mean stress and thus affect the fatigue life.) Beneficial compressive, near-surface residual stresses are introduced by various processes, such as shot peening, laser peening, low plasticity burnishing, and induction hardening [40].

In 1988, Landgraf and Chernenkoff [41] conducted a series of tests on axial specimens of steels, with the objective of evaluating the effect on fatigue life of mechanical or thermal processes employed to create residual stresses. They showed a dependence of mean stress relaxation on strain amplitude and material hardness, and they postulated the existence of a strain amplitude threshold below which no relaxation is exhibited. The relaxation behavior is modeled as an exponential with the number of cycle as base,

$$\sigma_{mN} = \sigma_{mi} \mathrm{N}^{r}\,, \qquad \text{where } r = A\left(1 - \frac{\varepsilon_a}{\varepsilon_{aTh}}\right) \qquad \text{(a,b)} \qquad (2.5)$$

Here, σ_m is mean stress, with an additional subscript i indicating the initial value, and an additional subscript *N*, the value after *N* cycles. Also, ea is the strain amplitude (half-range), and ε_{aTh} is the threshold value of this quantity. The dependence of the relaxation exponent, r, on strain amplitude was modeled with the linear expression (b) shown, along with $r = 0$ for $\varepsilon_a \leq \varepsilon_{aTh}$. For steels, A = 0.85 is employed in [41], and ε_{aTh} is expressed as a function of hardness.

For application to a particular metal that is not a steel, A and ε_{aTh} can be treated as fitting constants.

In a study on cyclic relaxation of mean stresses in a nickel-based superalloy, Fang and Berkovits [42] found a transition between regions of strong and weak relaxation effects around 0.5% strain amplitude. This value is on the same order as the threshold levels in the Landgraf work. Stable values of mean stress at half of the fatigue life were recorded in the present work for various test conditions, and a relationship was found with strain amplitude. The variation of stable mean stress with strain amplitude was approximately linear up to the transition, and then followed a nonlinear relationship [43].

Zhuang in 2001 proposed an experimental formula to model residual stress relaxation, involving a greater number of fitting constants [40]. Two factors are considered as key points in the prediction of relaxation effects: the amount of cold working and the relaxation occurring in the first cycle. This relationship has its roots in the Morrow and Sinclair model mentioned before [39] and in the Landgraf model for residual stresses [41]; the final formulation is the following:

$$\frac{\sigma_N^{re}}{|\sigma_0^{re}|} = A\left(\frac{\sigma_a^2}{(1-\mathrm{R})\left(\mathrm{C}_w\sigma_y^2\right)^2}\right)^m (N-1)^B - 1 \qquad (2.6)$$

where σ_N^{re} and σ_0^{re} are the residual stresses at cycle number N and the one at cycle number 0, σ_a is the stress amplitude of the test, R is the strain ratio of the test, C_w is the parameter for the degree of cold working, σ_y is the yield strength and all the other parameters are fitting constants. No experimental work was presented in the paper, but it is predicted that by increasing the number of material constants from one of the Landgraf model to three of the Zhuang model, a higher accuracy will be observed.

Various rheological models show time-dependent relaxation when subjected to biased strain and provide a mathematical formulation that seems to lend itself to ease of computation. A Maxwell model with a nonlinear dashpot, represented by Figure 2-5, can be adapted to model cyclic mean stress relaxation [43] .

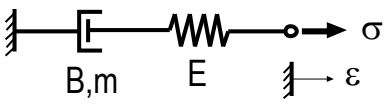

Figure 2-5. Spring and nonlinear dashpot model.

In the model there are three constants: a coefficient B and exponent m for the dashpot, which provides creep strain according to $\dot{\varepsilon}_c = B\sigma^m$, and an elastic modulus E for the spring, giving elastic strain $\varepsilon_e = \sigma/E$. When this rheological model is subjected to a step function of constant strain ε, the relaxation response of stress s with time t is given by:

$$\log\frac{\sigma}{\sigma_i} = \frac{1}{1-m}\log(tBE(m-1)\sigma_i^{m-1}+1) \qquad (m \neq 1) \qquad (2.7)$$

To adapt this model to cyclic loading, an analogy between the constant strain e and the mean strain for cyclic loading was created, $\varepsilon_m = (\varepsilon_{max} + \varepsilon_{min})/2$. Further, the time t was replaced with the number of cycles N, the initial value of stress σ_i with the initial mean stress σ_{mi} , and the stress σ with the mean stress σ_{mN} after N cycles. Thus, we obtain

$$\log\frac{\sigma_{mN}}{\sigma_{mi}} = \frac{1}{1-m}\log(NBE(m-1)\sigma_{mi}^{m-1}+1) \qquad (m \neq 1) \qquad (2.8)$$

Some other rheological models show relaxation formulas applicable to the relaxation observed cyclically in aluminum alloys, but, as considered by Arcari et al., a non linear Maxwell model seems to be the most reasonable tradeoff between complexity of rheological models and fitting feasibility of the relaxation formula [43].

2.4 Introduction to Plasticity Models

The application of plasticity models in a strain-based fatigue approach is not usually considered convenient because of the increase in computational difficulty in the calculation of

the stress-strain response, and the high number of fitting constants required. An advantage in using a plasticity theory is that transient effects, like hardening or softening, relaxation or ratcheting, non-Masing behavior and Baushinger effects [44] [45] are embedded in the stress-strain relationship. Also, global plasticity theories consider the combined effects of multidirectional loadings and are able to predict deformations in all directions.

Plasticity theories define a time independent relationship between stress and strain in materials when deformations deviate from being proportional to loading. Plasticity theories usually define a yield criterion through the use of yield surfaces, and they postulate the change in deformation due to loading once the yield point has been passed through the use of plastic flow rules [46].

Plasticity models describe yielding by using a yield surface in the deviatoric stress space. A flow rule controls the deformation once the yield point has been passed and it is typically included in a hardening rule for the material. In most cases the type of hardening described can be an expansion of the yield surface, isotropic hardening, or a translation of the surface, kinematic hardening and in some cases a combination of both. Among yield criterions, the most common is the von Mises criterion and the surface defined is:

$$f(s-\alpha) = \left[\frac{3}{2}(s-\alpha)(s-\alpha)\right]^{\frac{1}{2}} = \sigma_0 \qquad (2.9)$$

where s is the deviatoric stress tensor, α is the center of the yield surface and σ_0 is the yield strength. The Von Mises criterion determines the yield point of the material with energy concepts: if the elastic distortion energy per unit volume in the material exceeds the elastic distortion energy during yielding in a uniaxial test, the material undergoes plastic deformations [46].

The second element composing a plasticity theory is the flow rule; this can be split into an associated flow rule or a non associated flow rule. The plasticity theory assumes that a potential function exists, such that the velocity components of the plastic flow can be established

at any point of the loading and are proportional to the partial derivatives of this potential function F with respect to the stress:

$$d\varepsilon_{ij}^{p} = \lambda \frac{\partial F}{\partial \sigma_{ij}} \qquad (2.10)$$

where the coefficient λ is called plastic multiplier [47].

If the function F is the same as the yield function, the flow rule is defined as the associated flow rule and Eq. 2.10 establishes the perpendicularity of the plastic flow to the yield function [48].

Once the direction of the plastic flow is described, the consequence on the yield function is determined through a hardening rule. Kinematic hardening is usually preferred to isotropic hardening when dealing with metals due to the Baushinger effects. These effects are that when a material, isotropically hardening, is subjected first to a loading and then to unloading until the compressive yield point is reached, the elastic region in between the start point of unloading and the yield point in compression leads to a yield stress equivalent to the highest stress reached in the loading part due to the expansion of the yield surface. In a material kinematically hardening, the yield point in compression will be lower than the highest stress reached in the loading part of the curve due to the shifting of the yield surface, and this behavior is observed to be the same in aluminum and metals in general. Many plasticity theories hypothesized a combined isotropic-kinematic type of hardening for some metals, considering it too simple to use only one or the other [49].

In regards of kinematic hardening, depending on the way the center of the yield surfaces moves on the stress plane, this can be linear or non linear. The center of the yield surface in literature is usually referred as “back stress”.

All the incremental plasticity theories that will be shown in the following paragraphs define a relation between stress and strain in a material, therefore they have to respect physical constraints and be formulated such that they obey four basic rules derived from thermodynamics

concepts [46]. These rules are a continuity condition, a consistency condition, an irreversibility and stability condition, and a uniqueness condition.

The continuity condition simply postulates continuity in the stress-strain relation when the yield point is passed. This is accomplished stating that any movement of the stress in the tangential direction with respect to the yield surface is elastic.

The consistency condition relates the hardening rule and the flow rule, requiring that after yielding, no matter the form of the hardening rule, stress must satisfy the yield surface. In other words, the stress state is represented by continuous yielding events. Both kinematic and isotropic hardening in fact satisfy this condition, the stress always lays on the yield surface in its movements or expansions [50].

The irreversibility condition is a pure energy concept, defining the plastic event as irreversible in the sense that the work done in plastically deforming a material is not recoverable and it must be that:

$$\sigma_{ij} d\varepsilon_{ij}^{p} > 0 \qquad (2.11)$$

The stability concept also determines the acceptance of the hardening rule by energy concepts; one of its most important consequences is the convexity of the yield surface [51].

Uniqueness, along with stability concepts, establishes for a set of external conditions applied to the material the existence of a unique solution to the elastic problem, therefore leading to an acceptable state of stress and strain [51].

The development of hardening rule is effectively obtained by first assuring the validity of all the conditions briefly mentioned above. It will be assumed, but not demonstrated, that all the hardening rules shown work in respect to those principles.

Amstrong and Friederick (A-F) hypothesized a non linear hardening equation with a dynamic recovery term for the back stress α [45]:

$$d\alpha = a_{\alpha} d\varepsilon^{p} - c_{\alpha} dp \qquad (2.12)$$

where ε^p is plastic strain, p is plastic strain increment and a_α and c_α are material constants.

A good number of models expanded the A-F idea, decomposing the back stress α, in a linear summation of back stresses $\alpha_{(i)}$ [52] and changing the formulation of the infinitesimal increments $d\alpha_{(i)}$:

$$\alpha = \sum_{i=1}^{M} \alpha^{(i)} \qquad (2.13)$$

Chaboche in 1979 directly expanded the A-F incremental formulation introducing a $W_{(i)}$ as a function of stress state:

$$d\alpha^{(i)} = c^{(i)}\left(r^{(i)} d\varepsilon^p - W^{(i)}\alpha^{(i)} dp\right) \qquad (2.14)$$

where $c^{(i)}$ and $r^{(i)}$ are scalar functions.

Jiang and Sehitoglu in 1996 proposed radical changes to the increments of back stress $d\alpha^{(i)}$

and showed a better correlation of test data with simulations in terms of ratcheting amplitude and rate [53]. The model incorporated in the dynamic recovery term a threshold, capable of holding the back stress bounded:

$$d\alpha^{(i)} = c^{(i)} r^{(i)} \left[n - \left(\frac{\left|\alpha^{(i)}\right|}{r^{(i)}} \right)^{\chi^{(i)}+1} L^{(i)} \right] dp\,, \qquad \text{with} \qquad L^{(i)} = \frac{\left|\alpha^{(i)}\right|}{\alpha^{(i)}} \qquad (2.15)$$

where $c^{(i)}$, $r^{(i)}$ and $\alpha^{(i)}$ are positive single valued scalar functions.

They also introduced in their model a stress based memory surface controlling the Non-Masing behavior of the material and the variations of the exponents $\alpha^{(\iota)}$.

More recently Doring [54] successfully introduced the dependence of the threshold term $r^{(i)}$ from the plastic strain increment and introduced a plastic strain based memory surface controlling Non-Masing behavior of the material and the variations of the exponents $\alpha^{(i)}$:

$$d\alpha^{(i)} = c^{(i)}\left[r^{(i)}n - \left(\frac{\left\|\alpha^{(i)}\right\|}{r^{(i)}}\right)^{\chi^{(i)}}\alpha^{(i)}\right]dp + \frac{\alpha^{(i)}}{r^{(i)}}dr^{(i)} \quad \text{(a)}$$

$$dr^{(i)} = b\left(r_T^{(i)} - r^{(i)}\right)dp \quad \text{(b)}$$

$$r_T^{(i)} = r_0^{(i)}\left[1 + \frac{a_1^{(i)}}{(1+b_1p)^2} + \frac{a_2^{(i)}}{(1+b_2p)^2} + \frac{a_3^{(i)}}{(1+b_3p)^2}\right] \quad \text{(c)}$$

$$dr^{(0)} = b\left(r_T^{(0)} - r^{(0)}\right)dp \quad \text{(d)}$$

$$r_T^{(0)} = r_0^{(0)}\left[1 + \frac{a_1^{(0)}}{(1+b_1p)^2} + \frac{a_2^{(0)}}{(1+b_2p)^2} + \frac{a_3^{(0)}}{(1+b_3p)^2}\right]q_P \quad \text{(e)}$$

$$q_P = 1 + \frac{a_P}{(1+b_PR_\varepsilon)^2} \quad \text{(f)}$$

$$F = \|(\varepsilon^p - \beta)\| - R_\varepsilon \le 0 \quad \text{(g)}$$

$$d\beta = (1-\eta)H(F)\langle n : n^*\rangle n^* dp \quad \text{(h)}$$

$$dR_\varepsilon = \left[\eta H(F) - \left(1 - H(F)\right)(\xi R_\varepsilon)^\omega\right]\langle n : n^*\rangle dp \quad \text{(i)} \qquad (2.16)$$

where $r_0^{(i)}$, $a_1^{(i)}$, $a_2^{(i)}$, $a_3^{(i)}$, are positive single scalar function, b, $r_0^{(0)}$, $a_1^{(0)}$, $a_2^{(0)}$, $a_3^{(0)}$, a_P, b_P are material constants and R_ε is the center of the strain-based surface. F is the function that defines the memory surface and the $\langle \quad \rangle$ brackets are short for $\langle x \rangle = (x + |x|)/2$; the values of β, ξ and ω are material constants describing the contraction and expansion movements of the memory surface.

The Jiang and Sehitoglu model was widely discussed in literature and applied to several practical problems and situations [55], [56]; Jiang proposed other changes to the model in 2008, introducing an increment in back stress as the one proposed by Doring, introducing in a similar way the dependence of the threshold term $r_{(i)}$ from the plastic strain increment, and using a plastic strain based memory surface [57]:

$$d\alpha^{(i)} = c^{(i)}\left[r^{(i)}\boldsymbol{n} - \left(\frac{\left\|\alpha^{(i)}\right\|}{r^{(i)}}\right)^{\chi^{(i)}+1}\alpha^{(i)}\right]dp + \frac{\alpha^{(i)}}{r^{(i)}}dr^{(i)} \qquad \text{(a)}$$

$$F = (\varepsilon^p - \beta) : (\varepsilon^p - \beta) - q^2 \leq 0 \qquad \text{(b)}$$

(2.17)

$$d\beta = (1-\eta)H(F)\langle n : n^* \rangle n^* dp \qquad \text{(c)}$$

$$dq = [\eta H(F) - \xi q(1 - H(F))]\langle n : n^* \rangle dp \qquad \text{(d)}$$

The radius of the memory surface changes following the second power in this version of Jiang, differently from Doring; the values of β and η are material constants describing the contraction and expansion movements of the memory surface, and all the rest of the variable are defined as in Doring.

Valuable results have been shown by Wetzel in 1971 [58] [59] with the implementation of a plasticity model incorporating hardening or softening, relaxation or ratcheting with the use of a single constant for stress relaxation: M_r. The model decomposes the stress-strain curve in a

series of segments and to obtain cyclic relaxation modifies the slope of each segments during life, multiplying it by:

$$f(\bar{\sigma}_m) = 1 - \frac{\bar{\sigma}_m}{M_r} \qquad (2.18)$$

where $\bar{\sigma}_m$ is the mean stress of the single segment. This model is sometimes referred as kinematic hardening multi-surface model. With every segment decreasing its slope according to its mean stress, cyclic relaxation is obtained, as shown in a random loading simulation in Figure 2-6.

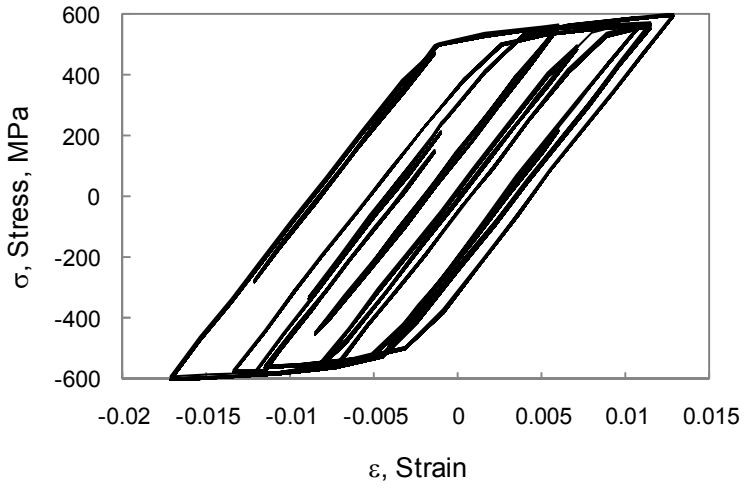

Figure 2-6. Simulation of random loading pattern with Wetzel model and constants fitted to 7075-T6511 aluminum.

Some of these models will be implemented in this study to obtain a valid reference on material behavior and computational time. A choice regarding what model to include in a life calculation software is restricted by computational problems. Current life calculation software implementing a strain-based approach to fatigue, are able to manage millions of cycles in a time of the order of hours. If mean stress relaxation were included as a result of an implementation of

a comprehensive plasticity theory, it is highly probable that the performances will go down by a unacceptable factor.

2.5 An example of use of plasticity models for mean stress relaxation

A recent study on the application of plasticity models for the description of uniaxial ratcheting and mean stress relaxation in 7050 Aluminum was published by Hu et al. working for the Australian Defense Science and Technology Organization (DSTO) [60]. The interest was the assessment of transient phenomena at notches during cyclic deformation, and the application of more complex stress-strain relationships from plasticity theories to be able to model those phenomena and apply results to life predictions for a strain-based fatigue approach.

A combined isotropic and kinematic hardening rule is used to model material behavior. The isotropic part is modeled as described by Chaboche [51]; for the kinematic hardening part, a A-F approach with single and multiple back stresses is implemented.

Numeric results show an improvement in the capability of modeling transient effects for this aluminum alloy. They also show the possibility of reproducing mean stress relaxation and ratcheting at the notch simultaneously, which is expected to happen in real conditions.

The implementation of the model with a single back stress is shown to be unsatisfactory in terms of reproducing accurate values of stress and strain at the notch, and overestimating the rate of both cyclic relaxation and ratcheting.

The use of three back stresses seems to the authors a good tradeoff between simplicity and accuracy of response.

Chapter 3
Experimental Methods

3.1 Materials characterization and use

As stated in part I, the two aluminum alloys under investigation are the 7th series alloys 7075-T6511 and 7249-T76511; however, in preliminary tests a similar alloy, 7475-T651, left over from previous work by Dowling and Knipling [24], was used to obtain expectations from the official tests.

The 7075-T6511, 7475-T651, and 7249-T76511 aluminum alloys studied are all Al-Zn-Mg-Cu-Cr alloys that are members of the 7000-series of alloys, which are the highest strength class of aluminum alloys. Their strength arises from the combined effect of multiple precipitation hardening reactions involving the various alloying elements [61]. Percentages of the alloying elements vary somewhat and are specified by the initial four digits, such as 7075. In processing, these alloys are first subjected to a solution heat treatment, followed by quenching. Then there is a second stage of heat treatment, called artificial aging, where the strengthening precipitates form at a moderately elevated temperature. The designation T6 indicates this process. Then the additional digits in T651 indicate wrought material that has been stretched by about 2% after solution treatment, to relieve residual stresses, and the additional digits in T6511 indicate the same for extruded material, with some minor straightening after stretching also being permitted in this case [61].

The 7249 aging treatment is carried beyond the point of peak strength, called overaging, as indicated by the T7 designation. The moderate degree of overaging is specified by the next digit as T76, and then the remaining digits in T76511 indicate stress relief by stretching for extruded material, as above. The overaging treatment for this special alloy may involve more than one stage of time and temperature to meet the strength and other property requirements of the specification AMS 4293 [62], with the exact details generally being proprietary to the extrusion supplier.

Fatigue characterization of both alloys is of special interest to NAVAIR since those alloys are used in key components in the structure of P3 and F18 aircrafts, and also in key components of the H-53 and H-60 helicopters. The 7075-T6511 alloy is a classical well known aluminum alloy with improved mechanical behavior for aeronautical applications, while 7249 is fairly new and is known to have improved corrosion resistance. The concern of NAVAIR is the possibility of substitution of structural components made of 7075 aluminum, with the 7249 alloy, so that those parts will be less susceptible to corrosion cracking, but show the same mechanical properties.

The mean stress relaxation behavior is of concern for both alloys. Even if aluminum alloys of the 7th series show stability in stress-strain behavior and do not generally undergo an extreme degree of relaxation, as opposed to other aluminum or titanium alloys, the problem can cause inaccuracy of fatigue life predictions. An exploratory study on possible inclusions of transient effects in life predictions in software like FAMS, calculating the life of critical components with a strain-based approach, is needed.

Some loading profiles will be taken from actual measurements on aircrafts or helicopters; in helicopters service loadings, mean stress relaxation is of great interest due to the frequent presence of highly biased loading profiles.

3.2 Tensile Properties of 7075 and 7249

As previously introduced, the lack of data points with high values of plasticity, pushed towards the solution of running a tensile test. The tensile test will be added to the list of fatigue data and the true fracture strain of the material will be used in the fitting of the stain-life curve. It is referred to true plastic fracture strain, the value of plastic strain corresponding to the true fracture strength of the material and conventionally considered the fracture at cycles to failure equals to 0.5:

$$\tilde{\varepsilon}_{pf} = \tilde{\varepsilon}_f - \frac{\tilde{\sigma}_f}{E} \qquad (3.1)$$

where $\tilde{\varepsilon}_f$ is the true fracture strain and $\tilde{\sigma}_f$ is the true fracture strength.

The tensile test will also be used in the mean stress analysis, the true fracture strength for each alloy is needed in one of the two formulations for the Morrow model.

The need of tensile material properties in strain-life and mean stress analysis, required the manufacturing of tensile specimens with geometry shown in Figure 3-1.

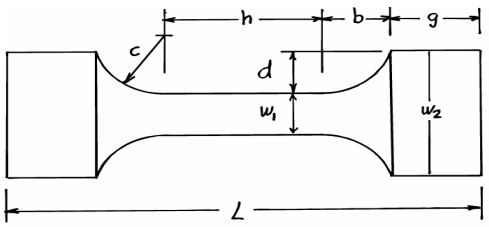

Figure 3-1. Tensile specimen geometry with c= 0.5, h=1.75, w_1=0.25, d=0.125 , b=0.331 , g=2.00 , w_2=0.5 , L= 6.42.

The specimens for tensile tests were machined at Virginia Tech from pieces of extrusions reserved for this purpose to sample the material for fatigue specimens. Manufacturing the specimens at Virginia Tech was considered convenient based on timing and expenses. A total of 6 tests were run for each material and the results are summarized in Table 3-1.

The material constants that can be obtained from a standard tensile test are: the elastic modulus, E, the yield strength, σ_0, the percent elongation after failure, $100\varepsilon_{pf}$, the percent reduction of cross sectional area, %RA, the true fracture strength and true fracture strain, $\tilde{\sigma}_{fB}$ and $\tilde{\varepsilon}_f$.

The elastic modulus is obtained by calculating the initial slope of the loading curve. Details will be described in the following section. The yield strength is obtained following the standard 0.2% offset line and details for calculation are shown in the following section. The engineering fracture stain ε_f is obtained from the final reading of the extensometer if its maximum strain capability is not exceeded. The elastic strain is then subtracted to estimate an after fracture value, ε_{pf}, expressed as a percentage, $100\varepsilon_{pf}$, to obtain the percentage elongation. The extensometer used for the tensile tests has limits of ±15%, and in some cases it is possible that the range might be exceeded. For this reason the gage length was marked with four equidistant points before each test, so that the final length could be obtained after fracture. To

avoid any interference between the test and the markings, colored markers are avoided since they could cause local corrosion cracking and initiate a preferential failure site. The true facture strength is the final point of stress recorded in the test, normalized by the reduction of area and adjusted for heap stress due to necking. The true fracture strain[1] is calculated as:

$$\tilde{\varepsilon}_f = \ln \frac{A_i}{A_f} \qquad (3.2).$$

Table 3-1. Tensile properties from tests run at Virginia Tech.

Aluminum Alloy	7075-T6511	7249-T76511
Elastic Modulus, *E*, MPa (ksi)	68,711 (9965)	68,932 (9997)
Yield Strength, σ_o, MPa (ksi)	559.4 (81.1)	567.6 (82.3)
Ultimate Strength, σ_u, MPa (ksi)	620.0 (89.9)	607.1 (88.0)
Elongation, $100\varepsilon_{pf}$, %	13.21	13.32
Reduction in Area, %	18.31	26.77
True Fracture Strength $\tilde{\sigma}_{fB}$, MPa (ksi)	711.3 (103.2)	686.8 (99.6)
True Fracture Strain, $\tilde{\varepsilon}_f$	0.2022	0.3120

3.3 Specimen Design and Laboratory Equipment

Fatigue and tensile specimens were cut from extrusions of 7075-T6511 and 7249-T76511. The long axes of the specimens are parallel to the longitudinal direction of the extrusion for the 7075 and 7249 alloys with a cross section shown in Figure 3-2. In order to avoid significant scatter of material properties, material very near the edge is not used, and only the base plate is employed for specimens, not the projections.

Another specification about the extrusions for 7075 is a bound of acceptance of ultimate and yield strength of the material. Since not all the extrusions present the same tensile characteristics, based on the Certificate of Conformance from the extrusion supplier, the ultimate

[1] Another interpretation would be to consider $\ln(A_i/A_f)$ to be the plastic strain at fracture, but this quantity was interpreted to be the total strain.

strength should be between 83 and 90 ksi and yield strength between 75-80 ksi before proceeding to cut specimens from the extrusion.

Specimens of 7249 came all from the same extrusion and therefore didn't need specifications on the extrusion properties at this stage.

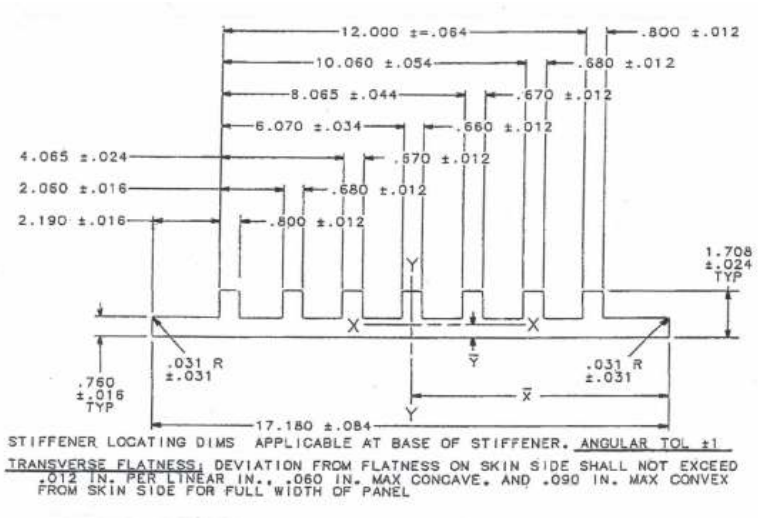

Figure 3-2. Projection of the extrusion from which all test specimens are taken; dimensions in inches.

Axial unnotched (AU) specimens are used for testing at constant amplitude loading to obtain fatigue life constants and evaluate mean stress sensitivity. The same specimens are also used for testing of mean stress relaxation under both constant and variable amplitude loading.

The specimen designs are shown in Figure 3-3 and dimensions obtained following ASTM standard guidelines [5]. The first of the two designs (a) refers to 7475-T651 aluminum alloy and the second (b) to 7075-T6511 and 7249-T76511. As it can be observed from the drawing, the diameter of the testing section in Figure 3-3 (b) is approximately 0.3 inches and the diameter of the part in the grips is around 0.6 inches; it was observed from previous experimental work that increasing the diameter of the section in the grips can be helpful to reduce the probability of grip failure and therefore the number of tests discarded [24]. Consequently, the test section increases due to geometry constraints.

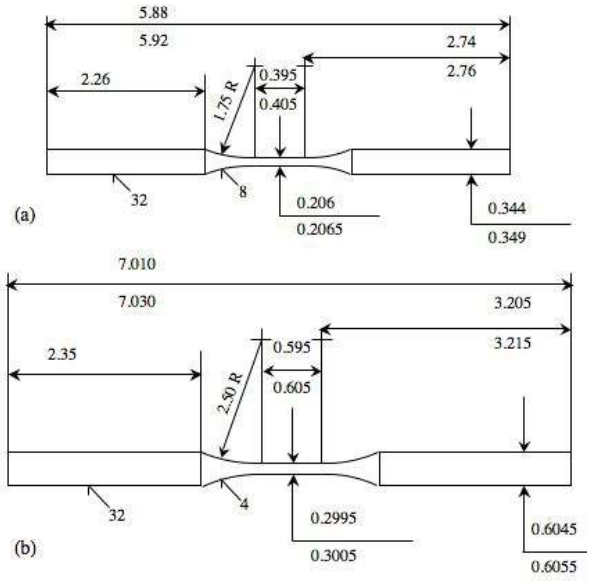

Figure 3-3. Test specimen geometries; dimensions in inches.

The longer and larger straight section of the 7075 and 7249 design is also aimed to accommodate future work on small surface crack detection with acetate replica or rubber material replica method, RepliSet [63], and possibly also with an infrared camera. Future work on small crack detection with the use of x-ray diffraction methods is also planned, these measurements will be better accommodated with a larger specimen geometry.

The surface finish required for the 7075 and 7249 specimens is particularly high, with a value of 4 μin. This was chosen for the same reasons; crack detection methods are particularly sensitive to surface finish, and the use of a shinier surface makes the overall process easier. The way such a high level of finish is obtained is through longitudinal polishing with sand paper. This eliminates the circumferential marks of the machining process which affect fatigue behavior because they are transverse to the loading direction. Diamond paste is then used to obtain the shiny finish. The polishing process highly increases the cost per specimen, but it is essential, especially in the case of crack detection research.

An MTS servo-hydraulic, closed-loop testing machine with capacity of 50 kN and maximum frequency of 20 Hz is used to run all tests. The system used is fully computer

controlled using recent upgrades of MTS TestStar interfaces and software; all the tests were programmed using Multi Purpose Testware from the MTS software package.

Alignment of the cross heads of the machine is checked following ASTM standard guidelines [5]. A cylindrical specimen of 0.5 in diameter is prepared with a set of 6 strain gauges attached to the surface with a specific configuration with respect to the center of the specimen. Three gauges are attached above the central section of the specimen. Each gauge is glued vertically with the length of the specimen and ¾ in from the center and 120° apart from the other two. The other three gauges are attached below the center section in the same configuration. The standard procedure requires the specimen to be elastically loaded three times to be rotated 120° before each loading cycle, so that any differences in the strain reading of the gauges caused by mounting the gauges imperfectly is canceled. If the averaged six readings for the three directions show less than 1% difference, then the cross heads of the machine are aligned properly. A tolerance lower than 0.001 inch over 0.5 inch of vertical movements is required to meet the standard.

A 0.5 (in) MTS extensometer with ±15% maximum capacity is used for all tests to record the strain. In strain controlled tests, the signal coming from the extensometer is the control signal used by the servo-hydraulic machine. Calibration of the extensometer is performed following guidelines given by the MTS TestStar service manual and performed with the use of an extensometer calibrator. The extensometer calibrator is essentially a high resolution micrometer, shaped in a way that the extensometer can be attached. The movements of the micrometer open or close the edges of the extensometer. The bottom edge of the extensometer moves with the bottom part of the micrometer and through a rotating indicator where a known amount of strain is applied to the extensometer. The indicator is labeled with marks indicating the vertical movement of the micrometer, with sensitivity up to 0.0001 (in). Going through different values of strain in tension or compression, the gains of the channel where the instrument is connected are adjusted in the software so that the signal coming from the extensometer indicates the value of strain manually applied.

A 50KN load cell is used in the MTS machine to measure force. Calibration of the load cell is certified by MTS and regularly checked by the laboratory technicians. The load cell signal is the control signal for all stress controlled tests.

The usual procedure before each test is the following:

a) The diameters of the specimen is measured with a micrometer caliper before each test

b) The value is recorded in the laboratory notebook along with date, information on the test and operator of the machine

c) The elastic modulus is measured once the specimen is gripped in the machine by applying a force of 5kN and recording the reading of the extensometer.

d) The value is recorded in the lab notebook. This measurement is not the way the value of the elastic modulus is calculated for each specimen, but just a routine procedure to check if the specimen and extensometer are mounted correctly or if some slipping is occurring in the grips.

e) The test is started and pre-strain is applied if needed.

Part e) of the procedure refers to the use of an initial pre-strain loading profile: following the logic of Topper and coworkers [28], [29] , initial overstrain is applied to all the specimens, except for the first tests which receive constant amplitude loading that will be described in the next section. This is done to advance the fatigue damage process and the initial transient cyclic hardening, so that the behavior is similar to that during service loading with occasional severe cycles and to partially reduce the sequence effects.

When performing the relaxation tests, the response of the servo-hydraulic testing system needed to be carefully tuned. The results of a test before tuning the system are shown in Figure 3-4. The strain amplitude and mean strain values gradually shifted and stabilized to the desired values only after 100 cycles. This problem in controlling the strain affected the mean stress response as shown. Stable control of strain during the entire test was possible by carefully optimizing the response settings of the test control system, along with using the automated peak-valley control option of the test system software. For data obtained prior to solving the above test

control problem, the entire results of some tests were discarded, and for others, some of the initial data were discarded, especially where the mean strain was not within ±1% of the stable strain value at half life. For example, only the data collected for N_f > 100 cycles were employed for the experimental results reported in Figure 3-4.

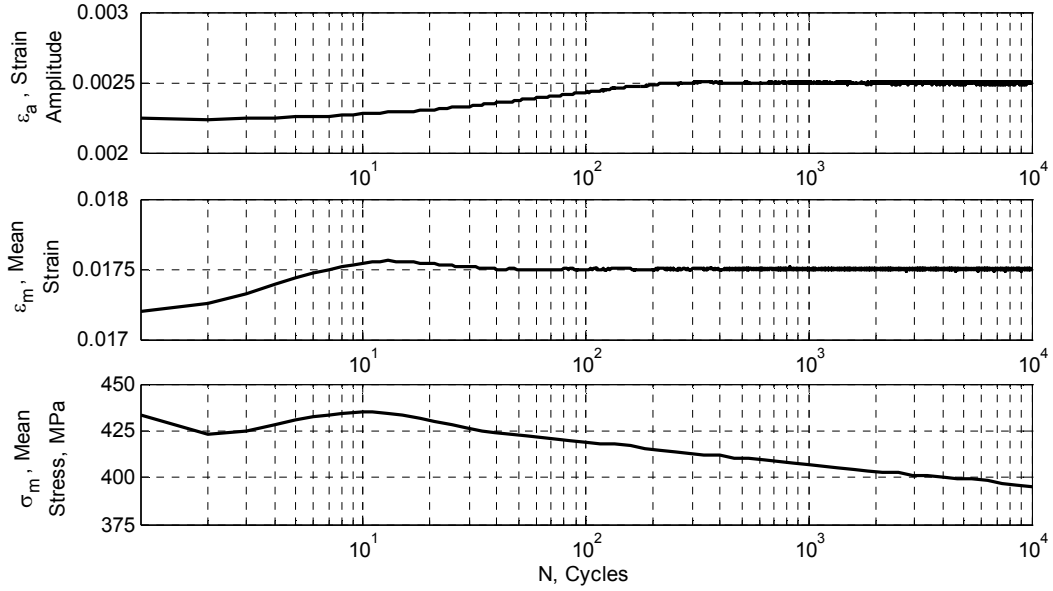

Figure 3-4. Variations in the controlled strain amplitude and mean, and the resulting mean stress, during an early test.

3.4 Test design

3.4.1 Constant Amplitude Loading Zero Mean

The first set of tests is intended to obtain preliminary fatigue life constants for 7075 and 7249 from non pre-strained specimens. This is done to observe the difference in strain-life curve between pre-strained specimens and non pre-strained specimens. The loading pattern is a sine wave with constant strain or stress limits, and the final number of cycles, N_f, is recorded. Each test is run with a sinusoidal waveform at a frequency that varies with the plastic strain amplitude involved, ranging from 0.1 Hz at very high strains to 2 Hz where the deformation was primarily

elastic. For each test, peak and valley stress-strain data are recorded for all cycles, along with data for complete stress-strain hysteresis loops at logarithmic intervals.

In the first phase of testing it is important to obtain material constants and evaluate the strain-life behavior and stress-strain behavior of both alloys to help in the design of the non zero mean tests and the mean stress relaxation tests. The test plan conceived divides the strain-life curve in segments, to obtain lives to failure approximately equally spanned in a logarithmic scale, so that both ε_{ea} vs N_f and ε_{pa} vs N_f relations could be fitted properly. With strain-life material constants for a similar 7075 alloy taken from Dowling [3], a rough approximation of the strain levels needed in the tests to have cycles to failure falling in the ranges identified was obtained. Two limits for low-cycle fatigue (the first part of the strain-life curve) and high-cycle fatigue (the last part of the strain-life curve) were set to be ±1.8% strain amplitude and 10^6 cycles. The first limit was set to prevent buckling in the specimens at high strain amplitude. When dealing with high completely reversed deformations in test specimens, it is possible for deformations of the straight section of the specimens consisting of localized bending phenomena to occur, called buckling. This happened even with careful machine alignment

.

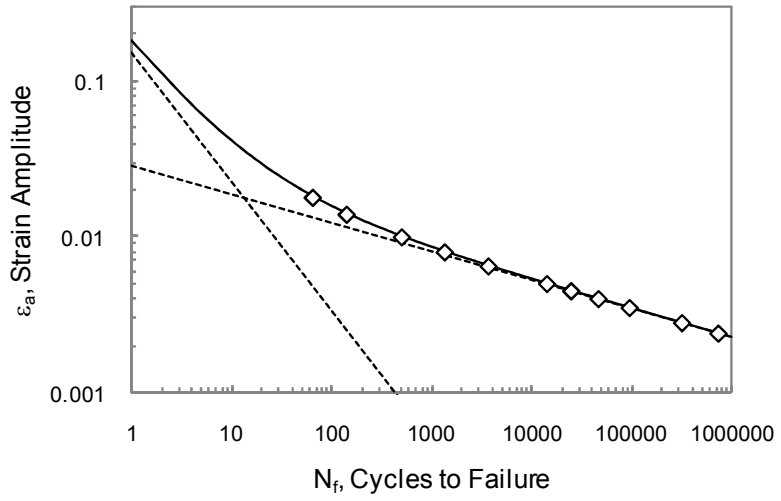

ε_a, Strain Amplitude	Strain or Stress Control
0.018	ε
0.014	ε
0.01	ε
0.008	ε
0.0065	ε
0.005	ε
0.0045	σ
0.004	σ
0.0035	σ
0.0028	σ
0.0024	σ

Figure 3-5 and Table 3-2. Graphical representation of the points in the plan for the first part of the research on 7075-T6511 and 7249-T76511.

The high cycle fatigue limit was set because it would be sufficient to get a significant value for the slope of the elastic strain-life line. The resulting plan is shown in Figure 3-5, and the calculated strain limits are shown in the Table 3-2.

It is immediately evident that the first point at 1.8% strain is probably not going to be a test short enough to characterize the plastic strain curve completely, and tests with higher strain amplitude are needed; however, buckling problems can be caused by an excessively high strain. The problem is solved with tension tests, that are used to find tensile properties of both materials and also to set a pivot point for the ε_{pa} vs N_f line at 0.5 cycles, the number of cycles to failure of a standard tension test.

3.4.2 Pre-strain effects

For most elastic strain amplitudes, a large part of the life is spent in the nucleation of a micro crack in the materials and less in the growth of the crack to the critical size; for strain amplitudes with a higher degree of plasticity involved, life is spent mostly in growing the micro crack, while nucleation happens in the very first part of the life. Pre-strain is used to evaluate the effects of strain amplitudes on life so that every test is starting from the same level of damage, introducing in all the specimens a micro crack or precursor damage nucleated by the same pre-straining cycles.

To evaluate the effect of pre-strain on the strain-life behavior of the materials for constant amplitude loading with zero mean stress, all the rest of the constant amplitude loading tests were run with pre-strain constituting the second major set of tests. The pre-strain consisted of 5 completely reversed, strain-controlled cycles at ±1.2% strain, followed by 10 additional cycles with peaks and valleys progressively decreasing to zero. To obtain a direct comparison between pre-strained behavior and non pre-strained behavior, the same constant amplitude tests with strain amplitude equal to or less than 0.65% from the previous test plan were rerun applying pre-strain. The effects of pre-strain at greater strain amplitudes are not significant as crack initiation occurs in the first part of the life, and pre-strain would not introduce any shortening in life for these tests. Table 3-3 summarizes the tests that were run to evaluate pre-strain effects.

Table 3-3. Constant amplitude zero-mean tests with pre-strain.

ε_a Strain Amplitude	Strain or Stress Control
0.0065	ε
0.005	ε
0.0045	σ
0.004	σ
0.0035	σ
0.0028	σ
0.0024	σ

Strain-life curves of some metals tested under constant amplitude completely reversed loading and non pre-strained show a so called fatigue limit, i.e. a leveling off of the curve where the strains are mostly elastic, decreasing the slope of the line representing high cycle fatigue to approximately zero. This point is considered the stress or strain level corresponding to an infinite fatigue life. The fatigue limit was found in the S-N curves mainly in steels since the beginnings of fatigue analysis and the first testing by Wohler. Fatigue limits for aluminum alloys are not seen in S-N curves generally.

The definition of fatigue limit is controversial and subject to debate. Fatigue life in the gigacycle regime is a popular research area for structural metals and, as the name suggests, it studies material behavior for lives to failure greater than 10^9. For the current scope of the research, 10^6 cycles is chosen as a maximum limit. The main reason is that to run experiment in the gigacycle regime, specific equipment is necessary, able to run tests at a frequency in the order of kHz. The MTS machine used in the current research has a maximum frequency limit of 20 Hz and a test running up to 10^9 cycles would take almost 2 years of testing. In addition the high scatter of test data in the gigacycle regime would require a high number of samples and a large amount of repetitive testing work. Note that in strain-life fatigue analysis and in software implementing it, a strain threshold is frequently used, below which no damage is taken into account. This is an approximation and it causes errors in predictions, but it is nevertheless used in commercial software.

During service loadings and when materials are tested in variable amplitude loading, the strain-life curve obtainable does not show this fatigue limit. This is mainly a problem when analyzing steels, while for the aluminum alloys of this study, there is not a large effect, as shown in Figure 3-6. Pre-strain affects the nucleation and growth of surface cracks in the materials, as introduced before. Pre-strain reproduces service life effects in materials, when sequence effects play an important role. Since the final objective is to run fatigue life analysis on variable amplitude loading, it is convenient to use pre-strain tests and obtain material constants in agreement with this type of loading [29].

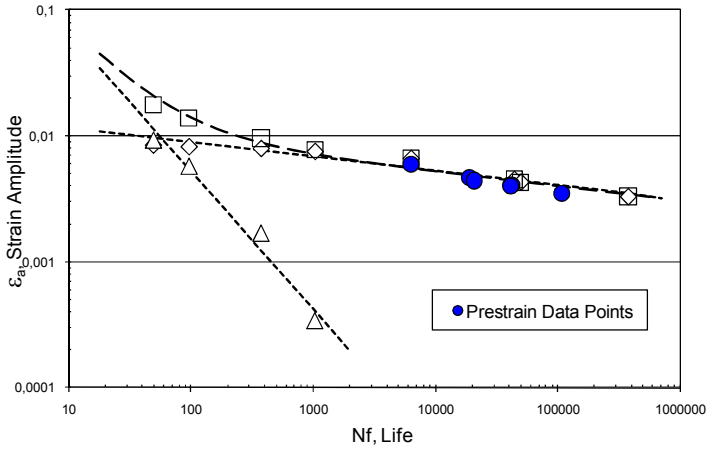

Figure 3-6. Pre-strain effects on strain-life curve of 7075-T6511.

3.4.3 Constant Amplitude Loading Non-Zero Mean

A third group of constant amplitude loading tests was planned. Most of the tests were controlled in strain. Differently from the first and second sets of tests, the loadings are not completely reversed, but biased with respect to zero. The intent is to characterize the mean stress sensitivity of both aluminum alloys and the mean stress relaxation behavior.

The mean strain, in the case of strain controlled tests, is fixed at either a positive or negative value. This biased state of deformation causes the mean stress to relax cyclically from a positive or negative initial value to a stable value. The relaxation curves were used to model

material behavior. Mean stress relaxation takes on average less than half of the life of a constant amplitude loading test. The stable value of mean stress at half life of the test can be considered the final stable value, and they will be used to perform mean stress sensitivity analysis.

Stress controlled tests are also run, mainly because of the need to have more data points for the mean stress sensitivity analysis. It is evident that stress controlled tests will not show relaxation behavior, but, if the loading conditions involve enough plastic deformation, ratcheting behavior will be observed. Ratcheting will not be analyzed in detail in this study, but some results will be shown as a general reference.

The preliminary work on 7475-T651 aluminum focused mainly on the relaxation behavior at high strains ($\varepsilon_a > 0.6\%$), therefore the strain limits for the tests on the 7075-T6511 and 7249-T76511 alloys were chosen to cover a wider range of strain amplitudes, 0.2% to 1%, to obtain mean stresses with values over a wide range, 50 to 450 MPa.

Similarly to what was done for constant amplitude loading, the strain-life curve was divided in equal segments, and fatigue lives of the tests were targeted to fall in the chosen life ranges. The strain-life fittings performed with the first two sets of data were used to obtain material constants for both alloys and plan this third phase of the research. Life calculations were done so the strain amplitudes corresponding to the targeted lives could be found, but this time mean stress effects had to be taken into account and the SWT method was used to estimate the change in fatigue life. A trial and error method was used in a Matlab software created ad hoc to get the desired cycles to failure, changing the strain limits and the mean stress.

Table 3-4 summarizes the mean stress relaxation tests run for alloy 7075-T6511; approximately the same tests were run for alloy 7475-T76511. Additional non zero mean tests were run for mean stress effects under stress control, as previously mentioned, depending on the level of mean stress of interest, and they are not included in Table 3-4.

Table 3-4. Non zero mean strain controlled test plan for both aluminum alloys.

Test Number	Specimen Number	Strain Amplitude ε_a	Mean Strain ε_m	Mean Stress σ_m, MPa	Cycles to Failure N_f
1	75LB-6	0.0095	0.0085	-15.12	439
2	75NLB-1	0.0090	0.009	-11.78	479
3	75LT-5	0.0085	0.0095	-5.18	655
4	75NLB-2	0.0072	0.0108	35.18	2010
5	75RB-5	0.00675	0.01125	70.38	2316
6	75NRB-1	0.0063	0.0117	164.9	2691
7	75LC-3	0.0050	0.013	225.65	4605
8	75LC-2	0.0045	0.0015	83.33	12793
9	75LB-5	0.004	0.014	279.35	9026
10	75LB	0.0030	0.001	60.16	59396
11	75RT-5	0.0025	0.0175	392.80	29054
12	75NLB-3	0.0020	0.015	403.10	37301
13	75RT-6	0.0020	0.006	352.55	36676

3.4.4 Variable Amplitude Loading

The last phase of testing involves the observation of mean stress relaxation in variable amplitude loading conditions. The tests are all controlled in strain and forces are recorded. The rationale behind the choice of variable amplitude loading profiles is the observation of relaxation with increasing level of complexity of the strain history.

The first phases of this research involved the observation of mean stress relaxation when only one strain amplitude is involved. This next part of the experimental work is aimed to observe mean stress relaxation when two, three or more strain amplitudes are alternated during a loading history. The goal is to obtain information on the relaxation of mean stresses, while stepping up to a variable amplitude loading with complexity comparable to service loadings.

With increasing level of irregularity, the behavior of relaxing loops is monitored so that general observations in the simplest cases can be verified or refuted in the more complex cases. From the point of view of a successful modeling, the less irregular histories are used in a screening process of the models under investigation. Only the most successful models in the less

irregular cases will be carried on in the analysis and tested for the more complex cases. The performance is in this way evaluated for each model step by step.

An overview of the loading patterns chosen, and the way those were grouped is presented here. The variable amplitude loadings used are divided into four categories:

1. Two-level Test: an alternation of two different strain amplitudes with different mean strain. The small strain amplitudes are repeated 10 times before the larger strain amplitude is repeated. For each test the mean or amplitude of the small cycle is changed (Figure 3-7 (a)).
2. Three-level Test: an alternation of three different strain amplitudes, with different mean strain The 2 smaller cycles are repeated 10 times each alternatively before the larger strain amplitude is repeated. For each test the mean or amplitude of the small cycles is changed (Figure 3-7 (b)).
3. Two-block Test: an alternation of two or more different strain amplitudes with different mean strain. The loading is constituted by a larger hysteresis loop containing 10 repetitions of each of the 2 smaller hysteresis loops. For each test the mean or amplitude is changed (Figure 3-7 (c)).
4. Random and/or service like type of loading: highly irregular histories with random variations of strain amplitudes, or typical variations of strain amplitudes, following loading patterns provided by NAVAIR (Figure 3-7 (d)).

All variable amplitude loading tests are run in strain control; Figure 3-7 visually summarizes the different types of loading. In later referring to these types of histories, they will be called Type A, Type B, Type C, and Type D, as labeled in Figure 3-7.

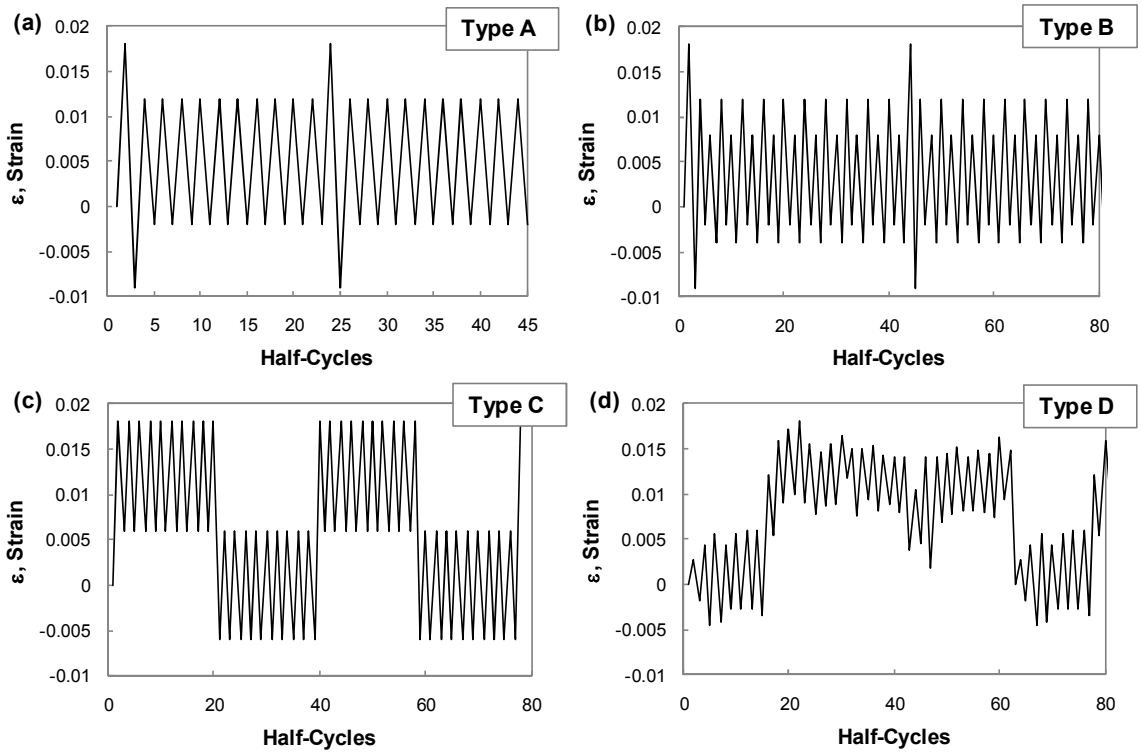

Figure 3-7. Strain controlled loading profiles for tests on Variable Amplitude loading, Types A, B, C, and D.

Most of the loading patterns chosen are frequently used in fatigue life analysis in several studies about life predictions for variable amplitude loading [10], [14].

Chapter 4
Stress-strain, stress-life and strain-life fitting

The experimental data obtained in testing axial un-notched specimens of 7075-T6511 and 7249-T76511 aluminum alloys are presented and analyzed in this chapter. A table with all the tests run on both aluminum alloys is reported in Appendix A. A more detailed overview of test results in all the phases of the project is shown in Appendix B. The strain-life analysis of the test data obtained is also presented in this section, with separate subheadings treating the cyclic stress-strain, stress-life, and strain-life curves.

4.1 Representative Test Results

Two of the most typical responses obtained during fatigue tests on the aluminum alloys under investigation are shown in this section.

The first test is a low cycle fatigue test with 1.8% strain amplitude and cycles at a zero mean strain level. The strain control and the stress response of 7075-T6511 is reported in Figure 4-1. A low degree of cyclic hardening is observable in the first few cycles for this aluminum alloy, given by the slow increase in stress amplitude observable from the stress response. A small amount of cyclic hardening is also noticeable in the stress-strain plot of this test in Figure 4-2. The hysteresis loop has progressively lower width and higher height.

Another observation can be done looking at the stress response of the material: while the strain response is not biased with respect to zero being purely completely reversed, the material tends to stabilize the mean of its stress response to a small compressive value. This will be taken into account in successive analysis. This test failed at 49 cycles.

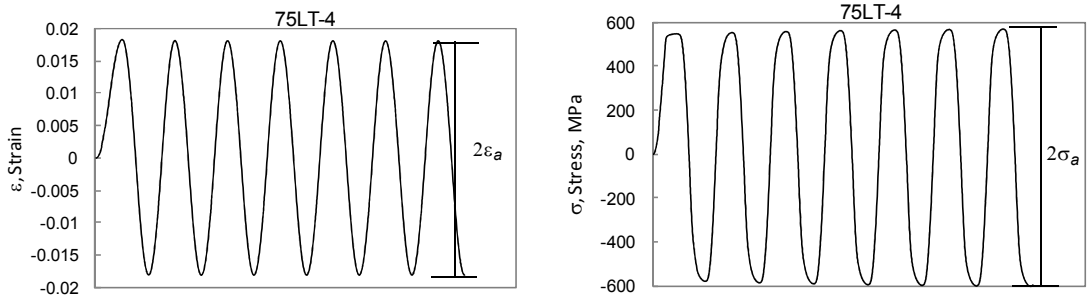

Figure 4-1. Stain control and stress response for test 75LT-4, the strain amplitude is 1.8% and the test is completely reversed.

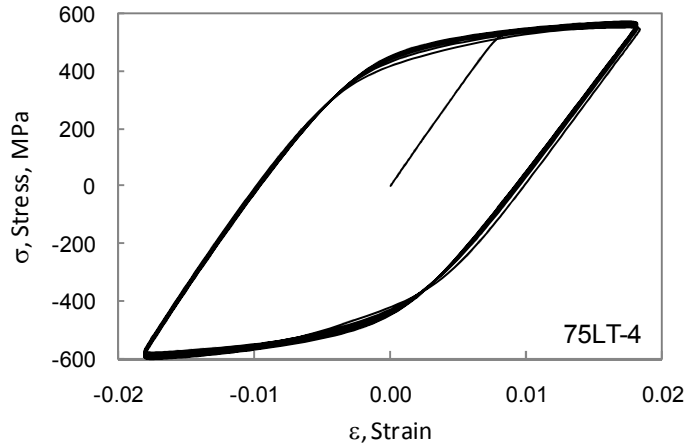

Figure 4-2. Stress-strain response from low cycle fatigue strain controlled test on 7075-T6511 aluminum.

The second test is a completely reversed high cycle fatigue test, non pre-strained, with a strain amplitude of 0.2%. The strain control and stress response are shown in Figure 4-3 and the stress-strain response is shown in Figure 4-4. The hysteresis loop formed by the cyclic deformation of the material is mostly elastic and since it is a non pre-strained test, the specimen never reached yielding. The behavior is mainly stable, with minor fluctuations in the stress response, probably due to the strain control. This is in fact one of the limiting cases of strain controlled tests in the high cycle fatigue regime. The stable mean stress obtained in this case is zero. From Figures 4-2 and 4-4 it is apparent that the stable stress-strain behavior varies markedly with the degree of plastic strain. This test (75RT-3) failed at around 50000 cycles.

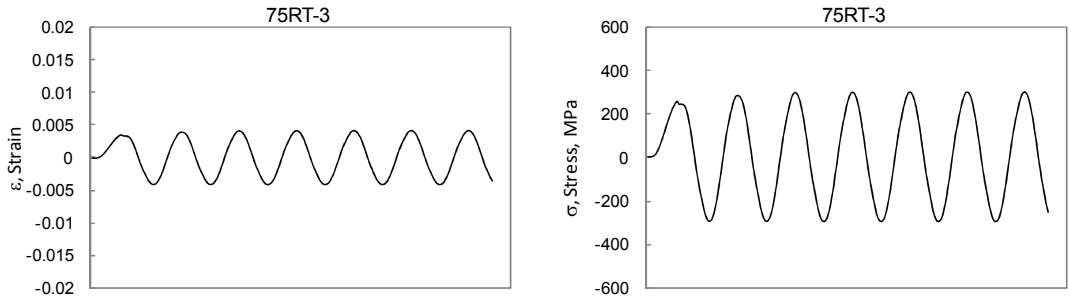

Figure 4-3. Stain control and stress response for test 75RT-3, the strain amplitude is 0.2% and the test is completely reversed.

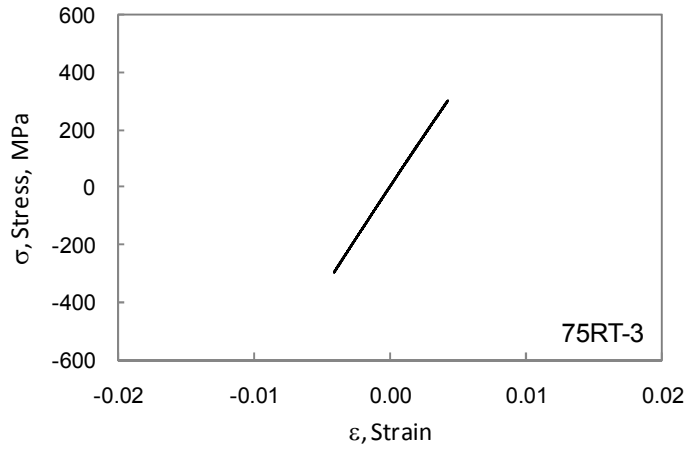

Figure 4-4. Stress-strain response from high cycle fatigue strain controlled test on 7075-T6511 aluminum.

The alloy 7249-T76511 has similar stress-strain response in constant amplitude loading, with a lower degree of cyclic hardening. The only difference is the presence of a transient effect in the first five cycles of its cyclic behavior, when significant plastic strain deformation is involved. The stress-strain response to the same strain controlled test shown in Figure 4-1 for 7075 is shown in Figure 4-5 for 7249.

Once the cyclic yield point is reached in the first cycles, the hysteresis loop for 7249 shows an irregular path with respect to the stable loops. This deflection was observed for 7249 only and its effects did not show to be noticeable after the first five cycles. It is therefore not considered a source of error for the future analysis. In fact, the physical mechanisms of deformation in

aluminum alloys and some other metals are known to cause hysteresis loops with a reverse curvature effect similar to that observed [64], [65].

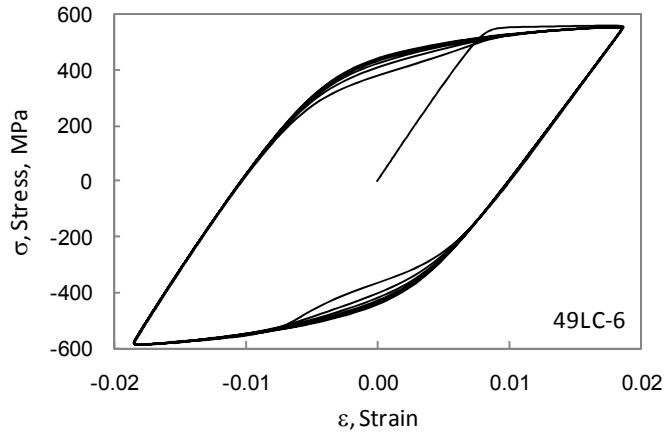

Figure 4-5. Stress-strain response from low cycle fatigue strain controlled test on 7075-T6511 aluminum.

4.2 Cyclic stress-strain curve fit

As introduced in Chapter 3, for each tests the system records the peaks and valleys of force and strain, and the cyclic material response following a logarithmic rule based on the number of cycles. If pre-strain is applied, the pre-strain sequence is recorded in a separate file. From the peaks and valleys response, the values of ε_a and σ_a at half life can be obtained, as shown in Figure 4-1. No exception is done for mean stress relaxation tests, since half life is considered the point where stable behavior is manifested in the material. From cyclic response, the closest cycle to the half life of the test is used as the representative stable loop for the particular test and ε_{pa} is calculated from this stable loop. The pre-strain file is used to obtain the value of elastic modulus and yield strength for the test.

As shown in the research plan in Chapter 3 some of the constant amplitude completely reversed tests are run with no initial pre-strain. For tests with no pre-strain, if the test level is higher than the ±1.2% pre-strain level, then the data are included with the pre-strain data for stress-strain, stress-life and strain-life curves. For tests with no pre-strain where the test level is below ±1.2%, the data are included with the pre-strain data for fitting the cyclic stress-strain

curve, but not for any fits involving the fatigue life, as the life is expected to be affected by the absence of pre-strain.

It can be noticed in Appendix A that some of the tests were only partially successful due to failure occurring at an extensometer knife edge or in the collet grips. In some cases the test was suspended at a long life when failure was not occurring after 10^7 cycles, 10 times more the limit prefigured in the research plan. These results were included in fitting the cyclic stress-strain curve, but not in any fits involving the fatigue life.

Unfortunately, instabilities of the testing control in the machine invalidated some of the tests. This control difficulty has been observed in few specific cases, with certain values of force and testing frequency. The reason of this control failure has never been clarified, but careful examination of all the tests previously run confirmed that it was an isolated case. Except for the initial E and σ_o values, the data were discarded.

4.2.1 Elastic modulus, yield strength and Plastic Strain calculation from data

The plastic strain range for each test was calculated using an ad hoc Matlab code. The code receives the stress-strain data from the hysteresis loop taken near half the life of the specimen tested. The code calculates the plastic strain range as the difference between the two values of strain corresponding to stress equal to zero, as shown by an example in Figure 4-6. A linear interpolation is performed by the code to calculate the two points of intersection between the hysteresis loop and the strain axis.

For some of the larger hysteresis loops the code is really efficient and fast. For some of the smaller loops the accuracy in determing ε_{pa} highly depends on the number of data points stored for the loop. The sampling frequency of the data has to be changed with the frequency of the test. At least 100 data points per hysteresis loops to have a good representation were usually collected.

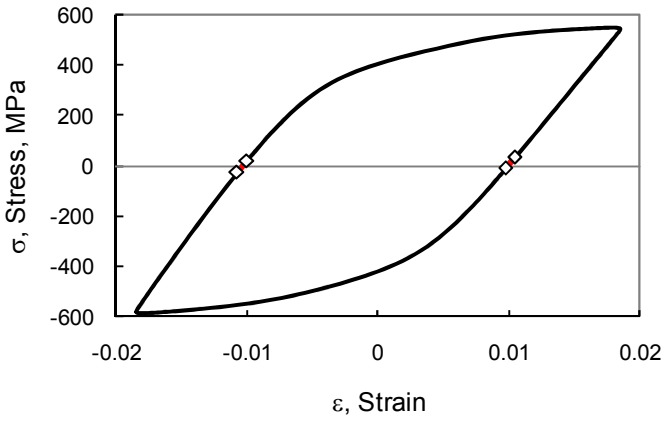

Figure 4-6. Hysteresis loop of low cycle fatigue test on 7075-T6511; data points for calculation of plastic strain amplitude are shown.

To calculate the elastic modulus and the yield strength on the initial loading of the specimen, a second Matlab code was written. The code takes the data for the first loading cycle, in the case no pre-strain is performed, or from the pre-strain file, and the elastic modulus is calculated from values of strain between 0.01% and 0.5%. When the maximum value of strain is less than 0.5%, which occurred for some tests in high-cycle fatigue, the code takes the highest value reached as the ending point. The yield strength is calculated with the 0.2% offset strain criterion as shown by an example in Figure 4-7. A linear interpolation is performed to calculate the point of intersection.

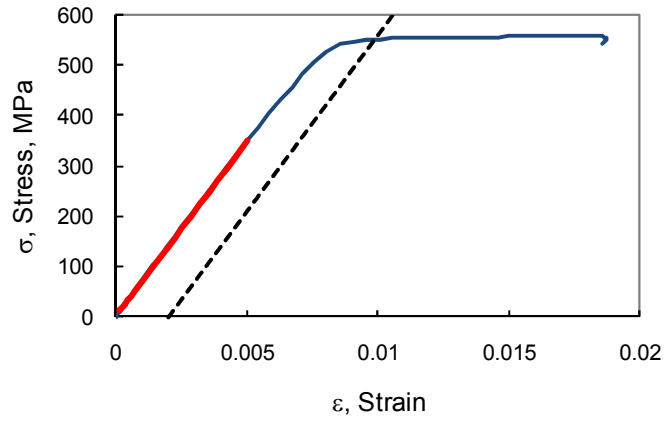

Figure 4-7. Initial loading in a low cycle fatigue test on 7075-T6511; the initial part of the curve used to calculate the elastic modulus is shown, along with the 0.2% offset line to calculate yield stress.

4.2.2 Cyclic Stress-Strain Curve Fits

When performing a cyclic stress-strain fit, there is no need to differentiate between completely reversed loops and biased loops: whatever the mean strain is, the relationship between stress and strain amplitudes is assumed to be the same, which agrees with experimental observations. Cyclic stress-strain curves are then fitted to the test data at all mean stresses for the two alloys, as shown in Figure 4-8. Ramberg-Osgood equation, Eq. 1.1, was found to represent the data very well, and the resulting constants are given in Table 4-1. In tests where a small amount of plastic strain is involved, the signal to noise ratio of the cyclic data is not high enough to obtain accurate values of plastic strain amplitude. The values calculated present a high scatter when plotted versus stress amplitude beyond a certain plastic strain amplitude limit. Therefore data with $\varepsilon_{pa} < 0.00025$ are not employed in the Eq. 1.1 fit. The stress-plastic strain fits are shown along with the stress versus plastic strain data in Figure 4-9.

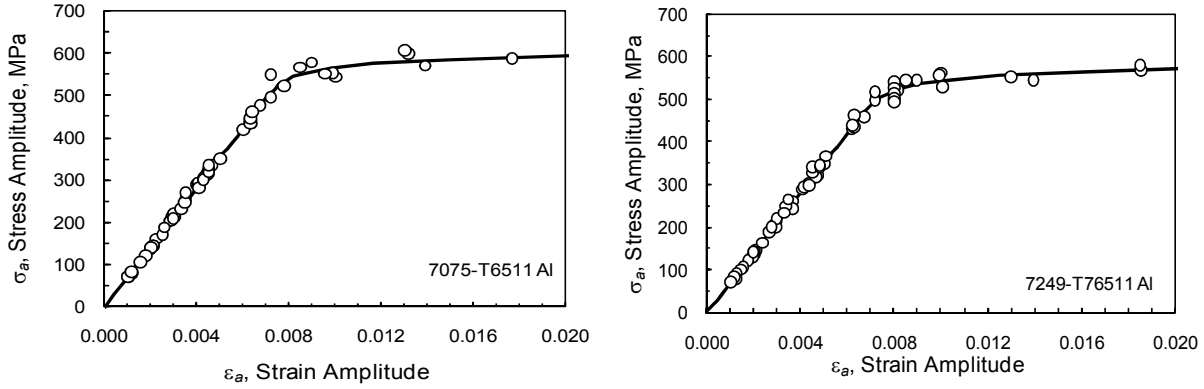

Figure 4-8. Cyclic stress-strain curves for the two alloys.

The 0.2% offset cyclic yield strengths average for all the tests are included in Table 4-1. These differ by only a small amount from the corresponding 0.2% offset yield strengths from tensile tests in Table 3-1. This indicates that these alloys have nearly stable behavior under cyclic loading, that is, they exhibit very little cycle-dependent hardening or softening.

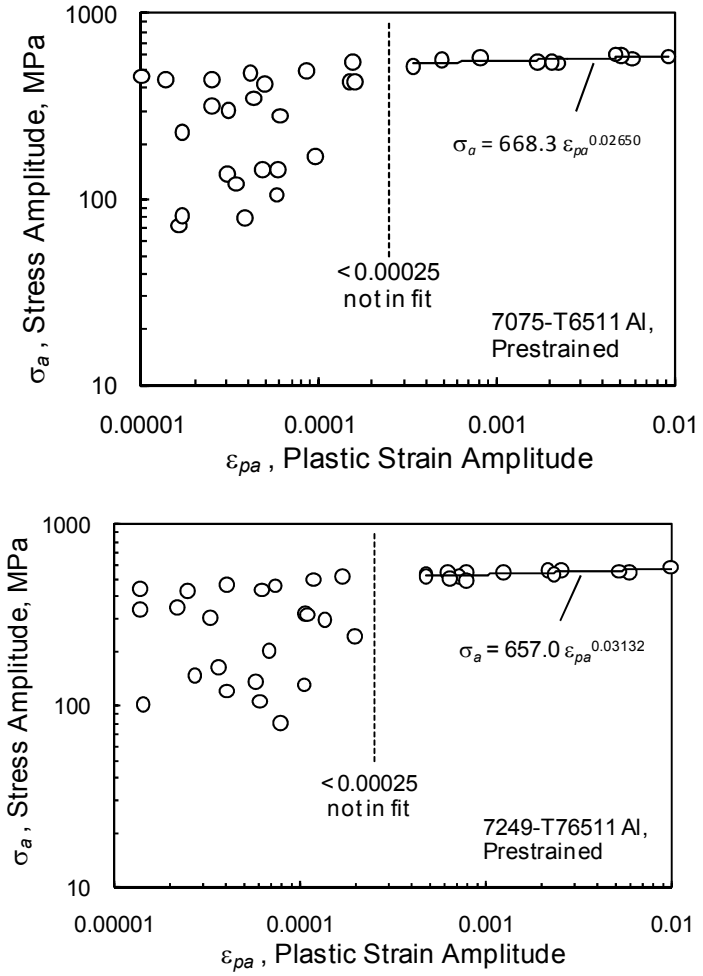

Figure 4-9. Stress amplitude versus plastic strain amplitude data and the fitting of Eq.1.1.

4.3 Stress-Life Curve Fit

The effects of mean stresses on fatigue are observable from the values of life to failure in the table summarizing all the tests performed (Appendix A). With high values of mean stress, life is severely reduced and a test with the same strain amplitude that could last more than 10^6 cycles has a life reduced by a factor of approximately 10 when the mean stress is more than 333 MPa.

The scatter of all the mean stress data on a strain-life curve obtained from fitting zero-mean tests only is shown in Figure 4-10.

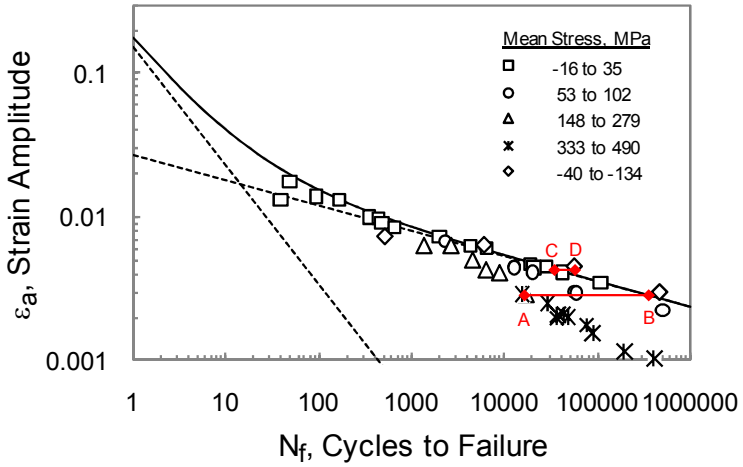

Figure 4-10. Strain-life curve fitted with 0-mean data only and scattered mean stress data points.

Two segments are shown in Figure 4-10, AB and CD, representing the distance (in log scale) between the theoretical life that would be predicted using a zero-mean curve and the experimental life of the test. When the mean stress is highly tensile, there is a great difference between the two. Life can change up to a factor of 10. In the same way life is altered when mean stresses are compressive, as observable from segment CD. In the case shown life is lengthened by a factor of 5 for a test with mean stress around -50 MPa.

A strain-life curve obtained with zero-mean tests only is clearly not giving satisfactory life predictions when mean stresses are involved in the loading. This is the reason why mean stress models are employed in the strain-based approach to fatigue. To obtain a successful representation of the strain-life behavior for both alloys, the fitting of the stress-life data has to be performed first.

Equivalent zero-mean stress amplitudes σ_{ar} for all tests are obtained with the use of a mean stress model, so that test data with different levels of mean stress can be fitted together to Eq. 2.1. The mean stress model chosen is the Walker model since it showed to be the most accurate for mean stress analysis [37], [38].

A first tentative fitting of all the test data was performed using the Walker model, as shown in Figure 4-11. Mean stress data are fitted using a multiple linear relation so that the value of γ is obtained for the model. The value of γ obtained is then used to get equivalent zero-mean stress

amplitudes σ_{ar}. The σ_{ar} values are then fitted to 2.1 so that $\sigma_f^{'}$ and b can be obtained.

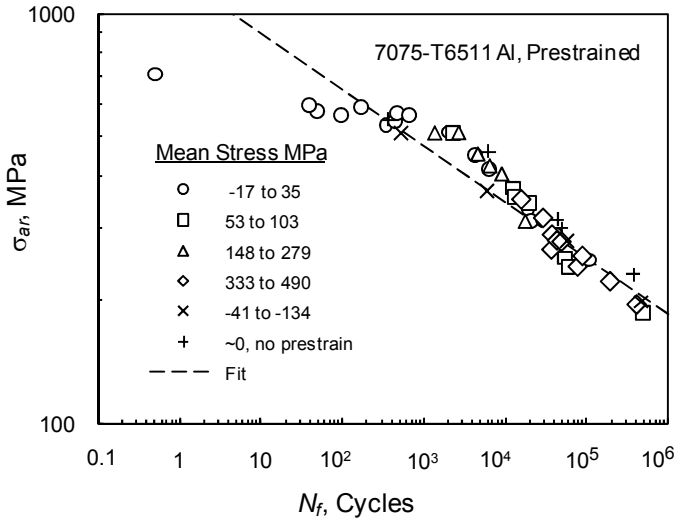

Figure 4-11. Unsuccessful attempt to fit the Walker equation to the non-zero mean stress data points obtained experimentally.

A trend is observed in the σ_{ar} versus N_f plot above: the fitted line represents better the high cycle fatigue region than the low cycle fatigue region. This is not surprising because values of stable mean stress in the low cycle fatigue regime are all small compared to the ones in the high cycle fatigue regime. It was then decided to fit two lines, one representing high cycle fatigue and the other low cycle fatigue.

The fitted lines are shown in Figure 4-12 for both aluminum alloys. A distinct trend appears in the fitting, differentiating shorter lives to intermediate and longer lives. The fitted line has a shallow slope at short lives and a steeper slope at intermediate and long lives. A number of cycles N_2 = 2000 was chosen by judgment as the separation between the two regions, with this value applying to both alloys.

For each alloy, the fit employing Eq. 4.1 is applied only to the data with $N_f > N_2$, which included all data with mean stresses that differed significantly from zero. The resulting equation is represented by

$$\sigma_{ar} = \sigma_{fw}^{'}(2N_f)^{b_w} \qquad (N_f \geq N_i) \qquad (4.1)$$

The subscript *w* is added to the fitting constants to indicate the fitting of data at various mean stresses using the Walker equation. The value of γ has to be obtained in the fitting procedure, with the fitting technique previously described. In some of the completely reversed tests, with strain amplitude larger than 1%, the mean stress is biased in compression. This value is in the order of 10 MPa.

The resulting material constants $\sigma_{fw}^{'}$, b_w, and the Walker constant γ, are reported in Table 4-1 for both alloys. Note that Eq. 4.1 can be used with Eq. 1.13 to estimate fatigue lives for cases of nonzero mean stress.

Table 4-1. Cyclic Stress-Strain and Strain-Life Constants

Aluminum Alloy	7075-T6511	7249-T76511
E, MPa	70,457	69,889
H', MPa	668.3	657.0
n'	0.02650	0.03132
σ'_o (cyclic yield strength)	566.8	540.8
σ'_{fw}, MPa (Walker fit)	2306	3002
b_w (Walker fit)	–0.1843	–0.2128
γ (Walker fit)	0.4836	0.5025
σ'_{f2}, MPa (short life)	720.0	680.1
b_2 (short life)	–0.04016	–0.03482
N_i, cycles (intersection)	1607.5	2099.2
ε_{ai} (intersection)	0.007724	0.007646
ε'_{fw}, MPa	0.2677	0.3302
c_w	–0.8276	–0.8149
σ'_f, MPa (zero mean only)	2184	2624
b (zero mean only)	–0.1777	–0.1965

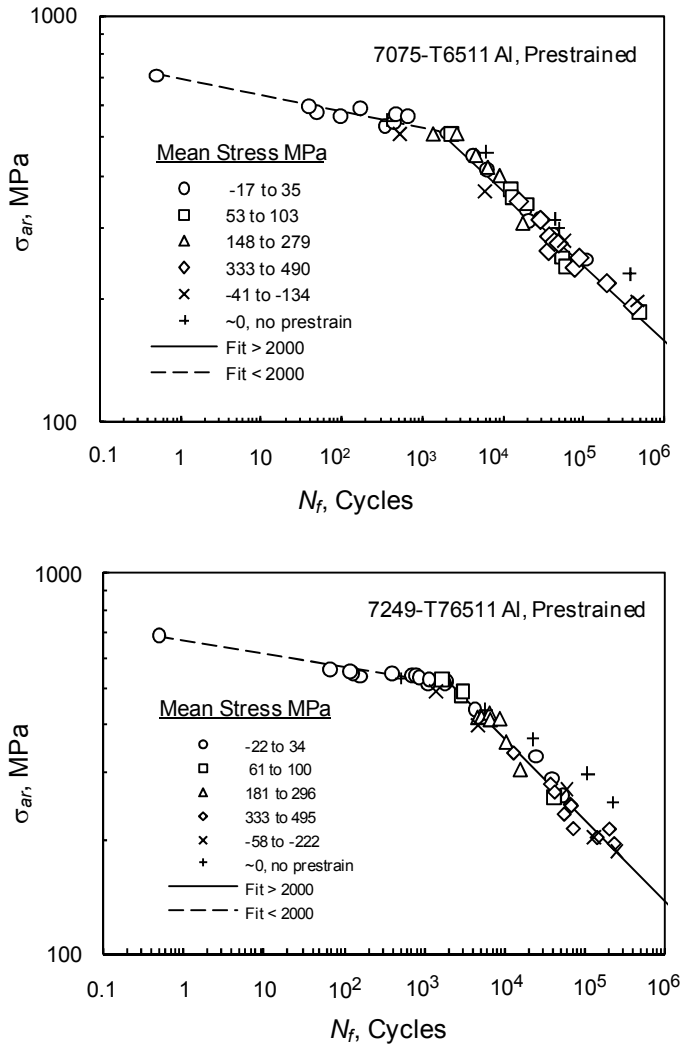

Figure 4-12. Stress-life data and fits for the two alloys. The fitted lines are based on the Walker mean stress equation at intermediate and long lives, and a separate fit is employed at short lives.

The data for $N_f < N_2$, where N_2 is the point corresponding to 2000 cycles, were then fitted separately, with the fitting constants being identified by adding a subscript 2.

$$\sigma_{ar} = \sigma_{f2}^{'}\left(2N_f\right)^{b_2} \qquad \left(N_f \le N_i\right) \qquad (4.2)$$

The use of a double linear fitting for the stress-life curve includes the need of finding the

actual intersection between the two fitted lines, N_i:

$$\log(2N_i) = \frac{\log\left(\sigma_{fw}^{'}/\sigma_{f2}^{'}\right)}{b_2 - b_w}, \quad N_i = \frac{1}{2}10^{\log(2N_i)} \qquad (4.3)$$

The equation comes from the intersection of the two fitted lines, i.e. equating the stress values of Eqs. 4.1 and 4.2 and solving for $N_f = N_i$. Values of N_i and the fitting constants for Eqs. 4.1 and 4.2 are also given in Table 4-1.

Data points corresponding to tests run with no initial pre-strain are also shown in Figure 4-12. These are not included in the fitting and at relatively long lives are seen to lie a little above the trend of the other data, indicating lives that are modestly longer than for pre-strained samples.

4.4 Strain-Life Curve Fit

The stress-life analysis gives the possibility of including the effects of mean stresses in the strain-life curve. The form of the strain-life curve is then represented by Eq. 1.7. With the use of $N^* = N_w^*$, the strain-life curve is generalized to include nonzero mean stresses according to the Walker equation.

The first term of Eq. 1.7 is seen to be equivalent to Eq. 4.1 or 4.2 used with Eq. 1.13 or 1.14, where the appropriate constants are employed, depending on whether the strain amplitude is greater or less than a value ε_{ai} that corresponds to N_i. As previously mentioned in the high strain, short life region, $\varepsilon_a \geq \varepsilon_{ai}$, mean stresses relax close to zero, and so it is not useful or even feasible to try to determine a specific γ value for this region. Hence, the same γ value as determined from the Walker fit at intermediate and short lives is used. The stress-life relationship for the strain-life curve is then taken to be the one obtained with the Walker analysis previously shown. The term of Eq. 1.7 relating plastic strain and life needs to be fitted. The Walker-equivalent life to failure, called N_w^*, is substituted to N_f accordingly to the Walker model:

$$\varepsilon_{pa} = \varepsilon_{fw}^{'}(2N_w^*)^{c_w} \quad , \quad N_w^* = N_f\left(\frac{1-R}{2}\right)^{(1-\gamma)/b} \tag{4.4}$$

Where the expression for N_w^* is obtained by substituting Eq. 1.14 into the second part of Eq. 1.7, noting that $2\sigma_a = \sigma_{max}(1\text{-}R)$

The calculated zero-mean-stress-equivalent life values N_w^* are fitted with plastic strain amplitudes. The value of b chosen depends on the value of life of the test: $b = b_w$ or b_2 depending on whether the N_f value for the particular test corresponding to ε_{pa} is longer or shorter, respectively, than N_i.

In a few cases if N_f is only modestly shorter than N_i, using b_2 might cause N_w^* to exceed N_i. It is then recommended that N_w^* be recalculated using b_w. Note that the constants from these fits again have subscripts *w* added, to distinguish them from constants obtained when the strain-life curve is characterized just with zero-mean tests.

For fitting the plastic strain-life relation, the same problem is observed as the stress-strain fitting: the plastic strain amplitudes becomes too small if calculated from thin, mostly elastic loops, and the high scatter of data points interferes with a correct fitting. Some of the test data with small values of plastic strain amplitudes are not included. The plastic strain amplitude threshold is chosen to be $\varepsilon_{pa} < 0.00025$.

Also, preliminary fitting gave a very high value of the intercept constant $\varepsilon_{fw}^{'}$ and did not seem to represent the shortest life data points very well. Hence the need of the inclusion of the tensile test in the strain-life fitting. It was decided to include in the fit the true plastic strain corresponding to the fracture point in a tension test, taking this to correspond to a fatigue test with failure at $N_f = 0.5$ cycles.

This procedure did indeed produce a more reasonable result, with Figure 4-13 showing the difference between data and two fitted lines, one calculated without the introduction of the tensile tests in the fitting and one calculated with the tensile test. This trend arises when fitting plastic strain amplitude and life to failure, where the inclusion of the tensile tests significantly improves the fitting results, as shown in Figure 4-14.

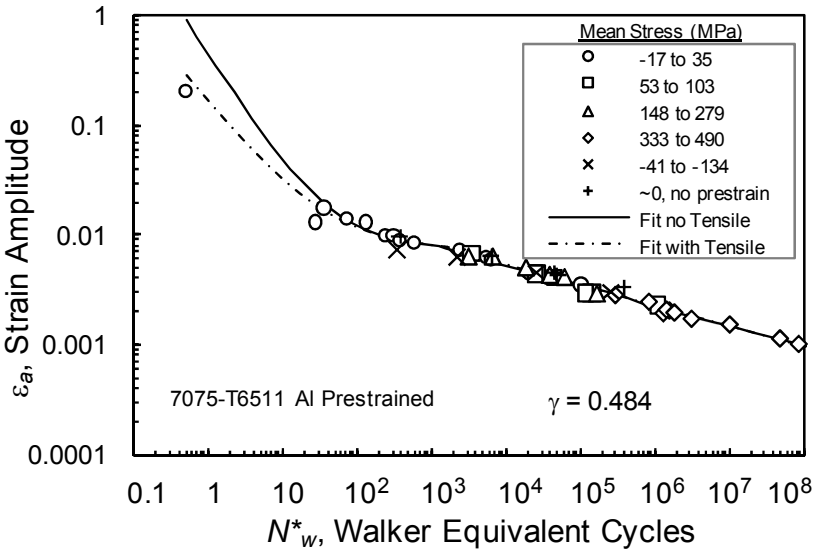

Figure 4-13. Fitted strain-life curve for 7075-T6511 with data point from tensile test and without data point from tensile test.

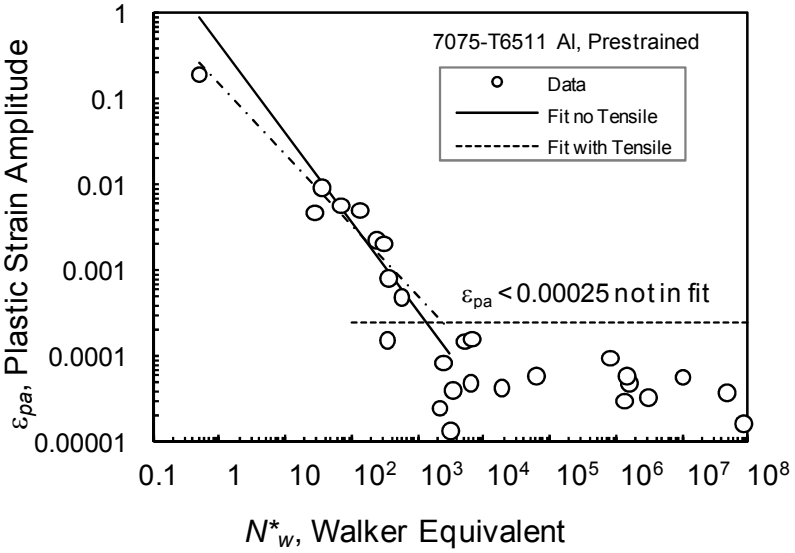

Figure 4-14. Fitted plastic strain-life curve for 7075-T6511 with data point from tensile test and without data point from tensile test.

The resulting fitting constants introducing the tensile test for both materials are listed in Table 4-1.

For consistency, since the true fracture strain from the tensile test was included in the strain life fitting, the true fracture strength $\tilde{\sigma}_{fB}$ was included in the Eq. 4.2 fit as a fatigue test with failure at N_f = 0.5 cycles. These points can be seen in Figure 4-12 and Figure 4-15.

A modified version of the strain-life curve is used in this study to fit all the experimental data. This form is the result of the assembling of the stress-life and plastic strain-life fitting just described. The complete version of this new formulation can be written as:

$$\varepsilon_a = \frac{\sigma_{fw}^{'}}{E}(2N_w^*)^{b_w} + \varepsilon_{fw}^{'}(2N_w^*)^{c_w} \qquad (4.5)$$

$$N_w^* = N_f\left(\frac{1-R}{2}\right)^{(1-\gamma)/b_w} \qquad (\varepsilon_a \le \varepsilon_{ai})$$

and

$$\varepsilon_a = \frac{\sigma_{f2}^{'}}{E}(2N_w^*)^{b_2} + \varepsilon_{fw}^{'}(2N_w^*)^{c_w} \qquad (4.6)$$

$$N_w^* = N_f\left(\frac{1-R}{2}\right)^{(1-\gamma)/b_2} \qquad (\varepsilon_a \ge \varepsilon_{ai})$$

Equation 4.5 applies at intermediate and long lives, specifically, for strain amplitudes $\varepsilon_a \le \varepsilon_{ai}$. Note that ε_{ai} can be calculated by substituting $N_w^* = N_i$, and calculating the strain amplitude. Then Eq. 4.6 applies at short lives, where $\varepsilon_a \ge \varepsilon_{ai}$, with the two curves joining at the discontinuity point (N_i, ε_{ai}).

Curves corresponding to the combination of Eqs. 4.5 and 4.6 are shown in Figure 4-16 along with all of the test data at all mean stresses for each alloy. There is only small scatter of the data about the discontinuous curves, indicating success of the manner of handling mean stress effects and the other aspects of the fitting procedure. Also shown in Figure 4-16 are data points for tests with no pre-strain, which were not included in the fitting. These are seen to lie a little above the

trend of the other data at relatively long lives.

It is interesting to note that the ε_{ai} values separating the two regions of strain-life behavior correspond to a point on the cyclic stress-strain curve below which there is only a small amount of plastic deformation. See Figure 4-17, where these points are compared with the points $(\varepsilon_o', \sigma_o')$ that locate the 0.2% offset cyclic yield strengths. (The mean stress relaxation transition ε_{a12} that is also shown will be discussed later.)

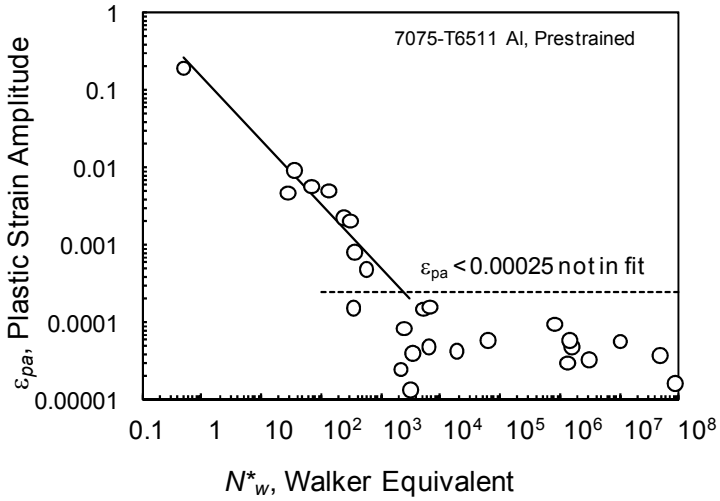

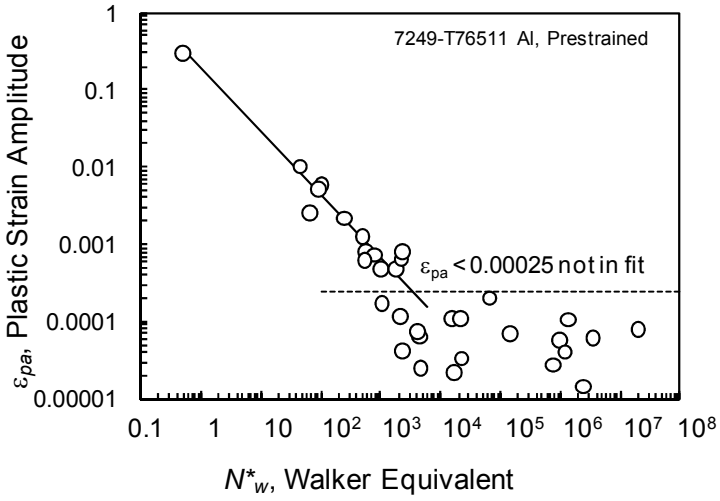

Figure 4-15. Plastic strain amplitude versus Walker equivalent life and the fitting of Eq. 1.7.

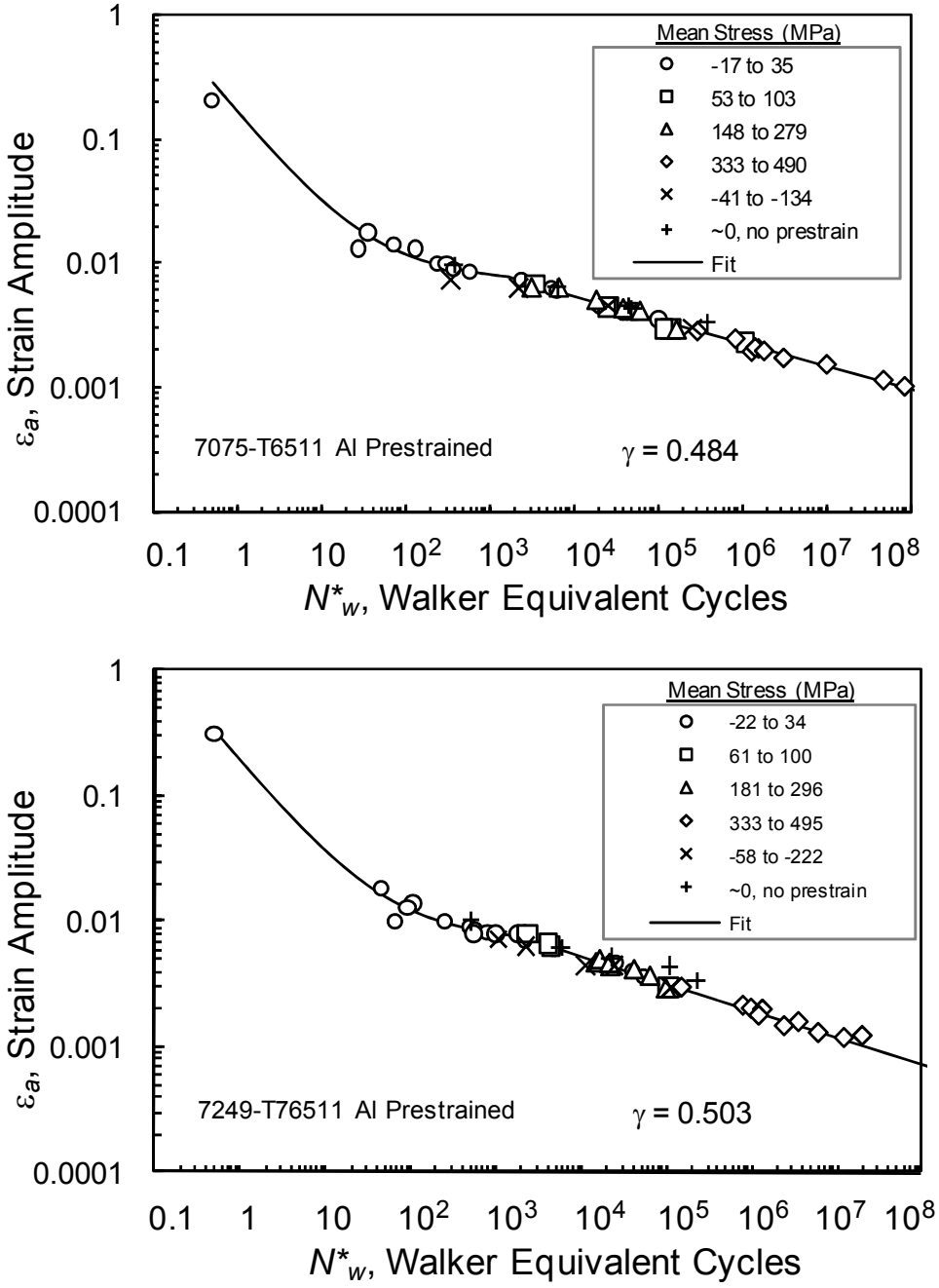

Figure 4-16. Strain amplitude versus Walker equivalent life for the two alloys.

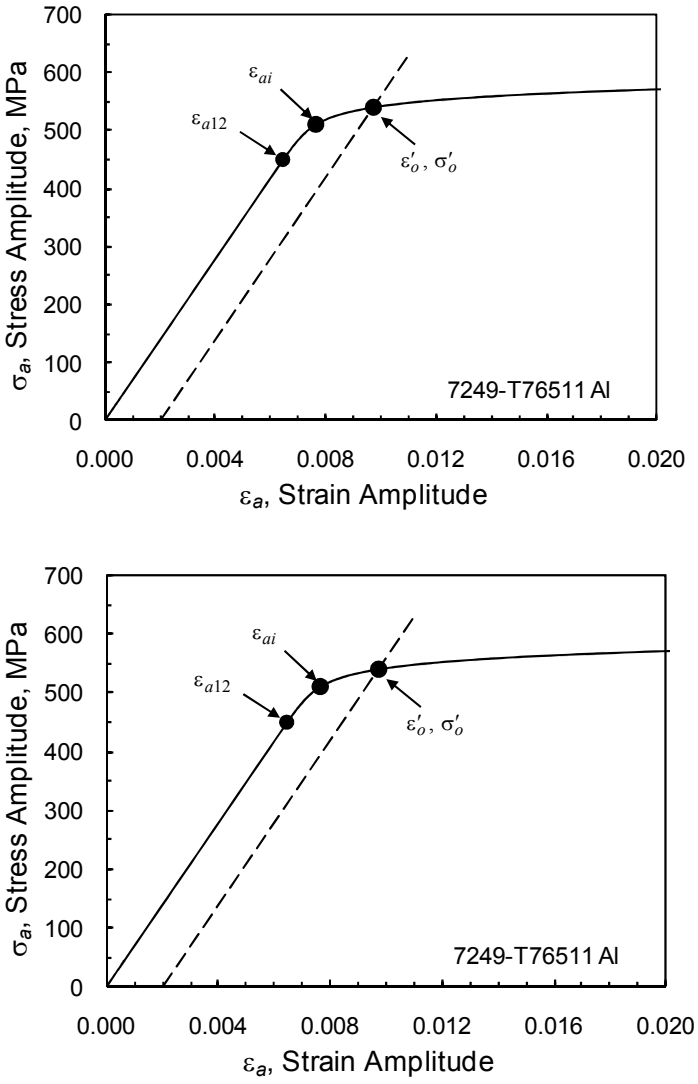

Figure 4-17. Cyclic stress-strain curves with points located corresponding to the strain-life transition strain ε_{ai} and the mean stress relaxation transition ε_{a12}. The 0.2% offset cyclic yield strength is also shown for comparison.

4.5
Mean stress models comparison

Two methods will be employed to observe the performance of the different mean stress models: stress-life plots and mean-amplitude plots. In a third subsection, the stress deviation

parameter for all the mean stress models will be calculated to quantify the scatter of the test data around the 0-mean line of each model.

4.5.1 Stress-Life Comparisons

The most direct way to compare test data to one of Eqs. 1.8 to 1.14 is to calculate σ_{ar} from the stresses applied in each test and plot the resulting values versus the corresponding experimental fatigue lives N_f. Comparisons of those plots are shown for both alloys in Figures 4-18 to 4-21 for the mean stress relations of the Goodman model, the Morrow model with $\tilde{\sigma}_{fB}$, the Morrow model with σ_f' and the SWT model respectively. As previously mentioned on each of these plots, a line for zero mean stress is also shown. The zero-mean line is obtained plotting the stress versus life relation for the materials, with constants obtained with zero-mean tests only. The constants were obtained in the stress-life analysis and can be found in Table 4-1. Since the scatter of the mean stress models is referred to the line describing the zero-mean relation, σ_f' and b are the ones at the bottom of Table 4-1 and indicated as "zero mean only". The analysis of the different mean stress models has to be performed with data points with mean stresses significantly different from zero, this is the case for data points with $N_f > N_i$, where N_i is the transition life otained in Section 4.4. Therefore only data in the range 10^3 to 10^6 cycles are included in these plots, as data at shorter lives involve only small mean stresses. The two alloys show quite similar trends.

The extent to which the data on such a plot agree with the zero-mean-stress line is a measure of the success of the σ_{ar} equation used. The Goodman relationship, Eq. 1.8, employs the ultimate tensile strength to "normalize" the mean stress data. It is clear from Figure 4-18 that the correlations are quite poor, indicated by the large scatter of mean stress data around the zero-mean line. Of particular concern is the scatter of the data for tensile mean stresses, lying well above the zero mean line. This means that that actual lives are often much longer than estimated, that is, the method is excessively conservative with respect to life estimates. Excessively conservative predictions translates into higher cost for inspection times and maintenance, which is of course undesirable.

The Morrow relationship of Eq. 1.9, employing the true fracture strength $\tilde{\sigma}_{fB}$, gives better results (Figure 4-19). The improvement with respect to the Goodman model is noticeable. However, from Figure 4-20, we see that Eq. 1.10, which uses the fitting constant $\sigma_f^{'}$, performs very poorly and is grossly non-conservative with respect to life estimates. The lack of correlation is so large that it was necessary to include an additional decade for the stress scale, which affects a visual comparison with the preceding similar plots. Non-conservative predictions mean a higher predicted life than the actual in service life, translating into possible catastrophic failures in service. The SWT relationship of Eq. 1.11 gives quite good results (Figure 4-21). The correlation seems at a first look better than for the Goodman relationship or either form of the Morrow equation. The SWT model doesn't use any material constant to reduce the mean stress data, but it shows a better correlation.

The same stress-life plot for the Walker relation has been shown in the stress-life analysis of the previous section (Figure 4-12). The $N_f > N_i$ portions are of primary interest here and can be compared with Figures 4-18 to 4-21. The zero-mean line for the case of the Walker method is calculated with the mean stress data reduced with the use of the fitted constant γ. Therefore the $\sigma_f^{'}$ and b constants are the $\sigma_{fw}^{'}$ and b_w fitting constants obtained in the previous section. The comparison is made to the Eq. 4.1 fit of data at various mean stresses with the σ_{ar} calculated with the value of γ for Eq. 1.13.

The correlation is similar to that for the SWT method, but slightly better, as might be expected from the ability to vary γ to obtain an optimum fit.

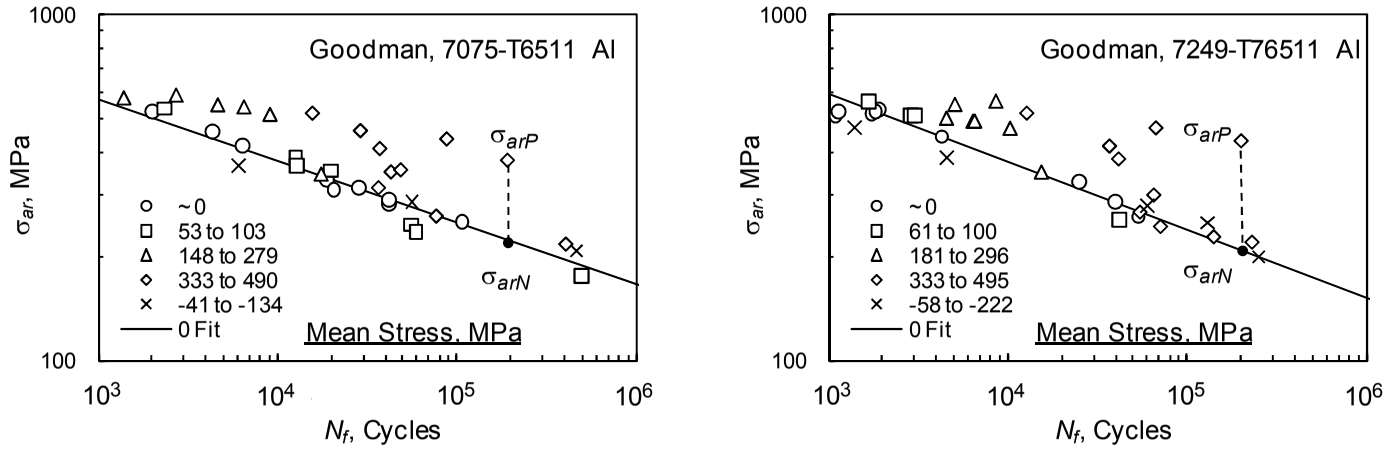

Figure 4-18. Equivalent completely reversed stress amplitude versus life correlations for the Goodman equation.

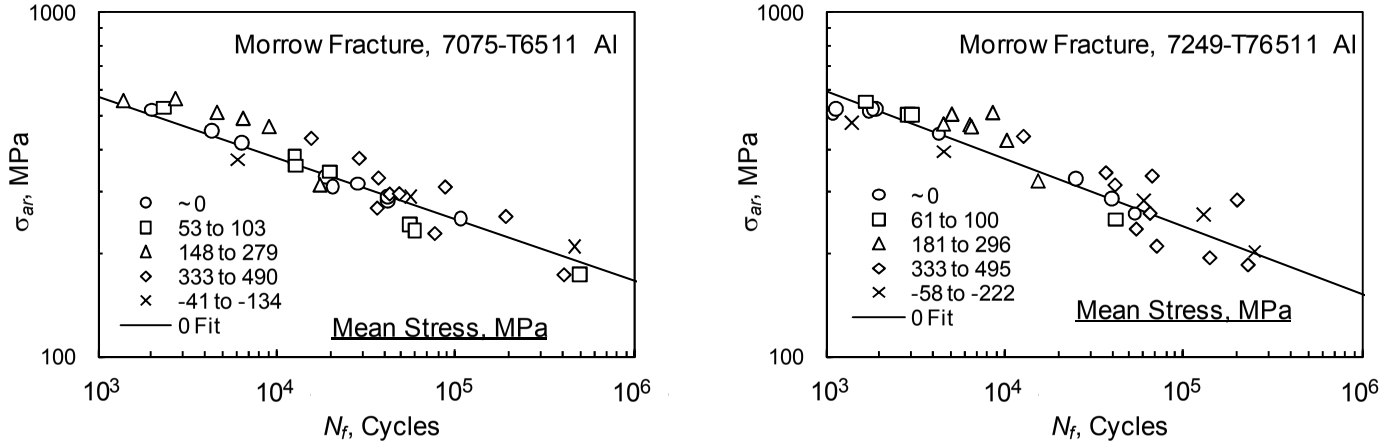

Figure 4-19. Equivalent completely reversed stress amplitude versus life correlations for the Morrow fracture strength equation.

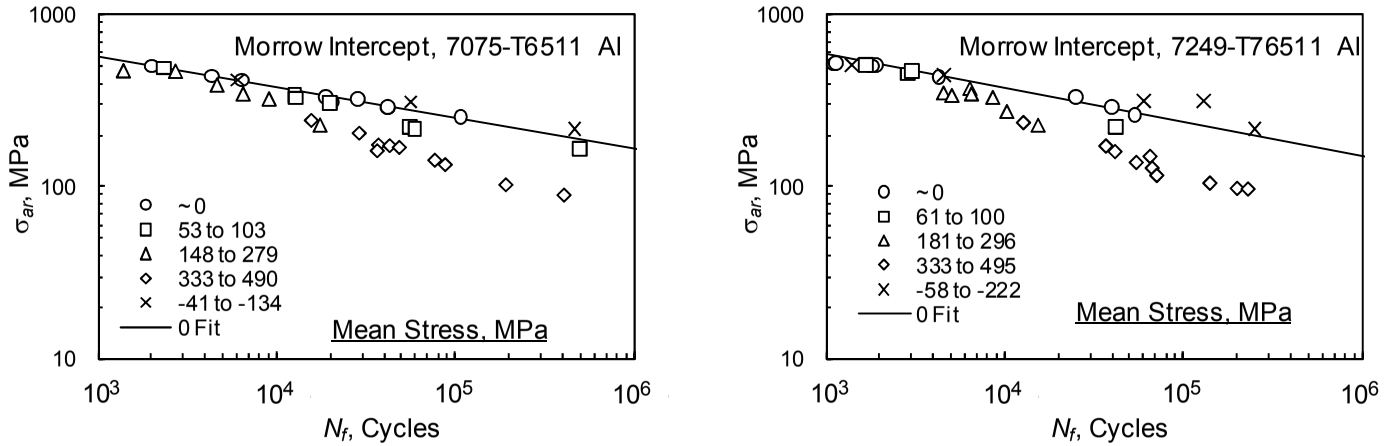

Figure 4-20. Equivalent completely reversed stress amplitude versus life correlations for the Morrow intercept equation. Note that it is necessary to use two decades for the stress scale to accommodate the large deviations from the zero-mean-stress line.

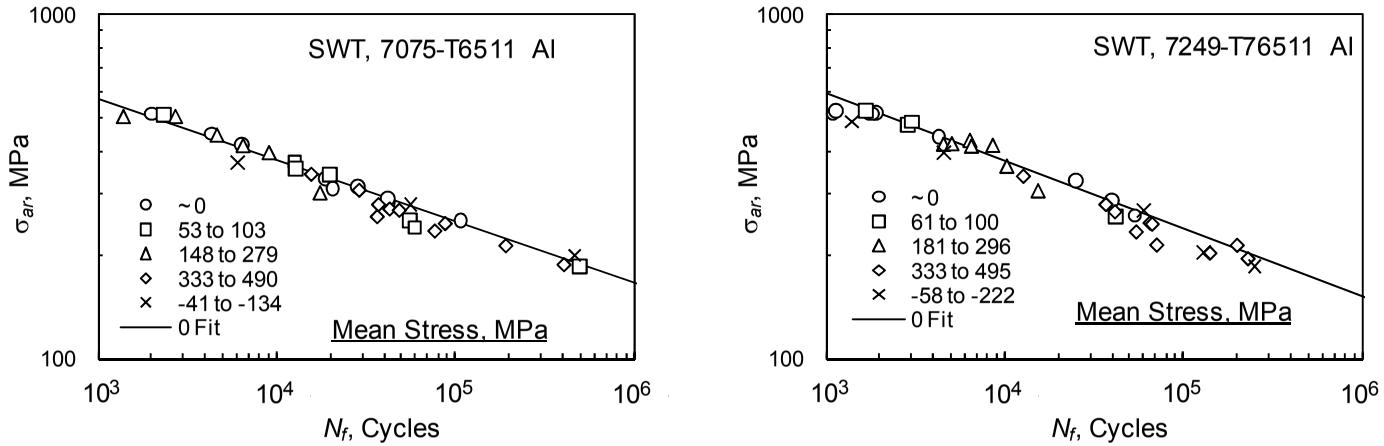

Figure 4-21. Equivalent completely reversed stress amplitude versus life correlations for the Smith-Watson-Topper equation.

4.5.2 Amplitude-Mean Plots

Another means of comparing mean stress equations to test data is to employ amplitude-mean plots, the same way it was shown to be employed in literature review. In this case, the σ_a and σ_a values for each tests are the experimental values. The equivalent stress amplitudes σ_{ar} for each point are calculated using the stress-life relation for zero-mean stress with the use of the experimental life N_f. The zero-mean data constants σ_f' and b from Table 4-1 are employed, except for with the only the Walker equation, where again Eq. 4.1 is used. The resulting mean-amplitude plots are shown in Figures 4-22 and 4-23. As shown in the introduction the expected behavior for the Goodman and Morrow relations is a line in a mean-amplitude plot. Equations 1.8, 1.9 and 1.10 represent a linear relationship for the corresponding mean stress models when σ_{ar} is normalized by σ_a and plotted versus σ_m. The x-axis intercept for the Goodman model is the ultimate strength, σ_u, while for the Morrow model it is in one case $\tilde{\sigma}_{fB}$ and in the other case σ_f'.

The previously noted performance of the mean stress models is confirmed by looking at the amplitude-mean plot. Data show some degree of scatter, but clearly mark a trend in the plot for both materials. Test data are scattered beyond the Goodman line, confirming the excessive degree of conservatism in life predictions. Hence, as for the life plots, for tensile mean stresses, this method is seen to be overly conservative with respect to life estimates. The Morrow equation with intercept $\tilde{\sigma}_{fB}$ gives good agreement. The form of the Morrow model with σ_f' gives a line visibly off the test data. This means that life predictions with this model would predict a lower effect of mean stress on life than is observed. The σ_a /σ_{ar} relation in fact decreases a lot more slowly than what it is predicted by the other models and observed from test data. The large deviation for the Morrow σ_f' model seems to be associated with the transition in stress-life behavior seen in Figure 4-12. The intercept σ_f' fitted in the intermediate and long life region is a very high value that is far above the intercept for the short-life region, which is more similar to the true fracture strength.

Equations 1.11 and 1.14 form a family of curves on plots similar to Figure 4-22, so a comparison of this type is not very useful. But a single curve is formed on a plot of σ_a

/σ_{ar} versus σ_m /σ_{ar}, as seen in Figure 4-23. Note that the SWT relationship, Eq. 1.11, corresponds to the $\gamma = 0.5$ special case of the Walker relationship, Eq. 1.13. Since the fitted γ values for the Walker equation were both near 0.5, the two curves for each alloy are quite close, and it is difficult to decide from these plots which provides better agreement with the test data.

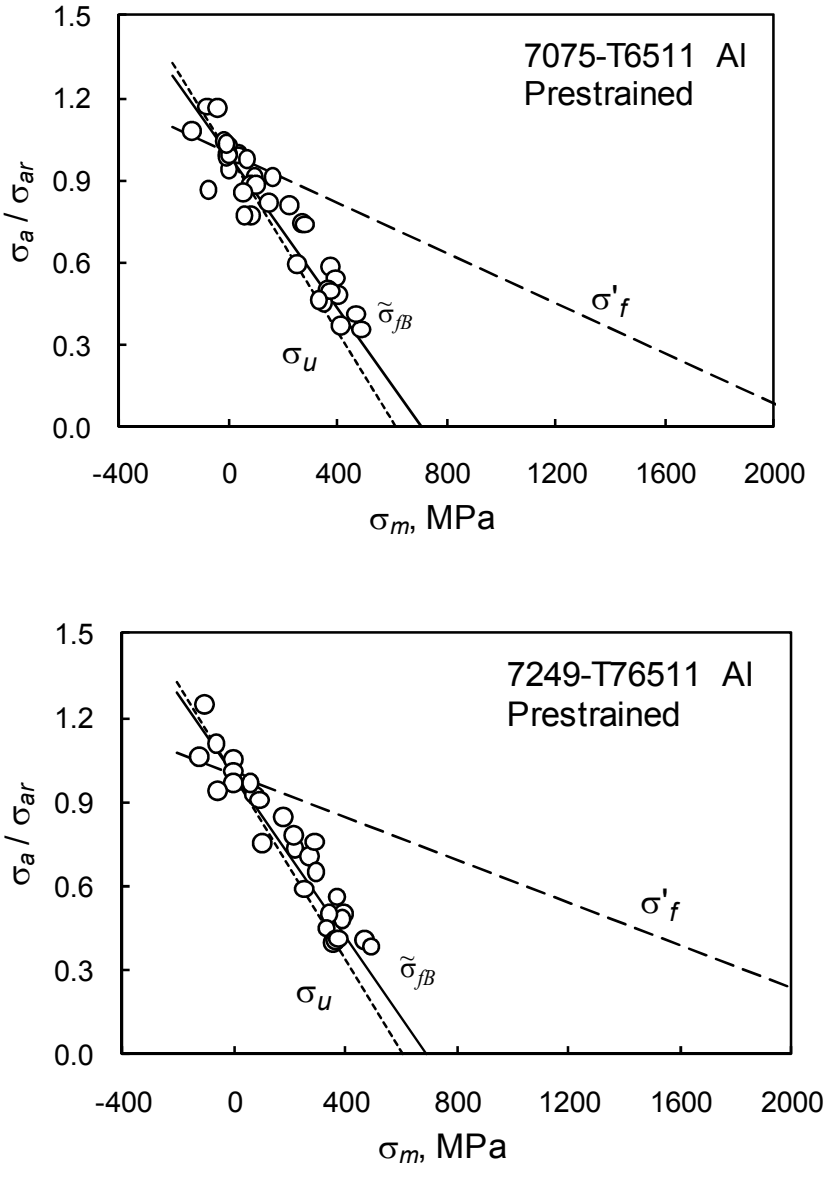

Figure 4-22. Normalized stress amplitude-mean plots for the two alloys.

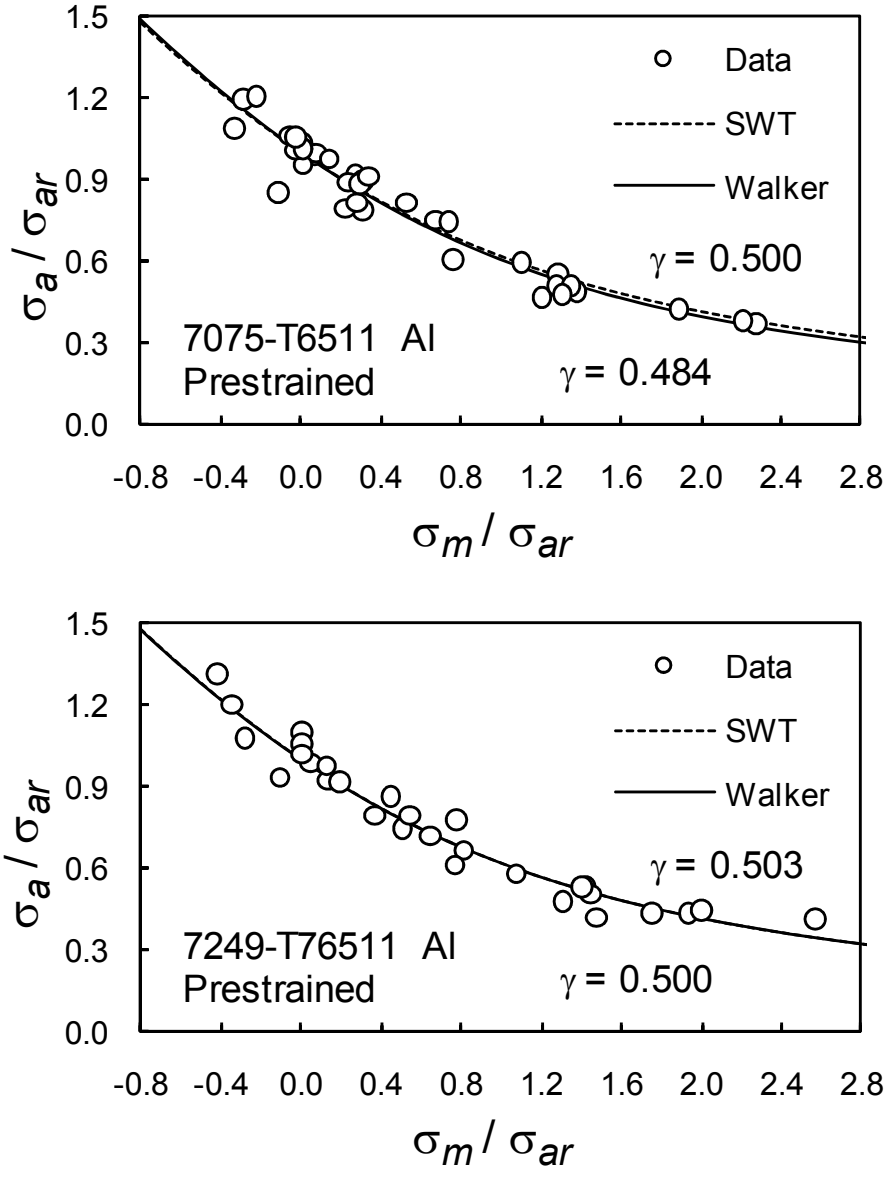

Figure 4-23. SWT and Walker amplitude-mean plots for the two alloys.

4.5.3 Stress Deviation Analysis

Following the analysis by Dowling et al. [37], [38] the stress deviation parameter is calculated for all the mean stress models. This parameter is a quantity that characterizes the degree of correlation on a life plot such as Figures 4-18 to 4-21 and it can be determined as follows: Consider the points σ_{arP} and σ_{arN} in Fig. 4-18. The former point corresponds to the applied stresses and experimental life for a fatigue test, and the latter to the point on the zero-mean-stress fit at the same life. The difference $\sigma_{arP} - \sigma_{arN}$ is a

measure of the lack of correlation, and a dimensionless measure is obtained by normalizing this difference to the σ_{arN} value [37].

$$z = \frac{\sigma_{arP} - \sigma_{arN}}{\sigma_{arN}} = \frac{\sigma_{arP}}{\sigma_{arN}} - 1 \qquad (4.7)$$

A measure of the overall scatter for a set of data is the standard deviation of this normalized variable z. Considering all nonzero mean stress data points in a given comparison, where n is the number of these, we have

$$s_z = \sqrt{\frac{\sum_{i=1}^{n} z_i^2}{n-1}} \qquad (4.8)$$

For the Walker model, since all the test data are included in the calculation of the stress-life zero-mean line, the zero-mean test data are also included in the s_z calculation. For all models, only the mean stress data with $N_f \geq N_i$ are used in the s_z calculation.

Values of s_z for each of the mean stress equations are given in Table 4-2. The trends noted with the use of stress-life and mean-amplitude plots are confirmed by the analysis of these values. The Goodman and Morrow σ_f' equations give relatively large values of s_z, indicating highly inaccurate results, whereas the Morrow $\tilde{\sigma}_{fB}$ equation is considerably better, and the SWT equation is better yet. The Walker equation gives a slightly lower s_z than the SWT one, and so it is the most accurate of the mean stress equations studied. Hence, its use in representing the strain-life curve is justified.

Similar trends in the success of the various equations occurred for the sets of aluminum alloy data that were included in the study by Dowling et al. [37], [38] reported in the Literature review. Values of γ were around 0.5 for all of the relatively high strength aluminum alloys, which included 2014, 2024, and 7075 alloys. But for relatively low strength alloys, such as 6061, the value of γ was around 0.65. For three sets of data on 2024 and 6061 alloys, where short fatigue lives were included from strain-controlled tests, similar flattening of the stress-life curve at short lives was also observed.

Using 2 segments in the stress-life curve for the Walker fitting may also provide a more successful fitting for some other types of alloys.

Table 4-2. Values of Stress Deviations for Mean Stress Equations

Mean Stress Equation	Values of s_z	
	7075-T6511	7249-T76511
Goodman	0.295	0.344
Morrow, $\tilde{\sigma}_{fB}$	0.142	0.166
Morrow, $\sigma_f^{'}$	0.294	0.336
Smith-Watson-Topper	0.074	0.072
Walker, fitted γ	0.061	0.059

Chapter 5
Mean Stress Relaxation in Constant Amplitude Loading

In this Chapter a complete analysis of all the mean stress relaxation tests performed under constant amplitude loading in this research is reported. Fitting methods are proposed to model this transient material behavior. In section 5.2 and 5.3, two empirical models are used to fit relaxation curves obtained from preliminary relaxation tests on three aluminum alloys: 7475-T651, 7075-T6511 and 7249-T76511. In section 5.4 all the relaxation curves obtained for 7075-T6511 and 7249-T76511 at the end of the experimental work are fitted to an improved versions of one of the models analyzed in the first part.

5.1 Representative test results

Constant-amplitude, strain-controlled, mean stress relaxation tests have been performed with the intent of characterizing this transient phenomenon in both aluminum alloys 7075-T6511 and 7249-T76511. Different behavior occurs depending of the level of plastic strain involved. As an example, the complete stress-strain response for test 75LB-6 is shown in Figures 5-1 and 5.2.

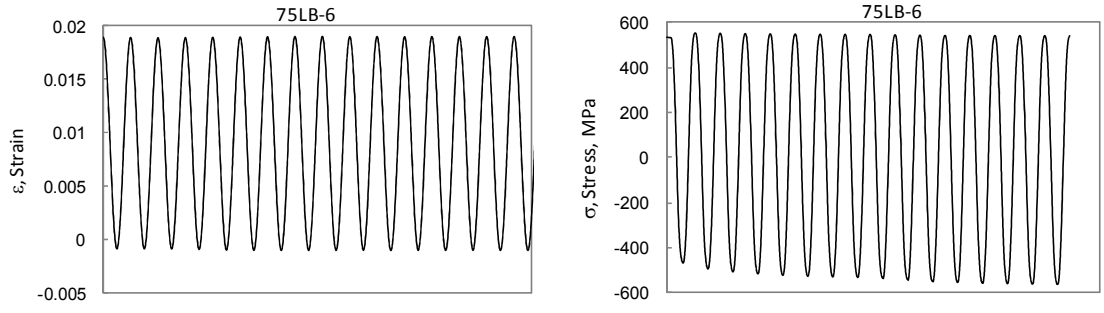

Figure 5-1. Strain control and stress response of mean stress relaxation test on 7075-T6511 aluminum alloy.

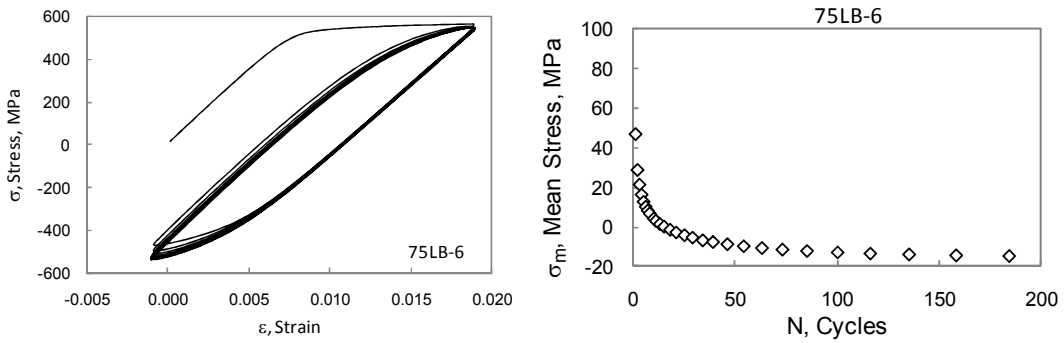

Figure 5-2. Stress-strain response and mean stress relaxation response of 7075-T6511 aluminum to strain controlled mean stress relaxation tests in Figure 5-1.

The relaxation response is evident from the observations of the valleys in Figure 5-1: the stress response is gradually shifting down towards a stable value. In Figure 5-2 the relaxation response is represented by the progressive shifting down of the hysteresis loop, confirmed by the plot of mean stress, σ_m, versus the number of cycles, N. Most of the relaxation for this low-cycle fatigue relaxation test happens in the first few cycles. The stable value of mean stress for the test shown is compressive and close to -20 MPa. This effect, observed also in Chapter 4 for zero mean stress tests, will be widely discussed in the next sections. The relaxation response for a strain controlled test with strain amplitude approximately equal to 0.2% is shown in Figure 5-3 and 5-4, the test name is 75NLB-3.

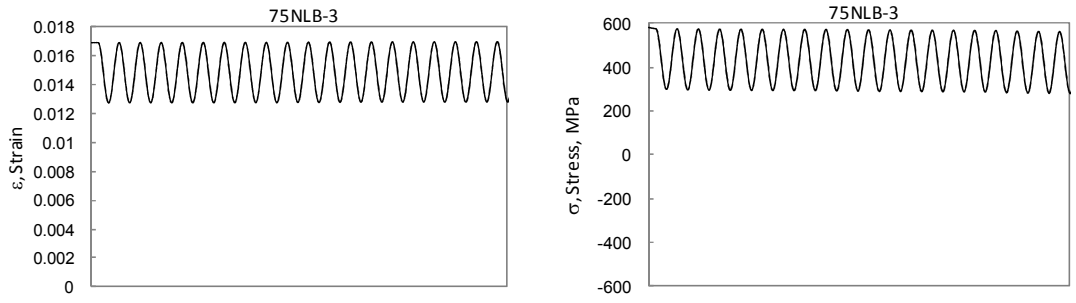

Figure 5-3. Strain control and stress response of mean stress relaxation test on 7075-T6511 aluminum alloy.

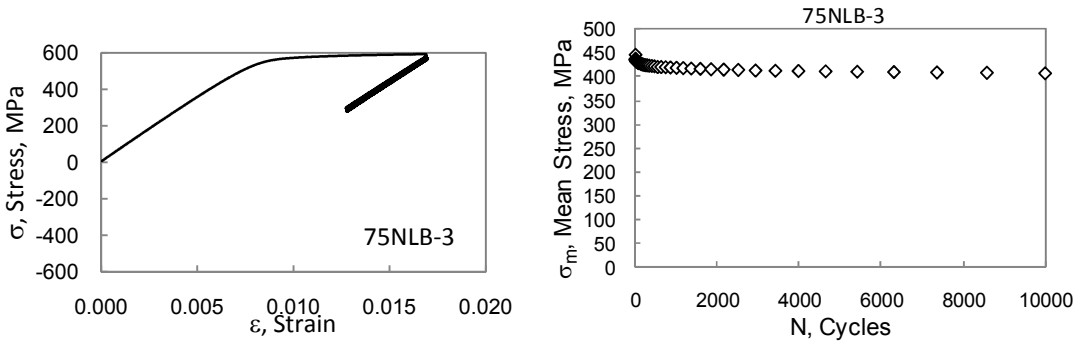

Figure 5-4. Stress-strain response and mean stress relaxation response of 7075-T6511 aluminum to strain controlled mean stress relaxation tests in Figure 5-3

The amount of relaxation and the rate of relaxation is highly different than observed for test 75LB-6. The hysteresis loop is totally elastic, with stress-strain response comparable to Figure 4-4. The difference in the stress-strain response with respect to a zero mean test is that the hysteresis loop is not stable at such high level of mean stress. In fact the hysteresis loop is slowly stabilizing at a lower mean level. This is confirmed by the plotting of mean stress, σ_m, starting at approximately 450 MPa and relaxing to about 400 MPa. In this case also a good level of relaxation is observed mainly in the first part of the life. The rate of relaxation seems lower for this high cycle fatigue case, with a decay spread over a large number of cycles. The observation of a significant relaxation in cases of negligible amount of plastic strain during cyclic deformation is of great importance for the scope of the current study.

5.2 The Landgraf Model

5.2.1 Preliminary fitting on 7475

Preliminary results on aluminum alloy 7475 obtained from mean stress relaxation tests were published by Arcari et al. in 2008 [43]. The initial study on 7475 data was used to carefully plan the tests for 7075-T6511 and 7249-T76511, as shown in Chapter 3. The preliminary work mainly showed a need for mean stress relaxation analysis for smaller strain amplitudes, and a need for a greater span of mean stresses, falling in the range 50-450 MPa.

The data collected were fitted to the Landgraf model, chosen for its simplicity of formulation, low number of material constants, and promising fitting capabilities.

The test data were normalized to σ_{mN}/σ_{mi} versus N form and fitted to a straight line in a log-log plot to obtain the relaxation exponents r of Eq. 2.5. Those normalized data are shown in Figure 5-5. Those exponents r were then plotted against the strain amplitude for each test to obtain a relationship between the two variables, which is shown in Figure 5-6. As stated by Landgraf [41], considering r as only a function of strain amplitude, the relationship is visibly linear.

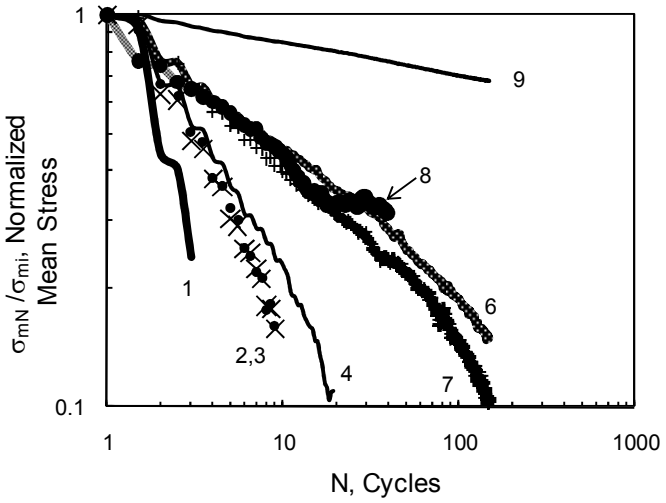

Figure 5-5. Mean stress relaxation curves for preliminary tests on 7475-T651.

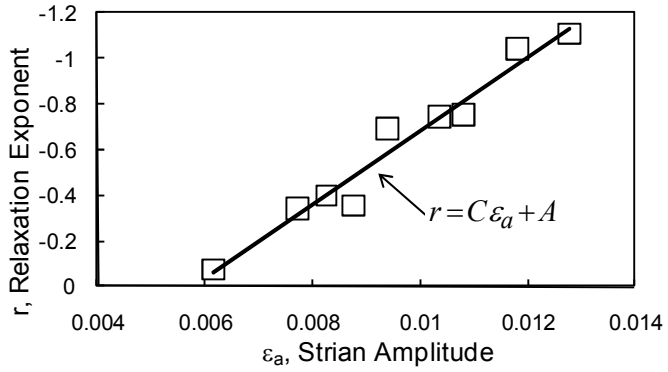

Figure 5-6. Linear fitting of relaxation exponents of the Landgraf formulation and strain amplitudes.

The relaxation exponent r is explicitly written as a function of ε_a, as shown in Figure 5-6, and the material constants are reported in Table 5-1. These are *C* and *A*, the slope and intercept of the line in the plot, and $\varepsilon_{a\mathrm{Th}}$, the threshold below which there is no relaxation. No relaxation corresponds to $r = 0$, giving $\varepsilon_{a\mathrm{Th}} = -A/C$.

Table 5-1. Fitting constants for the Landgraf formulation.

Landgraf Constant	C	A	$\varepsilon_{a\mathrm{Th}}$
Fitted value for 7475-T651	-161.6	0.931	0.00576

The results obtained show the ability of the Landgraf model to represent a wide variety of relaxation curves, and the possibility of relating the amount of mean stress relaxation to the amplitude of the strain involved. This will be the starting point of the next analysis that will take into account a larger number of experimental curves and strain amplitudes. Test details are given in Table 5-2 for the 7475 alloy, and the mean stress relaxation curves from Eq. 2.5 and the Table 5-1 constants are shown in Figure 5-7, along with test data. Note that the behavior of the mean stress relaxation crossing the stress cannot be accommodated by eq. 2.5.

5.2.2 Preliminary fitting on 7075-T6511 and 7249-T76511

Partial results on 7075 and 7249 were also published by Arcari et al. in 2008 [43]; the results of the fitting for this part of data showed a way to obtain significant improvements in the Landgraf model. The set of tests described in this initial part of the study is missing relaxation curves for negative mean stresses. These would be of particular interest because beneficial residual stresses, superficial mean stresses introduced frequently in high risk components, are always negative. These beneficial stresses are used to increase the time for crack initiation at the surface, but they are also similarly subjected to relaxation during service loading. A summary of the most important improvements in the fitting technique for the Landgraf model and of the possible improvements to the Landgraf model itself, shown by Arcari et al. [43], are summarized in the next paragraphs.

Table 5-2. Test details for 7475-T651 alloy.

Test Number	Strain Amplitude ε_a	Mean Strain ε_m	Mean Stress σ_m, MPa	Cycles to Failure N_f
1	0.01276	0.00350	-11.43	208
2	0.01075	0.00901	-13.84	369
3	0.01036	0.00973	-10.63	877
4	0.00937	0.00640	-9.04	560
5	0.00878	-0.00050	-12.41	423
6	0.00874	0.00361	17.85	306
7	0.00826	0.00720	8.34	928
8	0.00773	0.00700	-9.89	1660
9	0.00626	0.00319	110.31	2300

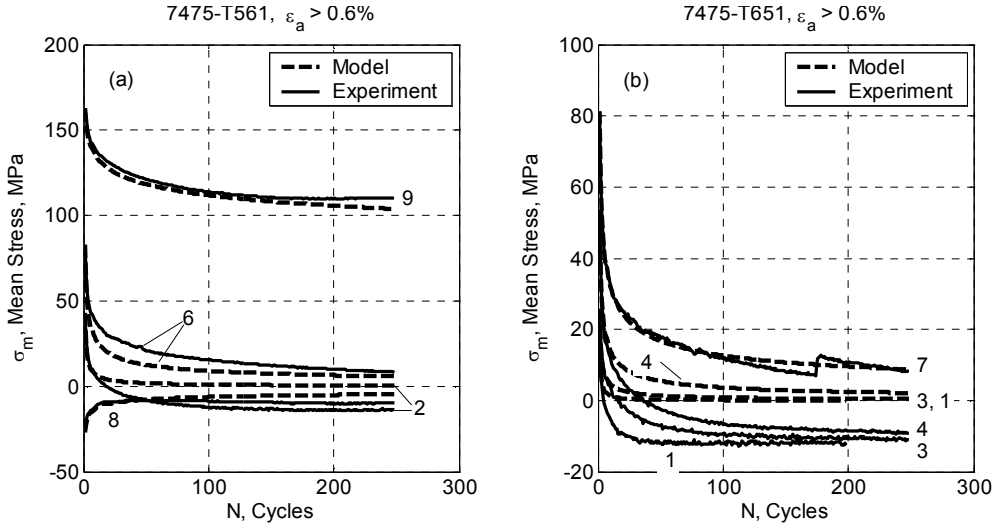

Figure 5-7. Mean stress relaxation tests on 7475-T651 aluminum alloys and Landgraf model curves.

With a greater number of tests and a wider range for both strain amplitude and mean stress, a different fitting technique was chosen for the calculation of the Landgraf constants. Expanding mathematically the Ladgraf formulation:

$$\frac{\sigma_{mN}}{\sigma_{mi}} = \mathrm{N}^{\mathrm{A}(1-\varepsilon_a/\varepsilon_{a\mathrm{Th}})} \quad , \quad \text{where } r = A(1-\varepsilon_a/\varepsilon_{a\mathrm{Th}})$$

$$\log\left(\frac{\sigma_{mN}}{\sigma_{mi}}\right) = \mathrm{A}\log\mathrm{N} - \frac{\mathrm{A}}{\varepsilon_{a\mathrm{Th}}}\varepsilon_a \log\mathrm{N} \tag{5.1}$$

It is possible to perform a multiple linear regression where:

$$\mathrm{y} = m_1\mathrm{x}_1 + m_2\mathrm{x}_2 + b$$

$$\mathrm{x}_1 = \log N, \qquad \mathrm{x}_2 = \varepsilon_a \log N, \qquad b = 0 \tag{5.2}$$

The obtained fitting parameters can be reconstructed to the slope and threshold of the original Landgraf fitting:

$$A = m_1, \qquad \varepsilon_{a\mathrm{Th}} = -\frac{A}{m_2} = -\frac{m_1}{m_2} \tag{5.3}$$

Partitioning the data for each material into low strain and high strain sets greatly improves its representation by the Landgraf model. The correlation factors are all near or above 0.8, with the fitting constants obtained being listed in Table 5-3. Plots of the relaxation exponent r of Eq. 5.1 versus strain amplitude ε_a are shown in Figures 5-8 and 5-9 for the two alloys, with a clear transition in behavior being evident around ε_a = 0.6% in each case. The straight lines shown in Figures 5-8 and 5-9 correspond to the equation in Figure 5-8, but with the constants *C* and *A* being obtained from the multiple regression results of Table 5-3. The strain amplitudes reported under Range in Table 5-3 correspond to transition values that are computed as intersection points of the fitted lines in Figures 5-8 and 5-9.

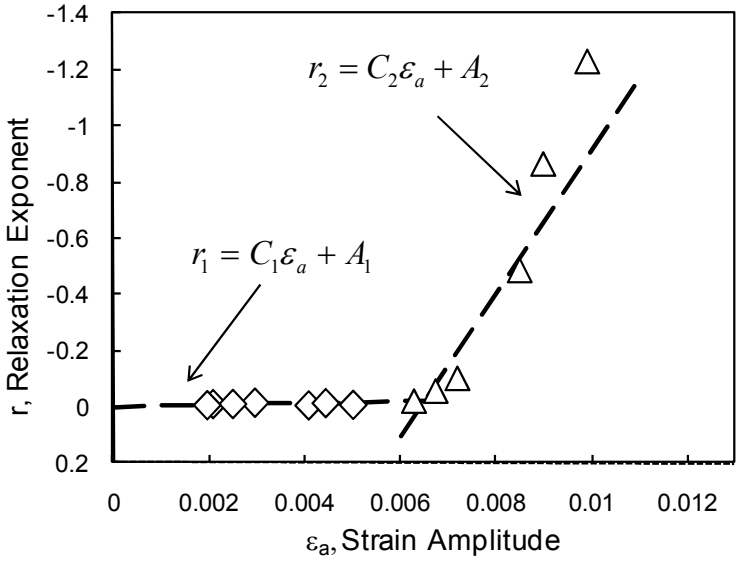

Figure 5-8. Relaxation exponent versus strain amplitude data for 7075-T6511 aluminum, with lines from the multiple regression constants also shown.

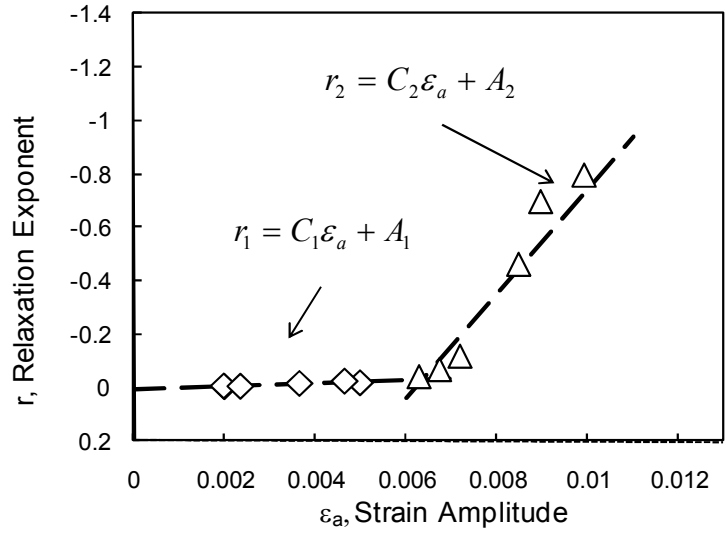

Figure 5-9. Relaxation exponent versus strain amplitude data for 7249-T76511 aluminum, with lines from the multiple regression constants also shown.

Table 5-3. Landgraf model fitting constants for 7075-T6511 and 7249-T76511 aluminum.

Alloy	Range	$m_1 = A$	m_2	$\varepsilon_{a\mathrm{Th}}$	Cor
7075-T6511	$\varepsilon_a \leq 0.648\%$	-0.000695	-2.92637	-0.0002374	0.8081
7075-T6511	$\varepsilon_a \leq 0.648\%$	1.635011	-255.205	0.006407	0.8425
7249-T76511	$\varepsilon_a \leq 0.637\%$	0.006347	-5.79367	0.001095	0.8019
7249-T76511	$\varepsilon_a \leq 0.637\%$	1.219585	-196.212	0.006216	0.8081

The relaxation curves and all the fitting results for the Landgraf model on the fitted data are shown in Figure 5-10.

The fitting technique proposed is an exceptional improvement to the Landgraf model, making the calculation of the constants fast and easy and showing a rationale similar to other fitting techniques used in the strain-based approach. A larger variety of strain amplitudes with respect to preliminary data on 7475 lead to the interesting discovery of significant relaxation behavior, even well below the proportional limit of the material, a phenomenon never reported before in literature [43].

The main issue with fitting the relaxation curves to the Landgraf formulation is the fact that some of the curves corresponding to the highest values of strain amplitudes tend to stabilize at a negative value. This creates problems in the calculation of $log(\sigma_{mN}/\sigma_{mi})$, making it necessary to exclude the affected data points from the fitting. The effect is noticeable for both alloys, where the linear fitting for the $\varepsilon_a > 0.6\%$ region deviates from the data points, that involves crossing zero.

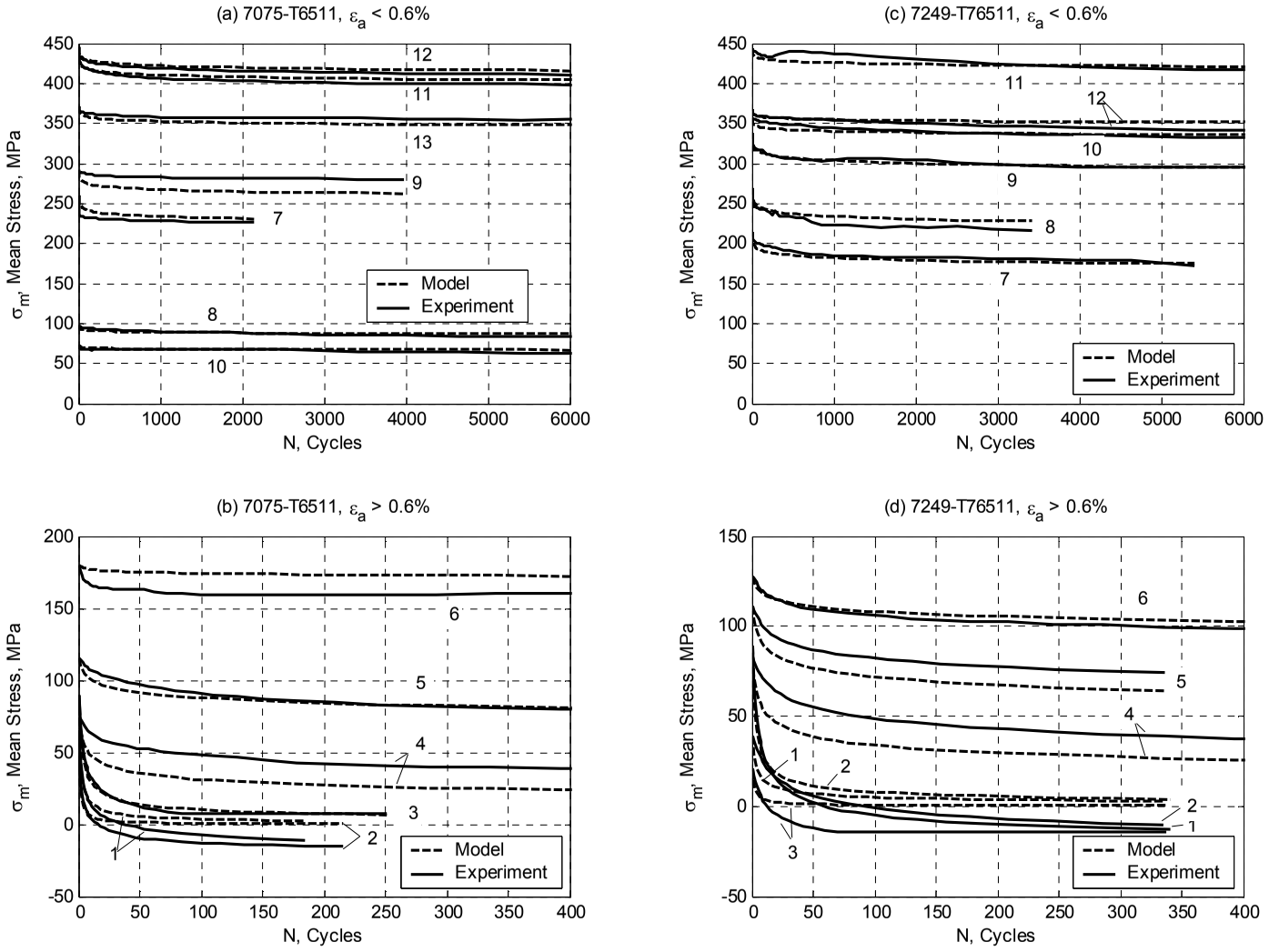

Figure 5-10. Experimental curves and Landgraf model curves for mean stress relaxation tests on 7075-T6511 and 7249-T76511.

5.3 The non linear Maxwell model

5.3.1 Preliminary fitting on 7075-T6511 and 7249-T76511

Even if at first sight the application of a non linear rheological model seemed appropriate with the right calibration between number of constants and application of relaxation formula to a cyclic case, the nonlinear Maxwell model was found to be difficult to handle when applied to fitting of experimental curves.

The same initial set of data are fitted to the nonlinear Maxwell curve and considerations are expressed in comparison to the Landgraf model. Given the corresponding results for Landgraf, the data sets for the nonlinear Maxwell model are also divided in two regions depending on the strain amplitude. A stepwise fitting procedure is used by the authors, and the normalized curves are fitted to Eq. 2.8 by using a Levenberg-Marquardt fitting procedure [66]. Preliminary set of mean stress versus cycles fits was done for each test. The values of the exponent m obtained were then averaged in order to run a second set of fits with the average m values for the high and low strain regions for each material. This preliminary fitting showed that for $\varepsilon_a < 0.6\%$, the values of the exponent m were extremely high, in the range m = 50 to 100, while for $\varepsilon_a > 0.6\%$, the exponents were lower, in the range 2 to 20.

The second step in the published study by Arcari et al. was to run fits employing a form that is equivalent to Eq. 2.8; the fitting routine used a Levenberg-Marquardt fitting function with the following form:

$$\log\frac{\sigma_{mN}}{\sigma_{m1}} = A\log(CN+1) \tag{5.4}$$

where $A = \frac{1}{1-m}$, $\quad C = BES^{m-1}(m-1)\left(\frac{\sigma_{mi}}{S}\right)^{m-1}$

Since the exponents m were quite high, difficulties in managing the values of B required the additional parameter S to be included, to avoid working with extremely

small or extremely large numbers. The value of S was chosen arbitrarily to correspond to a typical σ_m value.

A strong correlation was found between the logarithm of the first multiplying factor of the fitting coefficient C, i.e. the quantity $\log(BES^{m-1})$, and the initial maximum stress, $\sigma_{max,i} = \sigma_a + \sigma_{mi}$, for the tests, where σ_a is the stress amplitude; the mathematical expression of the correlations for $\varepsilon_a < 0.6\%$ is shown in Figure 5-11. Correlation coefficients for the fits in the low strain region were 0.999 for 7075 and 0.986 for 7249. For $\varepsilon_a > 0.6\%$, similar trends were observed, but with more scatter, and correlation values between 0.7 and 0.8.

The final values of fitting constants were found from data from both regions of the two alloys with m as the average value employed in the final fitting. Note that the fitting constants *F* and *G* provide a convenient way to express the constants so that B values can be calculated for any desired condition of initial stress $\sigma_{max,i} = \sigma_a + \sigma_{mi}$.

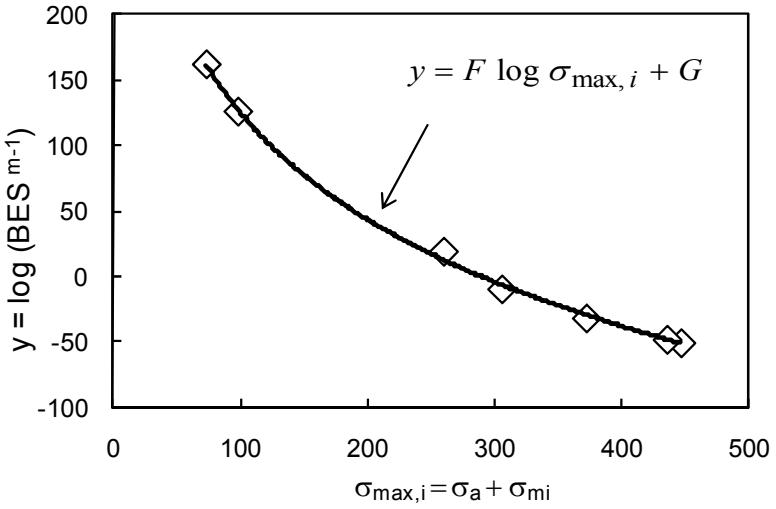

Figure 5-11. Correlation of with $\sigma_{max,i}$ for 7075-T6511 aluminum.

Although the relaxation formula for the nonlinear Maxwell model is mathematically simple, the high values of the constant m, necessary for accurate fitting, interfered with the manageability of the values of the parameter *B*, which in turn compromised the final

accuracy of the model in comparisons with experimental data for ε_a > 0.6%. From a computational point of view, the errors for the nonlinear Maxwell model are mainly due to two factors: (1) Since the values of *B* are obtained from fitting $\log(BES^{m-1})$ against $\sigma_{max,i} = \sigma_a + \sigma_{mi}$ small differences between the data points and the points on the fitted line will be magnified in modeling. (2) Since the values of m are much greater than unity, every source of error is amplified when the simulation is implemented.

Table 5-4. Nonlinear Maxwell model fitting constants for 7075-T6511 and 7249-T76511 aluminum.

Alloy	Range	*m*	*S*, MPa	*E*, GPa	*F*	*G*
7075-T6511	$\varepsilon_a \leq 0.6\%$	117.28	300	70	-137.58	334.89
7075-T6511	$\varepsilon_a \geq 0.6\%$	5.77	300	70	-29.75	59.97
7249-T76511	$\varepsilon_a \leq 0.6\%$	50.99	300	70	-270.79	666.22
7249-T76511	$\varepsilon_a \geq 0.6\%$	7.20	300	70	-25.63	55.67

The choice of a constant m for the two regions was based on observations of the trends in this value from individual fitting of different tests, and also from previous simulations of relaxation response with varying values of m and *B*. The dependence of *B* on the maximum stress was found to provide the strongest correlation with the variables involved in the fitting. It is also notable that differences with strain amplitude within the high or low strain region are not taken into account by a constant value of *m*.

Fitting results with the relations obtained for the Maxwell model are shown in Figure 5-12. It is significant that, despite the disadvantage noted above, the correlations and predictions obtained for the ε_a < 0.6% region were quite good.

Also, for the nonlinear Maxwell model, the degree of relaxation in the high strain region is more strongly dependent on the starting point of the curve than is seen in the experimental data. This is likely related to the necessity of using an average m value. Hence, as applied here, this model is not able to incorporate the effects of plastic strain amplitude variation as successfully as the Landgraf model.

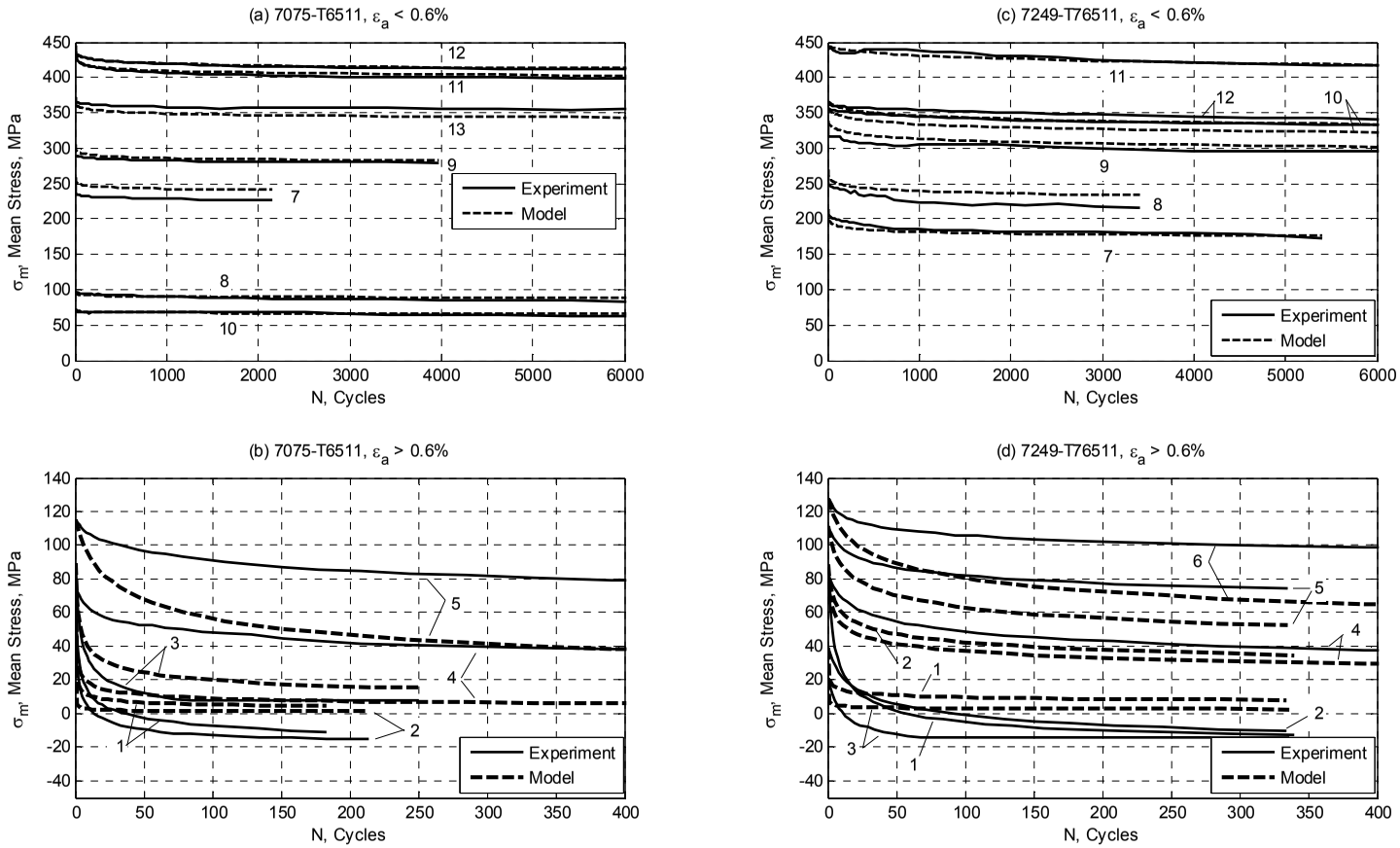

Figure 5-12. Experimental curves and Maxwell model curves for mean stress relaxation tests on 7075-T6511 and 7249-T76511.

A summary of all the preliminary tests run on 7075-T6511 and 7249-T76511 is shown in Table 5-5 and Table 5-6. The test number in the first colomn refers to the numbers in the figures and the specimen number in the secondcolumn can be referred to Tables A.1 and A.2 for more details on the specific test.

Table 5-5. Test details for 7075-T6511 alloy.

Test Number	Specimen Number	Strain Amplitude ε_a	Mean Strain ε_m	Mean Stress σ_m, MPa	Cycles to Failure N_f
1	75LB-6	0.0095	0.0085	-15.12	439
2	75NLB-1	0.0090	0.009	-11.78	479
3	75LT-5	0.0085	0.0095	-5.18	655
4	75NLB-2	0.0072	0.0108	35.18	2010
5	75RB-5	0.00675	0.01125	70.38	2316
6	75NRB-1	0.0063	0.0117	164.9	2691
7	75LC-3	0.0050	0.013	225.65	4605
8	75LC-2	0.0045	0.0015	83.33	12793
9	75LB-5	0.004	0.014	279.35	9026
10	75LB	0.0030	0.001	60.16	59396
11	75RT-5	0.0025	0.0175	392.80	29054
12	75NLB-3	0.0020	0.015	403.10	37301
13	75RT-6	0.0020	0.006	352.55	36676

Table 5-6. Test details for 7249-T76511 alloy.

Test Number	Specimen Number	Strain Amplitude ε_a	Mean Strain ε_m	Mean Stress σ_m, MPa	Cycles to Failure N_f
1	49LB	0.00992	0.0090	-17.75	399
2	49LC-3	0.008968	0.00899	-12.48	697
3	49LC-1	0.008486	0.00949	-11.67	781
4	49RB-3	0.007198	0.0108	33.94	1823
5	49LC-4	0.006748	0.01125	61.11	3032
6	49LB-5	0.006298	0.01169	91.80	2851
7	49LT-1	0.004998	0.01299	180.84	6336
8	49NLB-4	0.004659	0.01345	217.96	6731
9	49LT-4	0.003665	0.01698	295.86	87992
10	49NRB-6	0.002363	0.00603	328.52	65000
11	49LC-5	0.002011	0.01487	390.72	41353
12	49MT-C	0.001996	0.00600	328.39	42595

5.4 Improved Ladgraf model fitting

5.4.1 Compressive mean stress relaxation

Several additional tests were performed, with the intent of better characterizing the relaxation in 7075 and 7249 aluminum alloys. A total of 21 and 19 constant amplitude loading test have been performed on 7075 and 7249, respectively and the relaxation curves were recorded during the tests. Initial mean stresses varied from 50 to 450 MPa in tension and -50 to -250 MPa in compression, and strain amplitudes ranged from 0.2% strain to 1.2% strain. Table 5-7 shows the numbering used for the relaxation tests and the correspondence with the specimen numbers name of the tests in Tables A.1 and A.2.

Recalling Figures 5-1 anto 5-4, data from additional representative mean stress relaxation tests are fully plotted in Appendix B, with stress-strain plots, peak and valley plot and mean stress relaxation curves. A global visualization of the tests run is included in this section in Figure 5-13, with numbers or letter referring to Table 5-7.

All of the tests shown were included in the relaxation test analysis described in the previous section, with new tests now added, with particular attention to compressive relaxation curves. Knowing that in tension two distinct regions of behavior were determined from preliminary analysis, the partitioning into two regions was also applied for this data that also includes compression.

As previously mentioned for tension, mean stress relaxation happens mostly in the first part of the life, and the amount of relaxation in both tension and compression is related to the strain amplitude of the test. The observed relaxation is not extreme, but in life calculation it would be of some importance to account for this phenomenon. For some of the highest strain amplitudes, tensile mean stresses are visibly stabilizing to small compressive values. It is noticeable that differently from the tension tests, the compression relaxation curves never stabilize at a tensile value. The relaxation curves in compression do not cross the x-axis, but they also stabilize at a small compressive value. This will be the starting point for modifications of the Landgraf model.

Table 5-7. Names of mean stress relaxation tests and identifiers on plots.

(a) 7075-T6511 Al		(b) 7249-T76511 Al	
Identifier on Plot	Specimen Number	Identifier on Plot	Specimen Number
1	75NLB-1	1	49LC-3
2	75LB-6	2	49LC-1
3	75LT-5	3	49LB
4	75NLB-2	4	49RB-3
5	75RB-5	5	49LC-4
6	75NRB-1	6	49LB-5
7	75LC-3	7	49LT-1
8	75LC-2	8	49NLB-4
9	75LB-5	9	49LT-4
10	75LB	10	49NRB-6
11	75RT-5	11	49LC-5
12	75NLB-3	12	49MTC
13	75RT-6	a	B49-27
a	B75-47	b	B49-52
b	B75-40	c	B49-40
c	B75-46	d	B49-22
d	B75-50	e	B49-53
e	B75-31	f	B49-37
f	B75-38	g	B49-12
g	B75-43	---	---
h	B75-25	---	---

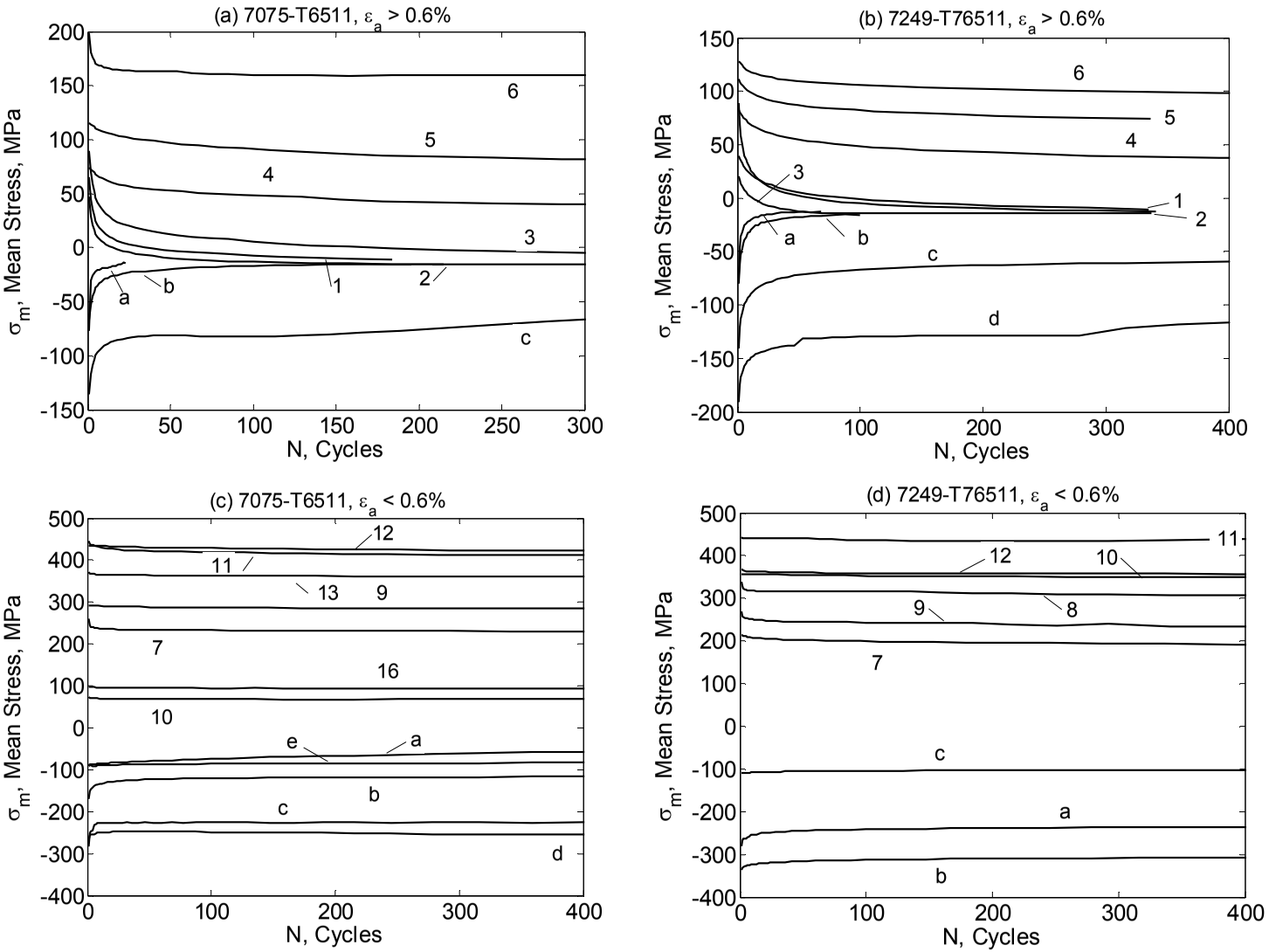

Figure 5-13. Summary of mean stress relaxation curves for 7075-T6511 and 7249-T76511.

In the low strain amplitude region, a noticeable amount of relaxation occurs in all the tests, with the compressive and tensile mean stress behaving similarly. The amount of relaxation is visibly less than observed in the high strain amplitude region, but nonetheless the change in mean stress can significantly interfere with life calculation. The only difference that can be pointed out between the compressive and tensile cases is a slight tendency of having a greater amount of relaxation at the same strain level when starting from a compressive value.

5.4.2 The mean stress offset

Looking at the plot of relaxation data and Landgraf model curves from the analysis for preliminary data, as seen in Figures 5-7 and 5-10, a limitation of the model is evident for the three tests at the highest strain amplitudes: an initially tensile mean stress can relax and stabilize at a small compressive value. In the fitting process, the data points of the relaxation curve below the x-axis had to be omitted in the preliminary fitting, due to mathematical incompatibility, so that useful information is lost, as reported by Arcari [43].

It is therefore proposed to modify the Landgraf formulation in a way that the relaxation for large strain amplitudes is driven to a stable compressive value, which can be accomplished by modifying Eq. 5.1 to include an offset stress σ_b.

$$(\sigma_{mN} + \sigma_b) = (\sigma_{mi} + \sigma_b)N^r \qquad \text{(a)}$$

$$\text{where} \quad r = A\left(1 - \frac{\varepsilon_a}{\varepsilon_{aTh}}\right) \qquad \text{(b)} \qquad (5.5)$$

The introduction of this offset σ_b allows the inclusion of all of the relaxation data for high strain tests in the fitting procedure. Also, this provides a framework for varying σ_b as necessary as a function of other test parameters.

The fitting procedure, as described previously, is substantially the same as for the Eq. 5.1 modified version of the Landgraf model. The only difference is that the stress data for tests with

relatively high strain amplitudes are included in the multiple linear regression as shifted by an offset value corresponding to their strain amplitudes. This in effect shifts the zero of each affected test to a stable compressive value. In particular, Eq. 5.5 causes Eq. 5.1 to be modified to a version that includes σ_b, leading to new values of *y* for the multiple regression, so that *y* in Eq. 5.2 is replaced by y in Eq. 5.6.

$$y = \log\left(\frac{\sigma_{mN} + \sigma_b}{\sigma_{mi} + \sigma_b}\right) \tag{5.6}$$

As an additional improvement to the quality of the fitting, since the number of data points per test may vary depending on the life to failure, a weighting technique is applied such that each test has a weight of 1.0 in the overall fitting procedure. Hence, each data point for a particular test is assigned a weight of 1.0 divided by the number of data points for the test.

5.4.3 Fitting 7075 and 7249 relaxation data

The relaxation curves obtained from testing are fitted to the Landgraf model. All the tensile and compressive mean stress curves are fitted to the model with the inclusion of the relaxation offset σ_b.

Before proceeding with the multiple linear regression to obtain the fitting constants from all the relaxation tests, the relation between σ_b and ε_a has to be determined. A careful examination of the variation in the offset for the tests conducted was performed. The values of stable mean stress for the tests with high strain amplitude in Figure 5-14 are plotted versus strain amplitude. The analysis of completely reversed tests lead to the observation that a stable compressive value was also obtained for some high strain tests with zero mean strain. This information was used to validate the relation between relaxation offset and strain amplitude.

The values of σ_b are taken to be zero for relatively small strain amplitudes, and then they are fitted as varying linearly with strain amplitude above 0.74% for 7075 Al, and 0.61% for 7249 Al, until they reach a constant value, corresponding to the stable negative stress reached in high

strain tests with zero mean strain. This fitting is shown in Figure 5-14, and values for the indicated points *A* and *B* are given in Table 5-8.

Note that the values plotted in Figure 5-14 are the observed offsets with negative values, which correspond to $-\sigma_b$. Hence, σ_b in Eq. 5.5 is a positive quantity, which causes σ_{mN} to approach $-\sigma_b$, as manipulation of Eq. 5.5(a) shows.

$$\sigma_{mN} = (\sigma_{mi} + \sigma_b)N^r - \sigma_b \qquad (5.7)$$

The multiple linear fitting can be performed once the relaxation offset is calculated. To assure the best possible fit for the relaxation results, the weighted fitting technique previously described is applied. The resulting values of *A* and ε_{aTh} for the two alloys and their ranges of applicability (as separated by ε_{a12}) are given in Table 5-9. Note that ε_{a12} = 0.675% for 7075 and ε_{a12} = 0.0645% for 7249. Figures 5-15 and 5-16 show the mean stress versus cycles curves from this modeling along with the test data. The numbers and letters identifying individual tests in Figures 5-15 and 5-16 refers to Table 5-7, and test details are found in Table A.1 and Table A.2. Further, Figure 5-17 compares *r* values fitted individually for each test to the lines resulting from the multiple regression, as given by the constants in Table 5-9. Also, the strain amplitudes ε_{a12} that separate the two regions of behavior are plotted on the cyclic stress-strain curves of Figure 4-17, where they correspond approximately to the level below which plastic strains are so small as to be difficult to detect, which might be considered a "proportional limit."

Good agreement is obtained between this modeling and the overall trends in the data, and significant improvements are achieved relative to the previous results [43], especially in the high strain region. The introduction of the empirical offset in the Landgraf model is considered to be successful.

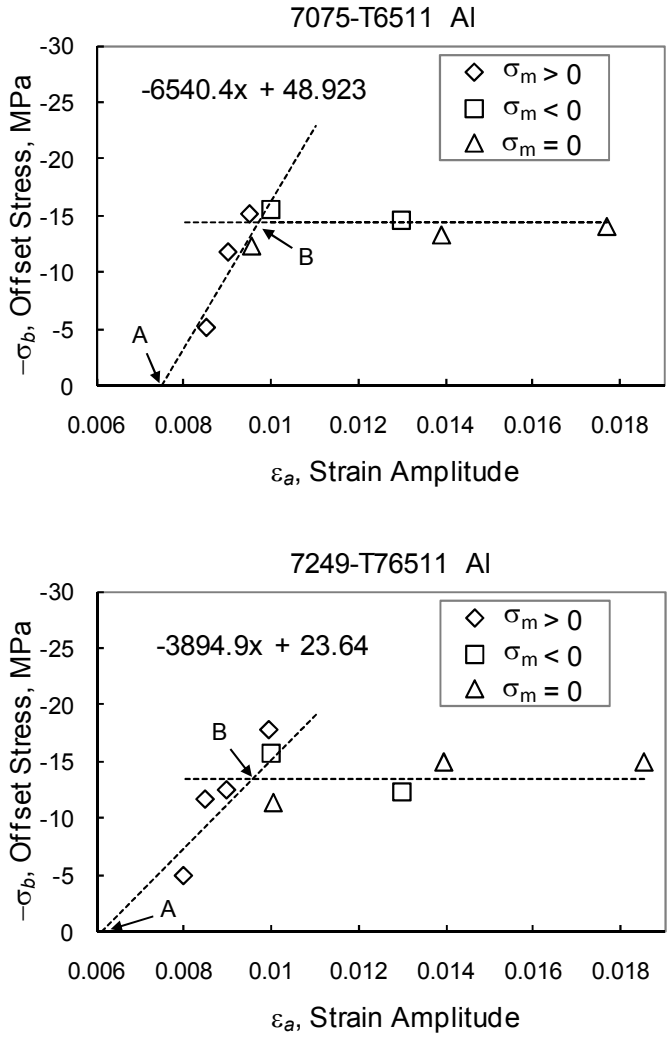

Figure 5-14. Empirical stress offset σ_b as a function of strain amplitude, as used in modeling.

Table 5-8. Points Identifying Empirical Mean Stress Offsets

Alloy	Point A		Point B	
	ε_a	σ_a, MPa	ε_a	σ_a, MPa
7075-T6511	0.00738	0	0.00968	−14.40
7249-T76511	0.00607	0	0.00952	−13.45

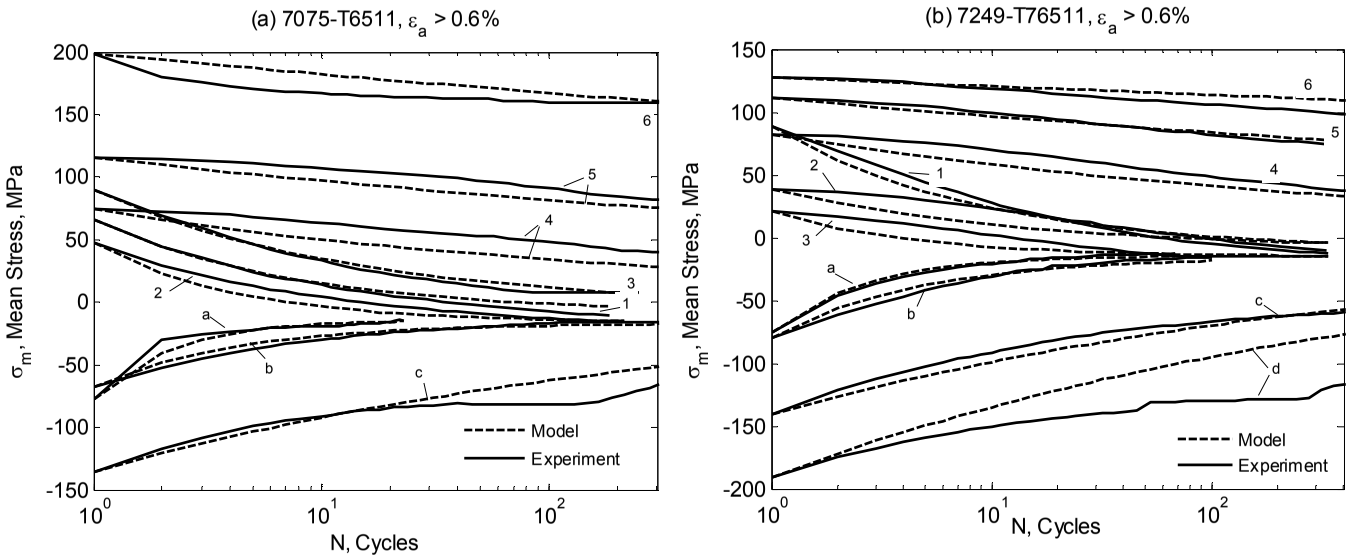

Figure 5-15. Mean stress relaxation and offset modeling for high strain amplitudes in the two alloys.

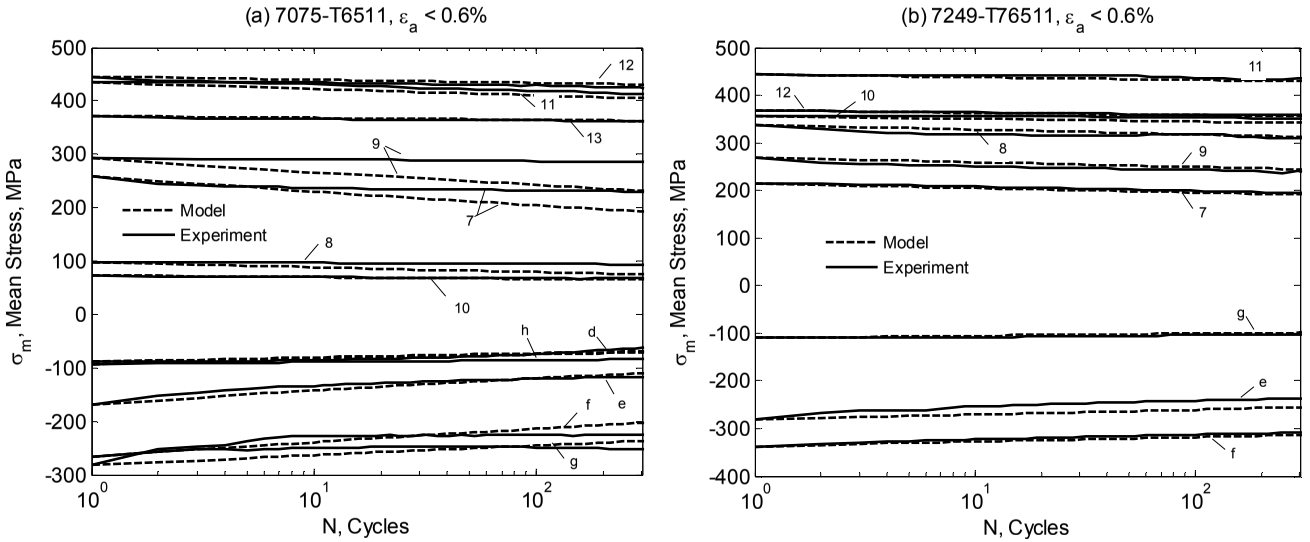

Figure 5-16. Mean stress relaxation and offset modeling for low strain amplitudes in the two alloys.

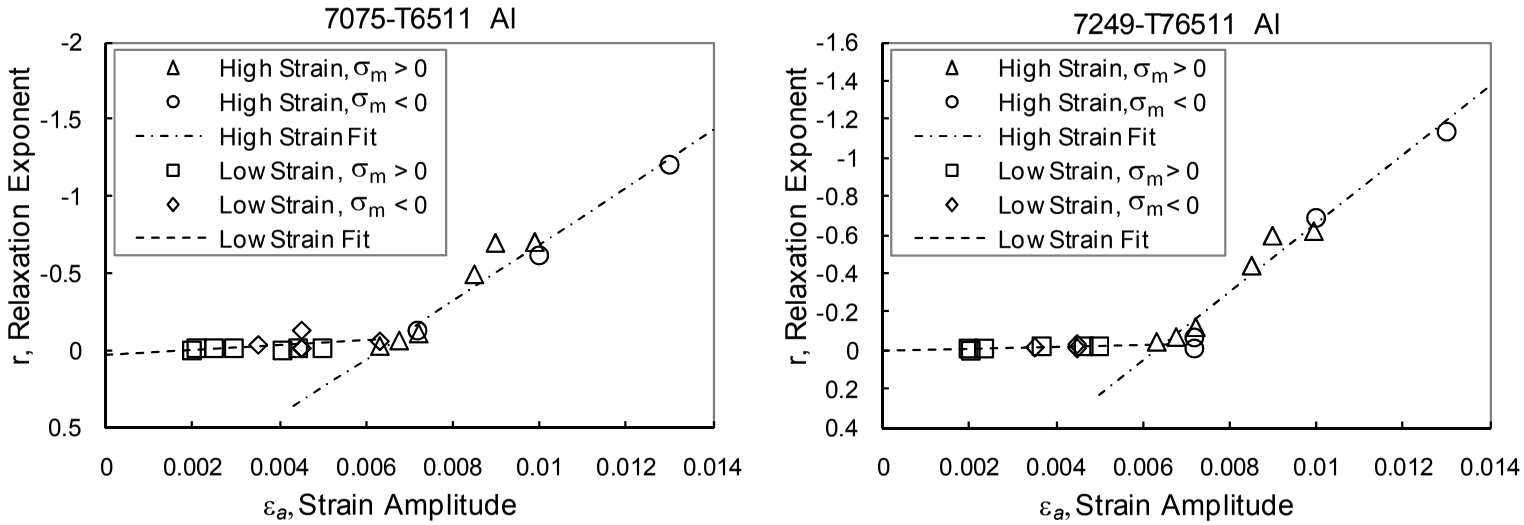

Figure 5-17. Relaxation exponent versus strain amplitude for the two alloys.

Table 5-9. Mean Stress Relaxation Constants for the Landgraf Model with a Stress Offset

Alloy	Range	A	ε_{aTh}	Corr. Coef.
7075-T6511	$\varepsilon_a \le 0.675\%$	0.02711	0.001641	0.672
7075-T6511	$\varepsilon_a \ge 0.675\%$	1.1759	0.006299	0.972
7249-T76511	$\varepsilon_a \le 0.645\%$	0.00384	0.000812	0.894
7249-T76511	$\varepsilon_a \ge 0.645\%$	1.1286	0.006305	0.943

Chapter 6
Mean Stress Relaxation in Variable Amplitude Loading

A total of 13 variable amplitude loading tests for 7075 and 12 for 7249 are run to observe mean stress relaxation in variable amplitude loading. One test per category of loading (shown in Figure 3-7) for alloy 7075 will be shown in this section, but all the variable amplitude loading results are shown in Appendix C. Simulations of variable amplitude loading are shown in Appendix D.

6.1 Representative test results

A total of thirteen Type A variable amplitude tests have been run on the two aluminum alloys. The attention to this simple type of loading, with schematic representation shown in Figure 3-7 (a), is due to a need in screening relaxation models for simple loading cases. The Type A test shown in Figure 6-1 has a larger hysteresis loop with amplitude equal to 0.9% strain and a smaller hysteresis loop with strain amplitude equal to 0.5% strain, repeated ten times. The larger hysteresis loop has strain amplitude and maximum and minimum strain limits equals to one of the constant amplitude loading tests run, namely 75NLB-1. The amplitude of the small loop is purposely chosen in the region $\varepsilon_a < \varepsilon_{a\mathrm{Th}}$, but close to the strain amplitude threshold observed in constant amplitude loading fitting.

In this case and as a general trend the larger hysteresis loop is the one leading the relaxation process in variable amplitude loading, as observed in Figure 6-1. The small loops undergo a certain amount of relaxation also, but the final position of the loop in the stress-strain space seems more due to the relaxation of the large loop. It is anyway noticeable that the small hysteresis loop relaxing inside the larger one has some influence on the overall relaxation . To visualize this, the relaxation of the same large hysteresis loop in constants and variable amplitude loading is plotted in Figure 6-2.

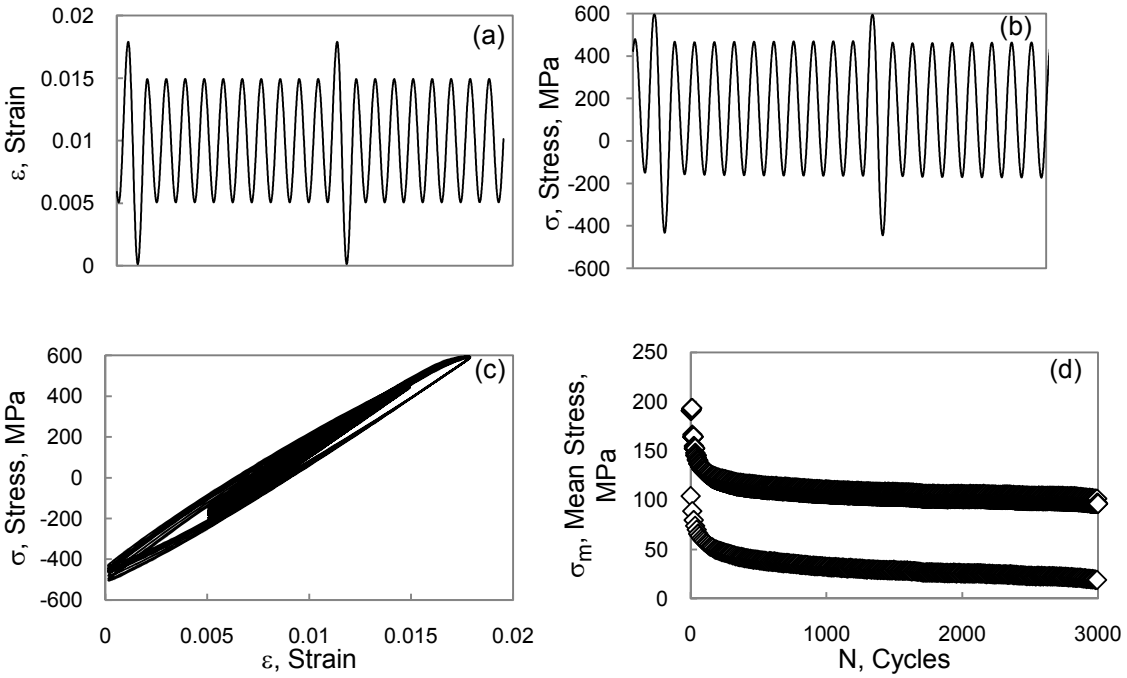

Figure 6-1. Type A variable amplitude loading test for 7075-T6511. Test number is B75-54 and show are the strain control (a), the stress response (b), the stress-strain response (c) and mean stress relaxation (d).

The relaxation of the hysteresis loop in constant amplitude loading is shown in Figure 6-2 (a) along with the variable amplitude loading test and with the bigger hysteresis loop alone in Figure 6-2 (b). Mean stress values for the constant amplitude test are chosen at a logarithmic interval with respect to the number of cycles. The relaxation response is also "expanded" so that each cycle number for the large loop in variable amplitude loading corresponds to the same cycle number in constant amplitude loading. The initial mean stress for the larger loop in constant amplitude loading is significantly lower than the one in variable amplitude loading. The amount and rate of relaxation is comparable, but for the constant amplitude loading case it seems slightly higher. Also, in the constant amplitude loading case the loop is relaxing to a compressive value, while in the variable amplitude loading case it is stabilizing at a tensile value. Such a high difference in initial mean stress value for the two cases is without doubts determining the stable value for the mean stress. This difference cannot be only due to scatter in test data. The relaxation of the small mainly elastic loop is potentially interfering with the stress-strain response of the material when loading up to the maximum point for the larger loop.

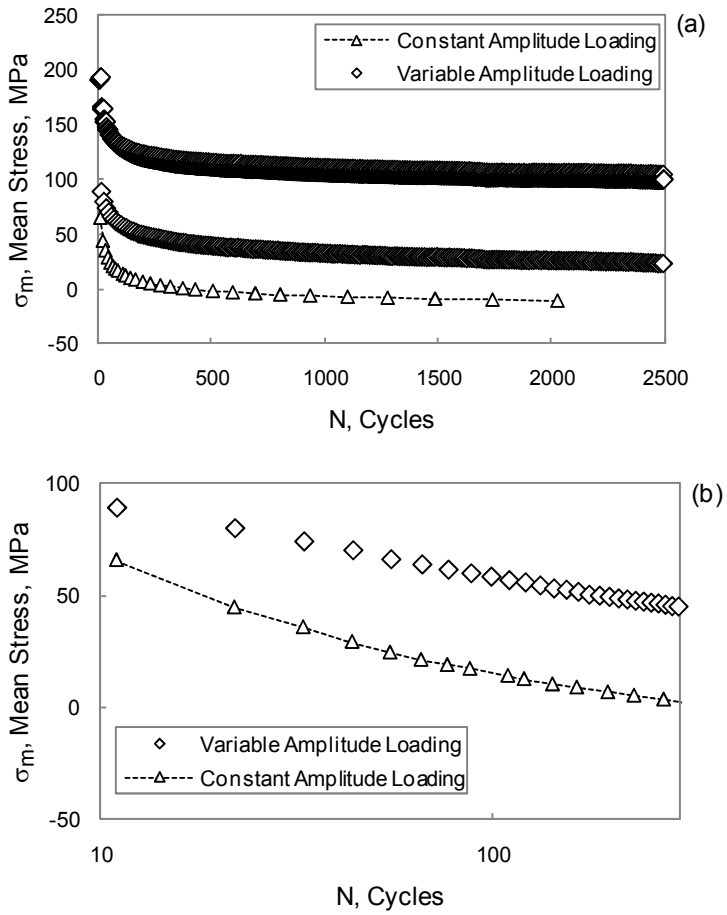

Figure 6-2. Comparison of mean stress relaxation for 0.9% strain hysteresis loop in constant and variable amplitude loading conditions.

One Type B relaxation test is shown in the Figure 6-3, in this case the big loop had a strain amplitude of 1.35% and the two smaller loops of 0.6% and 0.4% respectively.

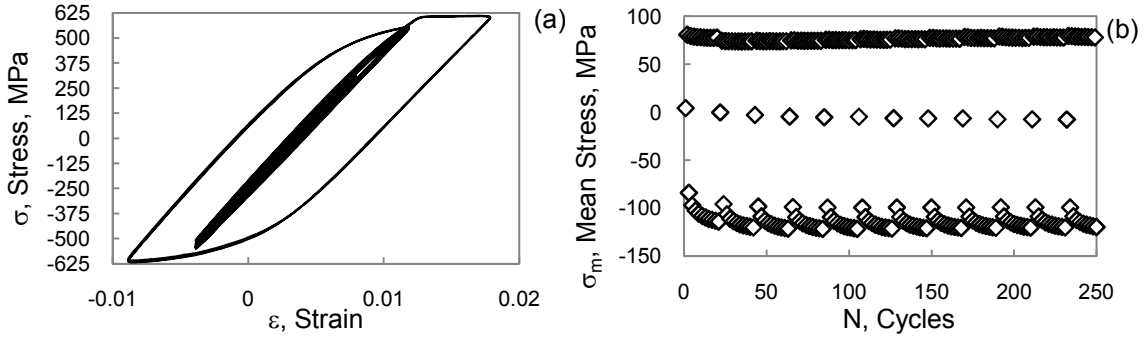

Figure 6-3. Type B variable amplitude loading test for 7075-T6511. Test number is B75-28 and the stress-strain response (a) and mean stress relaxation (b) are shown.

It is surprising that the smallest loop in the history is undergoing continuous cyclic relaxation of approximately the same amount each time it is repeated without stabilizing. The loop is shifting down following the largest hysteresis loop, but, during its ten repetitions, it is undergoing a significant level of cyclic relaxation. This phenomenon will be referred from here as: unstable repeated relaxation.

Not a lot of difference in the behavior can be identified with respect to the Type A tests for the larger loop, other than the mentioned unstable repeated relaxation behavior. The trend is generally similar to the Type A variable amplitude test, therefore only one test of this kind was performed.

An example for the third type of loading pattern studied, a Type C variable amplitude loading, is shown in Figure 6-4. In this case the large loop has a strain amplitude of 1.2% and two 0.6% strain amplitude hysteresis loops are repeated 10 times each inside it.

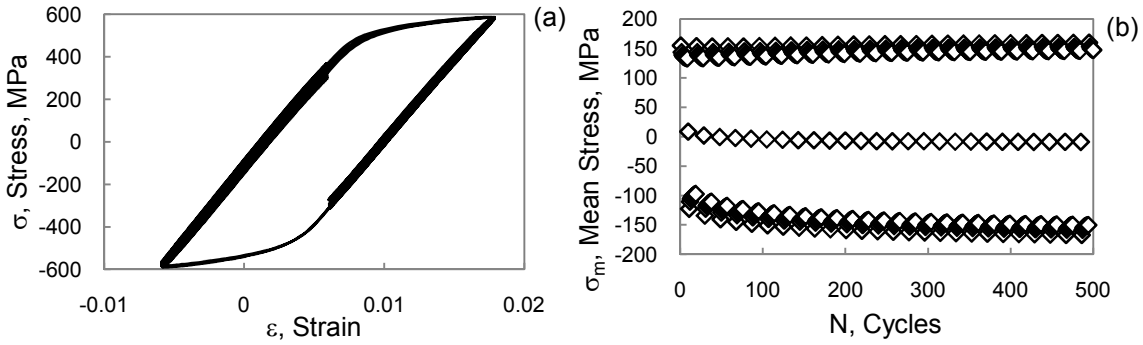

Figure 6-4. Type C variable amplitude loading test for 7075-T6511. Test number B75-26, and the stress-strain response (a) and mean stress relaxation are shown (b).

Unstable repeated relaxation for the smaller loops is even more evident in this type of loading. Surprisingly the small tensile loop is not gradually shifting down following the larger loop, but it seems constantly at the same mean level of stress. This can be possibly explained by the fact that it is generally observed for histories with tensile bias that valleys are more responsible for relaxation than peaks. The examples of constant amplitude loading relaxation reported in Appendix B generally show a higher degree of relaxation for valleys in the peak-valley plot. This is also confirmed by the stress-strain plot of the Type A test in Figure 6-1: the valleys of the hysteresis loops undergoes a

higher level of relaxation than the peaks. Therefore it is possible that the small tensile hysteresis loop, relaxing right after the peak of the larger hysteresis loop, is not as much influenced by the shift of the larger loop as the small compressive hysteresis loop.

The last example of results from variable amplitude loading test is a spectrum loading obtained from a helicopter loading profile. This profile was normalize so that the maximum strain was 1.8%.

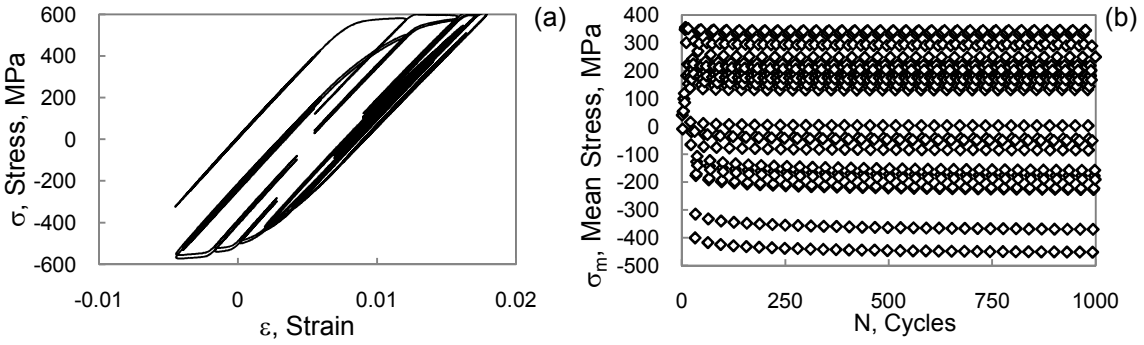

Figure 6-5. Service type of variable amplitude loading test for 7075-T6511.

The response to this loading is shown in Figure 6-5. In this service type of loading the amount of relaxation is comparable to the simpler cases, reassuring the validity of the strategy for studying relaxation phenomena.

In more complex loading, observations on the influence of small and large strain amplitude loops are more difficult, due to the high number of loops involved. Main trends can be generally confirmed, with a large loop leading the relaxation and compressive loops undergoing a more significant amount of relaxation than the tensile ones. Moreover, the compressive mean stresses are stabilizing at a higher compressive value than the initial ones. The large presence of hysteresis loops in the tensile portion of the stress-strain space might be the reason for a relaxation towards more negative values. The high degree of relaxation in the tensile side of the loop might drag down the compressive mean stresses, ideally directed to relax to a less severely compressive situation.

6.2 Tentative application of Landgraf model to variable amplitude loading

6.2.1 Landgraf approach to variable amplitude loading

The Landgraf model showed good agreement with experimental data for constant amplitude loading. The formulation proposed gives satisfactory results in all cases, for tensile and compressive mean stresses, with higher or lower values of strain amplitudes, as shown in Chapter 5.

The Landgraf model was adapted to simulate variable amplitude loading. A code was developed in Matlab to be used with any type of loading and capable of applying the principles of the Landgraf model to every segments that compose a loading.

The Landgraf model for variable amplitude loading uses the Ramberg-Osgood constants obtained from the stress-strain analysis. The program is able to apply the rain flow counting method to a loading history and assign to each cycle a certain amount of relaxation. This is performed by counting the number of cycles while the simulation is running and calculating for each segment the amount of relaxation based on the strain amplitude of the segment itself.

The program uses the counting method results to individualize the closing or potentially closing hysteresis loops in the loading. Once those points are obtained, the amount of relaxation for the closed or potentially closing loop is calculated by applying the constant amplitude loading Landgraf relation. For simplicity, the Landgraf model without the use of the offset σ_b is initially used.

For every loading segment a new value of *n'* for the Ramberg-Osgood equation (Eq. 1.1) is also calculated for the closed or potentially closing loop, based on the starting point and final point of the relaxed loading of the loop. This value is used in successive loading to calculate the ending point of the segment, in case it is different from the loading segment closing the loop.

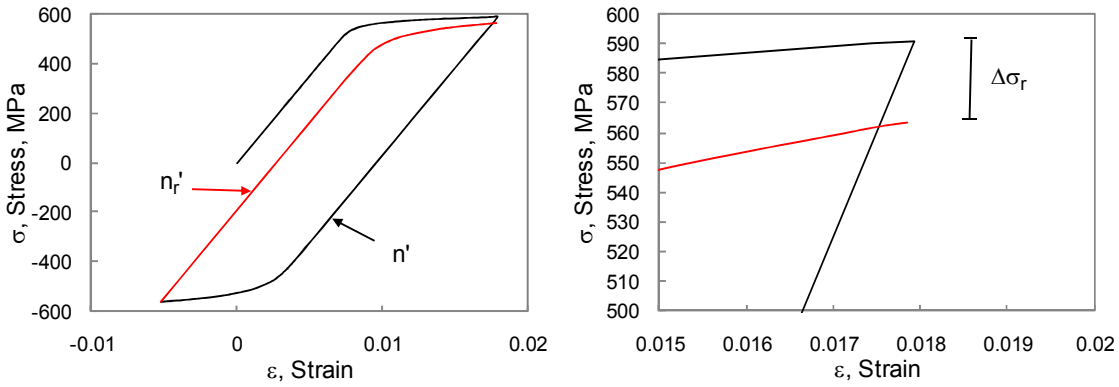

Figure 6-6. Example of Landgraf application to variable amplitude loading: a new hardening exponent for the Ramberg-Osgood relation is calculated with the use of $\Delta\sigma_r$.

In Figure 6-6 a relaxing loop is shown: a new hardening exponent n_r' for the Ramberg-Osgood equation is calculated given the amount of relaxation $\Delta\sigma_r$ as if the loop is closing. The new exponent is then used to calculate the ending point of the segment, that might or might not be closing the hysteresis loop. In Figure 6-7 the principle of the application of the Landgraf model to a variable amplitude loading is shown. The new hardening exponent, calculated as if the cycle is closed, it is used to find the peak of the loading segment. The STOP signs in Figure 6-7 show the possible ending points of the segment in the loading.

This way the amount of relaxation for each segment can be estimated with the Landgraf model and rain flow cycle counting can be performed at the same time. This formulation would be particularly convenient since it doesn't change the core of a strain-based approach.

Some perplexities arise about the way to account for the term N, number of cycles, in the Landgraf approach. First of all, relaxation is observed mainly as a transient phenomenon, so most of the decay happens in the early part of the life. If cycles are counted independently on their amplitude, most of the relaxation for smaller loops will be lost in the history and it will be highly reduced for bigger loops. Second, the simulated stress-strain behavior will not be reproducing real material behavior in variable amplitude loading, but forced to follow an empirical relation valid in constant amplitude loading.

At the moment, the cycles are counted one after another as they occur, and simulations observed.

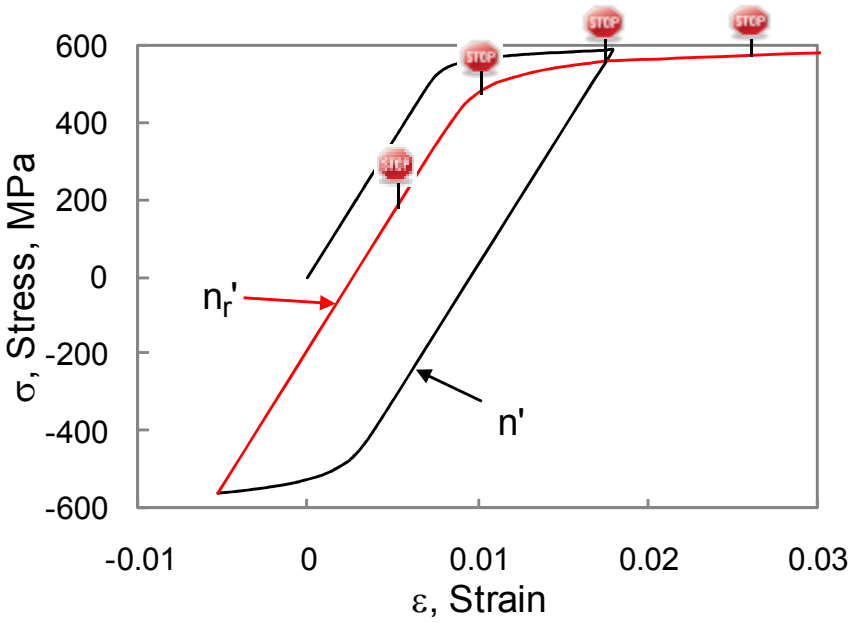

Figure 6-7. Possible ending points of the loading segment with new n_r', calculated with the Landgraf relation.

6.2.2 Simulations

Constant amplitude loading simulations are performed to test if the adaptation of the Landgraf approach to variable amplitude loading is successful in reproducing the tests run in constant amplitude loading. Experimental curves for 7075 are compared to the simulations, plotting the values of mean stresses obtained in Figure 6-8 and 6-9.

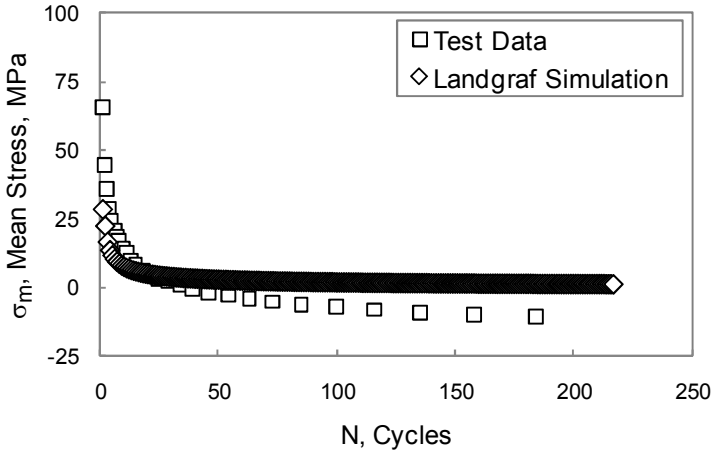

Figure 6-8. Constant amplitude loading simulation with Landgraf model, corresponding to 75NLB-1, test 2 Table 5.5 for 7075.

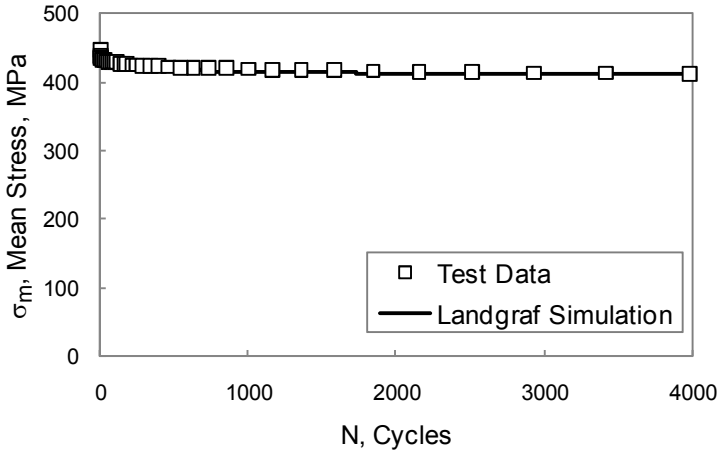

Figure 6-9. Constant amplitude loading simulation with Landgraf model, corresponding to 75NLB-3, test 12 Table 5.5 for 7075.

The simulation results in Figures 6-8 and 6-9 are close to the experimental data for constant amplitude loading cases. The first simulation tends to relax to a zero value for mean stress since the offset part of the Landgraf model is not included. In both cases there are differences in the initial stress-strain response, visible from a different value for the initial mean stress. This is expected since the Ramberg-Osgood constants and formulation is a model for the stable behavior of the material. Differences are limited and the real interest for life calculation is the stable value of mean stresses, since small differences for a small number of cycles are a negligible cause of life calculation errors.

Three representative variable amplitude loading patterns are simulated with the Landgraf model. The first simulation is shown in Figure 6-10 corresponding to a Type A variable amplitude loading whose experimental results are shown in Figure 6-1. The second simulation involves a Type C loading: the same loading pattern shown in Figure 6-4 is plotted in Figure 6-11 along with the simulated Landgraf response. Finally the service type of loading shown in Figure 6-5 is also simulated and mean stresses compared to the ones obtained with the Langraf model. The simulation along with experimental data is shown in Figure 6-12.

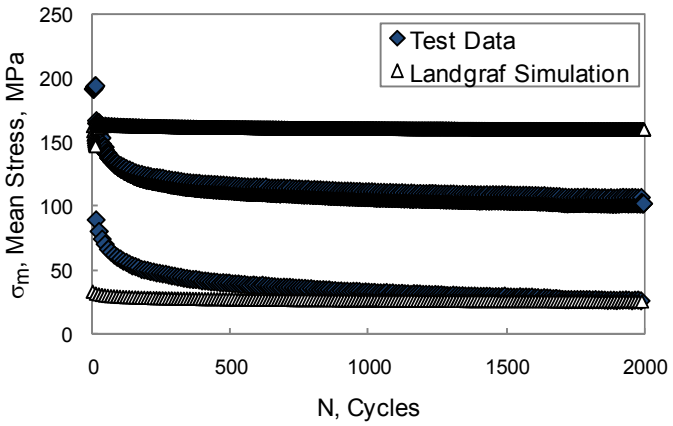

Figure 6-10. Type A variable amplitude loading simulation with Landgraf model, corresponding to test B75-54 for 7075. The mean stress relaxation response is shown.

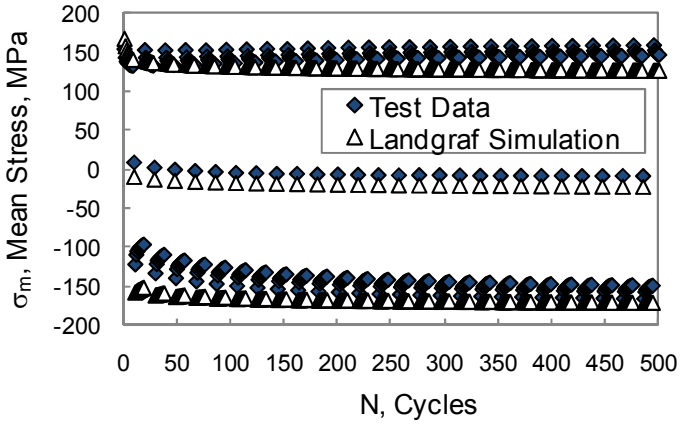

Figure 6-11. Type C variable amplitude loading simulation with Landgraf model, corresponding to test B75-26 for 7075. The mean stress relaxation response is shown.

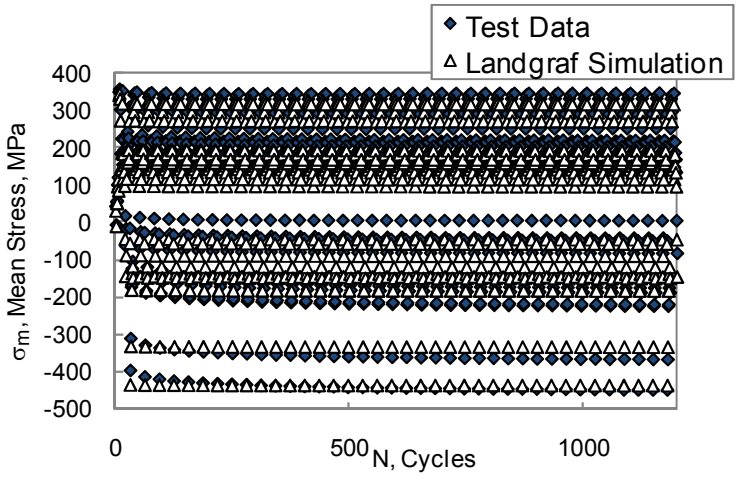

Figure 6-12. Spectrum variable amplitude loading simulation with Wetzel, corresponding to test NAV1-75-15 for 7075. The mean stress relaxation response is shown.

The results for variable amplitude loading are less satisfactory. In the case of the Type A variable amplitude loading, the stable value for the smallest of the two loops is off of approximately 50 MPa. The large loop starts from a different mean stress value, but stabilizes to a similar stable value.

The Type C loading shows the first main limitation of the Landgraf model: the relaxation occurring for the first ten repetitions of the small tensile biased loop is large, due to the fact that the number of cycles goes from 1 to 10 and it reproduces what it would happen in a constant amplitude case. It then suddenly stops, because the number of cycles is constantly increasing. This big difference between initial and final amount of relaxation is an artifact of the Landgraf model itself. It is not a totally unacceptable result, but it is the symptom of an erroneous application and handling of the relaxation process.

For the case of the spectrum-type of loading, results are not easily interpretable due to the large number of different curves of relaxation. Generally it doesn't seem that mean stresses are excessively off the ones obtained in testing, but they show a small amount of relaxation with increasing number of cycles. This is possibly due to the same artifact, relaxation practically stops when N, base of the exponential decays, becomes large enough.

6.3 The Wetzel model

6.3.1 The stress-strain curve

The striking simplicity of the Wetzel model made it a good candidate for the incorporation in a life calculation routine or program. The model falls in the category of incremental plasticity models with a multiple number of yield surfaces. The formulation of the model and a simulated response were introduced in Chapter 2. Despite the model definition, the implementation is fairly easy and the velocity of computation is impressive.

The Wetzel model is implemented in Matlab, and several loading profiles are tested to validate its performance. Data fitting is required for implementation, and the first constants needed in the model are the steps in stress and strain taken from the cyclic

stress-strain curve. In fact the stress-strain response of the Wetzel model is given by a summation of stress and strain increments, as in:

$$\sum_{j=1}^{n} d\sigma_j = k_{jj} \sum_{j=1}^{n} \varepsilon_j \qquad (6.1)$$

where the different $d\sigma_j$ and $d\varepsilon_j$ are obtainable from the segmentation of the stress strain curve, as shown in Figure 6-13.

To complete the implementation of the model, the constant M_r of Eq. 2.18, controlling the relaxation behavior is also needed.

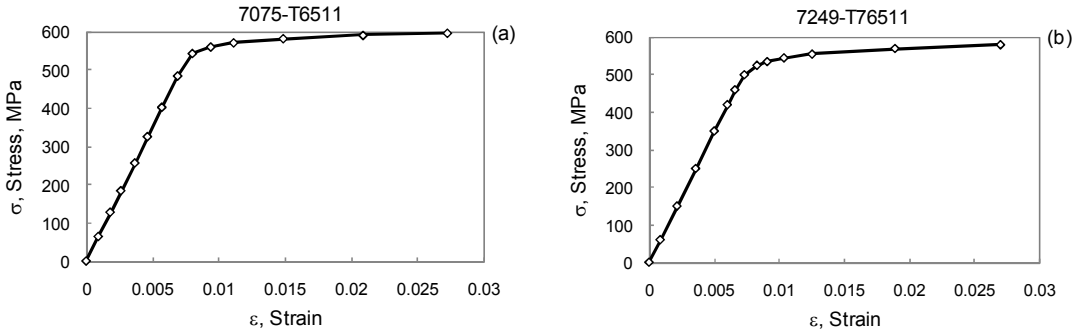

Figure 6-13. Stress-strain segments of the Wetzel model for 7075-T6511 (a) and 7249-T76511 (b).

In Figure 6-13, the division of the stable stress-strain curve is shown for both aluminum alloys. The way the curve is divided in segments was decided based on the principle that the elbow of the curve needed a greater number of segments than the elastic initial part or the flatter last part of the curve. There is a slightly different attention in the elbow section for the modeling of the two materials. For 7075, there are approximately three segments in the curving section, while for 7249, four segments are used to make the model. This was done with the intention of observing if any significant improvements would be obtained with a more accurate modeling of the section close to the cyclic yield point when dealing with the relaxation behavior.

The stress-strain modeling for Wetzel is easily obtainable and does not require any ad hoc tests to be run, making it convenient in the perspective of inclusion into life calculation. In addition, the modeling of the curve is derived from a rheological spring-

slider model. Therefore, once included into the routine of loading, it takes care of memory effects and hysteresis loops closure by itself, without further analysis on the loading.

The appeal of the Wetzel model among all the rest of the plasticity model is also due to the particularly efficient way of dealing with transient effects. Not only can mean stress relaxation be modeled in Wetzel, but also hardening or softening can be added to the stress-strain relationship. Hardening and softening are not implemented in the Wetzel model, since they are not of interest for the current study, as those alloys have little effect of this type.

The material constant needed to control relaxation is M_r; given a certain number of representative relaxation curves, trial and error methods can be applied to obtain the relaxation constant for a material. In this study, constant amplitude relaxation curves are used to estimate a value for M_r. The way this is done is through a target function to be minimized. This function is the difference between the peaks and valleys of simulated responses with the peaks and valleys of experimental data.

6.3.2 The relaxation constant M_r

The formulation of relaxation in Wetzel leads to the conclusion that all the mean stresses tend to relax to a zero mean stress condition; i.e. all the biased states of deformation tend to stabilize at the completely reversed state. Experimental data though clearly showed that if this is the case for large strain amplitudes, the relaxation of smaller loops highly biased in both tension or compression tends to a stable value different from zero. Since mean stress relaxation occurs mostly in the first part of the life, the stabilization of smaller loops to a completely reversed case will possibly lead in life calculation to dangerous non conservative predictions if the Wetzel model is used.

Data from simulations of constant amplitude loading relaxation tests and experimental data from the same tests are compared through the peaks and valleys of the stress response. Peaks and valleys from experimental data are recorded during the tests, and simulated peaks and valleys are collected during the simulation. The normalized root mean square value of the difference between the two is used as a parameter for comparison. Trial and error methods are used to minimize the normalized root mean

square: the best value of M_r for a constant amplitude relaxation test is the one that minimizes the difference between peaks and valleys from simulations and experimental data. The normalized root mean square is here called simulation residual:

$$s_r = \frac{\sqrt{\frac{\sum_{i=1}^{n}\left(\sigma_{\max/\min}^{\exp} - \sigma_{\max/\min}^{\text{simul}}\right)^2}{n}}}{\left(\sigma_{\max}^{\exp} - \sigma_{\min}^{\exp}\right)} \qquad (6.2)$$

where $\sigma_{\max/\min}^{\exp}$ and $\sigma_{\max/\min}^{\text{simul}}$ are the experimental and simulated peaks or valleys.

For all the constant amplitude relaxation tests run the values of s_r are plotted versus the values of M_r and the minimum of the curve is chosen to be the best M_r for for the specific relaxation test. The type of profile obtained is shown in Figure 6-14 where the range of M_r is set to go from a minimum of 10^3 to a maximum of 10^7. The steps from the lowest value up are chosen based on logarithmic rule, so that three to ten points per decades are used. Observations of the trends in areas of interest frequently lead to a decrease in the step, and a more detailed representation of the relationship is shown where needed.

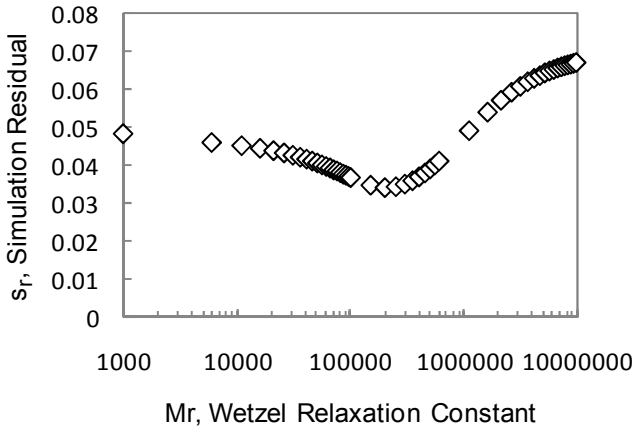

Figure 6-14. Simulation residuals for constants amplitude loading test plotted versus the value of Wetzel relaxation constant M_r.

The constants obtained are significantly high in the case of constant amplitude relaxation tests below the constant amplitude threshold $\varepsilon_{a\mathrm{Th}}$. The values obtained are in the order of 10^6. In the case of relaxation tests above the strain amplitude threshold $\varepsilon_{a\mathrm{Th}}$ the M_r's obtained are at least of two orders of magnitude smaller.

If an ideal value of M_r, able to reproduce both smaller and larger strain amplitudes, has to be obtained, this will probably be close to the mathematical average of those extreme cases.

An averaged value of Mr is then obtained from optimization of the constant amplitude relaxation tests and then used to reproduce two cases of relaxation, one with $\varepsilon_a < \varepsilon_{a\mathrm{Th}}$ and the other with $\varepsilon_a > \varepsilon_{a\mathrm{Th}}$.

The performance for larger strain amplitudes is poor because due to the influence of a high value of M_r obtained for matching test results for smaller strain amplitudes, the stress-strain response for the case of $\varepsilon_a = 0.95\%$ is showing almost no relaxation. On the other hand the simulation of the high cycle fatigue relaxation case is satisfactory, as shown in Figure 6-15.

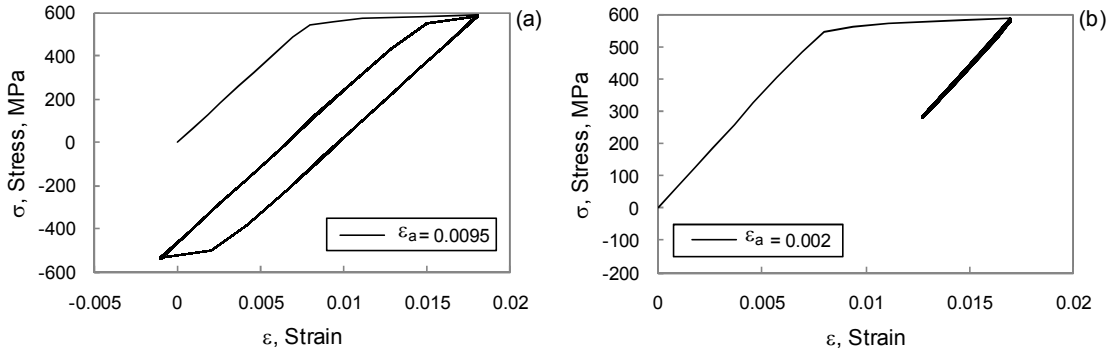

Figure 6-15. Simulations of constant amplitude loading relaxation tests with Wetzel model and averaged M_r for 7075.

The stress-strain behavior predicted by Wetzel is therefore not applicable to constant amplitude cases in the form described. An average value of M_r, obtained from optimized values of M_r at different strain amplitudes, leads to a poor response for larger strain amplitudes

If a weighted average with respect to strain amplitude is used instead of the mathematical average to obtain a value of M_r, results are very different. The value of M_r is significantly lower, in the order of 10^5, and the results are acceptable for $\varepsilon_a = 0.95\%$, but show excessive relaxation for $\varepsilon_a = 0.2\%$, as shown in Figure 6-16.

If a small value is chosen for M_r (Figure 6-17), in the order of 10^4, giving more emphasis to the large loop relaxation, the results for $\varepsilon_a = 0.95\%$ are still satisfactory, with a higher relaxation rate with respect to the weighted average. The results for $\varepsilon_a = 0.2\%$ show an even greater amount of relaxation, with respect to the weighted average case.

It seems that the Wetzel model cannot be adopted successfully to match simple constant amplitude loading cases, but successful simulations were shown in the study by Wetzel [57] for more complicated loadings. It was then decided to run a second set of simulations for cases more similar to the ones analyzed by Wetzel to observe what the behavior would be. The M_r is the one obtained from the mathematical average, since it proved to be the most conservative value.

The first loading is the Type A variable loading with experimental data shown in Figure 6-1 (a), the second loading (b) is the service type of loading in Figure 6-5.

In Figure 6-18, some of the stress-strain hysteresis loops at the beginning of the life and some at the end of the life are shown. The result of the presence of a higher number of small elastic loops in a variable amplitude loading and of relaxation handled with an averaged M_r value, leads the larger loop to relax excessively, pulling the hysteresis loop towards compression, well beyond the completely reversed case.

For both cases, the results are contradicting variable amplitude loading experimental data, where it was observed that the relaxation is mainly led by the larger hysteresis loops and it never stabilizes to such high negative mean stress values for the larger loops.

The relaxation of the large hysteresis loops in both simulations is mainly due to the fact that a greater number of smaller loops are relaxing inside, and if from one point of view, experimental data show some influence of smaller loops on larger hysteresis loops, they clearly do not show a predominance of relaxation of smaller loops on the bigger ones. It is possible that the results shown in Wetzel were given by the use of a high value for M_r, and that the high number of smaller elastic loops inside the larger loops of the

loading caused most of the relaxation behavior shown. Even if this could be acceptable from the point of view of results, in the sense that the large loop is effectively undergoing mean stress relaxation and most of the loading patterns in service are constituted by elastic cycles and occasional large overcycles, this is not acceptable from the sake of reproducing the stress-strain behavior correctly.

The Wetzel model in variable amplitude loading does not show good results, and it seems not to be applicable in its current formulation.

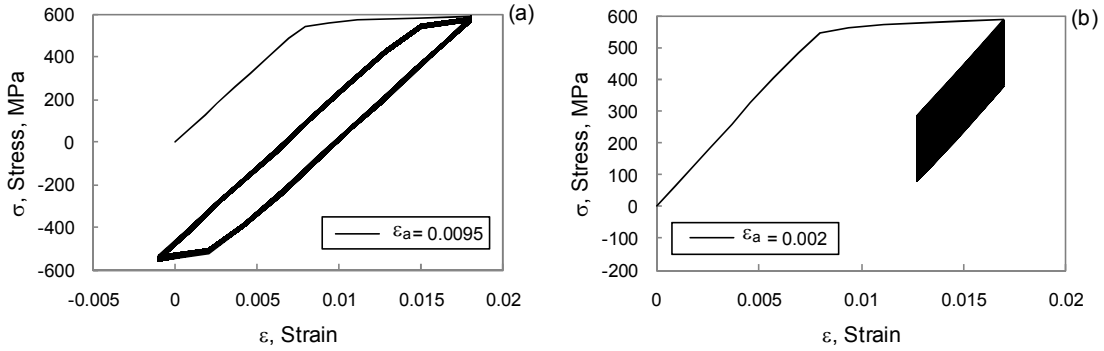

Figure 6-16. Simulations of constant amplitude loading relaxation tests with Wetzel model and weighted averaged M_r for 7075.

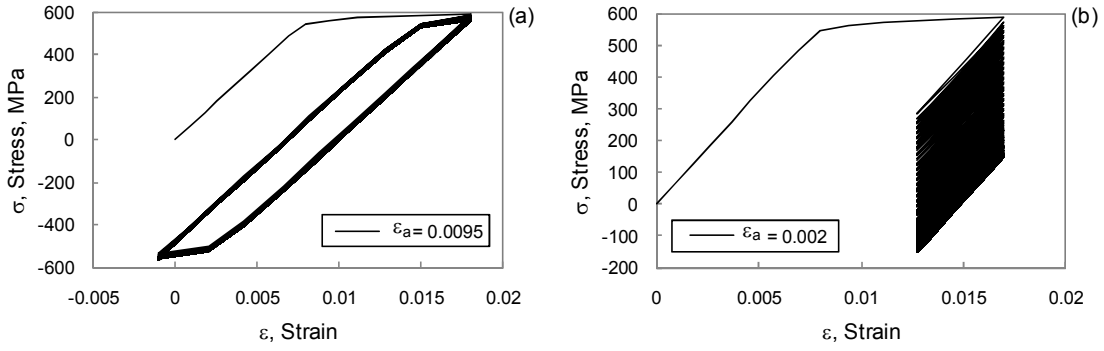

Figure 6-17. Simulations of constant amplitude loading relaxation tests with Wetzel model and optimum M_r for ε_a = 0.95% for 7075.

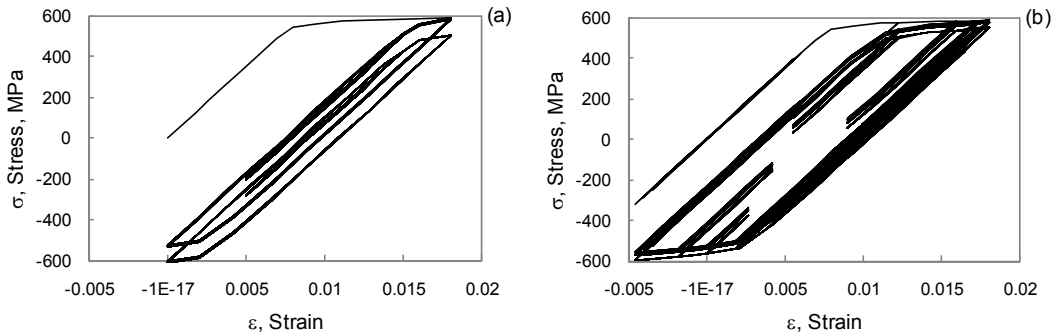

Figure 6-18. Simulations of variable amplitude loading relaxation tests with Wetzel model and averaged M_r for 7075.

6.3.3 Improvements to the Wetzel model

Given the radically different behavior observed in the two strain amplitude regions in the preliminary fitting for the Landgraf model, a distinction is needed also for the Wetzel model. The idea of having a single constant to model the relaxation behavior is convenient and appealing, but the consequences on both constant and variable amplitude loading are such that a single value for M_r has to be discarded.

It is then proposed to have a M_r constant dependent on ε_a, strain amplitude of the hysteresis loop in the loading. This means that bigger loops will relax following a smaller M_r and smaller loops, a larger M_r. To estimate the relationship between M_r and ε_a, a trial and error method is used to obtain the best value of M_r for all the constant amplitude loading tests run. The best M_r is here also the one able to minimize the simulation residual in Eq. 6.2. Then those values are plotted with respect to ε_a and trends are fitted to the data, Figure 6-19.

The fitting constants obtained from fitting of 7075 and 7249 constant amplitude loading tests are reported in Table 6-1.

Table 6-1. Summary of fitted constants for improved version of Wetzel model.

	k	p	ε_{aThW}	$M_{r\max}$
7075-T6511	-12.04	-20.86	0.00501	6433333
7249-T76511	-9.60	-15.73	0.00442	7433333

The proposed relation between strain amplitude and M_r is a good starting point in the modification of the Wetzel model, as it takes into account the observed material behavior and corrects possible misleading results that the original version would cause. The same trend is obtained with 7249, confirming a strain amplitude dependence.

The strain amplitude thresholds obtained in this case do not differ much from the ones obtained from the Landgraf model analysis and are again below the cyclic yield point for both materials.

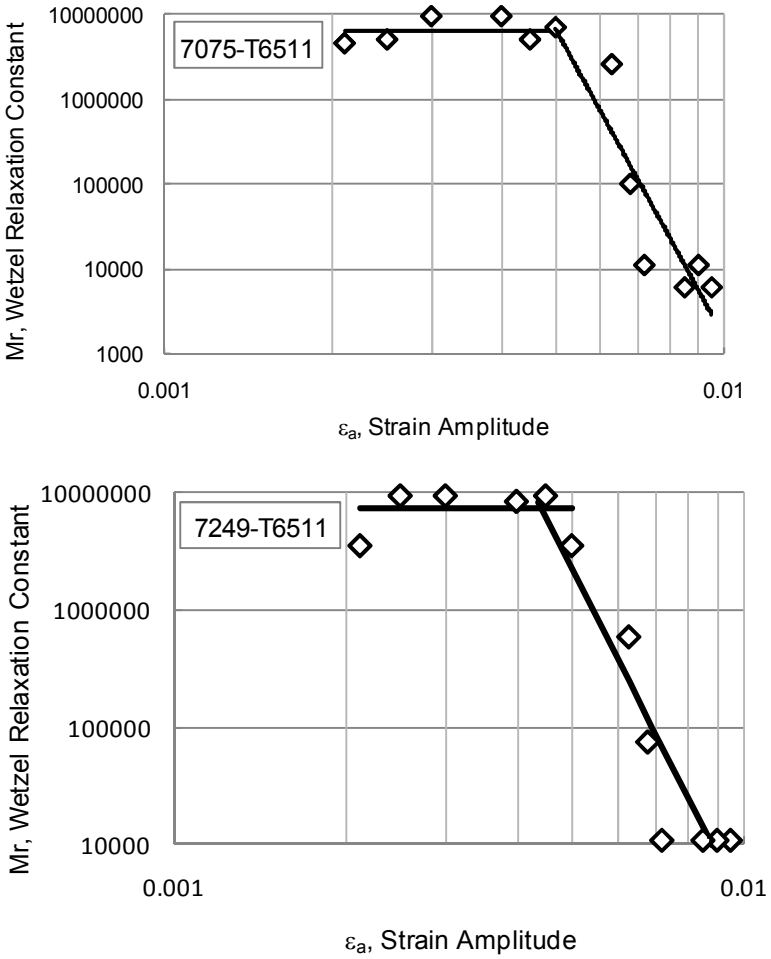

Figure 6-19. Correlation between M_r and ε_a for 7075 and 7249 in constant amplitude tests.

6.3.4 The Wetzel table approach

Even though the division of the stress-strain curve into segments is able to simulate memory effects and loop closure using a counting rule, it is not convenient when dealing with FAMS as it would require rewriting a significant part of the code.

It is possible to include the model into the life prediction software as an alternative option to the core program, but this might not be a good solution for the sponsor, as most of users trust the current version.

Since Wetzel does not have loading history memory in its formulation, but it responds to stimulation simply from its current state, a relationship among the amount of relaxation, called $\Delta\sigma_r$, the strain amplitude of the loading segment, ε_a, and the current mean stress, σ_m, can theoretically be derived from simulations in Wetzel (Eq. 6.4).

$$\Delta\sigma_r = f(\varepsilon_a, \sigma_m) \qquad (6.4)$$

The amount of relaxation per loading segment is defined as the difference between the stress at the peak or valley with respect to the stress at the previous peak or valley, as shown in the Figure 6-20.

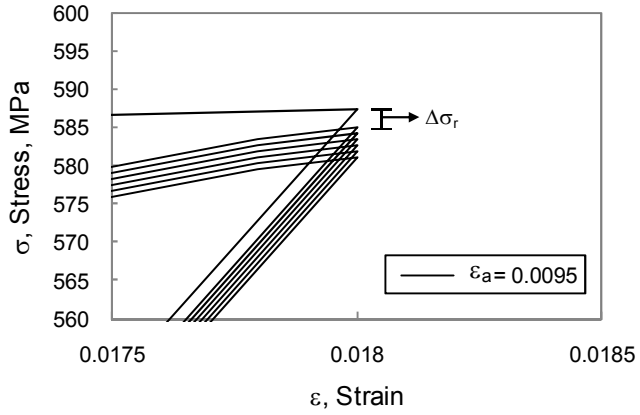

Figure 6-20. Visualization of $\Delta\sigma_r$ in a constant amplitude loading simulation with the Wetzel model for 7075.

As the modeling of a 2D function could require a high fitting effort, could need the determination of an excessive amount of fitting constants and could be of difficult

application in case of other materials, a table approach was thought more appropriate. The table will be a two entries, one exit table, where to each couple of strain amplitude, ε_{ai}, and mean stress, σ_{mj}, a corresponding relaxation delta, $\Delta\sigma_{r\,ij}$, is obtained.

Table 6-2. Exemplified relaxation table for the Wetzel model.

	ε_{a1}	ε_{a2}	…	ε_{an}
σ_{m1}	$\Delta\sigma_{r11}$	$\Delta\sigma_{r21}$	…	$\Delta\sigma_{r\,n1}$
σ_{m2}	$\Delta\sigma_{r12}$	$\Delta\sigma_{r22}$	…	$\Delta\sigma_{r\,n2}$
…	…	…	…	…
σ_{mn}	$\Delta\sigma_{r1n}$	$\Delta\sigma_{r2n}$	…	$\Delta\sigma_{r\,rnn}$

The table will be filled with values obtained from model simulations of relaxing hysteresis loops in various positions in the stress-strain space, so that a wide range of strain amplitudes and mean stresses is covered. The limits in the table, respectively ε_{an} and σ_{mn} have to be set to obtain a representative sample of strain amplitudes and mean stresses. In the current study the limits were set in dependence of the highest tension strain used in experimental tests that was around 1.8% strain.

A series of simulations were run, following the logic shown in Figure 6-21. The largest loop is defined by the limit chosen in tension and compression, respectively +1.8% and -1.8%. The mean stress relaxation loops used to fill the values of the Wetzel table are all contained in the largest loop determined by the strain limits, 1.8% and -1.8%. At a point such as P on the "container" hysteresis loop, 3 cycles P-a, 3 cycles P-b etc to P-n, are run to determine the relaxation behavior for each σ_m vs ε_a couple. Note that points such as a,b,c are spaced at intervals of 0.02%.Then the same routine is applied from point Q, spaced 0.05% from P, and similarly repeated for points all around the loop.

The discrete distribution of the points in the table will be applied to variable amplitude loading simulation with interpolation techniques. The two closest points in terms of strain amplitude and mean stress will be found with search methods in the table, and the values of $\Delta\sigma_r$ averaged, so that a value for the current (ε_a, σ_m) state can be obtained.

More refined techniques of interpolation could also be applied, but due to the low computational effort required by the Wetzel model, the best way is to increase the number of points in the Table. In addition $\Delta\sigma_r$ is frequently in the order of 1 MPa or less, and a high number of fast table search methods is available with most of the currently used software. Therefore a reduction of the maximum peak step or of the strain amplitude step will be the most efficient way to deal with a need of a higher accuracy of the Wetzel table.

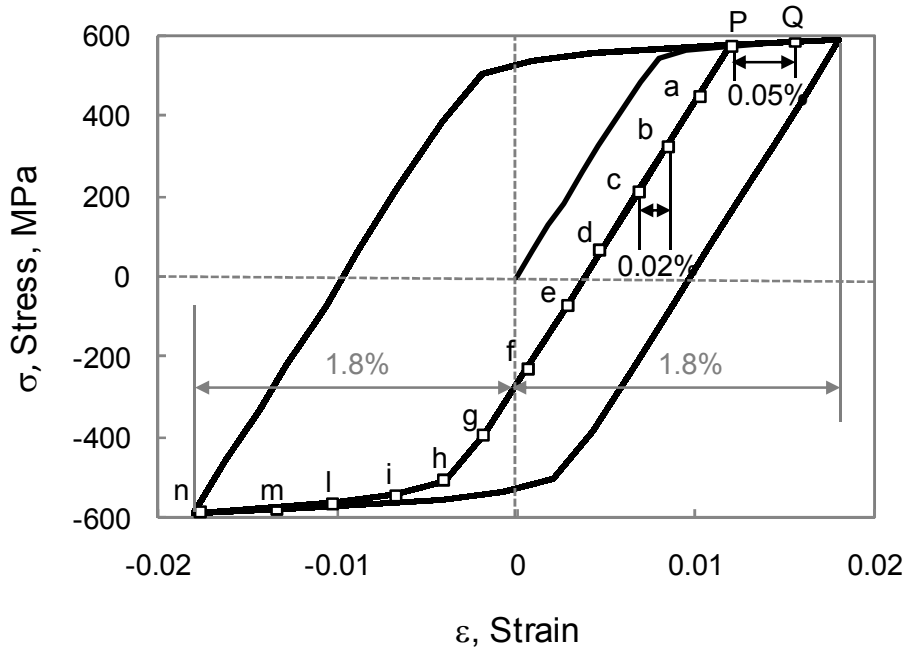

Figure 6-21. Scheme of constant amplitude loading relaxation tests to create a relaxation table for the Wetzel model.

All the steps and maximum peaks and valleys limits are adjustable according to any desired principle. In Figure 6-22 the way the stress-strain space is spanned and the 3D plot of a Wetzel table are shown.

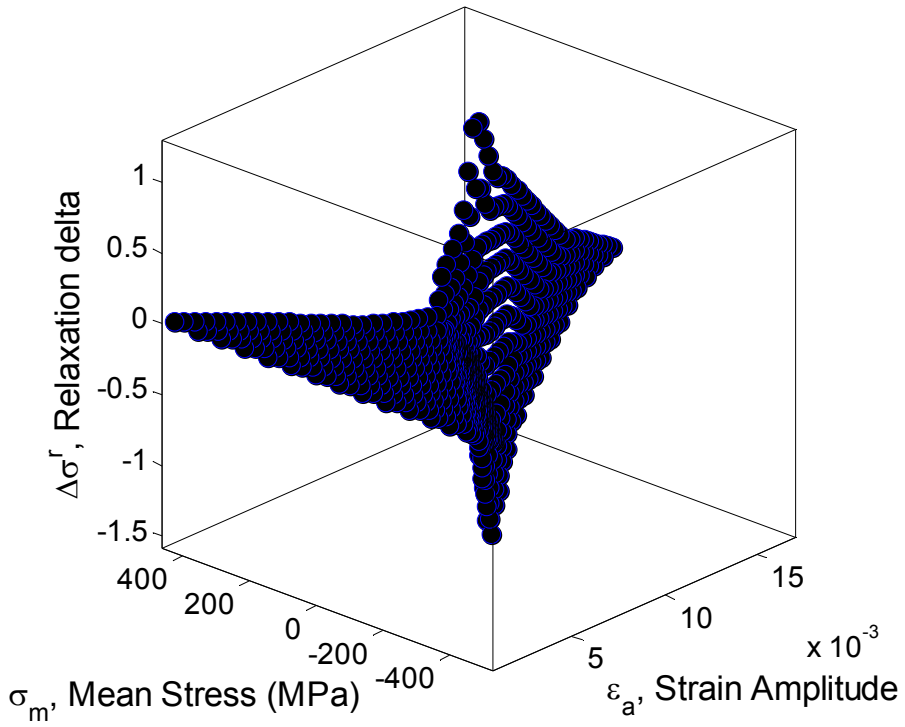

Figure 6-22. Graphical representation of the relaxation table for the Wetzel model.

As it can be observed, the more the strain amplitudes increase, the more the range of mean stresses decreases, accordingly to the highest peak and lowest valley limits set. The corkscrew type of shape in the center of the 3D plot is due to the bounded linear relationship used between M_r and ε_a and, as described previously, when the strain amplitude threshold is overcome, $\Delta\sigma_r$ values tend to increase exponentially with strain amplitude, determining a high relaxation for bigger hysteresis loops. The values of $\Delta\sigma_r$ in the region of high ε_a decrease with increasing ε_a. Note almost flat and small $\Delta\sigma_r$ at low strain amplitudes.

6.3.5 Simulations

The Wetzel model was chosen as a possible candidate for inclusion into life calculation for its computational manageability and elegant handling of the mean stress relaxation problem. The solution of using a relaxation constant M_r as a function of ε_a seems appropriate for the current scope of the research. The fitting technique used to

calculate the bounded linear relationship (in a log-log plot) between M_r and ε_a, and the M_r threshold was also successful for both aluminum alloys.

In the following section, several representative relaxation problems will be analyzed with the modified Wetzel model. The same loading profiles used for Landgraf will be included among the representative loading patterns, so that differences can be appreciated.

The Wetzel-table model will be used to reproduce mean stress relaxation in constant and variable amplitude loading, since the table version of this model is the first candidate for implementation into FAMS. The Wetzel-table model implements a version of the Wetzel model that first run independently, with a value of *f(m)*, the function responsible of changing the slope of the segments composing the loading and shown in Eq. 2.18, equals to 1. In a second step the corresponding strain amplitude and mean stress are calculated and the closest two values in the relaxation table are obtained through search methods. The corresponding values of $\Delta\sigma_{rij}$ are averaged and the $\Delta\sigma_r$ calculated is applied to the peak stress.

The Wetzel-table model is at first applied to simulate constant amplitude loading patterns. Positive and negative constant amplitude loading relaxation are also simulated with the Wetzel model for both 7075 and 7249. The results of the simulations are shown in Figures 6-23 to 6-26.

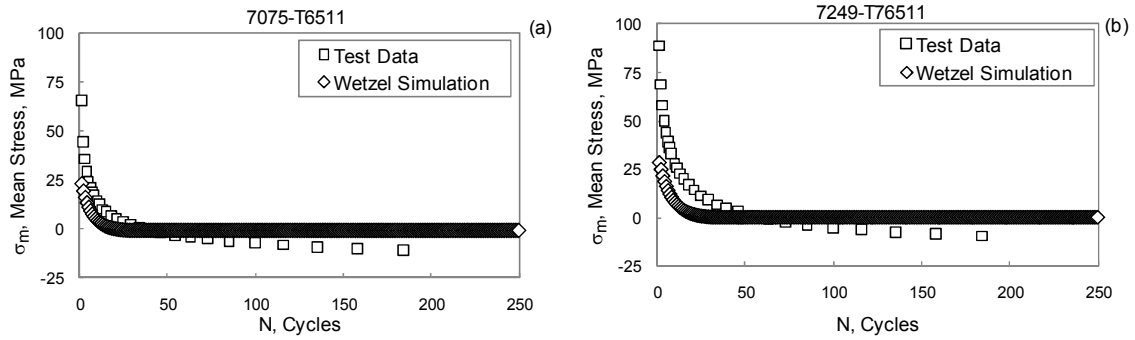

Figure 6-23. Constant amplitude loading simulation with Wetzel model, corresponding to 75NLB-1, test 2 Table 5.5 for 7075 and to 49LC-3, test 2 Table 5.6 for 7249. The mean stress relaxation response is shown.

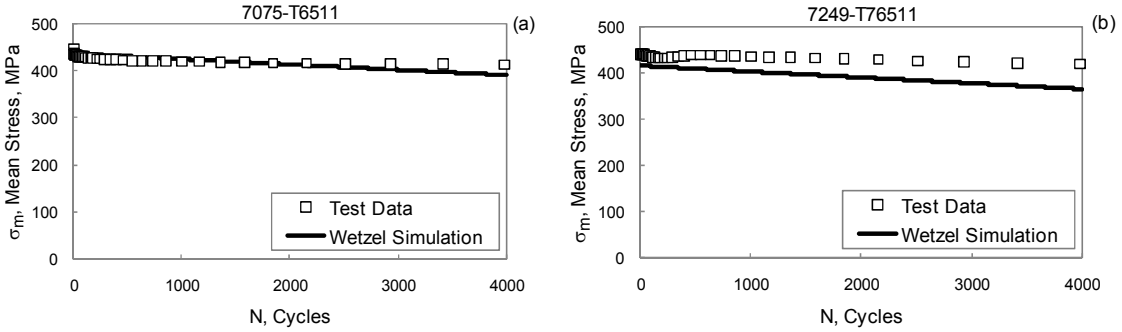

Figure 6-24. Constant amplitude loading simulation with Wetzel model, corresponding to 75NLB-3, test 12 Table 5.5 for 7075 and to 49LC-5, test 11 Table 5.6 for 7249. The mean stress relaxation response is shown.

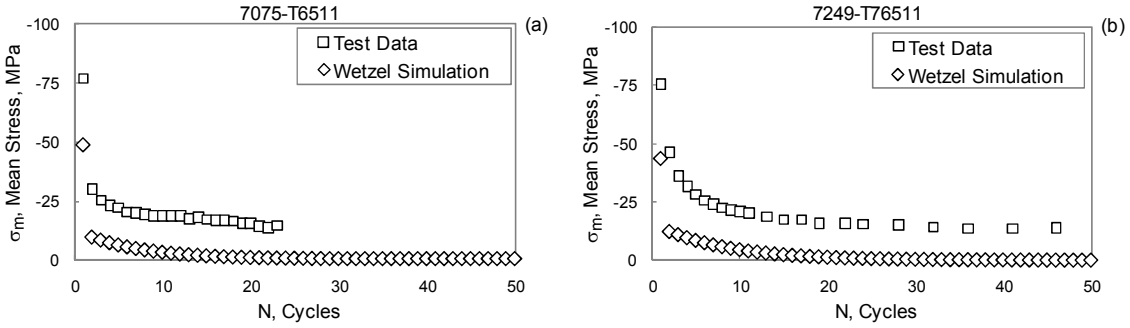

Figure 6-25. Constant amplitude loading simulation with Wetzel model, corresponding to B75-47, test (a) Table 5.5 for 7075 and to B49-27, test (a) Table 5.6 for 7249. The mean stress relaxation response is shown.

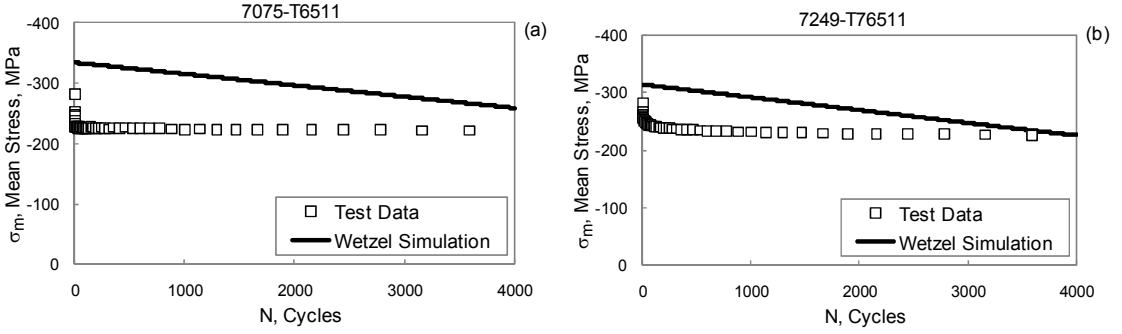

Figure 6-26. Constant amplitude loading simulation with Wetzel model, corresponding to B75-38, test (f) Table 5.5 for 7075 and to B49-53, test (e) Table 5.6 for 7249. The mean stress relaxation response is shown.

The stress-strain response of the Wetzel model causes the initial mean to be significantly different, especially when higher values of plastic strain are involved. This is expected since the stress-strain curve for Wetzel is fitted on the stable response of the material. Experimental mean stress values are usually higher than mean stresses obtained with the Wetzel model in tension, confirming the trend shown in the comparison of monotonic and cyclic behavior of Figure 1-4. In compression in the case of large strain amplitudes, Figure 6-25, the simulation has lower absolute value, while in th case of small strain amplitudes, Figure 6-26, it has a higher value with respect to test data. The errors are not excessive, with a maximum error bound of typically 50 MPa.

The relaxation response for strain amplitudes above the transition threshold for M_r ($\varepsilon_a > \varepsilon_{aThW}$) are satisfactory, having stable values that do not differ significantly at half-life of the test, as in Figures 6-23 and 6-25.

The positive mean stress relaxation test is relaxing towards a negative value, but in the Wetzel simulation this does not happen. The Wetzel model is relaxing all mean stresses towards zero in its current formulation. The relaxation rate in both cases is lower in Wetzel, mostly because the initial values of mean stress are higher experimentally, but relaxing to approximately the same stable value.

In the case of the compressive mean stress relaxation, test data show a stability close to a small negative mean stress. The Wetzel model is not able to predict this behavior and stable value is again zero. It is interesting to note that the rate of relaxation for the negative mean stresses is higher than the one for a comparable positive mean stress relaxation for test data. The model is able to predict this difference in relaxation rate for the two tests.

The response for strain amplitudes below the transition threshold for M_r ($\varepsilon_a < \varepsilon_{aThW}$) have a significantly different performance in the case of positive or negative initial mean stress. In both cases the test data show a higher initial relaxation rate while simulations show approximately a linear decay of mean stress with respect to number of cycles. This is unsatisfactory from the point of view of reproducing material behavior, but tends to be acceptable when dealing with service loadings. The relaxation decay underestimates the material behavior but it was shown that an overestimate of mean stress relaxation in variable amplitude loading for small hysteresis loops leads to unacceptable simulated

behavior, as shown in section 6.3.2. Even though the rate of relaxation is not respected, relaxation still occurs at a non insignificant level.

The simulation in the case of compressive mean stress relaxation is not fitting test data well. The main issue is the initial values of mean stress. Even if the relaxation behavior seems comparable to the one obtained for tensile mean, the initial value of mean stress can be a significant problem when dealing with the compressive part of the stress-strain space. The stable stress-strain response tends to differ more significantly in compression than in tension. This is a common problem of material simulation behavior and it is confirmed in this case. It is beyond the scope of this research to propose a solution for this problem, but in the case of the Wetzel model it seems easily resolvable: a second compressive stable curve could be divided in segments and employed when simulating the compressive part of the material response. This won't change the core of the Wetzel model and would help solve the difficulty in predictions.

For both materials the simulations are comparable, with no noticeable differences between the two alloys. Wetzel simulations for 7075 in case of tensile below threshold relaxation is better than the one for 7249, but in the case of compressive mean stress relaxation 7249 is doing better than 7075.

Variable Amplitude loading simulations are also run with the Wetzel model to evaluate its behavior when dealing with more complicated relaxation cases. The three variable amplitude loading patterns used to evaluate the Landgraf model are presented here, along with another Type C test in Figures 6-27 to 6-30. This test is chosen to further visualize and appreciate the capability of the Wetzel model to predict and simulate unstable repeated relaxation.

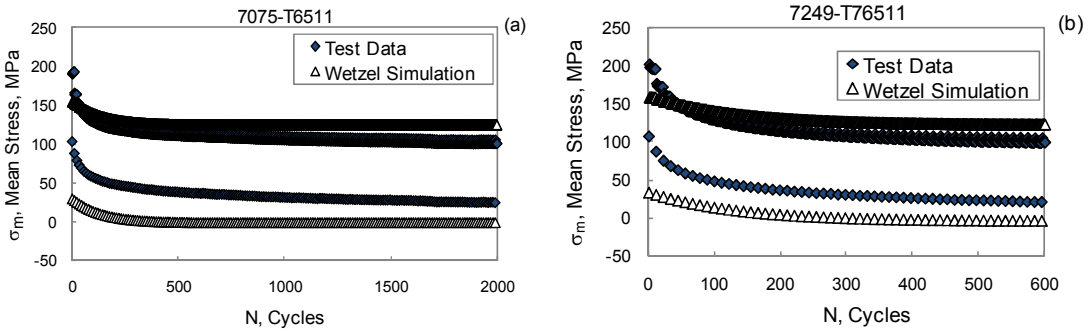

Figure 6-27. Type A variable amplitude loading simulation with Wetzel, corresponding to test B75-54 for 7075 and B49-60 for 7249.

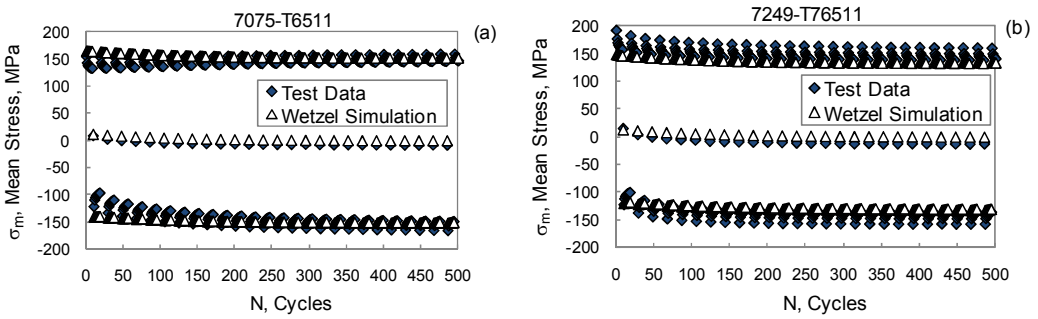

Figure 6-28. Type C variable amplitude loading simulation with Wetzel, corresponding to test B75-26 for 7075 and B49-44 for 7249.

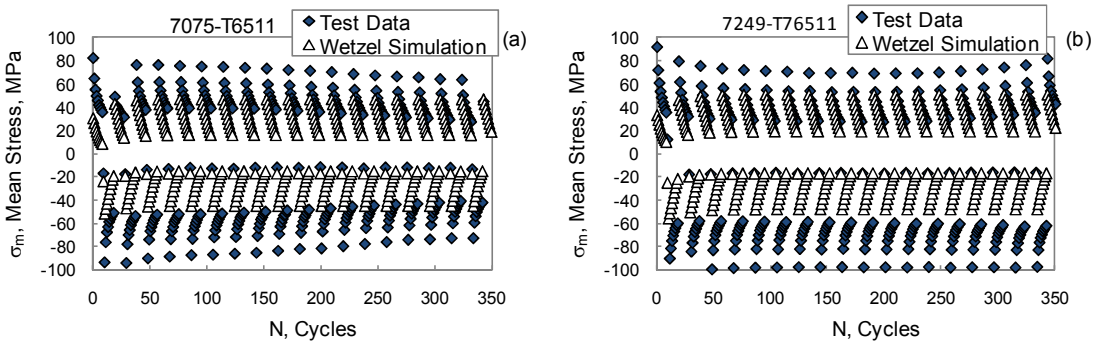

Figure 6-29. Type C variable amplitude loading simulation with Wetzel, corresponding to test B75-49 for 7075 and B49-41 for 7249.

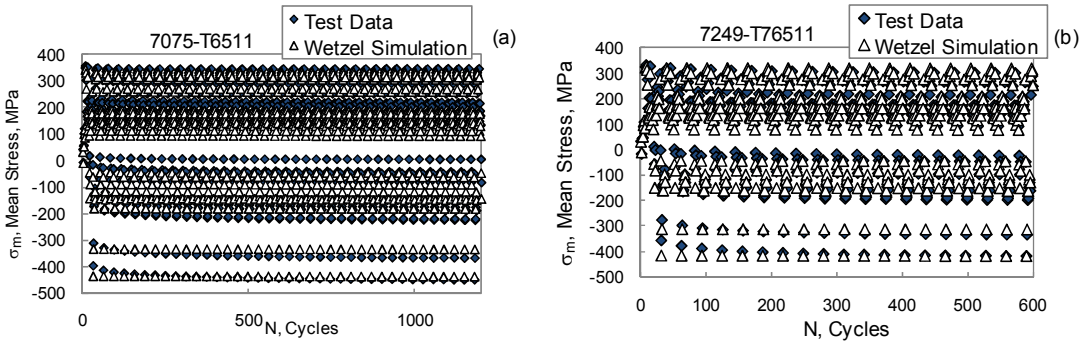

Figure 6-30. Spectrum variable amplitude loading simulation with Wetzel, corresponding to test NAV1-75-15 for 7075 and NAV1-49-1 for 7249.

As previously noticed for constant amplitude loading, in the case of variable amplitude loading also the initial values of mean stresses are influenced by the stable stress-strain behavior. The values are lower than the initial value from experimental data.

In the case of the Type A tests, the simulated response is satisfactory and close to the experimental data. The larger hysteresis loop leads the relaxation behavior with the

smaller one following its path down towards a stable value. The stable values for both are close to the experimental ones, with differences around 20 MPa at most. The response of the Wetzel model for the larger hysteresis loop is more similar to a constant amplitude loading response, with a mean stress stabilizing around zero. A lot less relaxation is observed for the smaller hysteresis loop, but even if not immediately visible, the contribution of its relaxation is taken into account in the global response.

The Type C loading simulations are particularly successful for both materials. Unstable repeated relaxation for the smaller hysteresis loops occurs in both cases, in accordance with test data. In the first case a lower degree of repeated relaxation is observed for the smaller hysteresis loops, while in the second Type C loading occurs at a higher degree, showing that the model is able to reproduce this phenomenon accordingly to the amplitude of the loop undergoing unstable repeated relaxation.

The rate of the unstable repeated relaxation does not correspond to the ones observe in experimental data. This could be due to the fact that the Wetzel table is obtained with simulations of simple constant amplitude loading inside a larger loop, without considering interactions of multiple repetitions of the same hysteresis loop in the bigger loop. Stable simulated value are close to the ones found in test data and only for the second Type C case relaxation behavior seems overestimated.

The overall performance is acceptable also looking at the last simulation of the service type of loading. Especially in the case of 7249, where they almost totally overlap, the stable mean stress values are really close to the experimental ones. The relaxation behavior in Wetzel for this loading is not really noticeable in the plot, while material behavior shows the characteristic relaxation decay.

6.4 The Jiang model

6.4.1 Route to the Jiang model

Among all other incremental plasticity models, the one developed by Jiang and Sehitoglu in 1996 is a successful improvement of the A-F formulation, and it showed particular accuracy in simulating different ratcheting rates for different loading conditions [53].

One disadvantage is that the number of material constants needed for a successful implementation of the Jiang model is higher compared to a A-F model with one or more back stresses.

It was decided to implement two versions of the A-F models, a version of Jiang and Sehitoglu model and a version of Doring model, shown in the literature review, and compare the results to decide what the most convenient model to suggest for implementation into FAMS is.

The simple A-F model with one or two back stresses requires only the fitting of the stable stress-strain curve for the material. In the case of a single back stress, two material constants must be found, along with the proportional elastic limit; in the case of multiple back stresses, the number of constants is 2n, where n is the number of back stresses and the proportional elastic limit. The fitting of the stress-plastic strain curve is performed with Matlab and using a Levemberg-Marquard method [66].

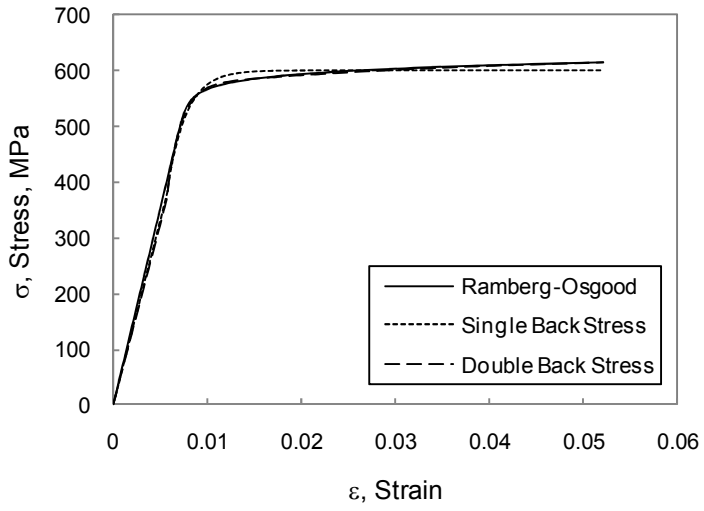

Figure 6-31. Comparison of Ramberg-Osgood fitted stress-strain curve for 7075 with the stable stress-strain response of A-F models with one and two back stresses.

The stress-strain responses of the A-F model with single and double back stress are shown in Figure 6-31 along with the Ramberg-Osgood curve obtained from fatigue analysis in the current study. The A-F model with a single back stress tends to have a more extreme response, with a more abrupt curving section immediately after the yield

point of the curve. The curve flattens down quickly, and a constant value for stress is reached immediately after 1.5% strain. The stress-strain response of the A-F model with two back stresses is very similar to the Ramberg-Osgood formulation, and practically indistinguishable from it.

This fitted stress-strain response is used to simulate one of the two constant amplitude loadings (ε_a = 0.95%), and one of the two variable amplitude loadings, the Type A loading, shown for Wetzel.

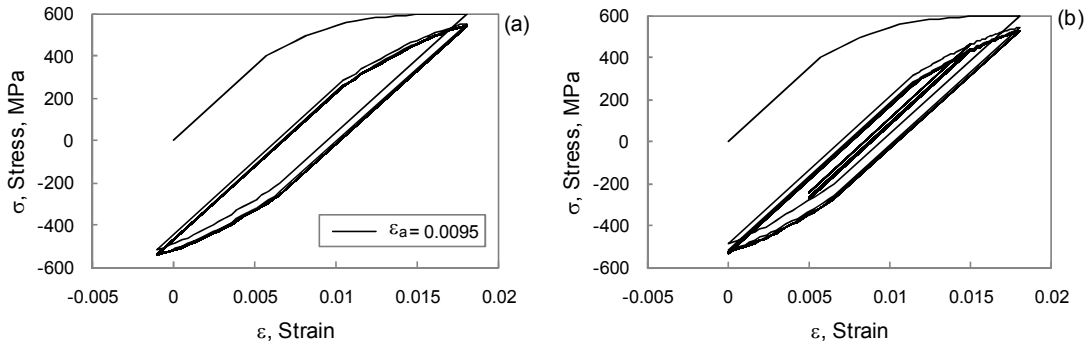

Figure 6-32. Simulation of a constant amplitude loading test and a Type A variable amplitude loading with a A-F model with one back stress for 7075.

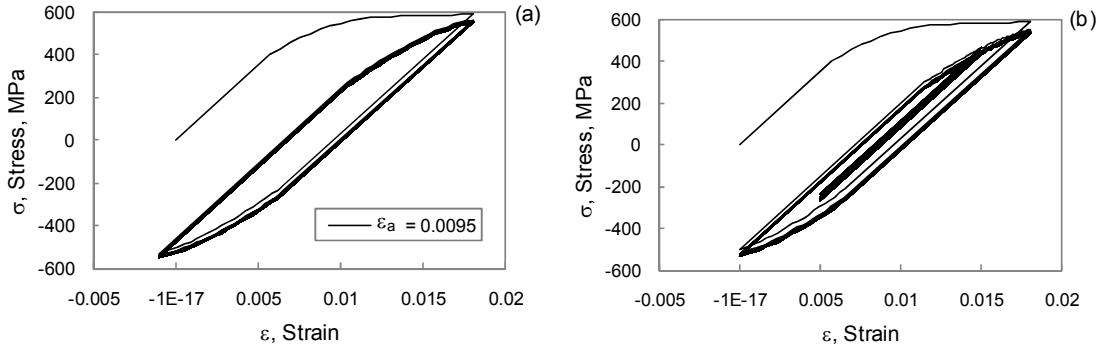

Figure 6-33. Simulation of a constant amplitude loading and a Type A variable amplitude loading with a A-F model with two back stresses for 7075.

The simulated results for the A-F models with one and two back stresses are shown in Figures 6-32 and 6-33. The simulated relaxation occurs mainly in the first few cycles of the life, and the small mainly elastic loops are not subjected to any relaxation for the variable amplitude loading case. The presence of a proportional limit is reflected in a total

absence of transient phenomena for loops below the strain amplitude threshold. Both models stabilize at the completely reversed state, and the smaller loops do not play a dominant role, but mostly follow the relaxation of the larger loop. The model with two back stresses is better able to reproduce the relaxation rate in both the constant and variable amplitude loading case. The monotonic stress-strain behavior for the case of two back stresses was also closer to the Ramberg-Osgood formulation.

The possibility of including three back stresses instead of only two was also taken into consideration. Simulations showed that introducing a third back stress is not adding any beneficial effects in the fitting of the stable stress-strain curve and in the relaxation response. This happens because the two additional fitting constants tend to converge to either of the two values of fitting constants obtained when the stress-strain is fitted with only two back stresses. Depending on the initial value of the additional two constants, these converge to the values of the ones previously obtained. The fitting of this type of curve with only two back stresses is therefore considered satisfactory.

Since any plasticity model requires a high effort in changing the current formulation of the life calculation software FAMS, a more accurate model would be a better compromise to justify significant changes.

The Jiang model requires a higher effort for obtaining the stress-strain constants for monotonic and cyclic behavior. A detailed explanation on how to obtain the constants is described in Jiang [53], and it is found in the next section of this Chapter for 7075 and 7249 Al. alloys. The method chosen is the one named "Obtaining $c_{(i)}$'s from constants $r_{(i)}$'s", therefore the $r_{(i)}$'s intervals are decided a priori once the proportional limit is set.

The implementation of the Jiang model also requires the determination of the $\chi_{(i)}$ constants controlling mean stress relaxation rates. No general method other than trial and error is suggested in literature.

A detailed analysis on the role of the $\chi_{(i)}$ constants is presented in the next section of this chapter, along with the trial and error methods for fitting.

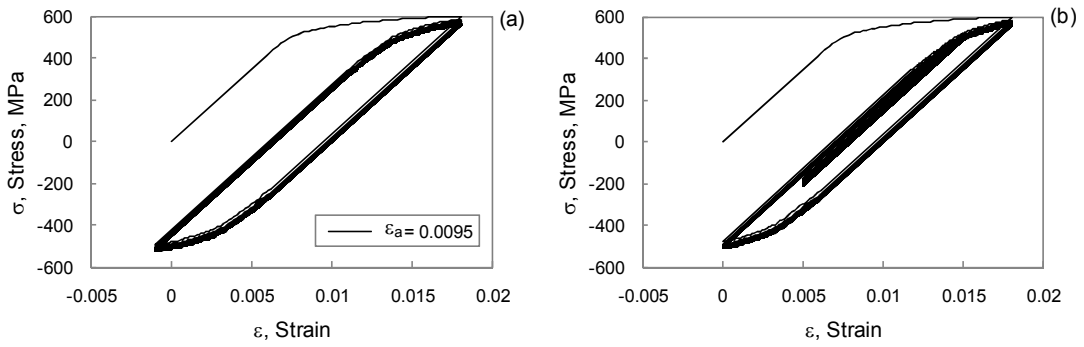

Figure 6-34. Simulation of a constant amplitude loading and a Type A variable amplitude loading with the Jiang model with constants obtained from fitting 7075 data.

Simulation results in Figure 6-34 show an acceptable rate of decay for mean stress in both cases. The simulated material response is more similar to test data obtained for 7075 and 7249. For the Type A loading case, the large hysteresis loop leads the relaxation with the smaller mainly elastic loop following its path towards the completely reversed state. With the use of the Jiang model, it is possible to fit the stress-strain curve and choose a lower proportional limit if compared to the A-F formulation. This makes relaxation possible for a large amount of smaller hysteresis loops in a variable amplitude loading.

The Doring model requires an even greater effort to obtain material constants for the stress-strain curve [54]. The results of the fitting of the stable stress-strain curve for 7075 and 7249 leads to the determination of a higher proportional limit, and a shape of the stress-strain curve that recalls an elastic, linearly hardening material. Simulations of the constant and variable amplitude loading cases are shown in Figure 6-35.

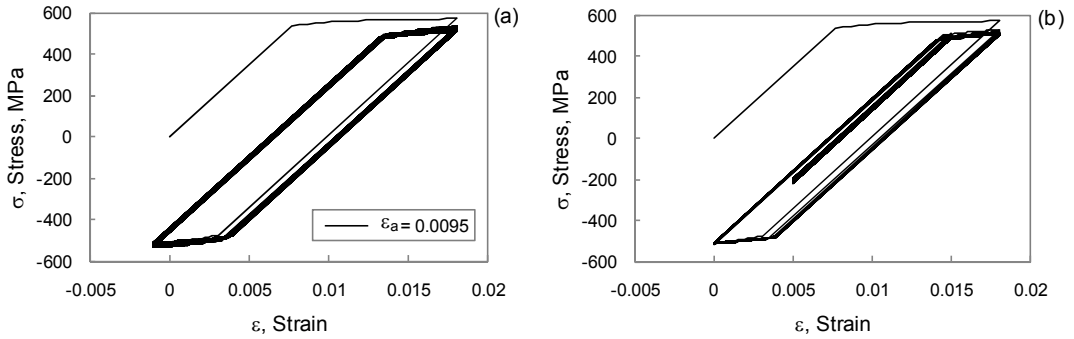

Figure 6-35. Simulation of a constant amplitude loading and a Type A variable amplitude loading with the Döring model with constants obtained from fitting 7075 data.

The details of the fitting for the Doring model will not be shown in this study as the model is not considered a good choice for incorporation into FAMS. The first reason is the difficulty in obtaining constants from the stress-strain curve. The second reason is the presence of an excessive amount of other constants regulating transient behaviors, not easily obtainable from experimental curves. As a final remark, the overall cyclic response does not justify the efforts in estimating material constants.

Comparisons of simulations show that among the four models used to estimate relaxation for constant and variable amplitude loading conditions, the Jiang model seems the best choice considering the observed response, the relative simplicity in obtaining stress-strain fitting constants, and a mean stress relaxation rate closer to material behavior. The Jiang model can also easily be simplified, leaving some of the other transient phenomena embedded in its stress-plastic strain formulation out of the implementation, by just setting the proper constants.

As previously considered, the fit backbone structure of the A-F model with one or two back stresses is attractive from the point of view of simplicity, but difficulties in matching the rate of mean stress relaxation or ratcheting behavior are noticeable. This is confirmed by other studies and also by Jiang and Sehitoglu [53].

The Doring model does not seem to be convenient for the purpose of the current research, as it requires an unwanted effort in fitting material constants of doubted physical significance. The model is also not easily reducible to a simpler form and fitting or implementing a number of unnecessary transient effects is undesirable.

6.4.2 Adaptation of the Jiang model and Monte Carlo Analysis

The Jiang model is then chosen as a candidate for inclusion into FAMS. A more detailed analysis about all the material constants used in the model and on how to fit those constants to obtain a more representative material behavior is presented in this section.

In the first part, it will be explained how the Jiang model is simplified and adapted to the scope of the current study. The second part will focus on the way the stress-strain curve is fitted. Some difficulties are encountered in using a stable stress-plastic strain curve in the Ramberg-Osgood form, so a curve from an incremental step test was used

instead. The third part will show the planning of a Monte Carlo analysis on the model to be able to give directions about which of the $\chi_{(i)}$'s constants is more influential in the control of the relaxation behavior.

6.4.2.1 Simplifications to the Jiang model

The first terms left out of the formulation of the model are the ones regulating the behavior of the Baushinger effects. These effects are not particularly evident in high strength aluminum alloys, and it is therefore decided to leave these out of the implementation. Those constants are not shown in Chapter 2.

The second set of constants that will be excluded from the model in this research are the ones controlling the stress memory surface and determining history effects. Constants β, η and ζ of Eq. 2.17 are set equal to zero. The transient effects of interest in this study happen mainly at the beginning of the life, and stability is frequently reached before the half life of the test. It is an unnecessary complication to obtain these constants and beyond the scope of this research.

The three sets of material constants left are: $c_{(i)}$'s, $r_{(i)}$'s and $\chi_{(i)}$'s in Eq. 2.17, in addition to elastic modulus and proportional limit. The way the first two sets are obtained will be shown in the following paragraphs.

6.4.2.2 $c_{(i)}$'s and $r_{(i)}$'s for the Jiang model

The fitting of the stress-strain curve in the Jiang model starts from defining a proportional limit for the material, and then calculates $c_{(i)}$'s and $r_{(i)}$'s from stress-plastic strain points. The use of the Ramberg-Osgood equation requires the choice of a high proportional limit, due to the shape of the curve for 7075 and 7249. Obtaining $c_{(i)}$'s and $r_{(i)}$'s from values of plastic strain smaller than 10^{-6} creates difficulties from a computational point of view. In addition with a high proportional limit, the shape of the stress-strain curve is not satisfactory enough, as shown for the A-F model and Doring model. Specifically for the current research, considering that small hysteresis loops will never show relaxation if their strain amplitude is lower than the corresponding proportional strain amplitude, a lower proportional limit for the model is desired.

To avoid an extremely conservative design of the stress-strain behavior, which would be obtained with a modeling of the stress-strain response from the Ramberg-Osgood formulation, an incremental step test is used in fitting. From test data of an incremental step test run at 15 different consecutive strain amplitudes, with maximum ε_a of 1.8% and a loading profile similar to the one shown in Chapter 1, the stress-strain response of the biggest of the incremental loops is used as a base line for fitting the Jiang constants.

The results of the incremental step test and the corresponding stress-plastic strain curve along with the cyclic stable stress-plastic strain curve from the Ramberg-Osgood analysis are shown in Figures 6-36 and 6-37. The values of $c_{(i)}$'s and $r_{(i)}$'s from the fitting are summarized in Table 6-3 and 6-4.

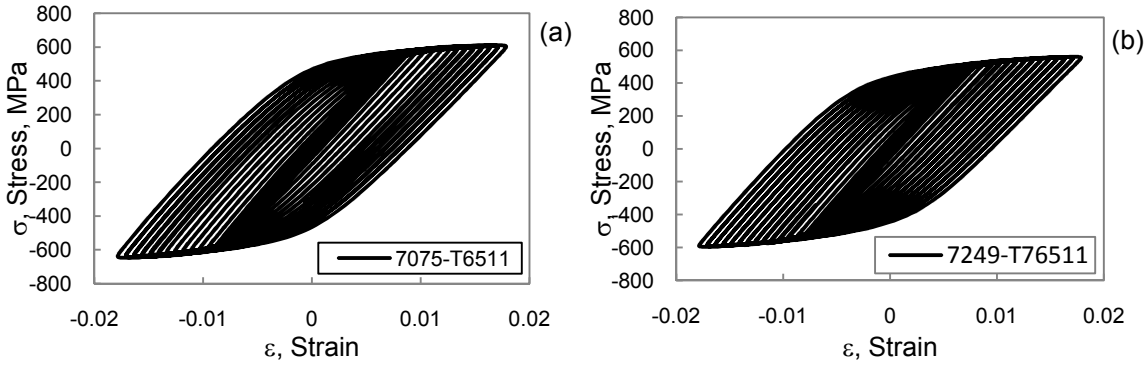

Figure 6-36. Incremental step test data for 7075 and 7249.

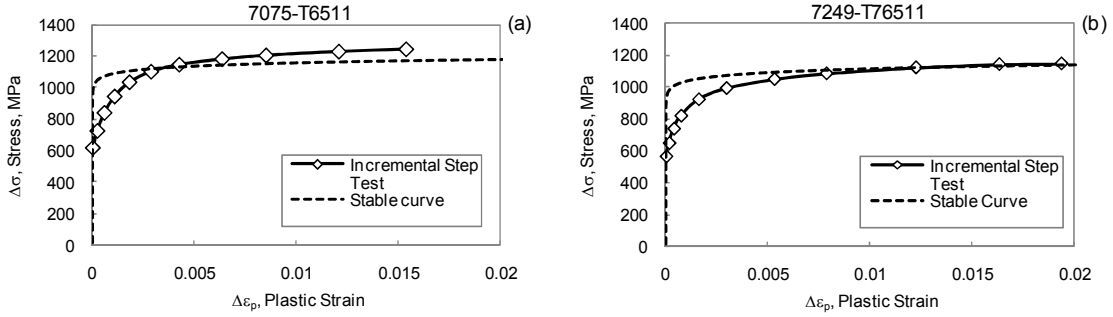

Figure 6-37. Ramberg-Osgood fitted curve and Jiang stress-strain curve for 7075 and 7249.

Table 6-3. Jiang model parameters $c_{(i)}$'s from fitted stress-strain curve.

$c^{(i)}$	7075-T6511	7249-T76511
$c^{(1)}$	4509.9	5952.22
$c^{(2)}$	3847.7	5235.08
$c^{(3)}$	2719	3732.62
$c^{(4)}$	1906.7	2197.51
$c^{(5)}$	974.04	919.58
$c^{(6)}$	490.74	320.22
$c^{(7)}$	191.81	179.59
$c^{(8)}$	123.85	120.76
$c^{(9)}$	72.745	113.94
$c^{(10)}$	142.35	47.43

Table 6-4. Jiang model parameters $r_{(i)}$'s from fitted stress-strain curve.

$r^{(i)}$	7075-T6511	7249-T76511
$r^{(i)}$, i=1 to 10	21.11	20.26

The stable stress-plastic strain curve plotted in Figure 6-37 comes from fitted constants in Chapter 4. This curve is extremely steep, with values of plastic strain less than 10^{-6} up to 900MPa, and this is the reason why it is not chosen as base line for $c_{(i)}$'s and $r_{(i)}$'s calculation in the Jiang model. Values of plastic strain in the order of 10^{-6} will cause the $c_{(1)}$ for both materials to be computationally difficult to manage.

The curve taken from the incremental test shows a lower proportional limit and a larger radius of curvature, making the $c_{(1)}$ constants manageable and the rest of the $c_{(i)}$'s decrease more gently, confirming the trends shown by Jiang [53].

For 7075, the deviation from the stable curve is higher. The maximum stress value reached in the curve is significantly higher than the one for the stable curve, meaning that

probably a larger degree of hardening occurred. The fitting for 7249 is more successful, with the stable curve and the fitted curve converging to the same maximum value for large plastic strains.

The technique used in this research is based on observations of hysteresis loop shape and comparison of different fitting procedures. The use of an incremental step test to model the stress-strain behavior in variable amplitude loading has been discussed in the literature review, and in this study also it is visible that it gives advantages in terms of reproducing more effectively material behavior in variable amplitude loading. It is unquestionable that this is an arbitrary choice, and it might cause an incorrect material behavior representation, but the Jiang model is taken in this study to be a more hazardous choice with respect to a conventional approach or with respect to the Wetzel approach; therefore it is justifiable to include this new idea also.

6.4.2.3 Monte Carlo Analysis and the $\chi_{(i)}$'s constants

The approach taken in this study is to run Monte Carlo analysis to understand which constants play the most important role in determining the relaxation response. Trial and error methods are then used to estimate optimized values for $\chi_{(i)}$'s.

The Monte Carlo analysis is structured to run the implemented version of the Jiang model with $c_{(i)}$'s and $r_{(i)}$'s found from the previous analysis with a number of different sets of $\chi_{(i)}$'s. The limits for the $\chi_{(i)}$'s constants is set to be from a value of 0 to a value of 50, and the statistical distribution chosen is a uniform distribution between the two limits. Limits are set based on values obtained by Jiang and Sehitoglu [52] and also by manual trial and errors performed in this study. These constants are not scattered around a mean value in between the limits, so a uniform distribution is the only possible choice.

The way the performance of each set of $\chi_{(i)}$'s is evaluated is through the use of the same parameter that was adopted for the evaluation of the Wetzel simulations, called simulation residual. The smaller the value of residual was, the better the correlation between the stress response of the model and experimental data.

The loading patterns used are a set of 11 variable amplitude loading patterns: the seven Type A loadings, one Type B loading and three Type C loading tests run for 7075.

All the simulations will be run to half life of the test, so the number of repetitions per loading varies depending on the life of the corresponding experimental test.

Those loading patterns will be simulated with 5000 different $\chi_{(i)}$'s sets, so a total of 55000 simulations is run and, calculating the number of cycles, a total of 30 millions cycles is obtained.

The ESM cluster server is used to run the simulation described and approximately 200 hours of server work are necessary to complete the simulation. The computational time is high compared to Wetzel, but still reasonable as the server has speed comparable to personal computers. The routine could also be programmed to run in parallel on a higher number of processors, if a multi processor server is available.

The 55000 residuals obtained are then analyzed along with the 55000 sets of $\chi_{(i)}$'s to obtain the correlation between the variation of each of the ten $\chi_{(i)}$'s constants and the value of the residuals. The Monte Carlo analysis is performed with the use of a statistical software, SIMLAB, funded by a project of the European Community and developed by Saltelli et al. [67]. This software is able to perform Monte Carlo simulations given the form of the model chosen, but also to analyze the results of simulations run with a different software and calculate the most used coefficients of correlation.

6.4.2.4 Results from Monte Carlo Analysis

The first step before running simulations with the Jiang model is the optimization of the exponents $\chi_{(i)}$'s in the model. As anticipated in the introduction to optimization in Chapter 4, a Monte Carlo analysis has to be performed to understand which ones of the $\chi_{(i)}$'s has the greatest influence in the relaxation behavior.

A total of 55000 simulations were run to obtain a large sample of performance indexes, the simulation residuals (Eq. 6.1), so that those could be related to the variations of $\chi_{(i)}$'s, scattered uniformly in a range 0 to 50. The results showed a growing correlation coefficient for the constants $\chi_{(i)}$'s. This means that the last 5 constants are mostly responsible for the relaxation behavior of the Jiang model.

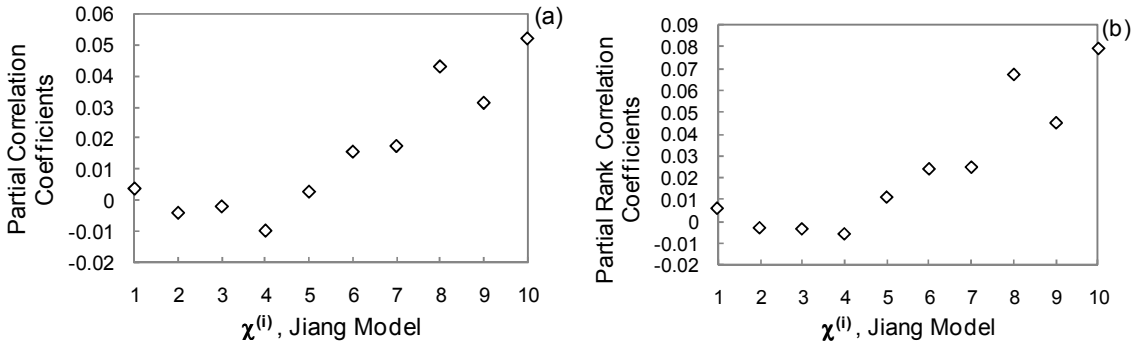

Figure 6-38. Partial Correlation Coefficient and Partial Rank Correlation Coefficients between constants $\chi_{(i)}$'s of the Jiang model and the simulation residuals for 55000 simulations of 11 variable amplitude loading patterns.

All the non linear correlation coefficients found with the help of SIMLAB [67] show that the last five correlation constants are responsible for most of the relaxation behavior in the model (Figure 6-38). Those coefficients are calculated with a 0.95% confidence level. The values for the first five constants are all smaller than ±0.01, while values for the last five start to be progressively higher. The last three $\chi_{(i)}$'s seem to be the most influential, with correlation coefficients in one case above 0.03 and in the second case above 0.05.

Linear correlation coefficients are not meaningful in the current context, mainly because the model is clearly non linear.

6.4.3 Optimization of $\chi_{(i)}$'s constants for Jiang

A series of optimization routines are run to obtain the best possible values for the ten $\chi_{(i)}$'s and especially for the 5 most significant ones. The way the optimization routine is structured has been shown in Chapter 4. The loading patterns chosen for the optimization are all the Type A, B, and C variable amplitude loading tests run for both materials. This was chosen because of the major interest in matching simulations and test data for the more complicated loadings. The two spectrum type of loading are purposely not used for the optimization, so that they could be used exclusively for comparison of material behavior.

The $\chi_{(i)}$'s are divided in two sets and alternatively the first five and the last five $\chi_{(i)}$'s are kept fixed. The non fixed set of $\chi_{(i)}$'s is chosen so that each time the routine runs, a sample of one hundred $\chi_{(i)}$'s is used for simulations. Ninety-nine of those are chosen following a uniform distribution between values of 0 and 50, 1 of those is chosen as the best set of $\chi_{(i)}$'s from the previous routine cycle. At the end of several different runs of the routine, an optimized set of $\chi_{(i)}$'s is obtained.

Results showed that the last five $\chi_{(i)}$'s in the sets, so the ones who are mostly influential for the relaxation behavior, are converging to the same five values after a large number of total cycles. This not only shows that the optimization routine is well structure and works in the desired way, but it confirms the results from the Monte Carlo Analysis. Since the last five constants are the most influential for the relaxation behavior, they are also the ones converging faster to the optimized values.

Table 6-5. Optimized values of $\chi^{(i)}$'s for 7075 and 7249; the values are used in simulations.

$\chi^{(i)}$	**7075-T6511**	**7249-T76511**
$\chi^{(1)}$	35.372	13.51045
$\chi^{(2)}$	28.705	6.556096
$\chi^{(3)}$	14.699	5.945286
$\chi^{(4)}$	0.21744	2.954271
$\chi^{(5)}$	17.161	11.59744
$\chi^{(6)}$	21.63	15.51248
$\chi^{(7)}$	7.6974	46.69625
$\chi^{(8)}$	3.8984	4.828717
$\chi^{(9)}$	0.17095	2.446377
$\chi^{(10)}$	20.419	12.69165

6.4.4 Simulations

The disadvantage of the Jiang model is the presence of a proportional limit in its formulation. This means that below a certain threshold, the material doesn't yield and the behavior is purely elastic. From the mean stress relaxation point of view, the proportional limit cause the smaller hysteresis loops to not relax. The simulations of the tests with relaxation of hysteresis loops below relaxation threshold shown for Landgraf and Wetzel are not shown for the Jiang model.

Mean stress relaxation for tests with high strain amplitudes are underestimated by the Landgraf model, especially for the tensile mean stress (Figures 6-39 and 6-40). This is expected since the optimization routine for the $\chi_{(i)}$'s is using variable amplitude loading patterns only. The relaxation for the larger loops in variable amplitude loading is modified by the presence of other hysteresis loops relaxing at the same time. As it was shown in Chapter 5, the relaxation of the same loop in constant and variable amplitude loading is different. The same features are revealed here, the relaxation in the case of variable amplitude loading is sensibly less than the one shown in constant amplitude loading.

The relaxation rate is comparable in both cases; in the compressive mean stress relaxation, the initial rate is observed to be higher than the ones for tensile mean stress, but the Jiang model also predicts this behavior. The stress-strain response for both materials is close to the experimental values, meaning that the at least for this case the fitting shown in Chapter 4 is successful.

The tensile mean stress relaxation and the compressive mean stress relaxation show a negative stable values, but the Jiang model is not able to predict this behavior.

The relaxation behavior in variable amplitude loading is observed for the Jiang model for the same loading patterns used for the Wetzel model. A Type B test is added to appreciate the potentiality of the Jiang model for all the 4 categories of loading patterns studied. Simulations are shown in Figures 6-41 to 6-45.

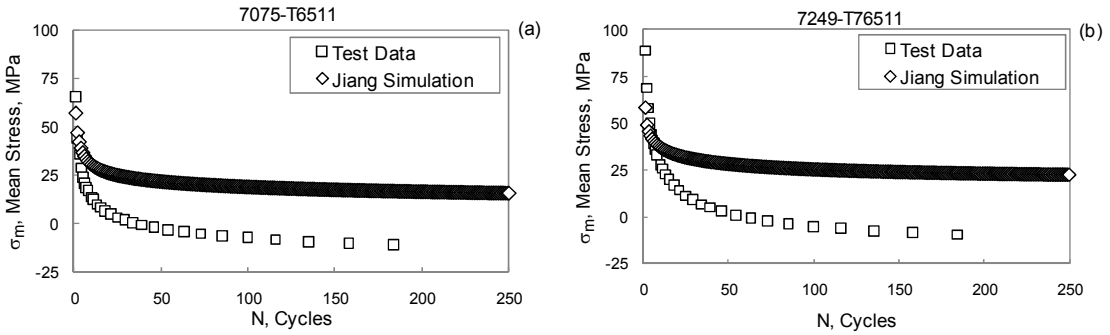

Figure 6-39. Constant amplitude loading simulation with Jiang model, corresponding to 75NLB-1, test 1 Table 5.5 for 7075 and to 49LC-3, test 1 Table 5.6 for 7249.

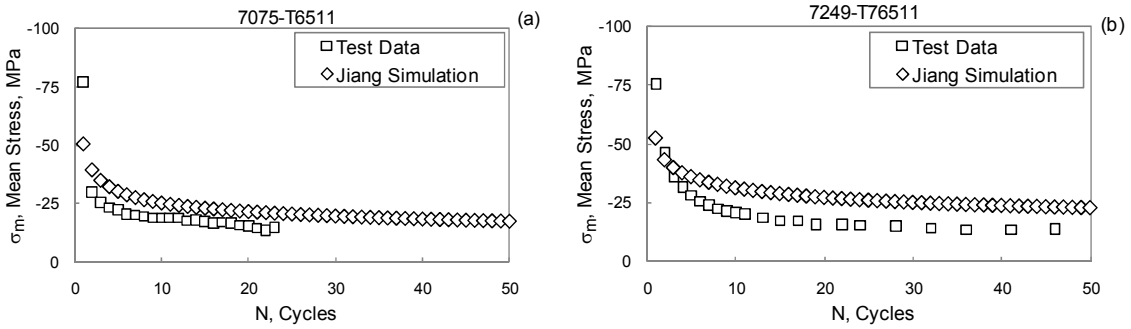

Figure 6-40. Constant amplitude loading simulation with Jiang model, corresponding to B75-47, test a Table 5.5 for 7075 and to B49-27, test a Table 5.6 for 7249.

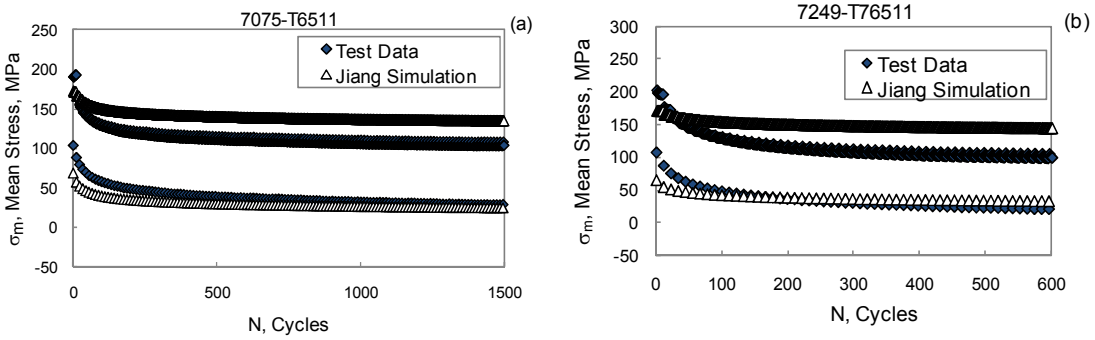

Figure 6-41. Type A variable amplitude loading simulation with Jiang, corresponding to test B75-54 for 7075 and B49-60 for 7249.

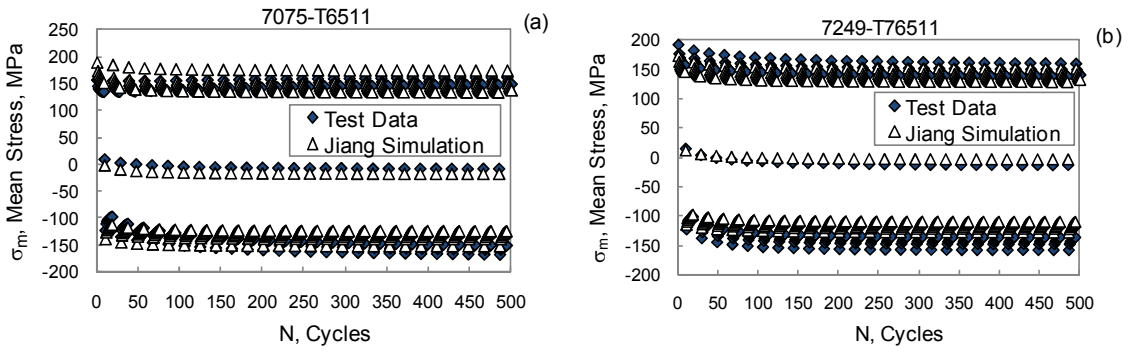

Figure 6-42. Type C variable amplitude loading simulation with Jiang, corresponding to test B75-26 for 7075 and B49-44 for 7249.

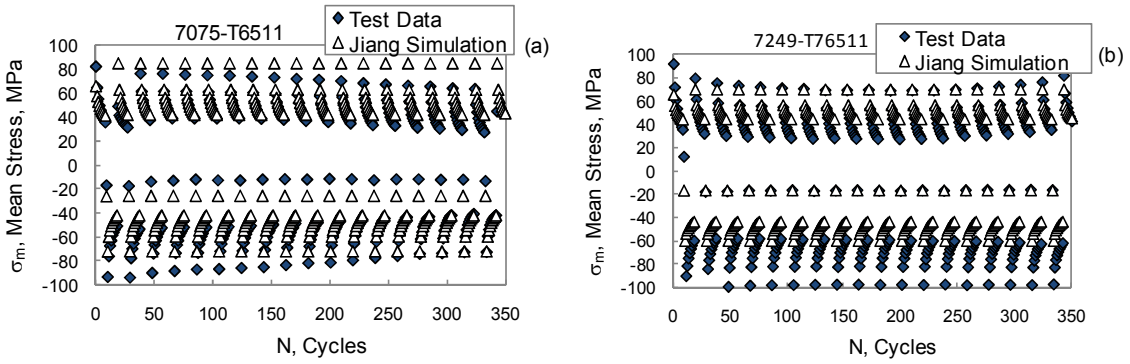

Figure 6-43. Type C variable amplitude loading simulation with Jiang, corresponding to test B75-49 for 7075 and B49-41 for 7249.

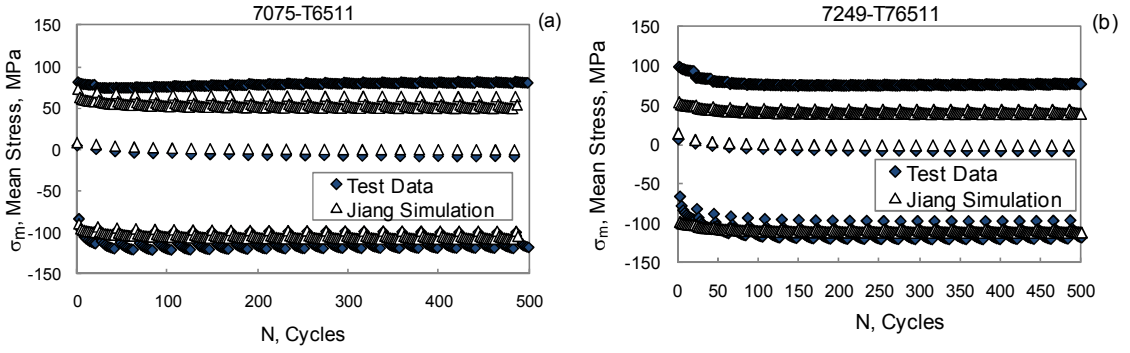

Figure 6-44. Type B variable amplitude loading simulation with Jiang, corresponding to test B75-28 for 7075 and B49-56 for 7249.

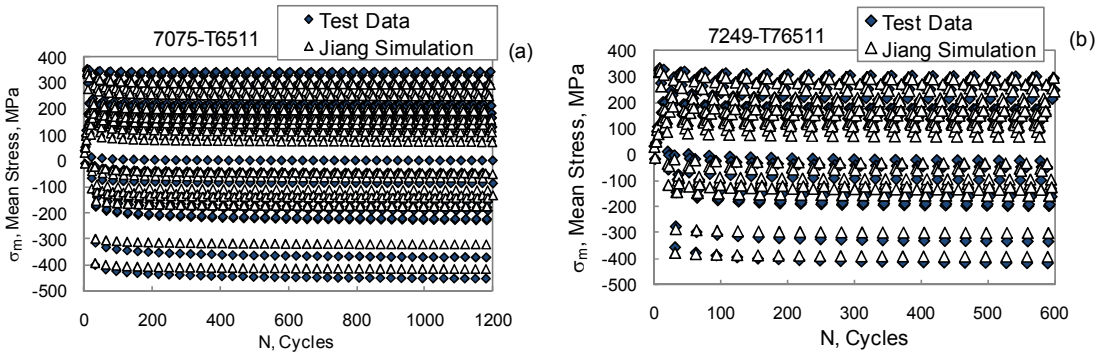

Figure 6-45. Service type of variable amplitude loading simulation with Jiang, corresponding to test NAV1-75-15 for 7075 and NAV1-49-1 for 7249.

Now let us summarize some overall trends seen in the tests just discussed. All the variable amplitude loading patterns chosen are satisfactory predicted by the Jiang model. The optimization method also showed to work well as in all the cases the relaxation is close to the experimental data.

The Type A variable amplitude loading simulation is able to predict the relaxation of the larger hysteresis loop better than what the Wetzel model was able to do. The difference with the Wetzel model is also that the bigger hysteresis loop in the Jiang model follows the relaxation behavior in variable amplitude loading more than the relaxation behavior observed in constant amplitude loading. This happens for the same reasons why the relaxation response in constant amplitude loading is off the experimental data: the optimization process involved variable amplitude loading only. A certain mutual influence for the small and large hysteresis loop is evident in the behavior of the relaxation for the larger one. The initial value of the relaxation in the first of the two Type C loadings is lower than what would be expected from the same loop in a simulation of constant amplitude loading.

A comparison of the relaxation of the loop in constant and amplitude loading with the Jiang model and the variable amplitude loading experimental data is shown in Figure 6-46. The rate of the relaxation in both simulated cases is the same, so the model does not change the rate of relaxation depending on the variable or constant amplitude loading case.

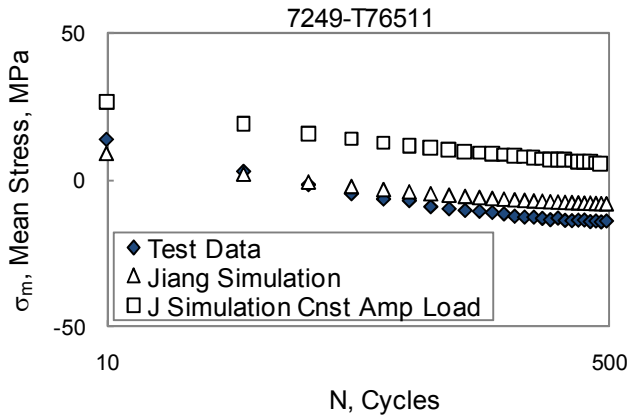

Figure 6-46. Comparison of a low cycle fatigue hysteresis loop in variable amplitude loading, Test data and Jiang model simulations, and in constant amplitude loading simulations with the Jiang model.

The Type C variable amplitude loading simulations are also really close to experimental data. For the first Type C loading the stable values differ from the experimental data of a maximum of 20 MPa. When larger hysteresis loops are relaxing inside the main loop (Figure 6-43), the model prediction becomes slightly less accurate, and the stable values are off of 30-35 MPa. Nonetheless the similarity in material behavior with the experimental data is surprising: in both cases the smaller hysteresis loops are showing unstable repeated relaxation with rate comparable to the one experimentally observed and they are following the relaxation of the larger loop at the same time.

In the Type B variable amplitude test it is appreciable the reproduction on unstable repeated relaxation for both the smaller loops in the history. This simulation is shown to appreciate the capabilities of the Jiang model with this type of loading also. The error in the case of 7249 is greater than the one observed for 7075, with an error for the stable value, being around 50 MPa.

The Spectrum loading shown in Figure 6-45 also gives good results in terms of mean stress relaxation prediction. The values are slightly less extreme in both the tension and compression part of the graph for 7075, but this could also be due to the stress-strain response to a complicated history of loading, rather than an issue regarding the relaxation behavior.

Chapter 7

Variable Amplitude Loading Life calculation

In this chapter the influence of mean stress relaxation in constant and variable amplitude loading conditions is evaluated. In a strain-based approach to fatigue, as discussed earlier, mean stresses can affect life predictions considerably. The possibility of mean stress relaxation during cyclic deformation of aluminum alloys adds a higher degree of uncertainty in life predictions, frequently causing over conservative life estimates. The role of the two mean stress relaxation models chosen for implementation into a life calculation software are also investigated in the second part of this Chapter.

7.1 Influence of mean stress relaxation on fatigue life analysis in a strain-based approach

The role of mean stress relaxation in life calculation in a strain based approach to fatigue has not yet been quantified. In this section two examples of life predictions is shown for each aluminum alloy.

A constant amplitude relaxation test and a variable amplitude relaxation test is analyzed with a standard strain-based approach for both alloys, without considering the effects of mean stress relaxation. This means that the Ramberg-Osgood curve is used to simulate the material response and that the rain flow counting method is applied to the loading profiles to deal with loop closure and memory effects. The strain-life curve is used to obtain the cycles to failure for the corresponding strain amplitudes involved in the loading, and the Palmgren-Miner rule is used to account for the damage of the different strain amplitudes in the loading. The Walker method is used to account for mean stress effects.

This method is equivalent to the method employed in FAMS to perform life predictions on notched members. The only difference is that in FAMS the Walker method is not implemented, but the SWT method is anyway a good substitute for this type of aluminum alloy, since the γ value is really close to 0.5. Future work on FAMS will probably include the implementation of the Walker method.

The material constants obtained in Chapter 4 are employed with the Ramberg-Osgood equation, the strain-life curve and the Walker method.

Secondarily the same constant and variable amplitude loading patterns are used to perform life calculations with inclusion of relaxation effects. This is done analyzing the experimental data for the tests and obtaining the stable values of mean stresses for the hysteresis loops in the loading. Those "relaxed" mean stress values are substituted to the stable values in the first analysis, so that the difference in life predictions for the two cases could be appreciated.

The constant amplitude loading pattern chosen for the purpose of this analysis is the one shown in Figure 5-1, corresponding to test 75LB-6. The rain flow counting method does not need to be applied in the case of constant amplitude loading, but the strain history and the amplitude of the loop in the loading are anyway shown in Figure 7-1.

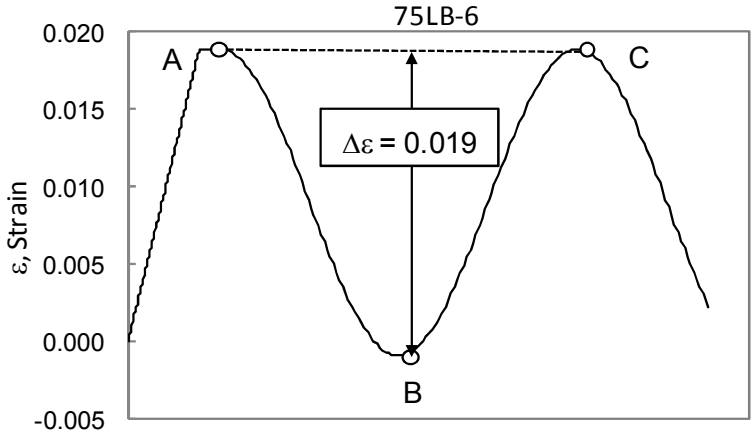

Figure 7-1: Schematic representation of cycle counting applied to a simple constant amplitude loading for test 75LB-6.

The analysis for this simple case is shown in Table 7-1, where the standard approach is applied.

Table 7-1: Analysis of constant amplitude loading for test 75LB-6.

Point	ε	Δσ	σ
A	0.018 (ε_A)	590.905 ($\Delta\sigma_{0\text{-}A}$)	590.90 (σ_A)
B	-0.001 (ε_B)	1125.31 ($\Delta\sigma_{A\text{-}B}$)	-534.41 (σ_B)
C	0.018 (ε_C)	1125.314 ($\Delta\sigma_{C\text{-}B}$)	590.90 (σ_C)

Table 7-2: Life calculation analysis with standard method of constant amplitude loading for test 75LB-6.

$\sigma_{a(ABC)}$	$\varepsilon_{a(ABC)}$	σ_m	N^*	R	N_j	N_f
562.66	0.0095	28.25	254.04	-0.904	1	135.32

Table 7-3: Analysis of constant amplitude loading for test 49LB.

Point	ε	Δσ	σ
A	0.018 (ε_A)	568.5 ($\Delta\sigma_{0\text{-}A}$)	568.5 (σ_A)
B	-0.001 (ε_B)	1077.816 ($\Delta\sigma_{A\text{-}B}$)	-509.32 (σ_B)
C	0.018 (ε_C)	1077.816 ($\Delta\sigma_{C\text{-}B}$)	568.5 (σ_C)

Table 7-4: Life calculation analysis with standard method of constant amplitude loading for test 49LB.

$\sigma_{a(ABC)}$	$\varepsilon_{a(ABC)}$	σ_m	N^*	R	N_j	N_f
538.9082	0.0095	29.59	315.6987	-0.8959	1	147.0863

To obtain the values of σ_A, $\Delta\sigma_{A\text{-}B}$ and $\Delta\sigma_{B\text{-}C}$, the Ramberg-Osgood relation is applied to the loading and given ε_A, $\Delta\varepsilon_{A\text{-}B}$ and $\Delta\varepsilon_{B\text{-}C}$, the corresponding values of stress can be found. Once then it is verified ith the use of the rain flow counting method that cycle ABC is closing, its strain amplitude ea(ABC) can be used to calculate the N* value with material constants from the strain-life curve. The value of mean stress can be obtained from sA and sB and the Walker method can be applied to get Nf from N*. finally since the ea(ABC) loop is the only one in this loading, the value of Nf is the predicted life for the test.

If mean stress relaxation effects want to be taken into account, the values (in this case on value only) of mean stress have to be substituted with the ones obtained experimentally at half life of the test. The analysis reported in Table 7-2 is the same, but

the mean stress, σ_m, is different. This analysis does not take into account the effects of the change in mean stress during the first part of the life for the test, but just considers the effects of the "relaxed" mean stress on life. This approximation simplifies the analysis of constant and variable amplitude loadings and it is used to give representative results on the influence of mean stress relaxation. This can be considered acceptable for the current scope of the study. Once the mean stress models are implemented into FAMS, the level of accuracy can be increased, since FAMS is able to manage life calculation cycle by cycle.

Table 7-5: Life calculation analysis with "relaxed" mean stress values of constant amplitude loading for test 75LB-6.

$\sigma_{a(ABC)}$	$\varepsilon_{a(ABC)}$	σ_m	N^*	R	N_j	N_f
562.66	0.0095	-15.12	254.04	-1.05523	1	360.6016

Table 7-6: Life calculation analysis with "relaxed" mean stress values of constant amplitude loading for test 49LB.

$\sigma_{a(ABC)}$	$\varepsilon_{a(ABC)}$	σ_m	N^*	R	N_j	N_f
538.9082	0.0095	-17.75	315.6987	-1.06812	1	509.43

The life predictions are significantly influence by the use of a "relaxed" or stable value for mean stress. In fact the life predicted in the first case is 135 cycles for 7075 and 147 for 7249, while with the "relaxed" state of mean stress life is 360 cycles for 7075 and 509 for 7249. The fatigue life obtained experimentally is 439 for 7075 and 399 for 7249.

The predictions with the stable values are overly conservative, around 70% conservative with respect to experimental life. The life predictions obtained with "relaxed" values of mean stress are slightly conservative, around 20%, for 7075 and slightly non-conservative, 22%, for 7249, but closer to experimental life than the standard approach.

The variable amplitude loading chosen is a Type A relaxation case, the same shown in Chapter 6, Figure 6-1.

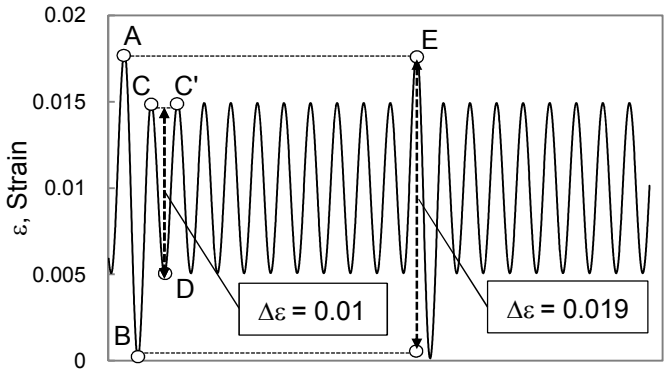

Figure 7-2: Schematic representation of cycle counting applied to a Type A variable amplitude loading for test B75-54.

The rain flow counting method is applied so that the number and amplitude of the hysteresis loops closing in each repetition of the loading are known. As show in Figure 7-2, this variable amplitude loading is constituted by ten repetitions of the smaller hysteresis loop with strain amplitude of 0.5% and one repetition of the larger hysteresis loop with strain amplitude equal to 0.95%.

Table 7-7: Analysis of Type A variable amplitude loading for test B75-54.

Point	ε	Δσ	σ
A	0.018 (ε_A)	590.905 ($\Delta\sigma_{0\text{-}A}$)	590.90 (σ_A)
B	0.00 (ε_B)	1115.40 ($\Delta\sigma_{A\text{-}B}$)	-524.49 (σ_B)
C	0.015(ε_C)	1080.78 ($\Delta\sigma_{C\text{-}B}$)	556.29 (σ_C)
D	0.005 (ε_D)	704.57 ($\Delta\sigma_{C\text{-}D}$)	-148.28 (σ_D)
E	0.018 (ε_E)	1115.40 ($\Delta\sigma_{B\text{-}E}$)	590.90 (σ_E)

Table 7-8: Life calculation analysis of Type A variable amplitude loading with standard method for test B75-54.

$\sigma_{a(CDC')}$	$\varepsilon_{a(CDC')}$	$\sigma_{m(CDC')}$	N^*	R	N_j	N_{fj}	N_f
352.285	0.005	204.0029	26809328	-0.26656	9	75348.73	
$\sigma_{a(ABE)}$	$\varepsilon_{a(ABE)}$	$\sigma_{m(ABE)}$	N^*	R	N_j	N_{fj}	1681
557.7011	0.009	33.20409	360.8623	-0.88762	1	171.5465	

Table 7-9: Analysis of Type A variable amplitude loading for test B49-60.

Point	ε	Δσ	σ
A	0.018 (ε_A)	568.5 ($\Delta\sigma_{0\text{-}A}$)	568.5 (σ_A)
B	0.00 (ε_B)	1068.49 ($\Delta\sigma_{A\text{-}B}$)	-499.99 (σ_B)
C	0.015(ε_C)	1039.49 ($\Delta\sigma_{C\text{-}B}$)	539.50 (σ_C)
D	0.005 (ε_D)	704.57 ($\Delta\sigma_{C\text{-}D}$)	-165.07 (σ_D)
E	0.018 (ε_E)	1068.49 ($\Delta\sigma_{B\text{-}E}$)	568.5 (σ_E)

Table 7-10: Life calculation analysis of Type A variable amplitude loading with standard method for test B49-60.

$\sigma_{a(CDC')}$	$\varepsilon_{a(CDC')}$	$\sigma_{m(CDC')}$	N^*	R	N_j	N_{fj}	N_f
352.285	0.005	187.21	101214645.8	-0.30597	9	229421.7	
$\sigma_{a(ABE)}$	$\varepsilon_{a(ABE)}$	$\sigma_{m(ABE)}$	N^*	R	N_j	N_{fj}	1800
534.25	0.009	34.25	440.45	-0.8795	1	181.2576	

The Ramberg-Osggod equation is again applied to calculate the initial point sa and then applied also to calculate the various Ds in the loading. Once the starting point sa and the Ds are calculated, the sb, sc, sd and se can also be calculated.

The sa and ea are then used to perform life calculation for the closed hysteresis loops obtained with the rain flow analysis. The Palmgren-Miner rule is applied to the loading and from the values of Nfj for each closing cycles, the total value of reversals to failure Nf is calculated.

The same analysis is then reapplied with the use of the "relaxed" mean stress values from experimental data.

Table 7-11: Life calculation analysis with "relaxed" mean stress values of constant amplitude loading for test B75-54.

$\sigma_{a(CDC')}$	$\varepsilon_{a(CDC')}$	$\sigma_{m(CDC')}$	N^*	R	N_j	N_{fj}	N_f
352.285	0.005	154.24	26809328	-0.39099	9	251422.1	
$\sigma_{a(ABE)}$	$\varepsilon_{a(ABE)}$	$\sigma_{m(ABE)}$	N^*	R	N_j	N_{fj}	2420.41
557.7011	0.009	17.205	360.8623	-0.94015	1	244.16	

Table 7-12: Life calculation analysis with "relaxed" mean stress values of constant amplitude loading for test B49-60.

$\sigma_{a(CDC')}$	$\varepsilon_{a(CDC')}$	$\sigma_{m(CDC')}$	N^*	R	N_j	N_{fj}	N_f
352.285	0.005	101.87	101214645.8	-0.55138	9	2686185	
$\sigma_{a(ABE)}$	$\varepsilon_{a(ABE)}$	$\sigma_{m(ABE)}$	N^*	R	N_j	N_{fj}	2956.828
534.25	0.009	15.07	440.45	-0.94512	1	295.9761	

The results of the application of the "relaxed" mean stresses instead of the stable values from the standard analysis show that for 7075 the predicted life goes from 1681 to 2420 cycles and for 7249 from 1800 to 2956. The experimental life for 7075 is 3568 and for 7249 is 2501 cycles.

The standard approach is again around 50% conservative for 7075, while the application of the "relaxed" state gives around 30% conservative results. For the case of 7249, the standard approach is less conservative, around 30%, and the application of the relaxed state of mean stress gives slightly non-conservative results, with a % difference in life of 16%.

Mean stress relaxation in life calculation has without doubt considerable effect. Life predictions are significantly changed in all cases when the "relaxed" state of mean stress is included in the analysis. The incorporation of mean stress relaxation in life calculation is possibly a way to overcome the highly conservative predictions sometimes obtained with a standard approach. In all the cases shown, involving strain with a tensile bias, the standard analysis is in fact, largely conservative, with an average ratio of predicted life and experimental life greater than 50%. This can be source of inaccuracies in life predictions also for more complex type of loadings. Opposite is expected for straining with a compressive bias.

The use of "relaxed" mean stresses in life calculation always gave less conservative results for 7075, but in both cases gave non-conservative results for 7249. Non-conservative results are undesirable in life calculations and potentially dangerous, but in all four cases life predictions were closer in absolute value to the experimental values.

7.2 Improvements with the Wetzel and Jiang model

The final goal of this study is to improve life calculation in the presence of mean stress relaxation. Some variable amplitude loading profiles or service type of loading profiles can cause more mean stress relaxation than others. This depends on how much the loading is biased with respect to a completely reversed condition and also on the amplitudes of the hysteresis loops involved in the loading. The predicted life with a traditional analysis can therefore highly differ from the life obtained experimentally.

Four life calculations methods are employed to observe the difference in predicted life for all the variable amplitude loading profiles obtained from laboratory tests for both aluminum alloys.

The first method analyzes the fatigue problem without considering mean stress relaxation. This method is the one implemented in the previous section with stable values of mean stress taken from the application of the Ramberg-Osgood formulation.

The second method performs life calculation with the stable values of mean stress obtained from experimental data, as shown in the previous section. The half-life values of mean stress for all the hysteresis loops in the loading are calculated with data points obtained from the tests. Since in this section all the different types of variable amplitude loading profiles are analyzed, in case of unstable repeated relaxation, where the choice of a single value of mean stress could be an oversimplification, all the mean stresses for the repetitions performed at half life of the test is used. This was the case for the single Type B and three Type C tests for each alloy.

The third method employs the Wetzel model to simulate mean stress relaxation in variable amplitude loading. The stable values are taken from the simulated data and used to perform life calculation. In the case of unstable repeated relaxation, the same approach employed in the second method is used.

The forth method employs the Jiang model to simulate mean stress relaxation. The stable values are taken from half-life of the simulated response and employed in life calculation. The same approach holds for unstable repeated relaxation.

Four values of predicted lives per test are therefore obtained. Those values are then compared to the experimental life of the test and results on the performance for the different methods can be obtained.

Similarly to what was done in the previous section, all the loading patterns are analyzed with the rain flow counting method, then the Ramberg-Osgood relation is applied to obtain the peaks and valleys of stress for each point in the loading and then the mean stresses are calculated. Life prediction is performed with the strain-life curve, the Walker correction method for mean stresses and the Palmgren-Miner rule to account for the different number of reversals in the loading.

For the second, third and forth cases, the analysis of the variable amplitude loading is not changed and the only values modified in the prediction are the mean stresses, taken from experimental data, the Wetzel model simulation and the Jiang model simulation.

Results of life predictions are shown in Figure 7-3 and 7-4, where the four predictions are plotted along with the experimental life to compare visually the results.

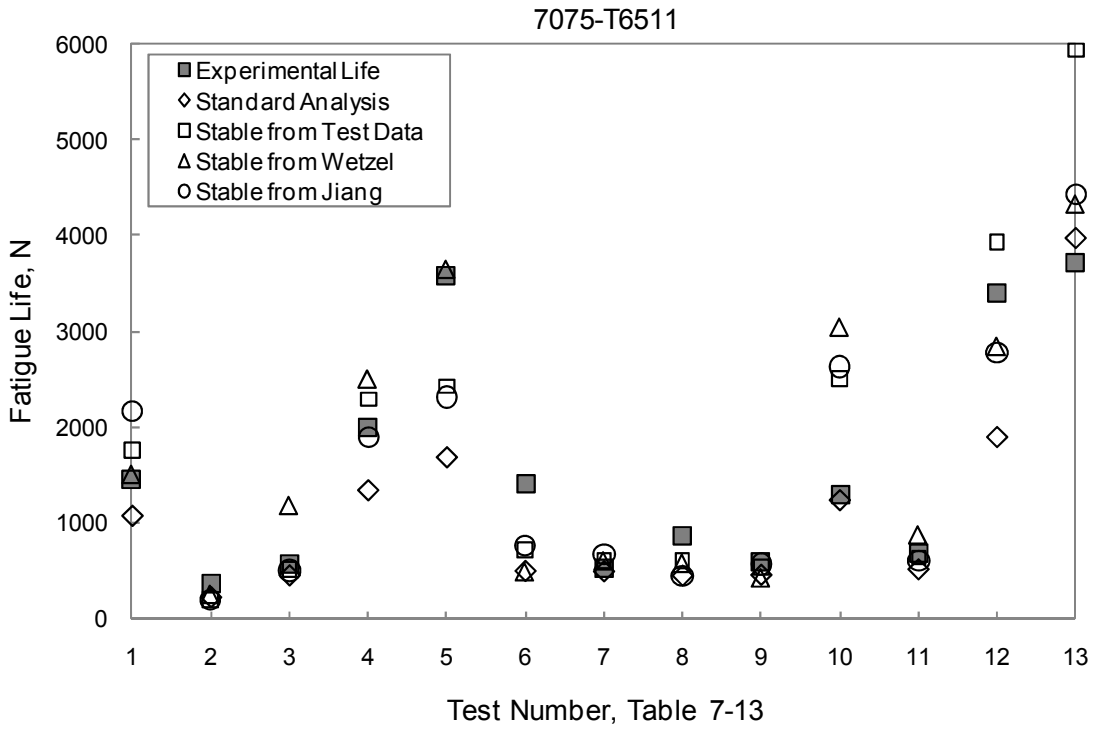

Figure 7-3. Performance of mean stress relaxation models in life calculation for 7075-T6511; the filled squares are the experimental lives.

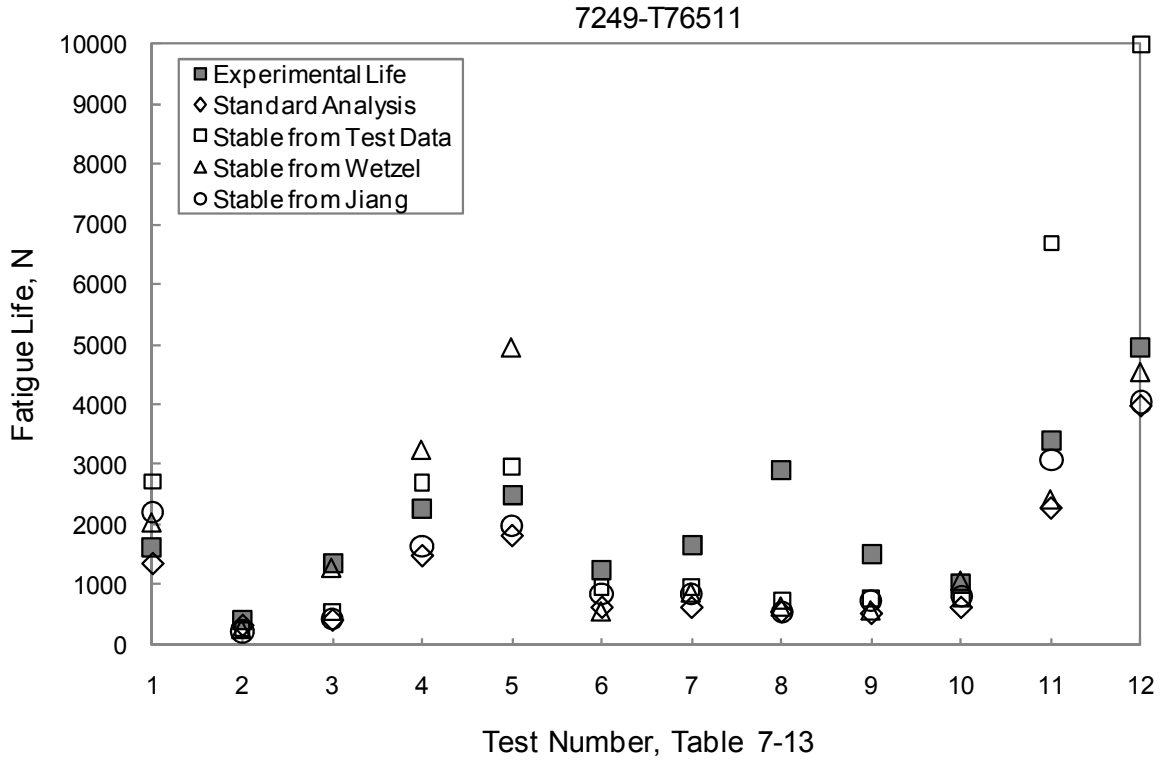

Figure 7-4. Performance of mean stress relaxation models in life calculation for 7249-T76511; the filled squares are the experimental lives.

Tables 7-13: Test numbers and test names of variable amplitude loading relaxation tests in Figure 7-3.

Test Number in Figure 7-3	Test Name	Type
1	B75-26	C
2	B75-49	C
3	B75-41	C
4	B75-71	A
5	B75-54	A
6	B75-44	A
7	B75-32	A
8	B75-2	A
9	B75-22	A
10	B75-63	A
11	B75-28	B
12	NAV-1-75-15	D
13	NAV-1-75-12	D

Tables 7-14: Test numbers and test names of variable amplitude loading relaxation tests in Figure 7-4.

Test Number in Figure 7-4	Test Name	Type
1	B49-44	C
2	B49-41	C
3	B49-13	C
4	B49-19	A
5	B49-60	A
6	B49-33	A
7	B49-8	A
8	B49-57	A
9	B59-50	A
10	B49-56	B
11	NAV-1-49-1	D
12	NAV-1-49-16	D

The success in material behavior representation shown in Chapter 6 for the models implemented is also shown in Figs. 7-3 and 7-4. The life calculated with the standard approach is most of the time further away from the experimental life than the life calculated with the mean stress relaxation models implemented in the current study. The standard approach is always calculating a predicted life shorter than the experimental life and in some cases shorter than any other predicted lives. The standard strain-based approach, without the use of any models to correct for mean stress relaxation, predicts highly conservative lives for the tensile biased strain histories.

Using stable values from test data is most of the time the closest to the experimental life. It has to be noticed that in both materials this method is not satisfactorily predicting life in the cases of irregular service types of loading. This might be due to the fact that the high presence of elastic loops in the loading causes retardation in the relaxation of the larger hysteresis loops. This difference in relaxation rate might influence the choice of using stable values in life calculations for this type of loading. This is just a way of saying that in the case of complicated loading histories or service type of loading histories, the use of a life calculation software able to analyze the loading cycle by cycle is suggested. For all the other cases the success of life predictions with stable experimental values shows that mean stress relaxation happens mainly in the first

part of the life and that most of the rest of the life is spent with mean stresses at their stable value.

The Wetzel model seems to be successful in more than half of the life calculations shown. In a few cases it is more conservative than the standard approach, and in some cases it is non-conservative. Both situations are therefore undesirable, but when predictions are non-conservative for the Wetzel model, the life predictions with the "relaxed" values of mean stresses from experimental data is also non-conservative. This situation happens for three Type A loadings for 7075 and 7249 and for one Type C loading for 7075. Those loadings involve the relaxation of hysteresis loops with comparable strain amplitudes. In fact, if compared with other loadings, the difference between the largest hysteresis loop and the smaller one in these variable amplitude patterns is reduced. This error might be overcome if the analysis is performed cycle by cycle and not with stable values only. Since the Wetzel model is frequently close to the life predictions obtained with stable "relaxed" value, the success in reproducing material behavior is confirmed.

The Jiang model is in most cases more conservative than the life prediction performed with the stable values from test data, but it is also in most cases less conservative than the standard approach. Consistent exceptions for both materials are the two predictions for the first type of Type C loading (tests B75-26 and B49-44) where the Jiang model is non-conservative and only for 7075 the relaxation of the Type B loading (test B75-63). It is possible that in this case also an analysis cycle by cycle would lead to significant improvements, since the life predictions with stable "relaxed" values is also slightly conservative in those cases. The Jiang model does not represent for all cases a large improvement with respect to the standard approach, but it is in the large majority of life predictions shows a less conservative tendency, without being non-conservative.

The percent difference in life for each model (standard, Wetzel, and Jiang) and the experimental data, calculated as:

$$\text{Difference in Fatigue Life, \%} = \frac{N_{\text{f_model}} - N_{\text{f_exp}}}{N_{\text{f_exp}}} * 100$$

Where N_{exp} is the experimental life of the test and N_{model} is the predicted life for the models. The calculated values are shown in Figures 7-5 and Figure 7-6.

Results show again that the standard model is always conservative, with an average percentage in life for the variable amplitude loading profiles tested of 29% for 7075 and 44% for 7249. This means that in average using the standard approach, without the use of a model to account for mean stress relaxation, the life predicted are from 29% to 44% shorter.

The use of a model to account for relaxation is desirable to avoid overly conservative predictions. The Wetzel model is able in some cases to reduce the error in life predictions, but in some other cases it becomes non-conservative. The average life prediction for Wetzel is a 11% error in favor of a non-conservative result for 7075 and a 11% in favor of a conservative result for 7249. These values are due to the fact that the conservative predictions (accounted as negative percentages) and non-conservative predictions (accounted as positive percentages) balance each other.

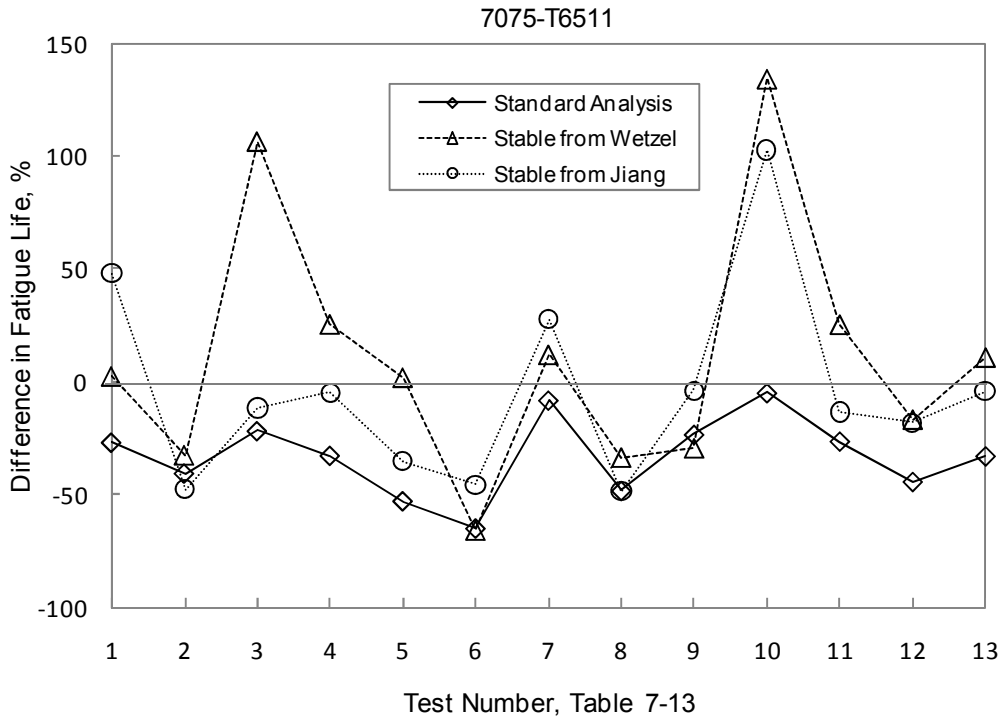

Figure 7-5. Percentage difference between predicting models and experimental life for 7075-T6511; the models used are a standard strain-based approach, and the improved version developed in this study, with the use of the Wetzel model or the Jiang model.

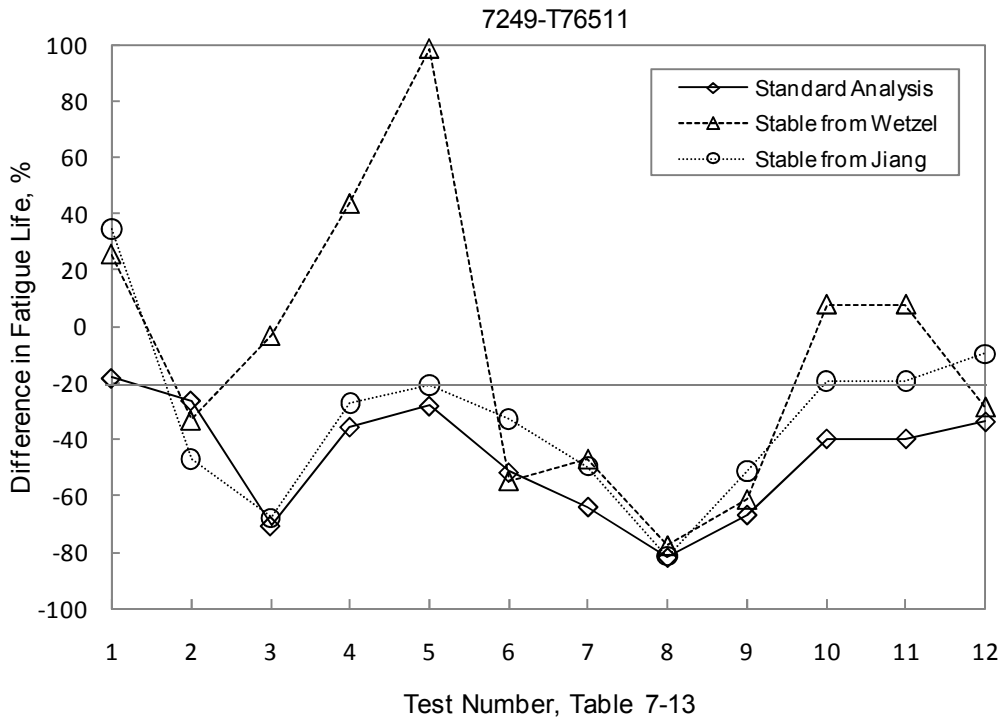

Figure 7-6. Percentage difference between predicting models and experimental life for 7249-T76511; the models used are a standard strain-based approach, and the improved version developed in this study, with the use of the Wetzel model or the Jiang model.

In few cases where the relaxed stable values gave a non-conservative life calculation, the Wetzel model gave a conservative one. Those cases seemed to confuse the comparison and so were next omitted in the comparison. The other percentage differences are calculated as absolute values and averaged to obtain a more significant performance index.

If the method described in the previous paragraph is applied, the Wetzel model has a percentage difference in life even lower in absolute value for 7075, 9%, but in favor of a conservative prediction. The percentage for 7249 goes up to 33%.

The Jiang model generally performs better than the Wetzel model from the point of view of stability of results, as it is most of the time conservative. Only in three cases the Jiang model has shown to be non-conservative and in all three of those case the life predictions with “relaxed” stable values also proved to be non-conservative.

Results show that the average error for life prediction of 7075 is 2% and the average error for predictions of 7249 is 32% for 7249. There is an improvement in both

cases, since the standard approach would lead to higher errors. The Jiang model is able to correct some of the overly conservative results in life calculation without frequently leading to non-conservative results as the Wetzel model. In some other cases though the model is non conservative, and if those points are taken out of the analysis, the percentages of improvements go up to 21% for 7075 and 38% for 7249 in favor of a conservative result.

In all cases it is interesting to notice that life calculation for service types of loading are always showing successful results. For 7075 life predictions of the two service type of loading with the standard approach show 18% conservative results, while with the use of the Wetzel model or the Jiang model the difference is reduced to 1% and , towards conservative predictions. For 7249 the two service type of loading have life predicted with an average of 26% on the conservative side for the standard approach, while the Wetzel model reduces this difference to 18% and the Jiang model to 14% towards a conservative prediction.

The use of the Wetzel or the Jiang models can be suggested as a good way to overcome the difficulties with life predictions for cases of high level of mean stress relaxation. The encouraging results with the two service type of loading tested on both materials confirm the convenience in introducing mean stress relaxation into life calculation.

An implementation into FAMS is therefore suggested as the difference in predicted and experimental life can be reduced with the use of both models. In some cases predictions are non-conservative, but this mainly happened when also predictions with the use of “relaxed” stable values from experimental results also gave non-conservative lives. The implementation into a life calculation software able to analyze cycle by cycle the different loadings might solve this problem.

Chapter 8
Discussion and Conclusions

8.1 7075 and 7249 Aluminum alloys

The first goal of this study was to collect fatigue life data with axial un-notched specimens of two aluminum alloys. One of the alloys under investigation, 7075-T6511, was of particular importance to the sponsor of the project because it has been intensely used to build structural components of airplanes and helicopters. The other of the two alloys was a fairly new type of high strength aluminum alloy, 7249-T76511, engineered to be more resistance to corrosion. This is of great interests especially for aircraft working in aggressive environmental conditions. High performance alloys, like most of the 7^{th} series alloys, are influenced by corrosion phenomena.

The data collected are used to characterize the performance of the materials, from the point of view of a stress-strain response, stress-life response and strain-life response. Once the mechanical behavior of the materials is characterized, comparisons can be done to evaluate similarities and differences.

Depending on their function, on the type of loading conditions, on the type of environmental conditions, on the desired cost and frequently also on environmental impact issues, mechanical parts are designed for a specific type of material. If some components are desired to be more corrosion resistant than the ones built with 7075-T6511, then the substitute material has to satisfy a certain bound of acceptance from a mechanical point of view.

In this Chapter the behavior of 7075-T6511 and 7249-T76511 are shown with direct comparison between the fitted lines of the models chosen. The model used to describe the stress-strain behavior is the Ramberg-Osgood equation.

The stress-strain behavior of the two alloys is quite similar. The stable stress-strain curve for 7249 has slightly lower yield point and is consistently lower with increasing strain amplitude. If a ± 5% bound is drawn in Figure 8-1 starting from the stable 7075-T6511 stress-strain curve, the 7249-T76511 stable stress-strain curve is included in this bound. The difference is therefore minimal and considering a practically

perfect match for the elastic part, a possible substitution of one material with the other can be acceptable.

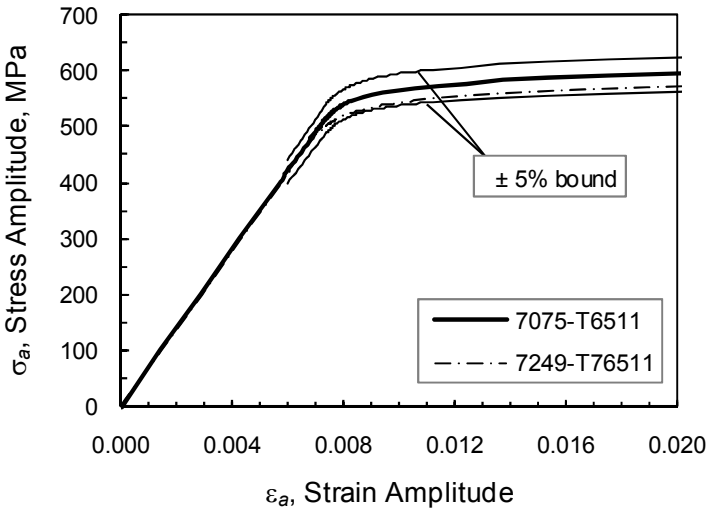

Figure 8-1. Comparison of stable cyclic stress-strain behavior for 7075-T6511 and 7249-T76511.

The Walker approach has been used to model the stress-life behavior for both materials and it was shown to be the most successful and accurate mean stress model. A mean stress model is needed as the high majority of tests were run with the intention to characterize the mean stress sensitivity of both alloys. These tests can be included in a stress-life analysis only with the use of a mean stress model.

In Figure 8-2 the trends are compared and it can be observed that the two materials have extremely similar equivalent stress-life behavior. The intermediate and long life region is of course of major interest in this type of analysis and the two curves for the materials are practically overlapping until approximately 10^5 cycles. After this point in life, the predicted lives for 7249 are lower than the ones predicted for 7075. Another difference is the intersection point for the two curves, with 7249 showing a slightly higher values of life for this point. The low cycle fatigue region for the two material shows comparable trends, with a close value of slope for the fitted line.

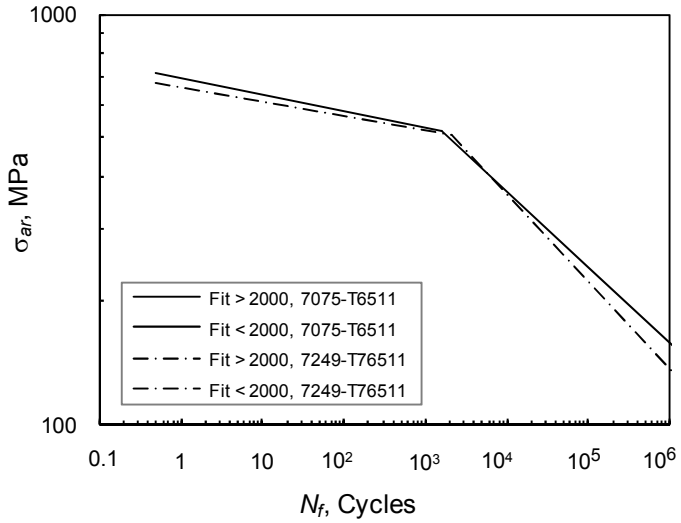

Figure 8-2. Comparison of stress-life Walker fit for 7075-T6511 and 7249-T76511.

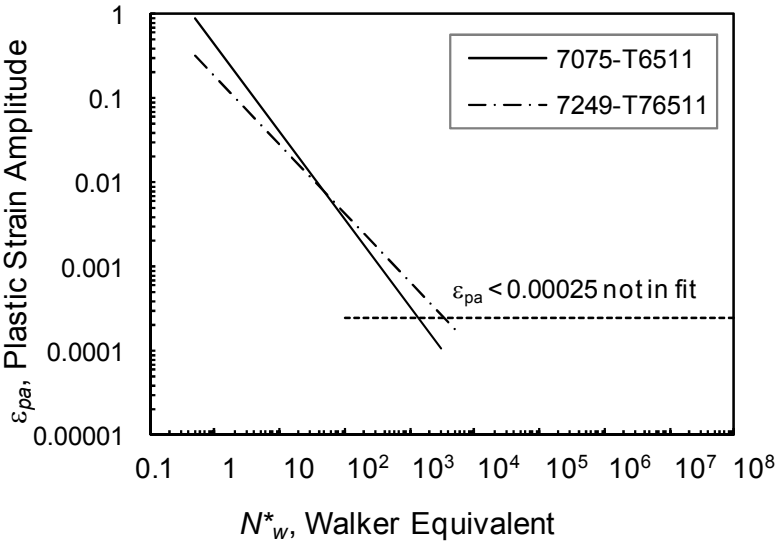

Figure 8-3. Comparison of plastic strain-life fit for 7075-T6511 and 7249-T76511.

A complete strain-based analysis, with formulation shown in Eq. 1.3, requires the characterization of the plastic strain-life relation for the materials, fitted lines for 7075 and 7249 are shown in Figure 8-3. The differences between 7075 and 7249 are more pronounced and this reflects into the values of the constants c and ε_f' for the materials. The slope of the fitted line is not very dissimilar, but this could be a factor when designing structural part with 7249. From approximately 0.5% plastic strain amplitude, the predicted lives for 7249 are actually higher than the ones predicted with the fitted line

of 7075. When plastic deformations become higher though the trend is reversed and the predicted lives for 7249 are lower than the ones predicted for 7075.Such high levels of plastic strain are unusual to be reached in service loading, therefore this part of the graph is not as important as the one corresponding to moderate plastic strain amplitudes.

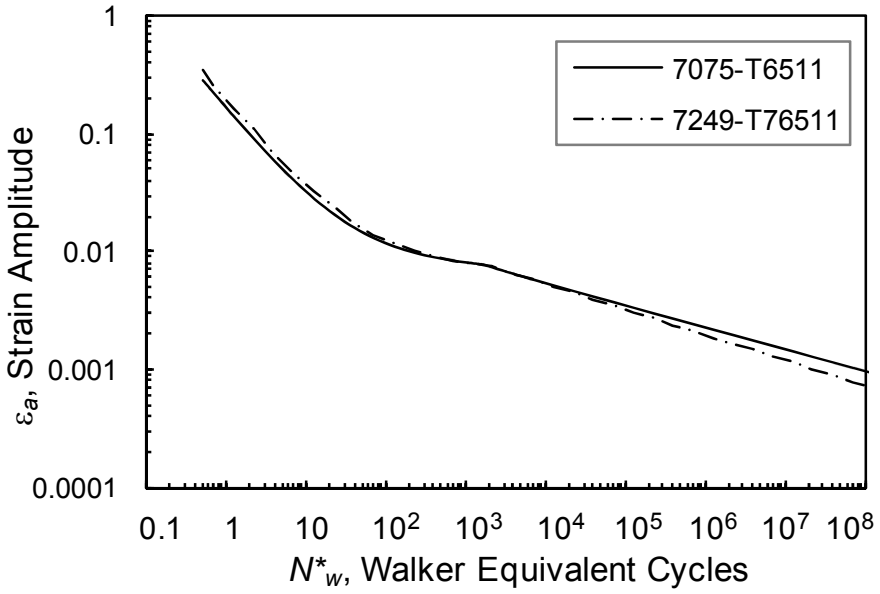

Figure 8-4. Comparison of strain-life fit for 7075-T6511 and 7249-T76511.

The strain-life behavior has high degree of similarity in the two alloys. There is almost no difference in the curve corresponding to high level of plastic strain deformations and the two curves almost overlap until approximately 10^5 cycles, where 7075 show a slightly less severe slope. This region is highly important when doing life calculations, since most of the life of the component will be spent deforming elastically in a typical service loading. The 7075 fit determines predicted lives higher than the 7249 fit.

Concluding, the materials have similar behavior, from the point of view of stress-strain, equivalent stress-life and strain-life behavior. More dissimilarities have been observed for the plastic strain-life fit, but this might also be due to the fewer points used for this fitting. More tests could be run to obtain a higher number of points in the plastic strain-life plot and evaluate better the differences between the two materials. As an additional factor, the same tests run in this study can be repeated several times to obtain

bounds of acceptance in strain-life trend, so that confidence levels and error bounds can be determined for both materials and reliability analysis can be performed.

The material constants obtained in this study are nonetheless accurately representative and details on the accuracy of the constants obtained with these fitting techniques can be found in ASTM standards [5].

As a general comment about the method used to analyze fatigue data, the use of a Ramberg-Osgood curve for the stress-strain is satisfactory. The agreement between fitted curve and experimental data is good and the curve represents well material behavior.

The Walker equation has been found to be a good solution to reduce mean stress data and obtain stress-life constants. The division of the set of data in two sets depending on the value of mean stress has also been proven to be successful. This was necessary from the point of view of fitting as it improved greatly the agreement between trend lines and experimental data.

The plastic strain-life relation is also able to it experimental data well. The shape of the strain-life curve, with the characteristic elbow corresponding to N_i, is due to the division of the stress-life curve in two segments. The success of the scatter of experimental data around the curve is a sign of good representation of the fatigue data collected.

8.2 Mean Stress Models

The Walker model has been shown to be the most accurate model in representing material sensitivity to mean stress. The values of γ obtained are comparable and really close to 0.5.

Among the other models, some have shown to be more representative than others for those materials. In the Figures 8-5 and 8-6 below, a summary of the scatter obtained for the Goodman, Morrow fracture, Morrow intercept and SWT models is shown.

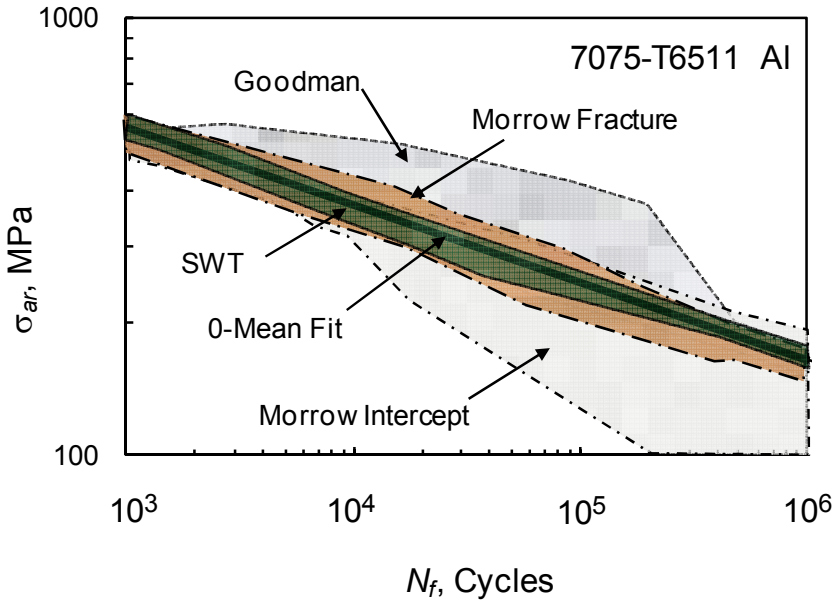

Figure 8-5. Area comparison of Goodman, Morrow fracture and intercept, and SWT mean stress models for 7075-T6511.

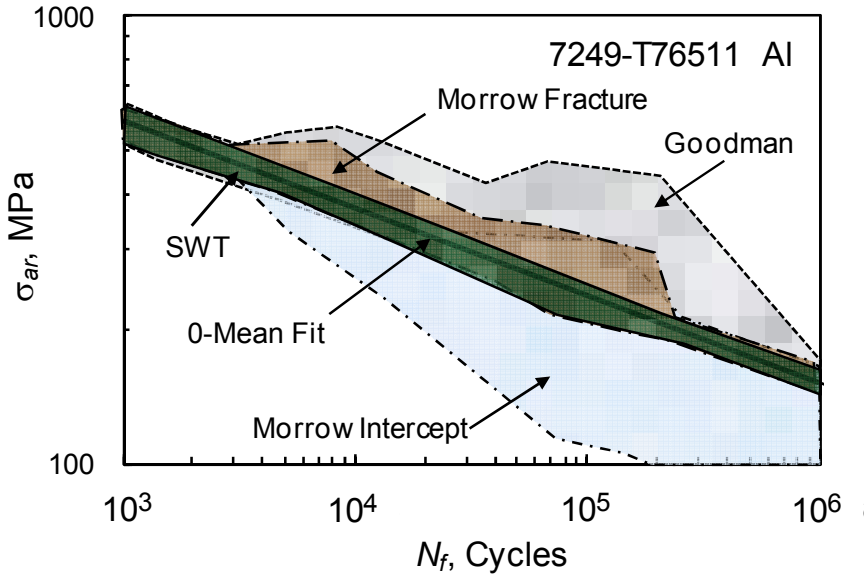

Figure 8-6. Area comparison of Goddman, Morrow fracture and intercept, and SWT mean stress models for 7249-T76511.

The areas highlighted represents the scatter obtained between the zero-mean line and the experimental data. The contours of the area are drawn based on the most external data points around the zero-mean line observed for each plot.

The regions including the areas around the zero-mean line are divided in conservative region, above the zero-mean line, and non conservative region, below the zero-mean line.

It is then at a first glance possible to determine that the Goodman model in both cases is highly conservative, with most of the area scattered above the fitted line. The Morrow intercept model is mostly non conservative, and by far the worst performing model, with a large area below the zero-mean line. The Morrow fracture model is able to reduce the scatter in both cases, with a slightly higher conservatism for 7249. The SWT model is the best among these four models as expected since it correspond to a Walker model with γ equal to 0.5. The area around the zero-mean line is minimal and not biased in conservatism or non conservatism.

FAMS implements SWT and Morrow Fracture models to analyze fatigue loading problems. For 7075 and 7249 aluminum alloys, the use of SWT is highly suggested. The possibility of inclusion of the Walker model could also be considered. The application of the Walker model depends on the availability of fatigue data with attention on tests with different mean stresses, so that a value for γ can be estimated. The implementation of the Walker model into a life calculation software does not differ much from the implementation of the SWT model.

8.3 Mean Stress Relaxation

8.3.1 Constant amplitude loading and the Landgraf model

The mean stress relaxation behavior of both aluminum alloys has been characterized. Relaxation curves for mean stresses have been shown to occur in different loading conditions and for different strain amplitudes. Surprisingly it was noticed that relaxation can occur even well below the yield strain of the material. This is an important aspect since elastic deformations can still be responsible of a high degree of relaxation. Large part of the life of mechanical components is spent in the elastic regime, with

occasional higher plastic overloading. In this scenario a significant level of relaxation could occur during service life, compromising the reliability of the mean stress analysis in fatigue.

The amount of mean stress relaxation has been successfully related to strain amplitude in constant amplitude loading. The decays were fitted with an exponential decay with the number of cycles N as base and a relaxation exponent dependent on the strain amplitude of the test.

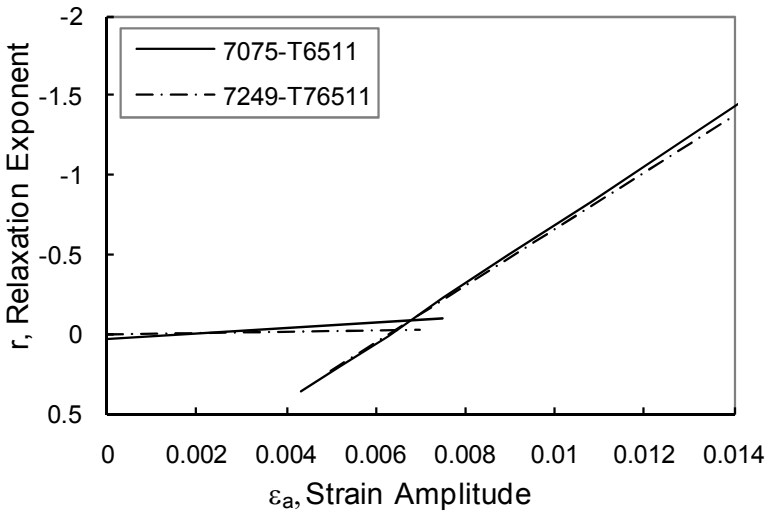

Figure 8-7. Comparison of Landgraf model behavior for 7075-T6511 and 7249-T76511.

Both materials behave similarly in constant amplitude loading, as shown in Figure 8-7, and the distinction between the two regions of behavior is clearly visible. One corresponds to relaxation curves for hysteresis loops with large amounts of plastic strain involved and one for hysteresis loops with a low and in some cases almost negligible amount of plastic strain. A strain amplitude threshold has been individualized and for both alloys is close to 0.6% strain, therefore not dissimilar to the cyclic yield point.

Most of the relaxation curves obtained experimentally were successfully reproduced with the use of the Landgraf model, proving this model to be particularly accurate in reproducing this transient phenomenon. Improvements have been made to the model with the introduction of σ_b and also a superior method for fitting has been developed to analyze relaxation curves.

8.3.2 Mean stress relaxation in variable amplitude loading

The problem of mean stress relaxation in constant amplitude loading is not of primary interest when dealing with life calculation. The main goal of the analysis is to be able to model mean stress relaxation in variable amplitude loading and in service type of loading.

A tentative attempt to adapt the Landgraf model to variable amplitude loading was performed, but the simulations results didn't show promising possibilities of development.

The focus was then shifted to plasticity models able to reproduce transient effects. Several models shown in literature were analyzed and finally a first screening revealed the interesting performances of the Wetzel model (1971) and the Jiang model (1996). Both models were optimized for the current scope of the research:

Thirteen variable amplitude loading tests were run on both alloys, following an increasing level of difficulty in the loading profiles. Two service type of loading were used to observe relaxation; the service loading was given by TDA, Inc and it is representative of a typical helicopter spectrum loading. The plasticity models performance was observed gradually from the simplest variable amplitude loading tests to the most complicated ones.

8.3.2.1 The Landgraf model

The application of the Landgraf model to variable amplitude loading seems to be a forcing of a good constant amplitude loading fitting formulation to a problem outside the correct context. Results are not totally unacceptable, but it doesn't seem very feasible to incorporate this model into a variable amplitude loading analysis. The main reason is that the counting of the number of cycles is not meaningful in variable amplitude loading. The relation between mean stress and number of cycles is lost in variable amplitude loading. The relaxation decays do not follow anymore a simple exponential decay with N as base.

One way to apply the Landgraf approach to variable amplitude loading could be to relate the decays to a value dependent on the number of cycles, mean stress and strain amplitude, i.e. damage:

$$d = f(N, \sigma_m, \varepsilon_a) \longrightarrow \Delta\sigma_r = f(N, \sigma_m, \varepsilon_a) \quad (6.4)$$

The amount of accumulated damage in the loading depends on $\sum \frac{N_j}{N_{jf}}$, if a Palmgren-Miner rule is used. At the same time N_{jf} depends on ε_a and σ_m in a strain-based fatigue approach, with the use of a mean stress model to account for mean stress effects. If a successful relation is obtained through the use of the Landgraf model between accumulated damage and $\Delta\sigma_r$, the relaxation delta can be applied to any model reproducing material behavior. This could be a similar approach to the Wetzel-table approach developed in the current study.

The damage model is not developed in this study, but it would possibly be developed as a viable application of the Landgraf model analysis.

8.3.2.2 The Wetzel model

The Wetzel formulation was adapted to accommodate different rates of relaxation for different values of strain amplitudes, and the Jiang model was simplified and optimized for mean stress relaxation in variable amplitude loading.

The Wetzel relaxation constant M_r was substituted by a M_r relaxation function, dependent on the strain amplitude of the loading segment undergoing relaxation. The model was then used to obtain a relaxation table, since it would be easier the use of a relaxation table in FAMS, than the complete implementation of the Wetzel model.

The Wetzel-table model is globally successful in reproducing relaxation behavior in both constant and variable amplitude loading cases. There are margins of improvements, especially for constant amplitude loading. For variable amplitude loading, the performance is acceptable with values of stable mean stresses always close to the experimental ones.

The simplicity in dealing with such a complicated transient effect is outstanding and the table version of the model makes possible to add the relaxation feature to any other models. In addition, the behavior in complicated loading patterns or service

loadings being the main interest in this research, the Wetzel model is suggested for implementation into FAMS.

8.3.2.3 The Jiang model

The Jiang model was applied without some of its features, like the Baushinger effects and the stress based memory surface. These would have just added difficulties in the managing of the model and in the fitting of material constants. Incremental step tests were considered a good choice for the stress-strain fitting of the Jiang model and this was proven to be a successful choice. A Monte Carlo analysis was also performed on the Jiang model to highlight the most important parameters responsible of mean stress relaxation. Optimization methods were finally applied, so that those parameters could be estimated.

The performance of the Jiang model is satisfactory, from the point of view of stable values reached at half life and reproduction of material behavior, with higher errors only in the reproduction of constant amplitude loading profiles.

The constant amplitude loading performance is influenced by the optimization process, run on variable amplitude loading only. This causes the larger loops to relax less than what would be observed in a simple constant amplitude loading case. The different rate of relaxation observed experimentally for the same hysteresis loop in constant and variable amplitude loading case is not reproduced by the Jiang model. Nonetheless most of the transient phenomena involved are reproduced correctly, like unstable repeated relaxation. This is clearly visible in the 2-Blocks loading, with smaller hysteresis loops relaxing inside a large one with decreasing rate, as observed in experimental data.

The formulation of the Jiang model is able to successfully reproduce most of the behaviors show during cyclic loading of aluminum alloys. The optimization process is able to focus the accuracy of the model towards variable amplitude loading and this leads to a improved performance for service type of loading. The computational effort in determining successful stress-strain constants and in running the optimization process, along with the computational effort required by the Jiang model itself is an obstacle to a successful implementation in a life calculation software. The table approach used for Wetzel would be a good solution for the Jiang model too.

The Jiang model, even in its simplified form, is not trivial to include into FAMS, and it is a cause of perplexities because of its different stress-strain formulation and the use of material constants of unclear physical meaning, like $\chi_{(i)}$'s. The fitting process described above is mainly aimed to reproduce material behavior and to obtain the closest transient response. It is desirable to individualize a set of standard variable or constant amplitude loading tests so that the same optimization process can be run for any material.

In case of reluctance in the change of the structure of FAMS or simply if a faster method to use the Jiang model is needed, the Wetzel table method could be applied also for the Jiang model. Considering also that the Jiang model in the form used in this study is deprived of its memory surface, an absence of memory could be postulated in this case also; in any case, because of the way the loadings are structured, this will not be influential on the relaxation for the first cycles.

8.4 Life Calculation

Analysis on life predictions with or without the use of methods to account for mean stress relaxation has been performed. Results show that a standard method is always conservative for tension-biased strain histories, but frequently predicted cycles to failure are excessively less than the experimental lives.

The Wetzel table model and the Jiang model were used to obtain stable relaxed states of mean stresses for the different variable amplitude loadings run on both alloys. Life calculation was implemented in a traditional way, with the use of Ramberg-Osgood formulation, rain flow counting method and the strain-life curve with the constants obtained from Chapter 4. The Walker model was then used to correct for mean stress.

Comparison of predicted lives to failure and experimental lives show that in some cases the analysis cycle by cycle is necessary to avoid non conservative predictions, especially for the case of the service type of loading. Even with inaccuracies derived from the consideration of stable "relaxed" mean stresses only, the Wetzel and the Jiang model were able to sensibly reduce the difference in predicted and experimental life for both service types of loading and in both material consistently.

Considering the tests where this effect was less influential on the analysis, the Wetzel and the Jiang model were able to predict life to failure in average better than the standard approach, with an average improvement varying from 7% up to 20%.

This number might not seem high at a first look, but the possibility of predicting lives with a 6-7% improvements for service type of loading with several millions cycles translates into a gain of thousands of cycles and possibly hours of service load.

In addition if the implementation of those models into FAMS is performed, both models could be applied cycle by cycle, eliminating a possible source of inaccuracy.

References

1. Stephens, R. I., and Fuchs H. O., 2001, *Metal Fatigue in Engineering*. New York: Wiley.
2. Sines, G., and Waisman, J.L., 1959, *Metal Fatigue*, McGraw-Hill, NewYork.
3. Dowling, N.E., 2006, *Mechanical Behavior of Materials*. 3rd ed. : Prentice Hall; 3 edition (April 15, 2006)
4. Kundu, T., 2008, *Fundamentals of Fracture Mechanics*. Boca Raton, FL: CRC Press.
5. Standard Practice for Strain-Controlled Fatigue Testing, in ASTM International, Vol. 03.01, E606.2005.
6. Ramberg, W., and Osgood, W. R., 1943, "Description of stress-strain curves by three parameters". *Technical Note No. 902*, National Advisory Committee For Aeronautics, Washington DC
7. JoDean Morrow, 1965, "Cyclic Plastic Strain Energy and Fatigue of Metals," *Internal Friction, Damping, and Cyclic Plasticity*, ASTM STP No. 378, Am. Soc. for Testing and Materials, Philadelphia, PA.
8. Carlson, R. L., and Kardomateas, George A., 1996, *An Introduction to Fatigue in Metals and Composites*. London: Chapman & Hall.
9. Lukas, P., Klesnil, M., and Polak J., 1974, "High Cycle Fatigue Life of Metals". *Materials Science and Engineering,* Elsevier Sequoia S. A., Lausanne, The Netherlands, Vol. 15, pp. 239-245.
10. Dowling, N.E., 1973, "Fatigue life and inelastic strain response under complex histories for an alloy steel". *Journal of testing and evaluation*, 1(4).
11. Manson, S. S., Freche, J. C., and Ensign, C. R., 1966, "Application of a Double Linear Damage Rule to Cumulative Fatigue". *Fatigue Crack Propagation,* ASTM STP 415, Am. Soc. for Testing and Materials, pp. 384-412.
12. Topper, T. H., and Lam, T. S., 1997, "Effective Strain Fatigue Life Data for Variable Amplitude Fatigue". *Int. Journal of Fatigue, Vol. 19, Supp. No. 1*, pp. S137-S143.
13. Matsuishi, M. and Endo, T., 1968, "Fatigue of Metals Subjected to Varying Stress". *Japan Society of Mechanical Engineers*. Fukuoka, Japan.
14. Dowling, N.E., 1972, "Fatigue Failure Predictions for Complicated Stress-Strain Histories". *Journal of Materials, Vol.7, No, 1*, pp. 271-287.

15. Iyyer, N., 1998, *" Fatigue Analysis of Metallic Structures (FAMS)",* Aerostructures Inc., Arlington, VA, Technical Report 98005.
16. Bílý, Matěj., 1993, *Cyclic Deformation and Fatigue of Metals*. Materials science monographs, 78. Amsterdam: Elsevier.
17. Goodman, J., 1919, *Mechanics Applied to Engineering*. Longmans, Green and Co., London, pp. 631-636.
18. Smith, J. O., 1942, *The Effect of Range of Stress on the Fatigue Strength of Metals*, Bulletin No. 334. University of Illinois, Engineering Experiment Station, Urbana, IL, Feb. 1942. See also Bulletin No. 316, Sept. 1939.
19. Morrow, J., 1968, *Fatigue Properties of Metals*, Section 3.2. Fatigue Design Handbook, Pub. No. AE-4. Soc. of Automotive Engineers, Warrendale, PA. Section 3.2 is a summary of a paper presented at Division 4 of the SAE Iron and Steel Technical Committee, Nov. 4, 1964.
20. Bridgman, P. W., 1944, *The Stress Distribution at the Neck of a Tension Specimen*. Trans. of the Am. Soc. for Metals, Vol. 32, pp. 553-574.
21. Smith, K. N., Watson, P. and Topper, T. H., 1970, "A Stress-Strain Function for the Fatigue of Metals". *Jnl. of Materials, ASTM, Vol. 5, No. 4*, pp. 767-778.
22. Walker, K., 1970, *The Effect of Stress Ratio During Crack Propagation and Fatigue for 2024-T3 and 7075-T6 Aluminum*. Effects of Environment and Complex Load History on Fatigue Life, ASTM STP 462. Am. Soc. for Testing and Materials, Philadelphia, PA, pp. 1-14.
23. Duga, J.J., Fisher, W.H., et al., 1983, Fracture costs US 119 billion a year, says study by battelle/NBS, *Int. J. of Fracture*, vol. 23-3, R81-R83.
24. Knipling, K. E., 2003, *High-cycle fatigue / low-cycle fatigue interactions in Ti-6Al-4V*. Blacksburg, Va: University Libraries, Virginia Polytechnic Institute and State University. http://scholar.lib.vt.edu/theses/available/etd-02252003-110749.
25. K. Koibuchi, and Kotani S., 1973, "*The Role of Cyclic Strain Behavior on Fatigue Damage Under Varying Load*," Cyclic Stress-Strain Behavior: Analysis, Experimentation and Failure Prediction, ASTM STP 519, Am. Soc. for Testing and Materials, pp. 229-245.
26. P. Heuler, and Seege, T., 1986, "A Criterion for Omission of Variable Amplitude Loading Histories," *International Journal of Fatigue, Vol. 8, No. 4*, pp. 225-230.
27. A. Conle, and Topper,T. H., 1980, "Overstrain Effects During Variable Amplitude Service History Testing," *International Journal of Fatigue*, *Vol. 2, No. 3*, pp. 130-136.

28. Topper, T. H., and Sandor, B. I.,1970, *"Effects of Mean Stress and Prestrain on Fatigue Damage Summation"* Effects of Environment and Complex Load History on Fatigue Life, ASTM STP 462, Am. Soc. for Testing and Materials, Philadelphia, PA, pp. 93-104.
29. Watson, P., and Topper, T. H., 1971, "*The Effects of Overstrains on the Fatigue Behavior of Five Steels*" 1970 Fall Meeting of the Metallurgical Society of AIME, Cleveland, OH, Oct. 1970. See also: Watson, P., The Effect of Mean Stress and Overstrains on the Fatigue Behavior of Structural Steels, PhD Dissertation, Department of Civil Engineering, University of Waterloo, Ontario, Canada.
30. M. Kikukawa, Jono, M. and Song, J., 1973, "Cumulative Damage and Behavior of Plastic Strain Below Fatigue Limit," Third International Conference on Fracture, Munich, West Germany.
31. Landgraf, R. W., 1970, "The Resistance of Metals to Cyclic Deformation". *Achievement of High Fatigue Resistance in Metals and Alloys*, ASTM STP 467, Am. Soc. for Testing and Materials, West Conshohocken, PA, pp. 3-36.
32. Landgraf, R. W., Morrow, J., and Endo, T., 1969, "Determination of the Cyclic Stress-Strain Curve". *Journal of Materials, ASTM, Vol. 4, No. 1*, pp. 176-188.
33. Rossino, L. S., Castro, F.C., Bose Filho, W.W., Araujo**,** J.A., 2009**,** *"Issues on the mean stress effect in fretting fatigue of a 7050-T7451 Al alloy posed by new experimental data". International Journal of Fatigue, Volume 31, Issues 11-12*, Pages 2041-2048
34. Wehner, T. and Fatemi, A., 1991, Effects of Mean Stress on Fatigue Behavior of a Hardened Carbon Steel. *Int. Jnl. of Fatigue, Vol. 13, No. 3*, pp. 241-248.
35. Dowling, N.E. and Thangjitham, S., 1999, *Overview and discussion of basic methodology for fatigue*, in 31st National Symposium on Fatigue and Fracture Mechanics: Cleveland, OH; USA. pp. 3-36.
36. Peterson, R. E., 1974, *Stress concentration factors; Charts and relations useful in making strength calculations for machine parts and structural elements*. New York: Wiley.
37. Dowling, N. E., Calhoun, C. A., and Arcari, A., 2009, "Mean Stress Effects in Stress-Life Fatigue and the Walker Equation," *Fatigue and Fracture of Engineering Materials and Structures, Vol. 32, No. 3*, pp. 163-179. Also, Erratum, Vol. 32, October 2009, p. 866.
38. Dowling, N. E., 2009, "Mean Stress Effects in Strain-Life Fatigue," *Fatigue and Fracture of Engineering Materials and Structures, Vol. 32, No. 12*, pp. 1004–1019.

39. Morrow, J. and Sinclair, G.M., 1958, *Cycle-Dependent Stress Relaxation*. Symposium on Basic Mechanisms of Fatigue. ASTM STP 237, Am. Soc. for Testing and Materials, Philadelphia, PA,. p. 83-109.
40. Zhuang, W.Z. and Halford, G.H., 2001, Investigation of residual stress relaxation under cyclic load. *International Journal of Fatigue, Vol. 23*, pp. 531-537.
41. Landgraf, R.W. and Chernenkoff, R.A., 1988, *Residual Stress Effects on Fatigue of Surface Processed Steels*. In: Champoux RL. et al. Analytical and Experimental methods for Residual Stress Effects in Fatigue. ASTM STP 1004, eds. American Society for Testing and Materials, West Conshohocken, PA, pp. 1-12.
42. Fang, D. and Berkovits, A., 1994, Mean stress models for low-cycle fatigue of a nickel-base superalloy. *International Journal of Fatigue, Vol. 16, No. 6,* pp. 429-437.
43. Arcari, A., De Vita, R., Dowling, N.E., 2009, "Mean Stress Relaxation During Cyclic Straining of High Strength Aluminum Alloys," *International Journal of Fatigue, Volume 31, Issues 11-12*, Fatigue Damage of Structural Materials VII, Pages 1742-1750, ISSN 0142-1123, DOI: 10.1016/j.ijfatigue.2009.01.021.(http://www.sciencedirect.com/science/article/B6V35-4VJ4WRR-2/2/88e318cc613aaca50c011939b8fed89a)
44. Bauschinger, J., 1886, On the change of position of the elastic limit of iron and steel under cyclic variations of stress. *Mitt. Mech. Tech. Lab*. München 13, 1–115.
45. Armstrong, P. J. and Frederick, C. O., 1966, *A mathematical Representation of the multiaxial Baushinger Effect,* Report RD/B/N 731, Central Electricity Generating Board.
46. Jain, S. K., 1989, *Introduction to theories of plasticity*. Blacksburg, Va. (P.O. Box 302, Blacksburg 24060): Engineering Publications.
47. Dunne, Fionn, and Nik Petrinic. 2005, *Introduction to computational plasticity*. Oxford: Oxford University Press.
48. Kaliszky, Sándor., 1989, *Plasticity: Theory and Engineering Applications. Studies in applied mechanics*, 21. Amsterdam: Elsevier.
49. Lee, W. B., 1992, *Advances in Engineering Plasticity and Its Applications: Proceedings of the Asia-Pacific Symposium on Advances in Engineering Plasticity and Its Applications*, AEPA '92, Hong Kong. Amsterdam: Elsevier, 1993.
50. Paglietti, A., 2007, *Plasticity of cold worked metals: a deductive approach*. Southampton: WIT Press.
51. Yu, Maohong, 2006, *Generalized Plasticity*. Berlin: Springer.

52. Chaboche, J. L. et al., 1979, *Modelization of the Strain Memory Effect on the Cyclic Hardening of 316 stainless Steel, structural Mehcanics in Reactor Technology*, Transactions of the Fifth Int. Conf. on Structural Mechanics in Reactor Technology, L11/3.
53. Jiang, Y., Sehitoglu, H., 1996, Modeling of Cyclic Ratchetting Plasticity, Part 1: Development of Constitutive Relations, *Transactions of the ASME, Vol. 63*.
54. Doring, R. et al., 2003, A plasticity model for calculating stress-strain sequences under multiaxial non proportional cyclic loading, *Computational Materials Science, Vol. 28*, pp. 587-596.
55. Yanyao Jiang, Huseyin Sehitoglu, 1999, A model for rolling contact failure, *Wear, Volume 224, No. 1*, pp. 38-49, ISSN 0043-1648, DOI: 10.1016/S0043-1648(98)00311-1.
56. Huseyin Sehitoglu, Kevin Verzal, Y.Jiang, 2004, University of Illinois at Urbana-Champaign Mechanical and Industrial Engineering Department, October 12, 2004, presentation on: "Modeling rail ratcheting under high adhesion contact loading"
57. Zhang, J. and Jiang, Y., 2008, Constitutive modeling of cyclic plasticity deformation of a pure polycrystalline copper, *Int. J. of Plasticity, Vol. 24*, pp. 1890-1915.
58. R. M. Wetzel, 1971, "A Method of Fatigue Damage Analysis," Ph.D. Thesis, Department of Civil Engineering, University of Waterloo, Ontario, Canada, see also Technical Report No. SR 71-107, Scientific Research Staff, Ford Motor Co., Dearborn, MI, Aug. 1971.
59. R. M. Wetzel, ed., 1977, Fatigue Under Complex Loading: *Analyses and Experiments, Vol. AE 6*, The Society of Automotive Engineers, 1977.
60. Hu W., Wang C.H., Barter S.A., 1999, "Analysis of cyclic mean stress relaxation and strain ratchetting behaviour of aluminium 7050". DSTO-RR-0153, Melbourne.
61. Davis, J. R., ed. 1998, Metals Handbook: Desk Edition, 2nd ed., ASM International, Materials Park, OH.
62. SAE. 2008, "Aluminum Alloy Extrusions, 7.9Zn-1.6Cu-2.2Mg-0.16Cr (7249-T76511), Solution Heat Treated, Stress-Relieved, Straightened, and Overaged," Aerospace Material Specification, AMS 4293, SAE International, Warrendale, PA.
63. Newman, John A., Willard, S. A., Smith, S. W., Piascik, R. S., 2009, "Replica-based crack inspection". *Engineering Fracture Mechanics, Volume 76, Issue 7*, Pages 898-910, ISSN 0013-7944, DOI: 10.1016/j.engfracmech.2008.12.012.
64. R. J. Asaro. 1975, "Elastic-Plastic Memory and Kinematic-Type Hardening". *Acta Metallurgica*, Vol. 23, pp. 1255-1265.

65. S. Suresh. 1991, *Fatigue of Materials*. Cambridge University Press, Cambridge, England, pp. 80-82. (See also 2nd edition, 1998.)
66. The Mathworks, Inc, "Matlab online reference documentation", www.mathworks.com
67. Saltelli, A., 2004. *Sensitivity Analysis in Practice: A Guide to Assessing Scientific Models*. Hoboken, NJ: Wiley. http://simlab.jrc.ec.europa.eu/ and http://www.trusteagle.com/

Appendix A

Fatigue Data Tables

A.1

Test Data for 7075-T6511

Date Run	Spec. No.	ε_a	ε_m	σ_a MPa	σ_m MPa	ε_{pa}	N_f cycles	Control ε or σ	Prestrain y or n	Initial Loading		Comment (σ_m range, MPa)
										E, MPa	σ_o, MPa	
9-Aug-07	75LT-4	0.017670	0.000000	586.6	-14.1	0.009290	49	ε	n	67335	538.6	
9-Aug-07	75RC-4	0.013900	0.000000	570.4	-13.4	0.005760	96	ε	n	70490	538.0	
14-Feb-08	75LC-C	0.013142	0.004467	598.5	-10.9	0.005033	169	ε	y	71230	572.2	
3-Feb-09	B75-40	0.012999	-0.006004	605.6	-16.1	0.004692	39	ε	y	70207	574.5	
4-Dec-08	B75-47	0.010000	-0.009000	543.8	-15.8	0.002233	348	ε	y	69324	540.3	
18-Apr-08	75LB-6	0.009890	0.008989	553.9	-15.1	0.002058	439	ε	y	70809	537.8	
8-May-08	75NLB-1	0.008977	0.008998	577.8	-11.8	0.000817	479	ε	y	71158	572.7	
6-May-08	75LT-5	0.008489	0.009502	567.0	-5.2	0.000490	655	ε	y	67306	564.5	
16-Apr-08	75NLB-2	0.007198	0.010800	496.6	35.2	0.000085	2,010	ε	y	70103	543.8	(-17 to 35)
17-Apr-08	75LC-4	0.006297	0.011700	433.2	34.6	-	4,306	ε	y	70576	540.9	
30-Oct-07	75LT-6	0.005990	0.000016	418.5	-0.2	-	6,354	σ	y	69248	536.2	
7-Nov-07	75LT	0.004660	-0.000080	334.6	0.6	-	18,935	σ	y	70070	557.1	
26-Jan-09	B75-50	0.004500	-0.001499	325.3	-16.8	-	28,415	ε	y	69469	552.6	
7-Nov-07	75RB-2	0.004410	-0.000049	310.4	4.2	-	20,653	σ	y	69251	545.9	
8-Nov-07	75RC-6	0.004110	0.000382	289.0	3.7	-	41,848	σ	y	65037	534.9	
2-Dec-08	75RT-1	0.003990	-0.000310	288.0	-6.7	-	41,608	σ	y	70566	544.6	
31-Jan-08	75RC-1	0.003500	-0.000190	254.0	-5.1	-	107,288	σ	y	71468	583.2	
25-Apr-08	75RB-5	0.006746	0.011250	475.8	70.4	0.000041	2,316	ε	y	70582	568.2	
28-Apr-08	75LC-1	0.004500	0.001499	328.0	97.3	-	12,574	ε	y	72654	582.9	

3-Apr-08	75LC-2	0.004430	0.001499	317.1	83.3	-	12,793	ε	y	70902	551.2	
10-Mar-08	75MT-C	0.004095	0.001608	295.1	102.6	-	19,716	ε	y	72435	574.3	(53 to 103)
13-Feb-08	75RT-4	0.003000	0.001000	213.5	84.7	-	55,171	ε	y	70102	544.7	
9-Apr-08	75LB	0.002957	0.000998	212.2	60.2	-	59,396	ε	y	68763	554.3	
15-Feb-08	75RB-4	0.002259	0.000702	160.8	53.4	-	498,254	σ	y	70084	540.7	
27-Jun-08	75NRB-6	0.006300	0.011700	438.1	148.1	1.38E-05	1,372	ε	y	75227	550.8	
13-Jun-08	75NRB-1	0.006295	0.011701	432.3	162.7	-	2,691	σ	y	67499	587.8	
24-Apr-08	75LC-3	0.005000	0.012998	349.2	225.7	-	4,605	ε	y	72168	577.3	(148 to 279)
28-May-08	75RC-5	0.004268	0.005541	303.2	272.7	-	6,450	σ	y	72404	577.3	
1-Feb-08	75LB-5	0.004073	0.014339	282.7	279.4	-	9,026	ε	y	71496	572.9	
3-Jun-08	75NLB-4	0.002873	0.004395	203.1	254.4	-	17,448	σ	y	69378	546.4	
29-May-08	75NLB-5	0.002873	0.007888	203.3	377.1	-	15,652	σ	y	71669	577.5	
19-Feb-08	75RT-5	0.002500	0.017502	169.4	392.8	-	29,054	ε	y	71182	569.4	
11-Feb-08	75RT-2	0.002122	0.014875	145.4	363.5	-	43,110	ε	y	70858	554.6	
5-Apr-08	75NLB-3	0.002086	0.014874	143.6	403.1	-	37,301	ε	y	71968	572.9	
12-Feb-08	75RC-3	0.001997	0.005999	141.0	374.7	-	48,822	ε	y	70352	580.2	(333 to 490)
7-Apr-08	75RT-6	0.001967	0.005998	136.4	352.5	-	36,676	ε	y	70856	538.6	
4-Jun-08	75NLB	0.001753	0.005494	121.1	333.4	-	77,231	σ	y	-	566.2	
2-Jun-08	75NRB-3	0.001557	0.011305	105.6	470.3	-	88,358	σ	y	-	578.2	
30-May-08	75NRB-5	0.001164	0.009108	79.3	490.5	-	193,458	σ	y	70799	573.7	
18-Feb-08	75RB-3	0.001038	0.006213	72.0	414.8	-	410,183	σ	y	71568	579.6	
6-Oct-08	B75-46	0.007200	-0.010800	548.6	-71.7	0.000154	518	ε	y	71496	574.1	
8-Oct-08	B75-31	0.006300	-0.011701	445.1	-134.1	0.000025	6,033	ε	y	69605	547.7	(-41 to -134)
12-Dec-08	B75-25	0.004500	-0.001499	323.3	-78.3	-	56,272	ε	y	69859	554.1	
4-Dec-08	B75-20	0.003003	-0.001001	221.1	-40.8	-	466,816	ε	y	71373	570.9	
8-Aug-07	75T1-2	0.009570	0.000000	551.5	-12.4	0.001690	373	ε	n	70030	543.0	
16-Aug-07	75MB-C	0.006379	0.000000	461.1	-37.2	0.000010	6,288	ε	n	69580	-	
21-Aug-07	75LC	0.004510	0.000000	316.0	3.5	-	44,005	ε	n	71051	-	(~0, no prestrain)
27-Aug-07	75RT-3	0.004290	0.000000	300.1	-0.1	-	49,840	ε	n	71658	-	
28-Aug-07	75LB-3	0.003300	-0.000036	231.3	0.0	-	375,893	σ	n	71421	-	
11-Jun-08	75RB-6	0.001173	0.005778	81.5	376.2	-	>9,891,016	σ	y	65905	588.3	runout
20-Feb-08	75LC-5	0.001015	0.002905	72.1	215.1	-	>7,644,193	σ	y	70664	577.6	runout
16-Aug-07	75RC-2	0.007800	0.000000	522.5	-4.0	0.000340	1,031	ε	n	69010	-	knife edge failure
10-Dec-08	B75-43	0.004500	-0.013498	336.1	-251.8	-	218,438	ε	y	70115	541.5	knife edge failure

13-Feb-08	75LT-1	0.004498	0.001501	318.4	101.4	-	24,569	ε	y	70981	584.3	knife edge failure
9-Oct-08	B75-38	0.003499	-0.010510	269.6	-222.0	-	65,287	ε	y	73312	586.4	failure in collet
9-Nov-07	75LB-4	0.003453	0.000304	247.0	0.0	-	76,558	σ	y	70512	542.5	knife edge failure
8-Apr-08	75LB-2	0.002960	0.000997	209.3	83.1	-	34,010	ε	y	70620	548.4	knife edge failure
29-Aug-07	75LT-3	0.002586	0.000000	187.6	-1.7	-	3,311,698	ε	n	-	-	failure in collet
29-May-08	75NRB-4	-	-	-	-	-	-	σ	y	71426	558.5	excess strain
5-Feb-09	B75-60	-	-	-	-	-	-	ε	n	70842	573.9	buckling
13-Jun-08	75NLB-6	-	-	-	-	-	-	σ	y	69524	544.2	control difficulty
2-Jun-08	75NRB-2	-	-	-	-	-	-	σ	y	-	553.6	control difficulty
6-Jun-08	75NMB-C	-	-	-	-	-	-	σ	y	71366	578.8	control difficulty
									Average	70457	560.8	
									Std. Dev.	1641	16.8	
									Count	59	57	

A.2

Test Data for 7249-T76511

Date Run	Spec. No.	ε_a	ε_m	σ_a MPa	σ_m MPa	ε_{pa}	N_f cycles	Control ε or σ	Prestrain y or n	Initial Loading		Comment (σ_m range, MPa
										E, MPa	σ_o, MPa	
1-Nov-07	49LC-6	0.018530	0.000000	567.7	-15.0	0.010220	67	ε	n	69300	552.2	
24-Sep-07	49RT-6	0.013950	0.000000	543.2	-15.0	0.005990	157	ε	n	68685	557.0	
9-Feb-09	B49-52	0.013000	-0.006000	553.0	-13.4	0.005200	129	ε	y	67145	564.6	
4-Dec-08	B49-27	0.010000	-0.009000	561.6	-22.4	0.002540	118	ε	y	71268	559.7	
7-May-08	49LB	0.009920	0.009003	555.1	-17.8	0.002159	399	ε	y	72367	571.9	
19-May-08	49LC-3	0.008968	0.008995	544.4	-12.5	0.001242	697	ε	y	69345	566.3	
8-May-08	49LC-1	0.008486	0.009499	545.1	-11.7	0.000786	781	ε	y	71185	565.7	
26-Sep-07	49RC-6	0.008130	0.000000	519.7	-11.4	0.000720	1,092	ε	y	69593	-	

26-Feb-09	B49-58	0.008000	0.005500	527.5	-5.0	0.000480	1,135	ε	y	72632	567.1	(-22 to 34)
26-Feb-09	B49-30	0.008000	0.006200	512.7	9.1	0.000480	1,743	ε	y	69830	566.4	
24-Feb-09	B49-25	0.008000	0.009000	502.1	33.1	0.000640	1,910	ε	y	62292	561.5	
3-Jul-08	49RC-5	0.007990	-0.000500	540.5	-17.1	0.000630	860	ε	y	71992	574.0	
1-May-08	49RB-3	0.007198	0.010800	497.3	33.9	0.000118	1,823	ε	y	71047	564.1	
27-Jan-09	B49-48	0.006197	0.000000	431.3	18.9	-	4,261	ε	y	69574	555.6	
3-Feb-09	B49-47	0.004624	-0.000410	330.4	0.0	-	24,898	σ	y	68400	562.1	
4-Feb-09	B49-11	0.004089	-0.000190	288.8	0.0	-	39,399	σ	y	68822	559.5	
4-Feb-09	B49-28	0.003657	0.000150	260.3	0.0	-	53,374	σ	y	72418	559.4	
25-Feb-09	B49-3	0.008000	0.007500	492.5	72.6	0.000790	1,684	ε	y	61529	568.4	
6-May-08	49LC-4	0.006748	0.011249	458.9	61.1	0.000074	3,032	ε	y	70140	557.9	(61 to 100)
5-May-08	49LB-5	0.006298	0.011698	435.8	91.8	-	2,851	ε	y	68780	557.7	
20-May-08	49RB-1	0.003000	0.001001	213.7	100.2	-	41,872	ε	y	66937	554.1	
5-May-08	49LT-1	0.004998	0.013000	347.8	180.8	-	6,336	ε	y	71522	563.7	
26-Feb-08	49NLB-6	0.004720	0.013569	322.4	220.0	-	4,508	ε	y	69902	565.3	
27-Feb-08	49NLB-4	0.004659	0.013452	317.9	218.0	-	6,463	ε	y	69160	567.3	
9-Jun-08	49RT-3	0.004388	0.011550	304.4	273.8	-	5,021	σ	y	71782	576.0	(181 to 296)
2-Mar-08	49NLB-1	0.004147	0.002158	293.8	292.3	-	8,500	ε	y	73915	582.4	
5-Mar-08	49LT-4	0.003665	0.016982	242.2	295.9	-	10,189	ε	y	68444	559.3	
8-Jul-08	49LB-3	0.002898	0.003830	204.1	255.7	0.000000	15,239	σ	y	71195	572.9	
26-Jun-08	49LB-2	0.002952	0.012792	201.5	372.1	-	12,688	σ	y	-	572.4	
1-Jul-08	49RC-3	0.002124	0.014874	146.5	394.1	-	36,780	ε	y	72264	575.5	
7-Mar-08	49LC-5	0.002011	0.014875	136.5	390.7	-	41,353	ε	y	70596	573.3	
12-Mar-08	49LB-1	0.001974	0.005915	130.6	343.5		65,000	ε	y	63323	577.2	
12-Jun-08	49NRB-4	0.001773	0.005802	121.1	332.9	-	54,423	σ	y	66229	568.2	(333 to 495)
16-Jun-08	49NLB-2	0.001575	0.014551	105.8	470.9	-	66,820	σ	y	69873	572.5	
18-Jun-08	49RB-6	0.001462	0.005760	101.2	354.7	-	70,892	σ	y	66572	565.6	
19-Jun-08	49NLB-3	0.001292	0.005415	91.0	363.9	-	140,581	σ	y	72626	576.3	
17-Jun-08	49RB-2	0.001224	0.016388	80.0	494.7	-	199,912	σ	y	-	566.9	
23-Jun-08	49RC-1	0.001179	0.005517	83.9	374.7	-	230,136	σ	y	72302	578.8	
15-Dec-08	B49-22	0.007198	-0.010800	517.6	-57.8	0.000170	1,398	ε	y	73780	568.6	
15-Dec-08	B49-40	0.006300	-0.011700	463.0	-120.6	0.000041	4,602	ε	y	68770	562.8	
16-Dec-08	B49-12	0.004499	-0.001500	327.9	-105.1	-	60,256	ε	y	74781	561.8	(-58 to -222)
22-Jan-09	B49-53	0.004499	-0.013500	341.7	-221.5	-	129,631	ε	y	-	-	

8-Dec-08	B49-49	0.003001	-0.001000	220.5	-63.7	-	251,613	ε	y	72396	566.1	
25-Sep-07	49LC-2	0.010050	0.000000	529.5	-11.5	0.002340	513	ε	n	69178	581.4	
27-Sep-07	49RC-4	0.006220	0.000015	438.3	-4.5	0.000014	5,849	σ	n	68306	-	
29-Jan-08	49RT-5	0.005110	-0.000550	366.5	-0.2	0.000000	22,330	σ	n	69652	-	(~0, no prestrain)
2-Oct-07	49LT	0.004390	-0.000240	297.2	1.4	-	108,309	σ	n	66886	-	
25-Jan-08	49RB-5	0.003390	0.000180	249.8	0.9	-	224,773	σ	n	71536	-	
24-Jun-08	49LC-C	0.001011	0.005688	71.2	385.5	-	3,624,095	σ	y	-	-	very long life
23-Jan-09	B49-37	0.003500	-0.010500	265.5	-298.7	-	>463,898	ε	y	71760	576.5	runout
21-Sep-07	49LT-5	0.018507	0.000000	579.2	-13.8	0.009962	51	ε	n	70846	568.0	knife edge failure
3-Feb-09	B49-10	0.004838	0.000000	344.0	-0.1	-	15,292	ε	y	70044	564.3	knife edge failure
27-Sep-07	49RC-2	0.004831	0.000000	340.6	46.4	0.000014	20,389	ε	n	68198	-	knife edge failure
4-Oct-07	49LT-2	0.003306	0.000347	233.1	0.0	-	624,641	σ	n	69929	-	failure in collet
29-Jan-08	49RT-4	0.002777	0.000140	199.5	0.0	-	831,320	σ	n	71331	-	failure in collet
1-Nov-07	49LT-6	0.002667	0.000030	188.5	0.0	-	608,183	σ	n	70325	-	failure in collet
4-Mar-08	49NRB-6	0.002363	0.006038	162.6	328.5	-	26,256	ε	y	70812	570.1	knife edge failure
27-May-08	49NMBN-2	0.002040	0.001918	143.5	129.3	-	1,264	σ	y	69724	558.3	failure in collet
19-May-08	49MT-C	0.001996	0.006001	140.6	328.4	-	42,595	ε	y	69841	565.5	knife edge failure
1-Jul-08	49-extra	0.001997	0.006000	140.7	366.2	-	30,044	ε	y	71829	579.9	knife edge failure
27-Jan-09	B49-35	-	-	-	-	-	-	ε	y	70755	571.2	control difficulty
10-Jun-08	49NRB-5	-	-	-	-	-	-	σ	y	-	568.9	control difficulty
									Average	69889	567.1	
									Std. Dev.	2572	7.3	
									Count	57	51	

Appendix B
Constant Amplitude Loading Stress-Strain Curves

B.1
Completely reversed non pre-strained tests

Three examples of stress-strain response in the low, intermediate and long life region are shown for each material in this section. It noticeable for 7075 a low degree of cyclic hardening. For 7249 the reverse curvature effect is visible for the low cycle fatigue test.

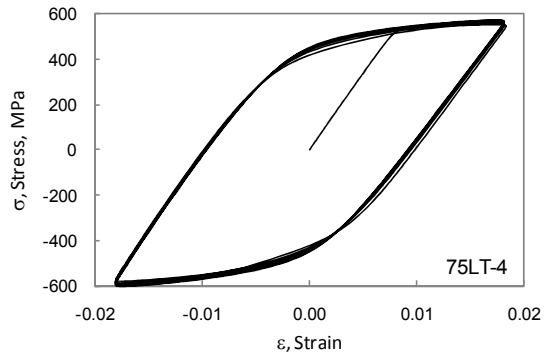

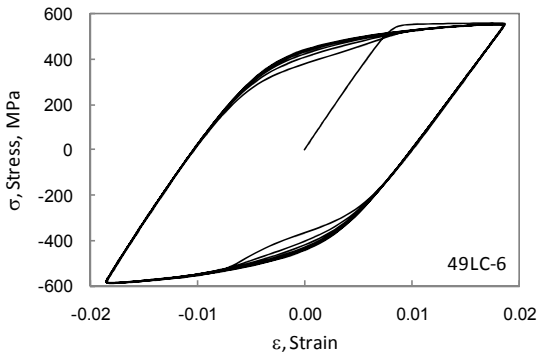

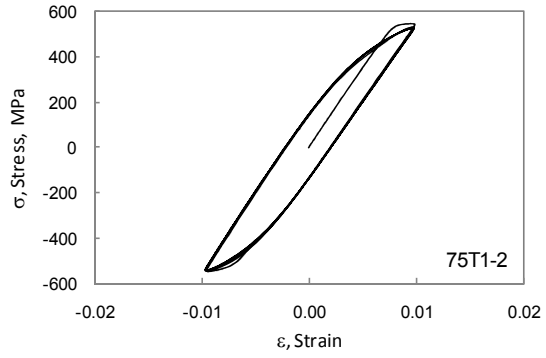

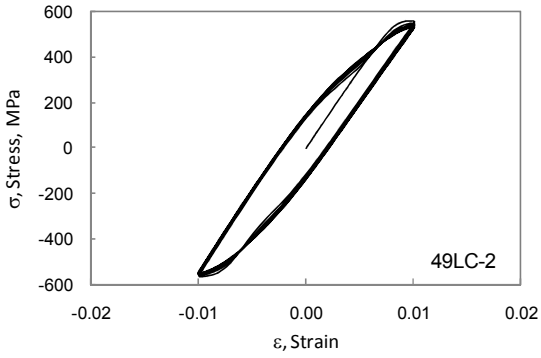

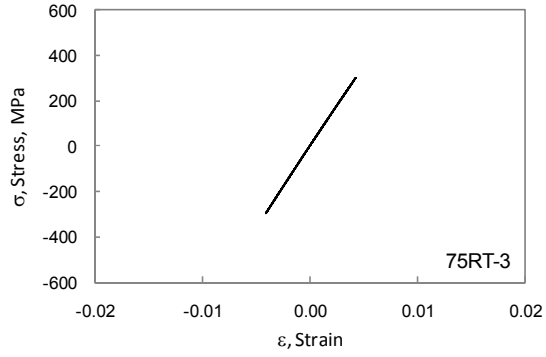

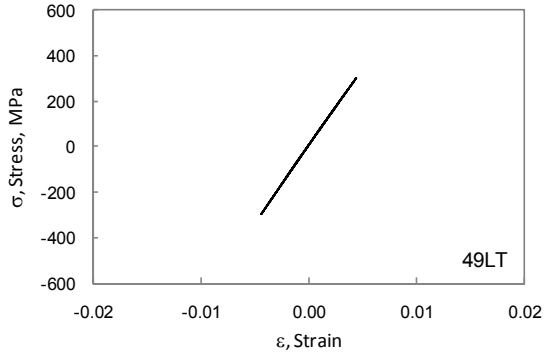

B.2
Completely reversed pre-strained tests

Some of the tests run in constant amplitude loading are rerun with initial pre-strain. The tests are all in the intermediate and long life regime, and differences in the shape of the hysteresis loops are barely noticeable for both materials.

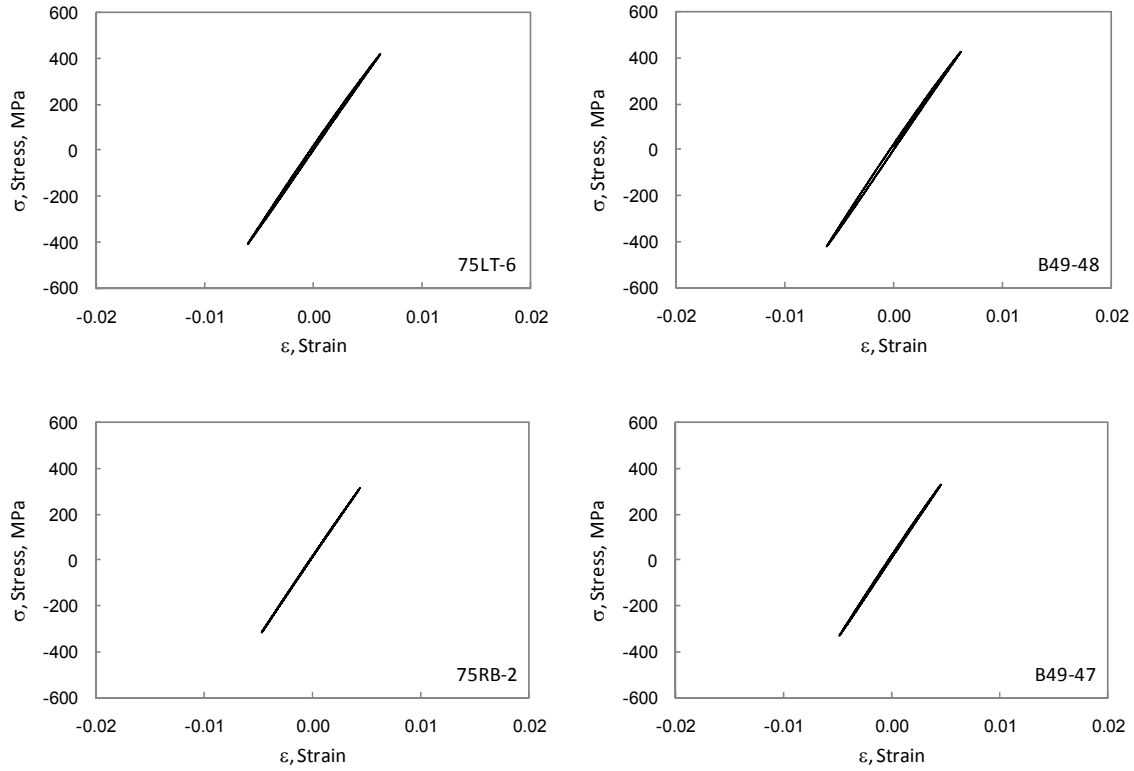

B.3
Mean stress and mean stress relaxation tests

Several constant amplitude non zero-mean tests are run with the intention of characterizing the mean stress sensitivity of both materials. Several constant amplitude relaxation tests are run to observe the relaxation behavior. In this section relaxation responses are visible from the stress plots, from the stress-strain plots and the mean stress plots of the tests. Four tests are presented, two for 7075 and two for 7249. For each material one in the low cycle fatigue regime and one in the high cycle fatigue regime are shown.

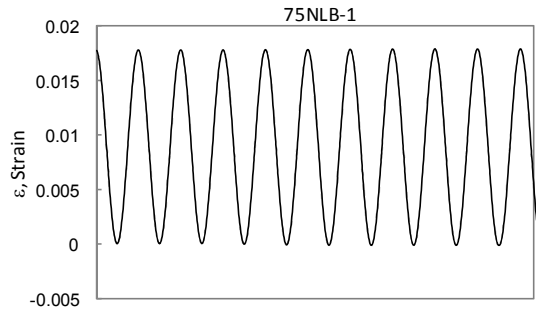
75NLB-1
ε, Strain

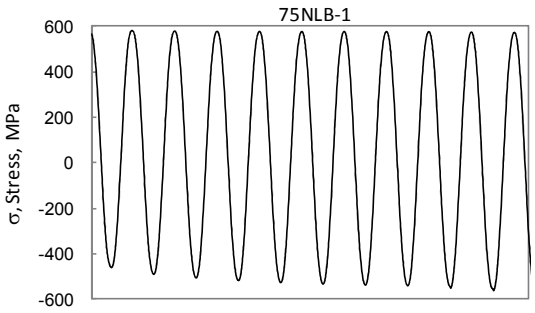
75NLB-1
σ, Stress, MPa

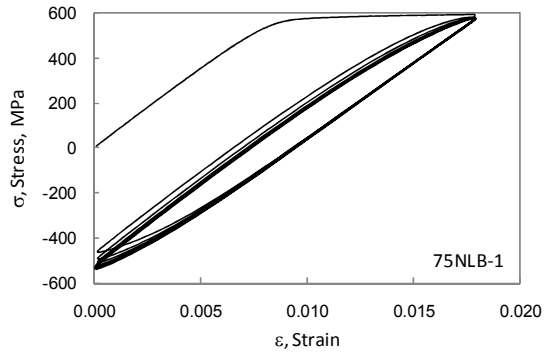
σ, Stress, MPa
75NLB-1
ε, Strain

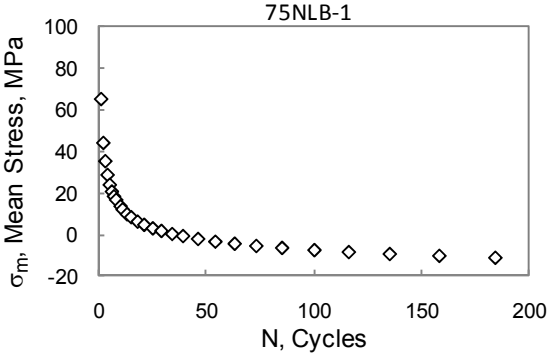
75NLB-1
σm, Mean Stress, MPa
N, Cycles

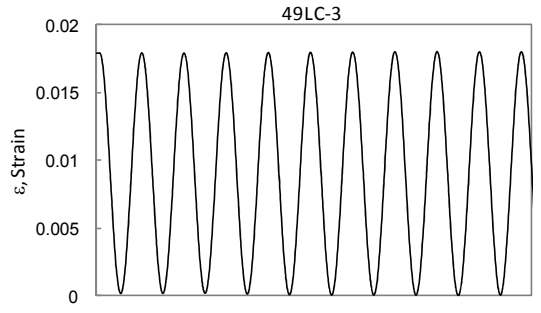
49LC-3
ε, Strain

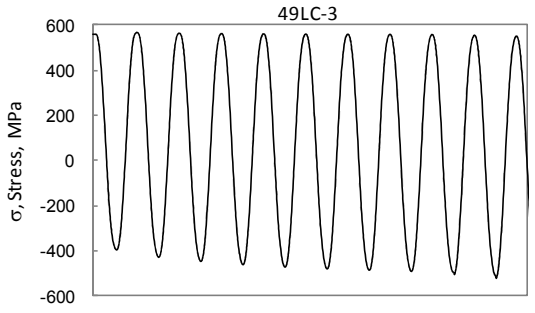
49LC-3
σ, Stress, MPa

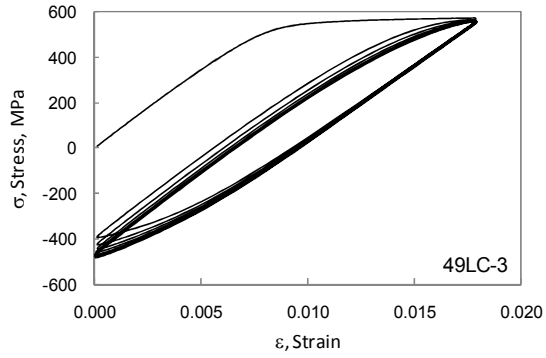
σ, Stress, MPa
49LC-3
ε, Strain

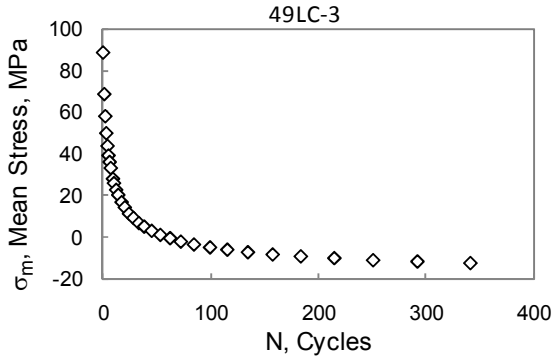
49LC-3
σm, Mean Stress, MPa
N, Cycles

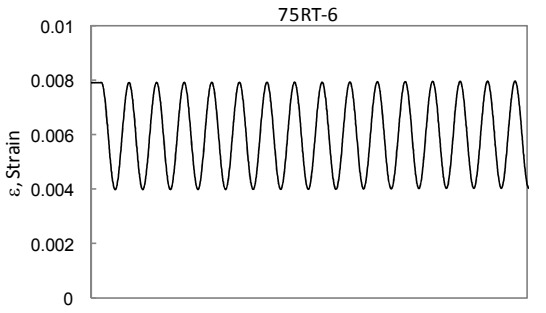
75RT-6
ε, Strain

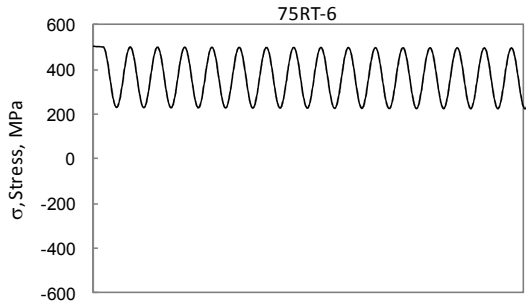
75RT-6
σ, Stress, MPa

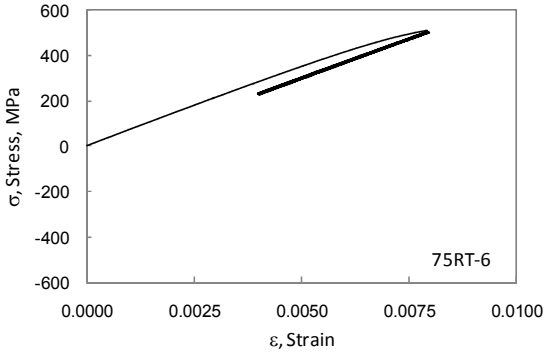
σ, Stress, MPa
75RT-6
ε, Strain

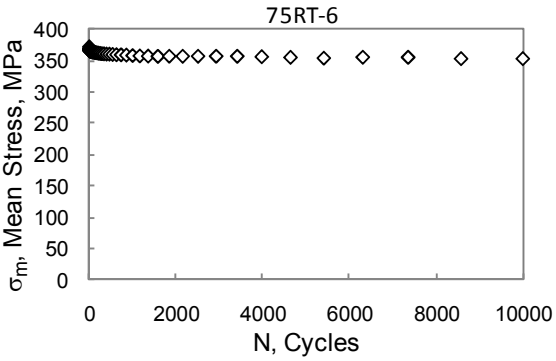
75RT-6
σm, Mean Stress, MPa
N, Cycles

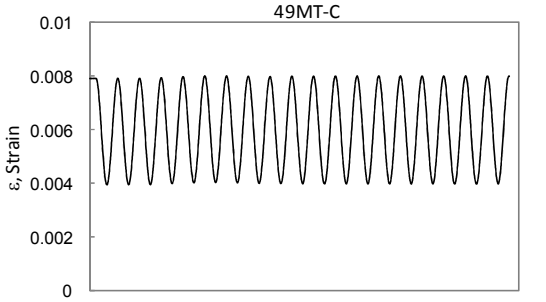
49MT-C
ε, Strain

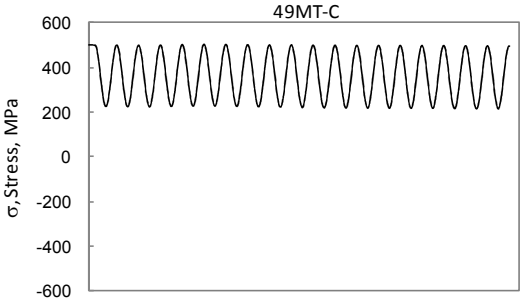
49MT-C
σ, Stress, MPa

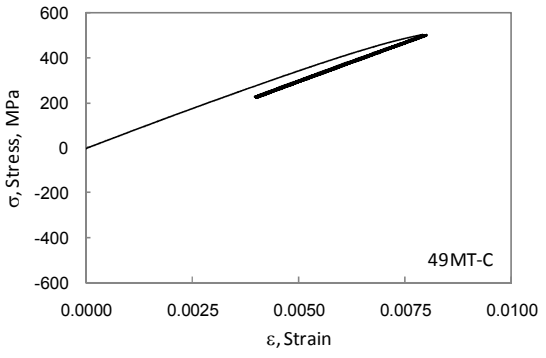
σ, Stress, MPa
49MT-C
ε, Strain

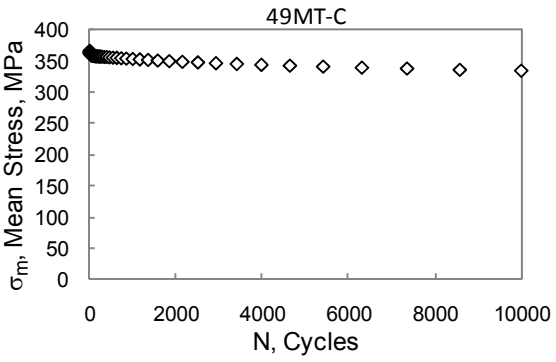
49MT-C
σm, Mean Stress, MPa
N, Cycles

B.4
Negative mean stress and mean stress relaxation tests

Among the relaxation tests, negative mean stress relaxation are also included. Four cases are shown, two for each material, one in the low cycle fatigue regime and the other in the high cycle fatigue regime.

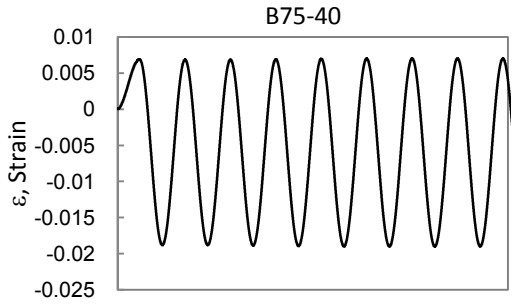

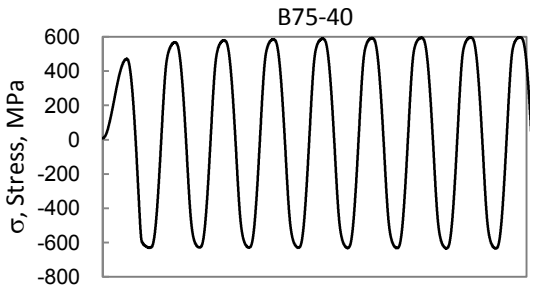

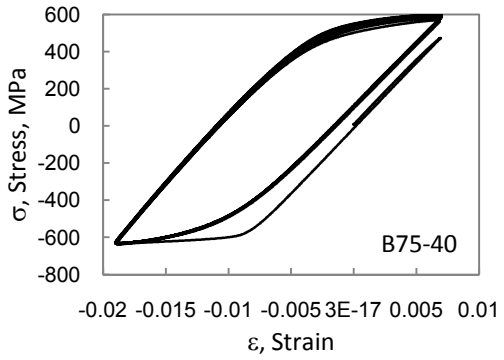

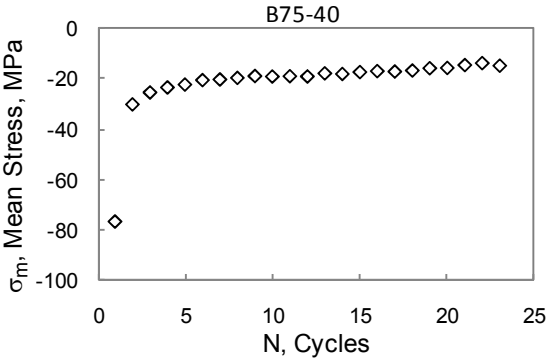

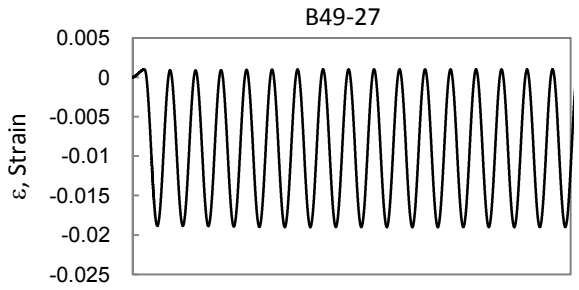

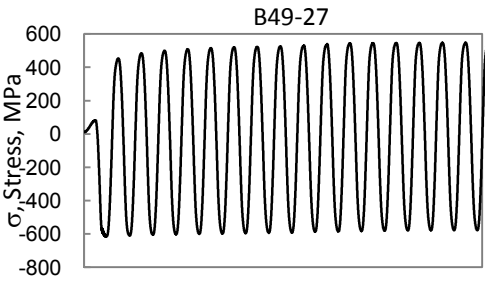

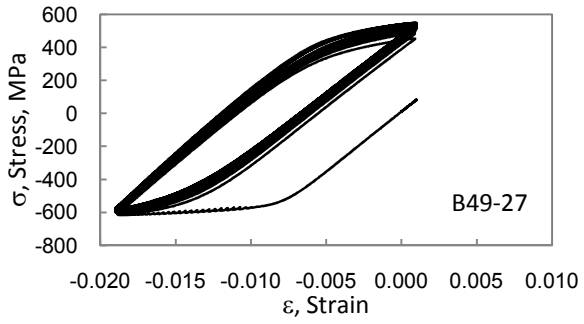

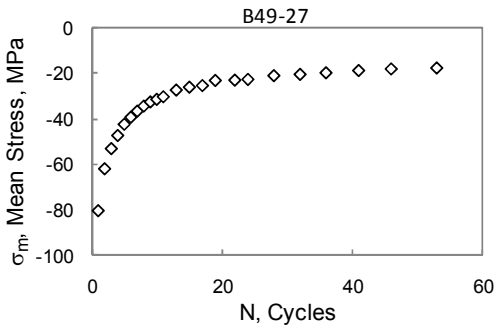

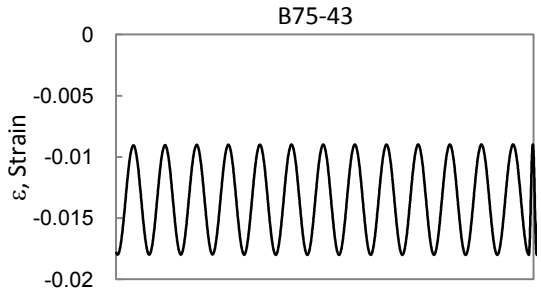
B75-43
ε, Strain
0
-0.005
-0.01
-0.015
-0.02

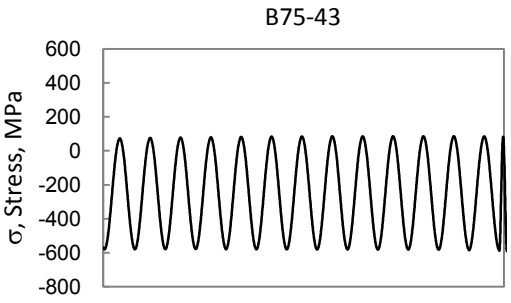
B75-43
σ, Stress, MPa
600
400
200
0
-200
-400
-600
-800

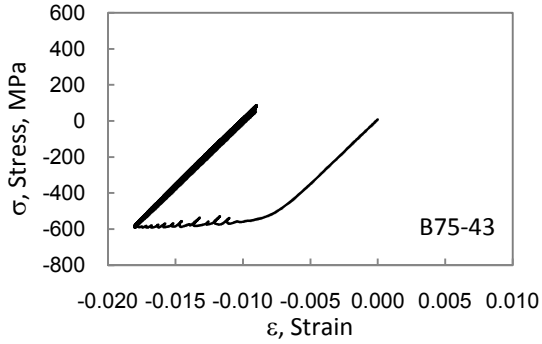
σ, Stress, MPa
600
400
200
0
-200
-400
-600
-800
B75-43
-0.020 -0.015 -0.010 -0.005 0.000 0.005 0.010
ε, Strain

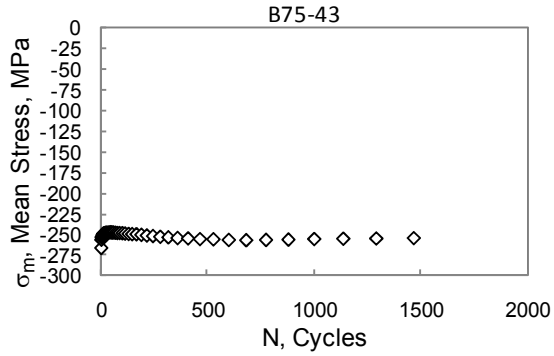
B75-43
σm, Mean Stress, MPa
0
-25
-50
-75
-100
-125
-150
-175
-200
-225
-250
-275
-300
0
500
1000
1500
2000
N, Cycles

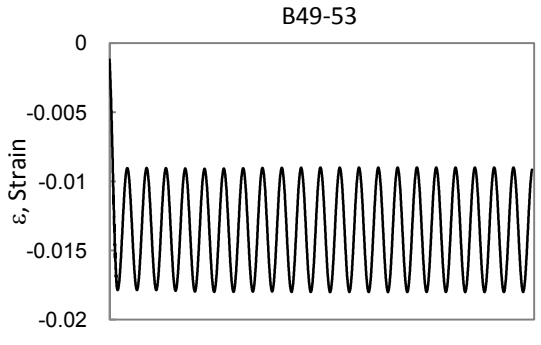
B49-53
ε, Strain
0
-0.005
-0.01
-0.015
-0.02

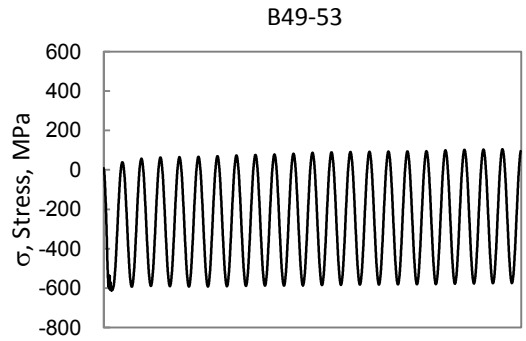
B49-53
σ, Stress, MPa
600
400
200
0
-200
-400
-600
-800

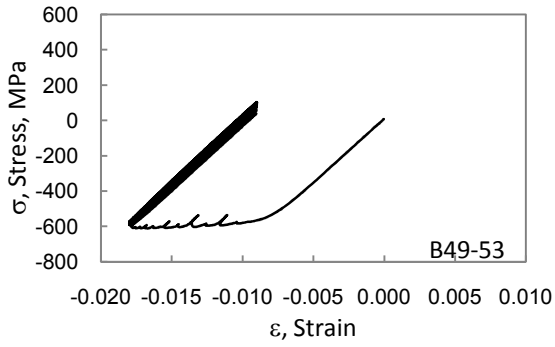
σ, Stress, MPa
600
400
200
0
-200
-400
-600
-800
B49-53
-0.020 -0.015 -0.010 -0.005 0.000 0.005 0.010
ε, Strain

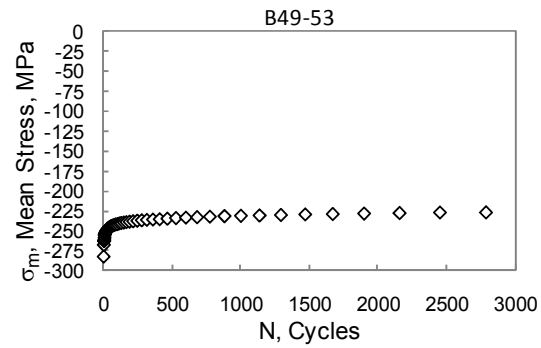
B49-53
σm, Mean Stress, MPa
0
-25
-50
-75
-100
-125
-150
-175
-200
-225
-250
-275
-300
0
500
1000
1500
2000
2500
3000
N, Cycles

Appendix C

Variable Amplitude Loading Stress-Strain Curves

C.1

7075-T6511

B75-26

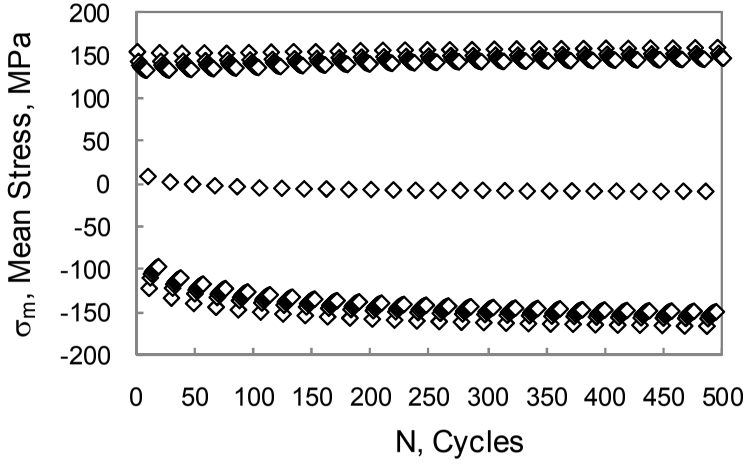

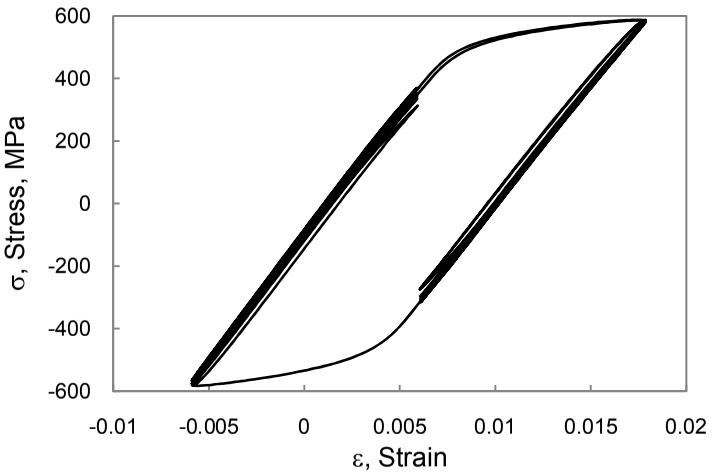

B75-4

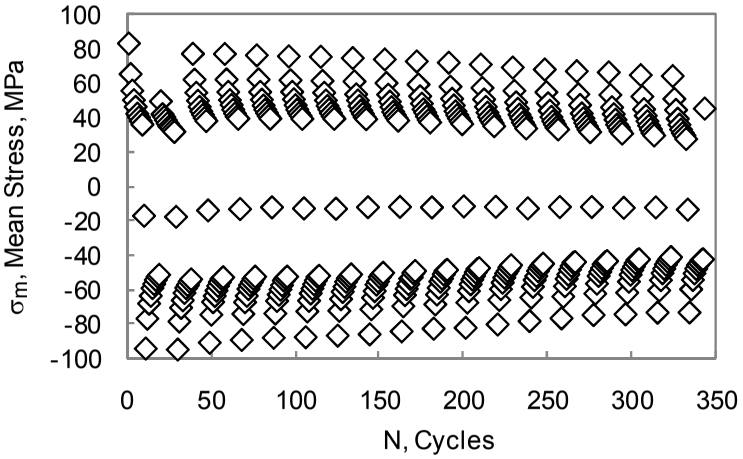
100
80
60
40
20
0
-20
-40
-60
-80
-100
σm, Mean Stress, MPa
0
50
100
150
200
250
300
350
N, Cycles

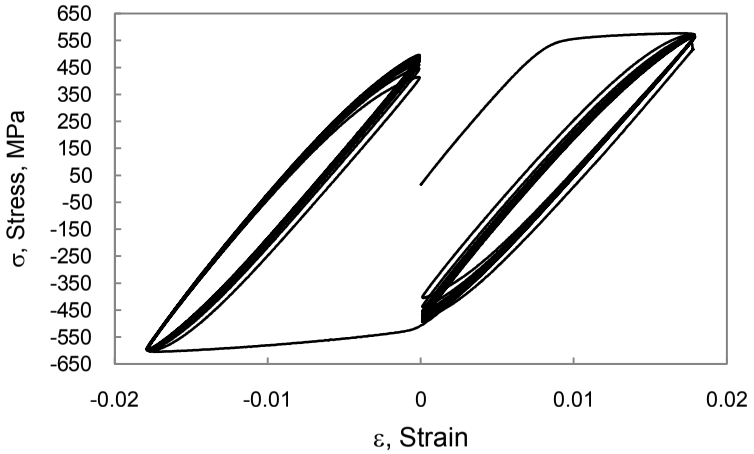
650
550
450
350
250
150
50
-50
-150
-250
-350
-450
-550
-650
σ, Stress, MPa
-0.02
-0.01
0
0.01
0.02
ε, Strain

B75-41

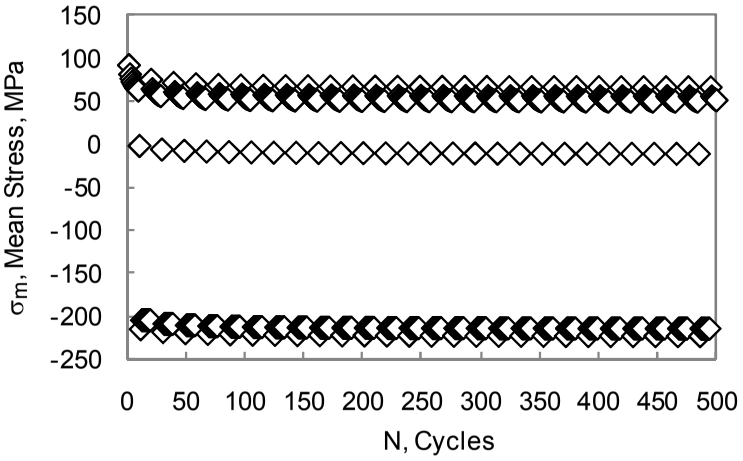
150
100
50
0
-50
-100
-150
-200
-250
σm, Mean Stress, MPa
0
50
100
150
200
250
300
350
400
450
500
N, Cycles

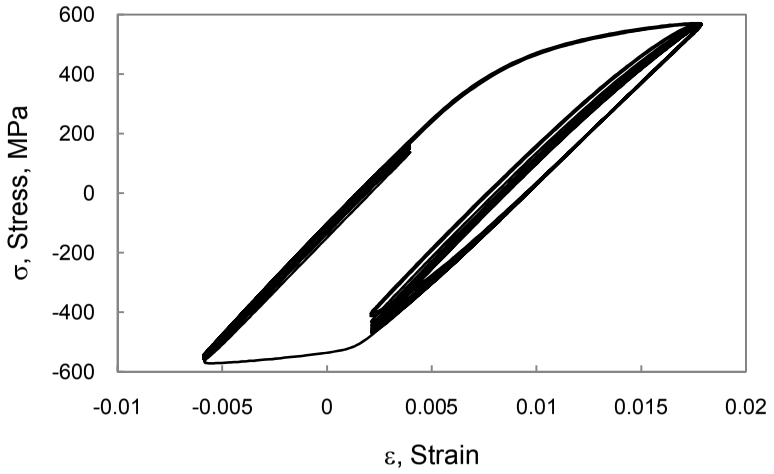
600
400
200
0
-200
-400
-600
σ, Stress, MPa
-0.01
-0.005
0
0.005
0.01
0.015
0.02
ε, Strain

B75-71

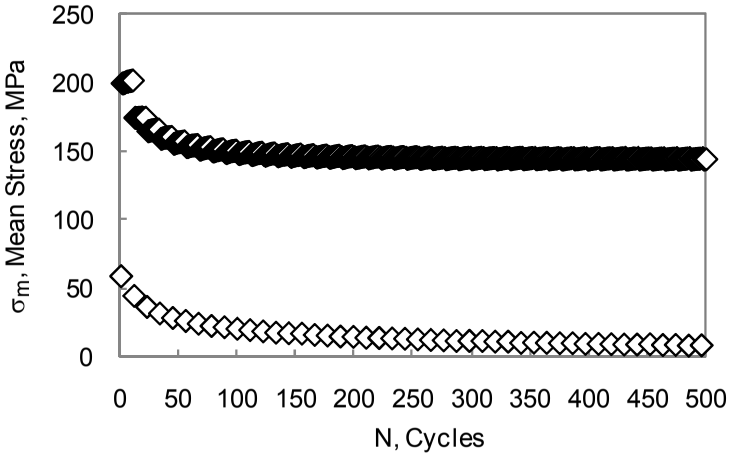
250
200
150
100
50
0
σm, Mean Stress, MPa
0 50 100 150 200 250 300 350 400 450 500
N, Cycles

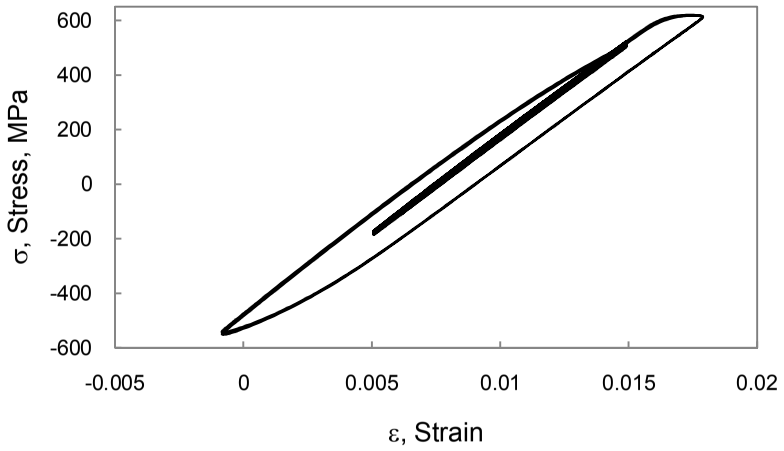
600
400
200
0
-200
-400
-600
σ, Stress, MPa
-0.005 0 0.005 0.01 0.015 0.02
ε, Strain

B75-54

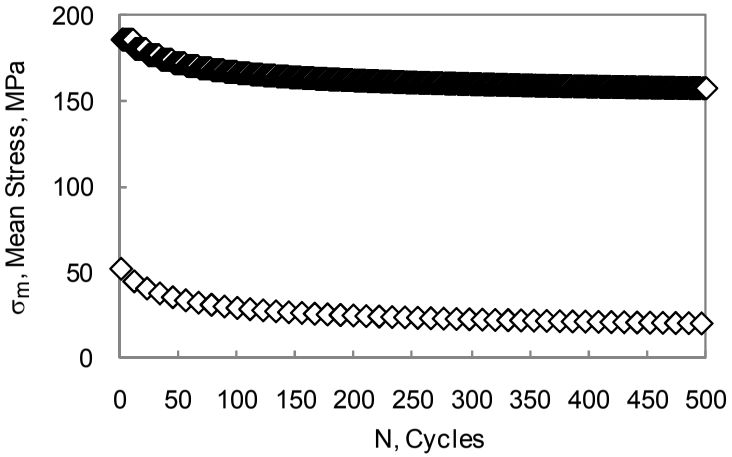
200
150
100
50
0
σm, Mean Stress, MPa
0 50 100 150 200 250 300 350 400 450 500
N, Cycles

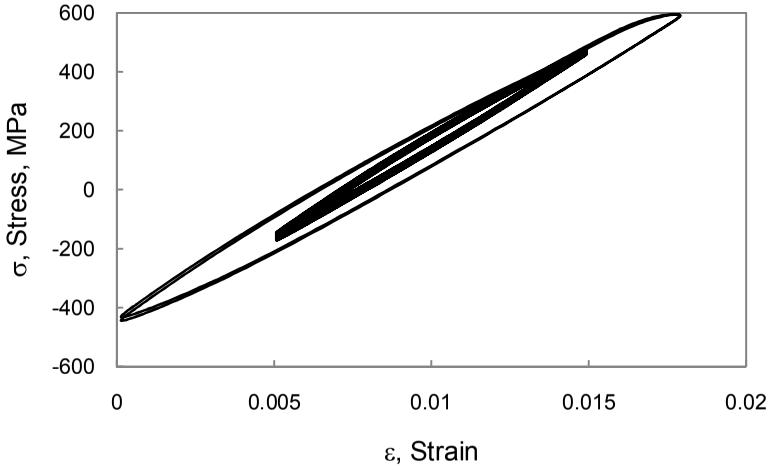
600
400
200
0
-200
-400
-600
σ, Stress, MPa
0 0.005 0.01 0.015 0.02
ε, Strain

B75-44

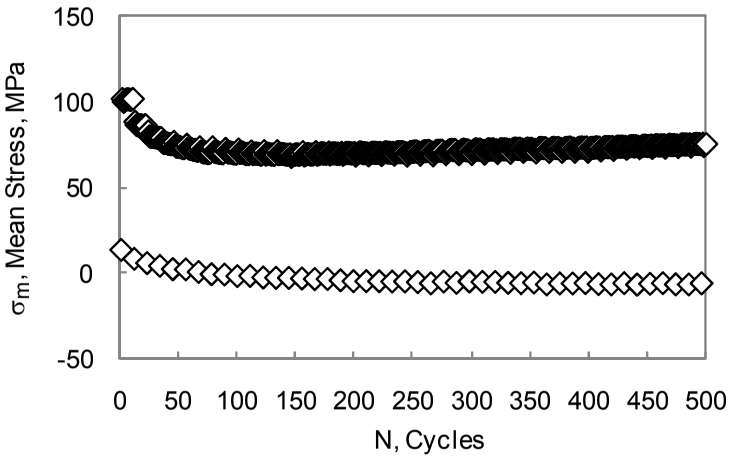
150
100
50
0
-50
σm, Mean Stress, MPa
0 50 100 150 200 250 300 350 400 450 500
N, Cycles

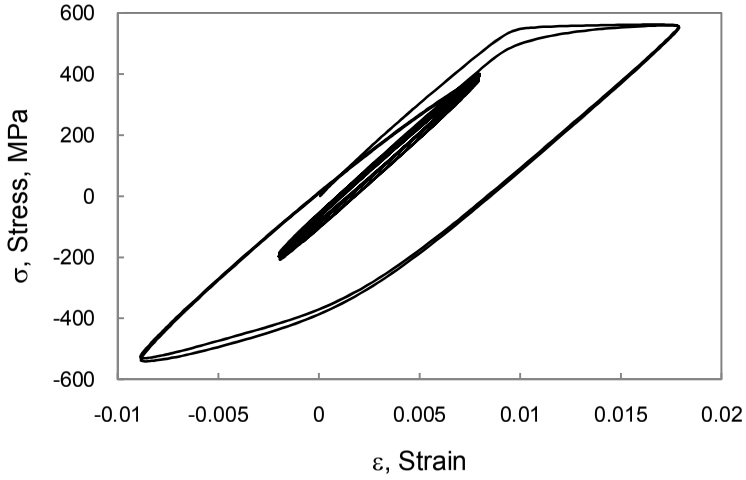
600
400
200
0
-200
-400
-600
σ, Stress, MPa
-0.01 -0.005 0 0.005 0.01 0.015 0.02
ε, Strain

B75-32

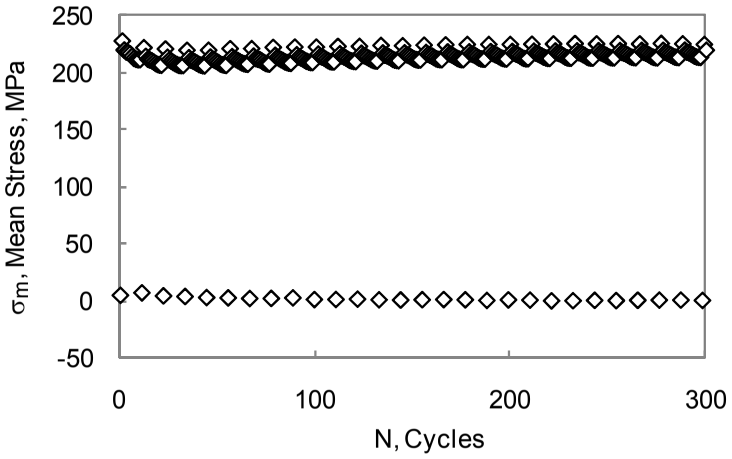
250
200
150
100
50
0
-50
σm, Mean Stress, MPa
0 100 200 300
N, Cycles

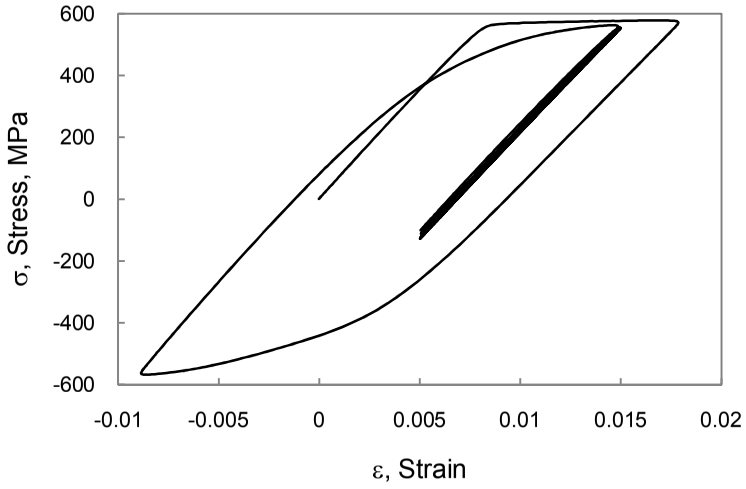
600
400
200
0
-200
-400
-600
σ, Stress, MPa
-0.01 -0.005 0 0.005 0.01 0.015 0.02
ε, Strain

B75-2

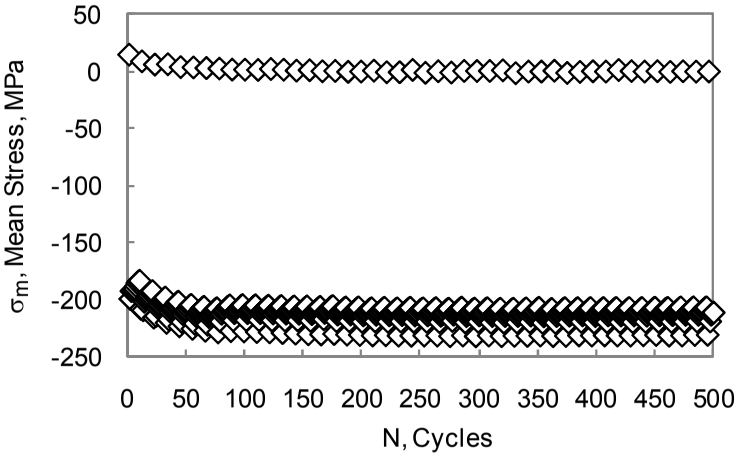
50
0
-50
-100
-150
-200
-250
σm, Mean Stress, MPa
0 50 100 150 200 250 300 350 400 450 500
N, Cycles

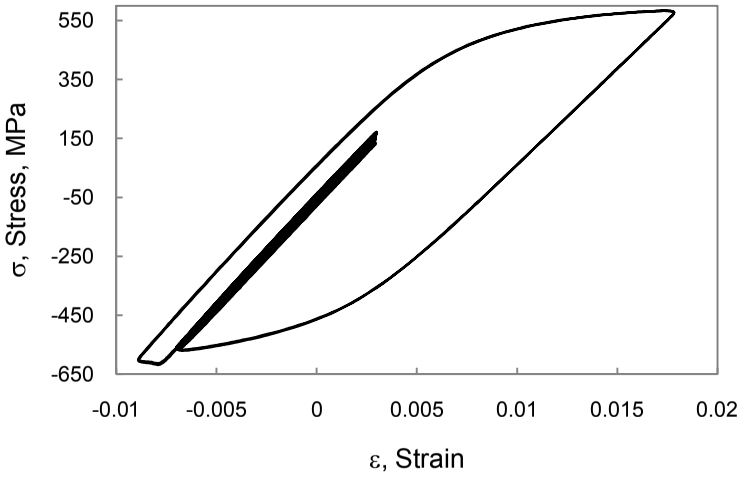
550
350
150
-50
-250
-450
-650
σ, Stress, MPa
-0.01 -0.005 0 0.005 0.01 0.015 0.02
ε, Strain

B75-22

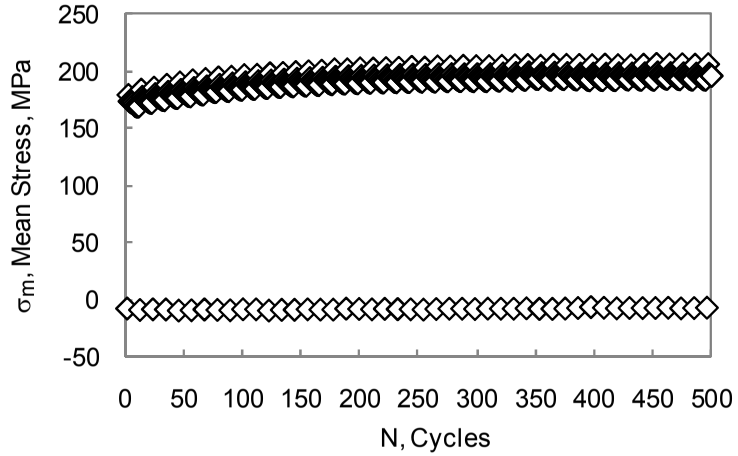
250
200
150
100
50
0
-50
σm, Mean Stress, MPa
0 50 100 150 200 250 300 350 400 450 500
N, Cycles

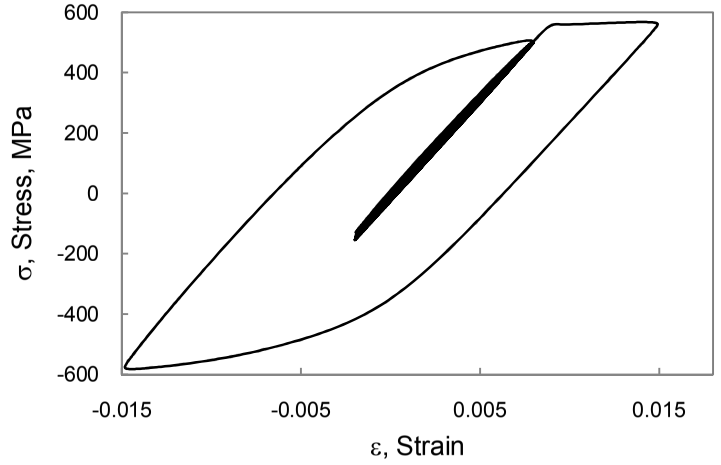
600
400
200
0
-200
-400
-600
σ, Stress, MPa
-0.015 -0.005 0.005 0.015
ε, Strain

B75-63

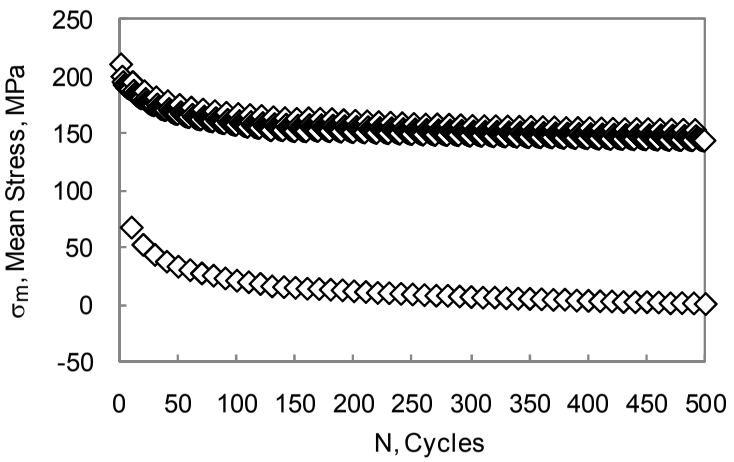
250
200
150
100
50
0
-50
σm, Mean Stress, MPa
0 50 100 150 200 250 300 350 400 450 500
N, Cycles

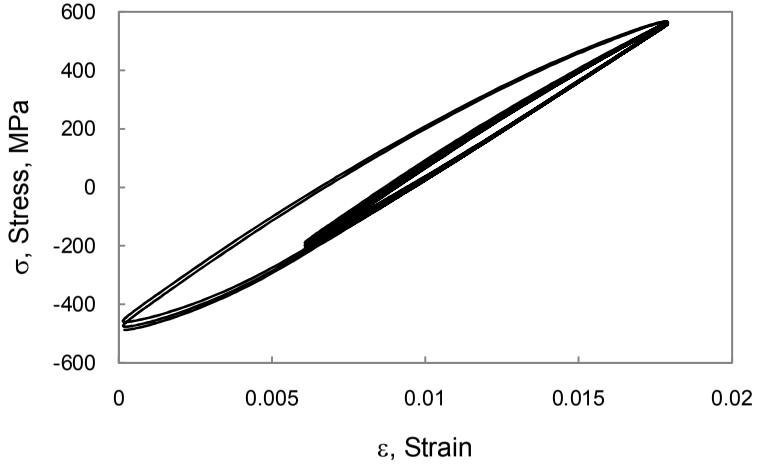
600
400
200
0
-200
-400
-600
σ, Stress, MPa
0 0.005 0.01 0.015 0.02
ε, Strain

B75-28

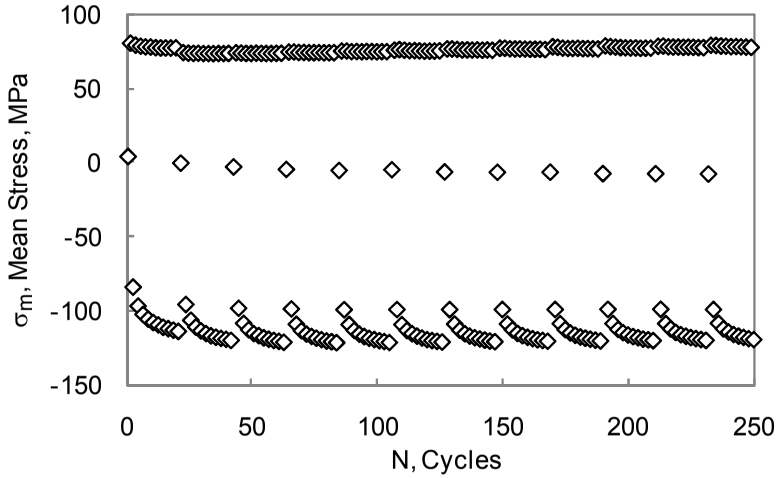
100
50
0
-50
-100
-150
σm, Mean Stress, MPa
0 50 100 150 200 250
N, Cycles

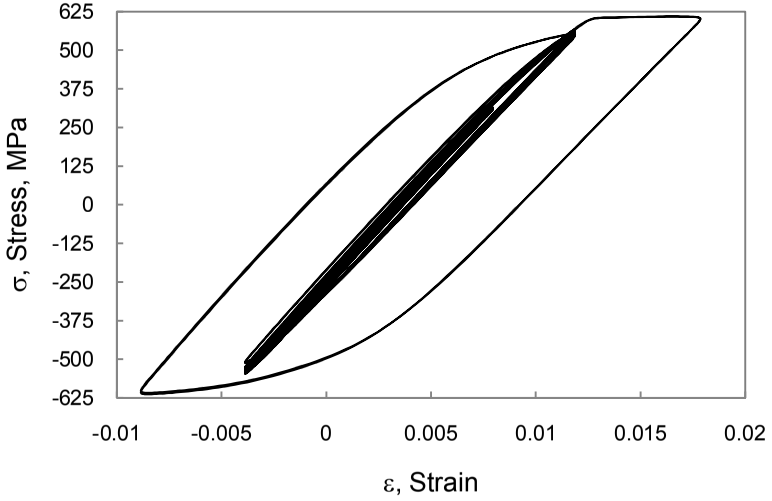
625
500
375
250
125
0
-125
-250
-375
-500
-625
σ, Stress, MPa
-0.01 -0.005 0 0.005 0.01 0.015 0.02
ε, Strain

NAV-1-75-15

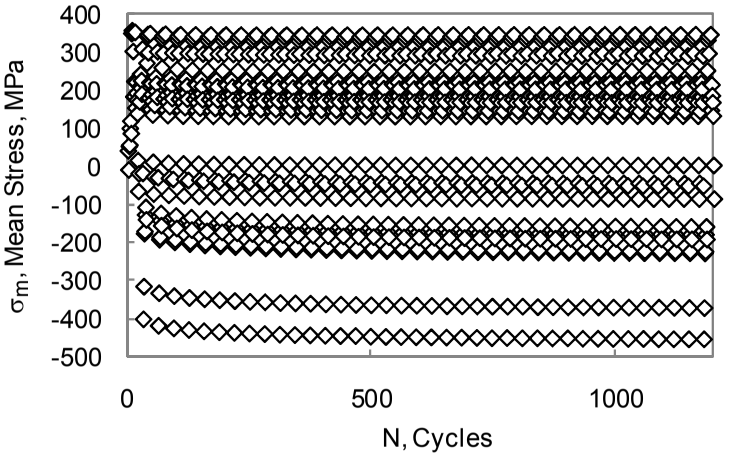

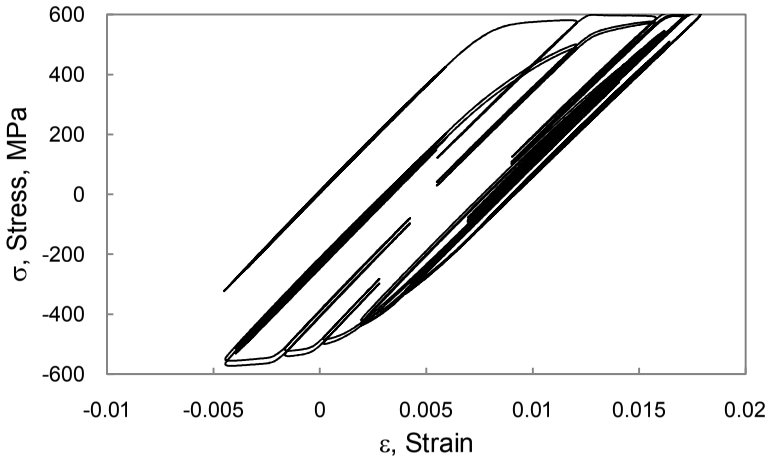

NAV-1-75-12

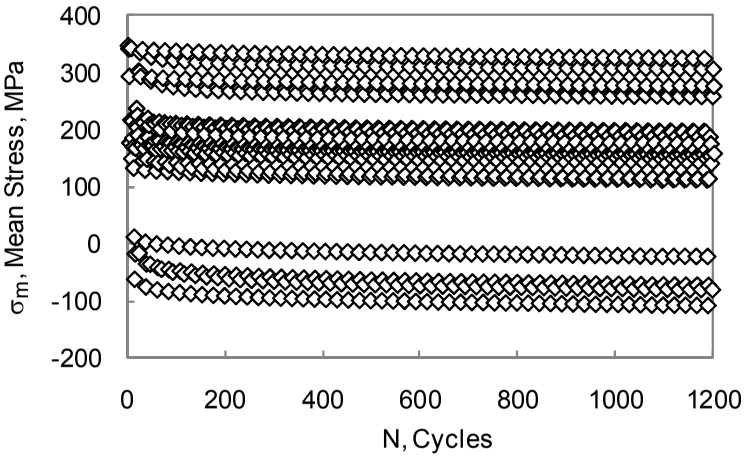

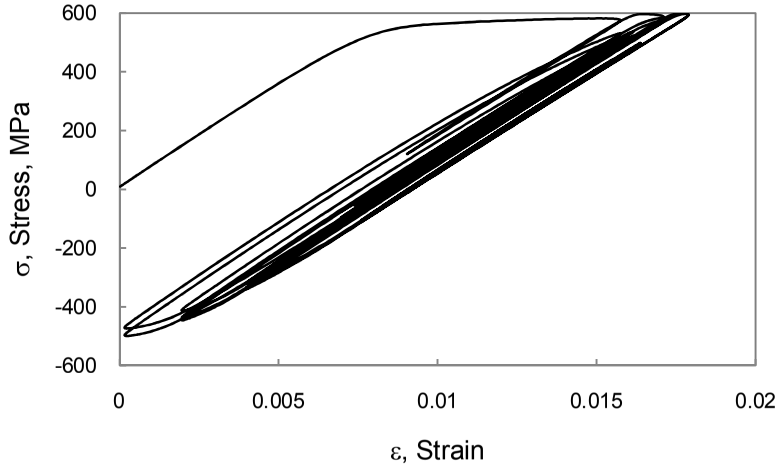

C.2

7249-T76511

B49-44

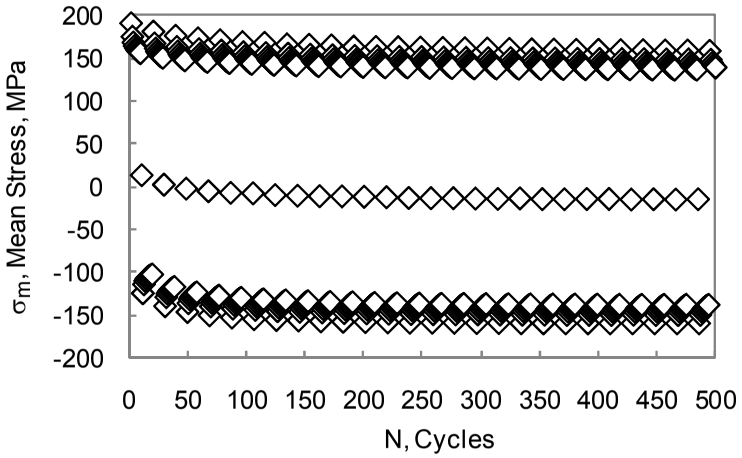

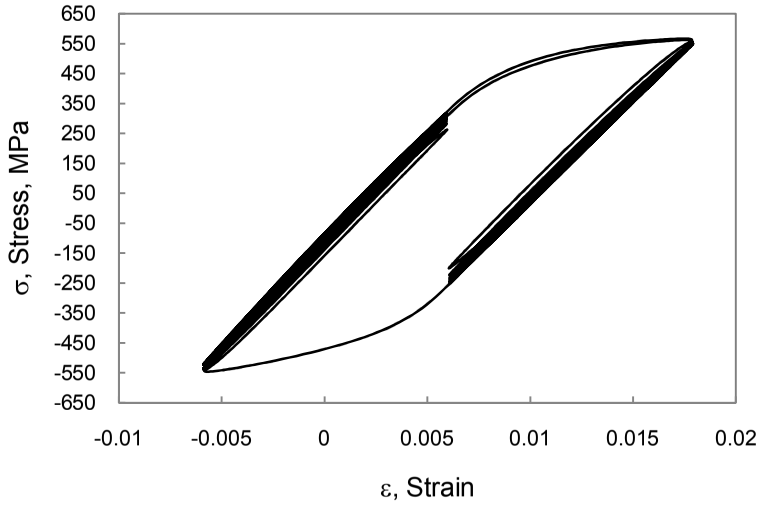

B49-41

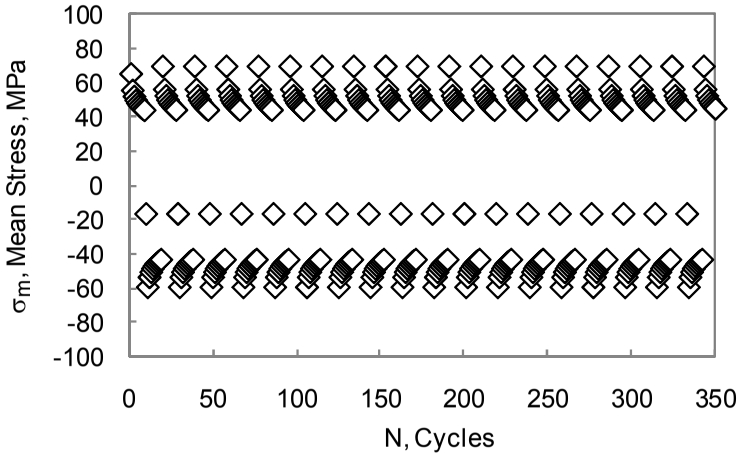
100
80
60
40
20
0
-20
-40
-60
-80
-100
σm, Mean Stress, MPa
0
50
100
150
200
250
300
350
N, Cycles

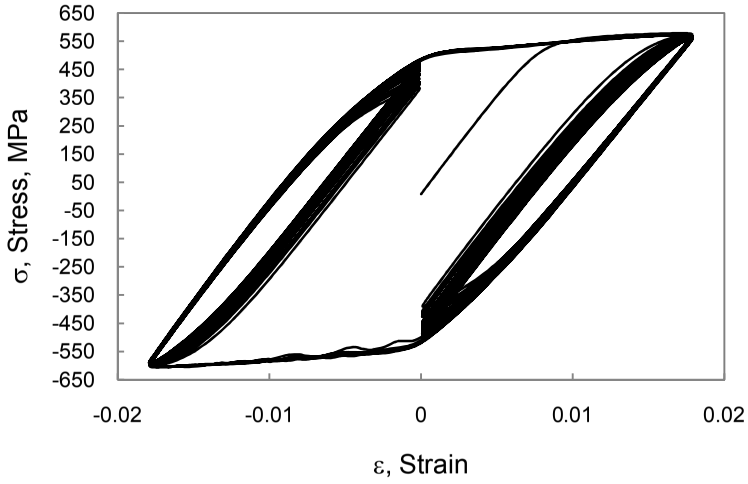
650
550
450
350
250
150
50
-50
-150
-250
-350
-450
-550
-650
σ, Stress, MPa
-0.02
-0.01
0
0.01
0.02
ε, Strain

B49-13

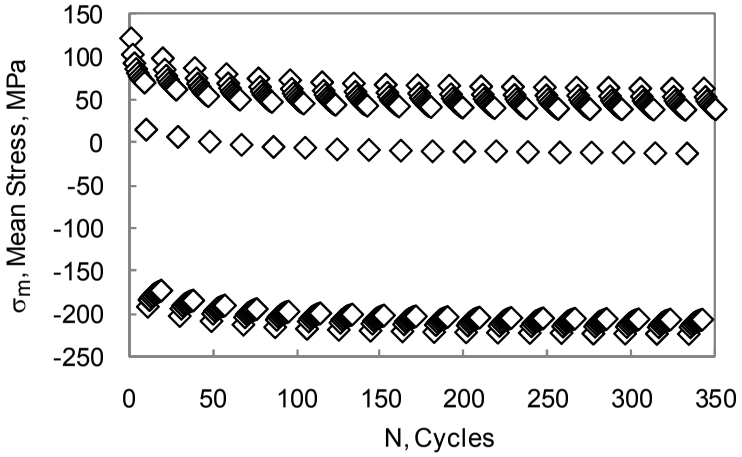
150
100
50
0
-50
-100
-150
-200
-250
σm, Mean Stress, MPa
0
50
100
150
200
250
300
350
N, Cycles

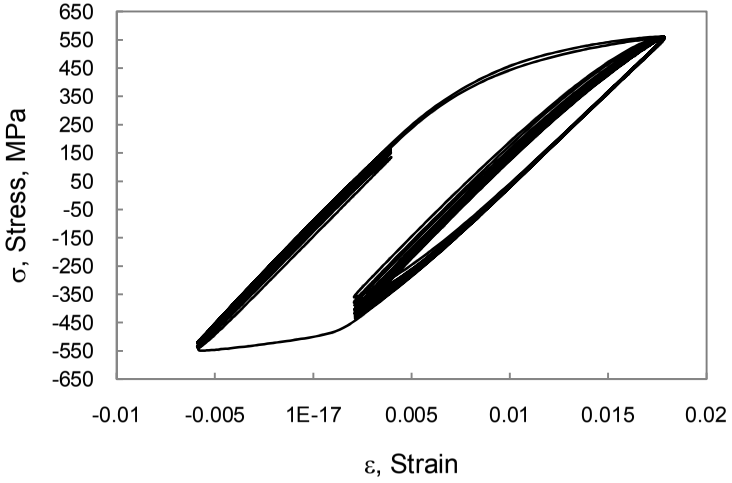
650
550
450
350
250
150
50
-50
-150
-250
-350
-450
-550
-650
σ, Stress, MPa
-0.01
-0.005
1E-17
0.005
0.01
0.015
0.02
ε, Strain

B49-19

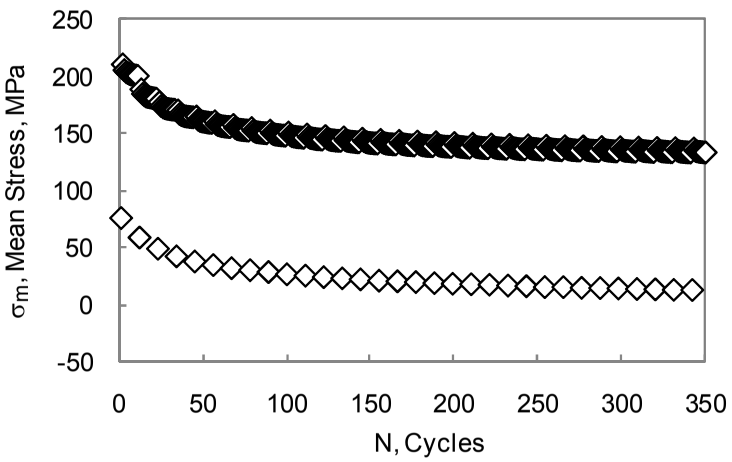
250
200
150
100
50
0
-50
σm, Mean Stress, MPa
0
50
100
150
200
250
300
350
N, Cycles

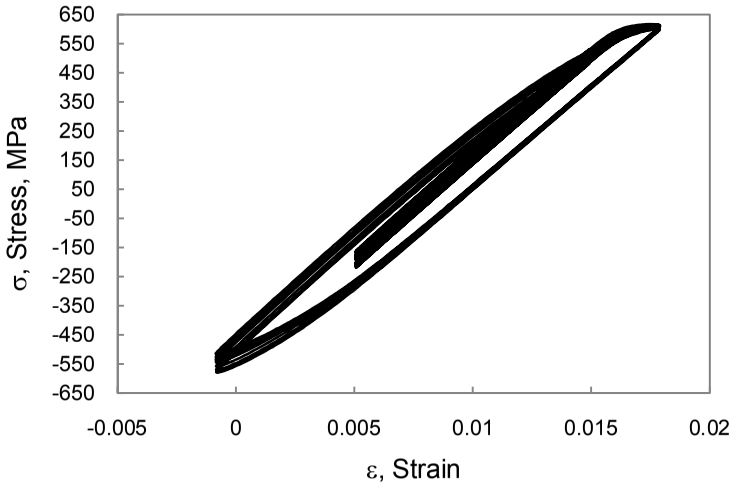
650
550
450
350
250
150
50
-50
-150
-250
-350
-450
-550
-650
σ, Stress, MPa
-0.005
0
0.005
0.01
0.015
0.02
ε, Strain

B49-60

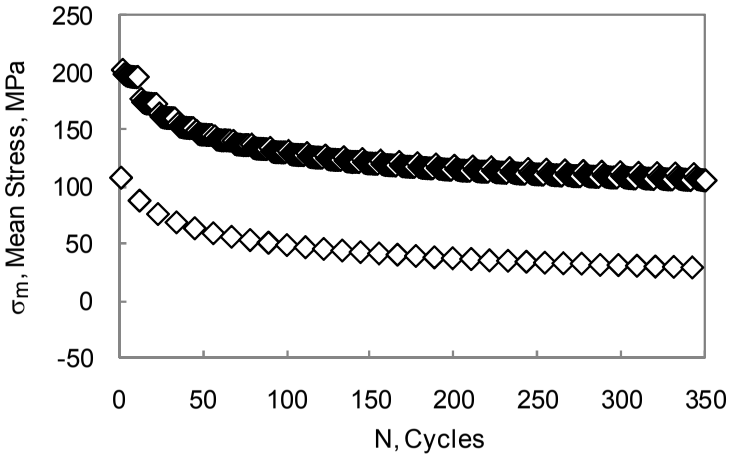
250
200
150
100
50
0
-50
σm, Mean Stress, MPa
0
50
100
150
200
250
300
350
N, Cycles

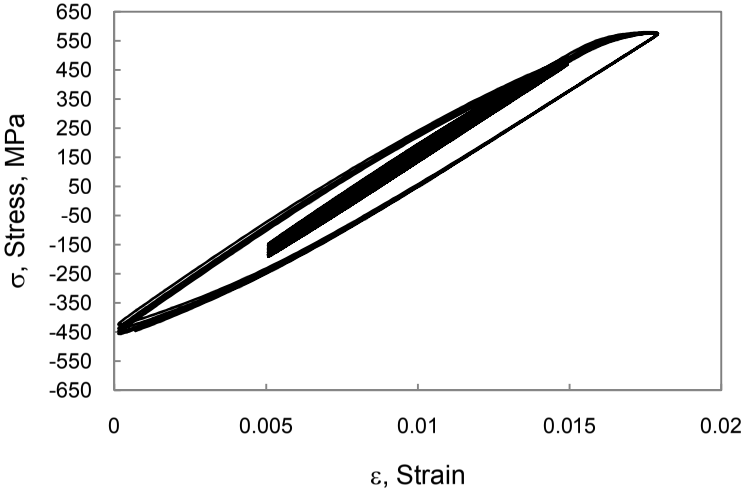
650
550
450
350
250
150
50
-50
-150
-250
-350
-450
-550
-650
σ, Stress, MPa
0
0.005
0.01
0.015
0.02
ε, Strain

B49-33

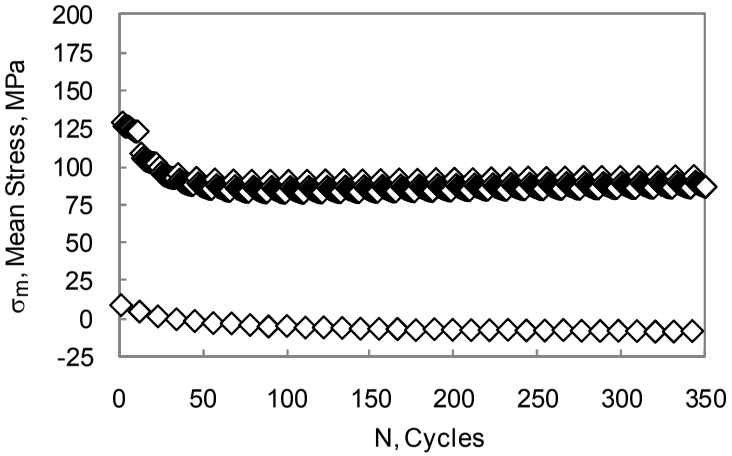
200
175
150
125
100
75
50
25
0
-25
σm, Mean Stress, MPa
0
50
100
150
200
250
300
350
N, Cycles

B49-8

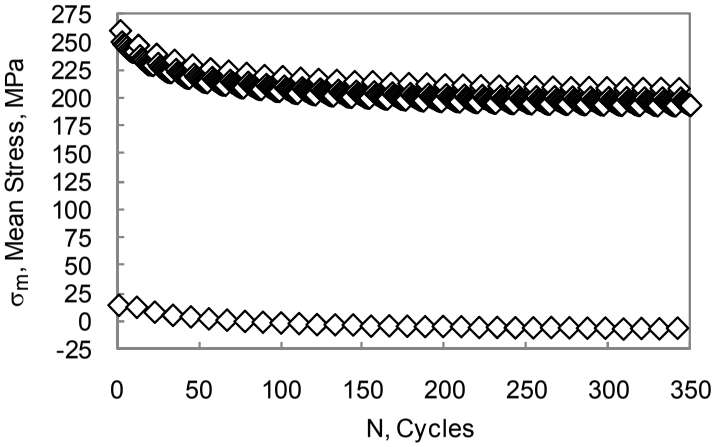
275
250
225
200
175
150
125
100
75
50
25
0
-25
σm, Mean Stress, MPa
0
50
100
150
200
250
300
350
N, Cycles

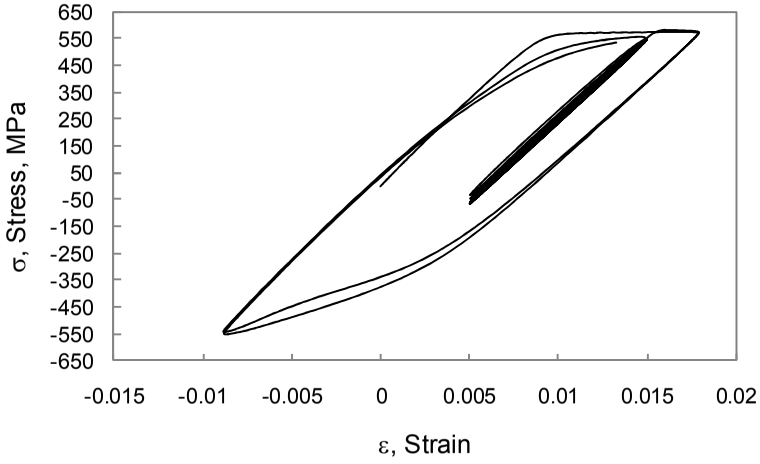
650
550
450
350
250
150
50
-50
-150
-250
-350
-450
-550
-650
σ, Stress, MPa
-0.015
-0.01
-0.005
0
0.005
0.01
0.015
0.02
ε, Strain

B49-57

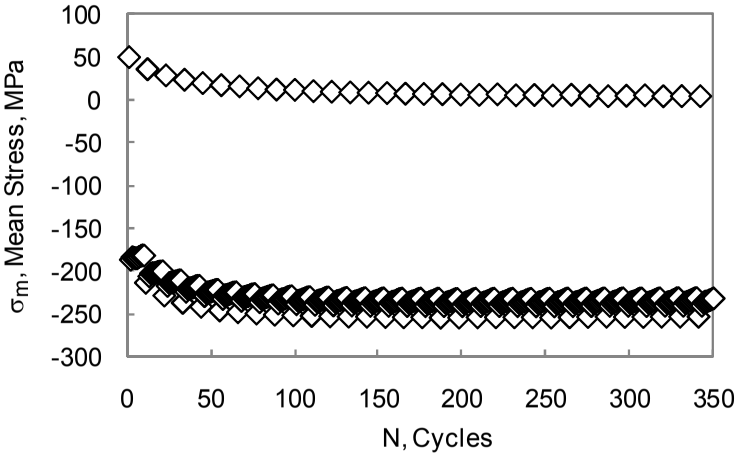
100
50
0
-50
-100
-150
-200
-250
-300
σm, Mean Stress, MPa
0
50
100
150
200
250
300
350
N, Cycles

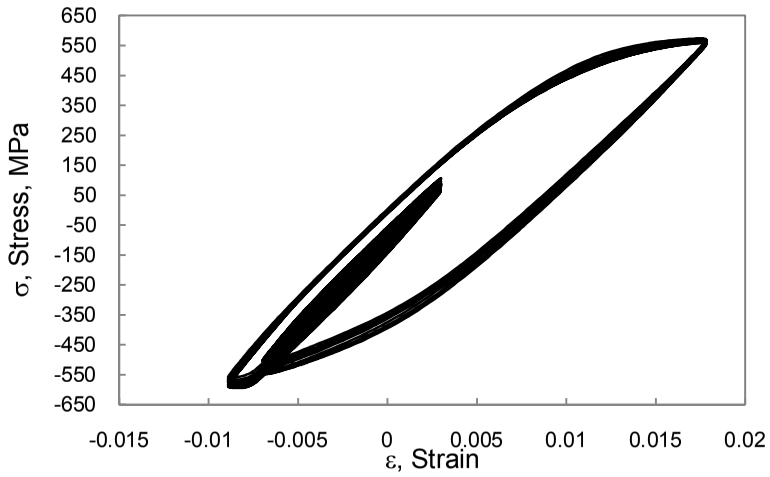
650
550
450
350
250
150
50
-50
-150
-250
-350
-450
-550
-650
σ, Stress, MPa
-0.015
-0.01
-0.005
0
0.005
0.01
0.015
0.02
ε, Strain

B49-50

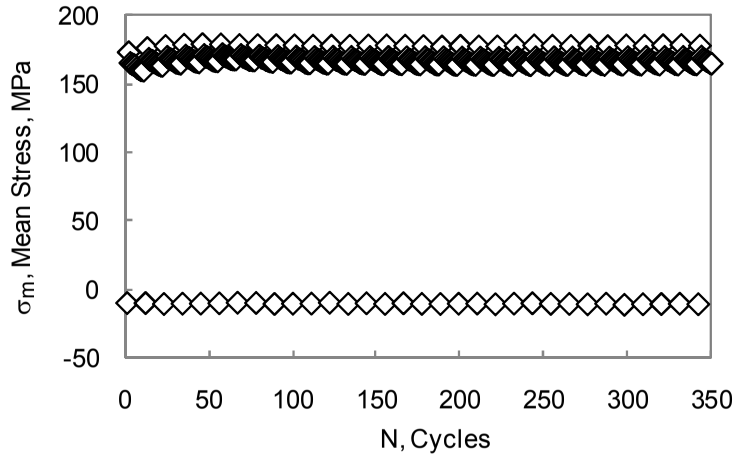
200
150
100
50
0
-50
σm, Mean Stress, MPa
0
50
100
150
200
250
300
350
N, Cycles

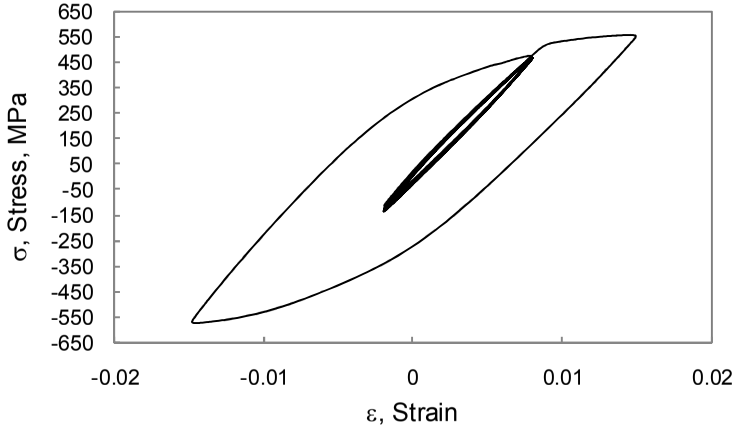
650
550
450
350
250
150
50
-50
-150
-250
-350
-450
-550
-650
σ, Stress, MPa
-0.02
-0.01
0
0.01
0.02
ε, Strain

B49-56

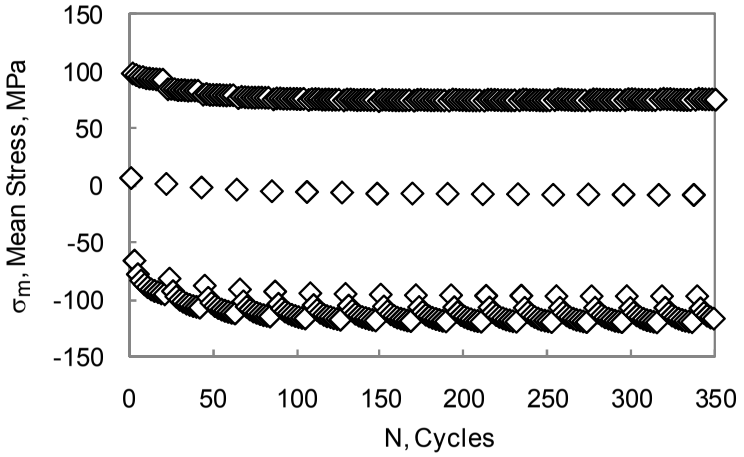

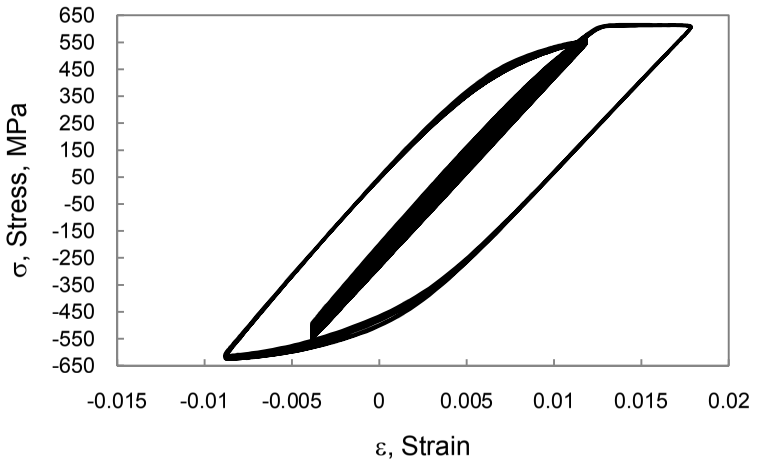

NAV-1-49-1

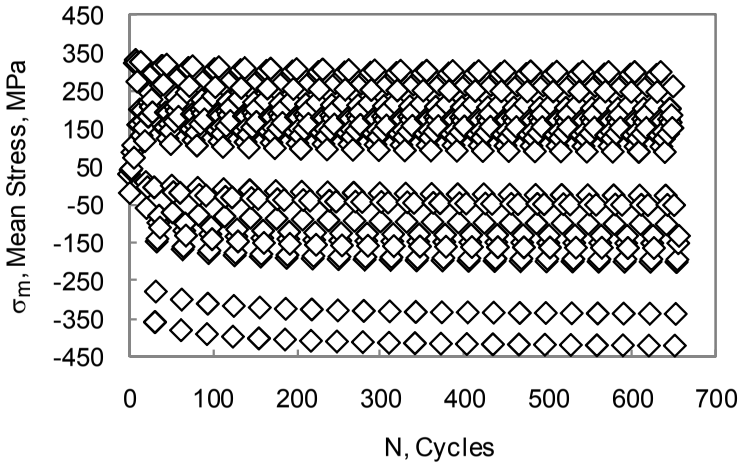

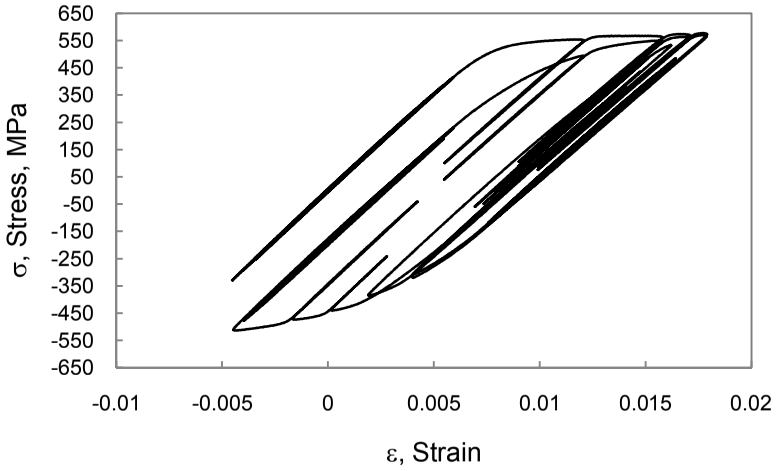

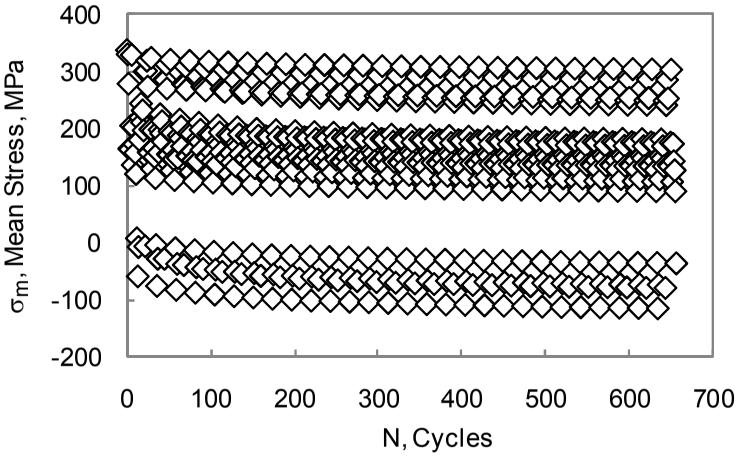
400
300
200
100
0
-100
-200
σm, Mean Stress, MPa
0
100
200
300
400
500
600
700
N, Cycles

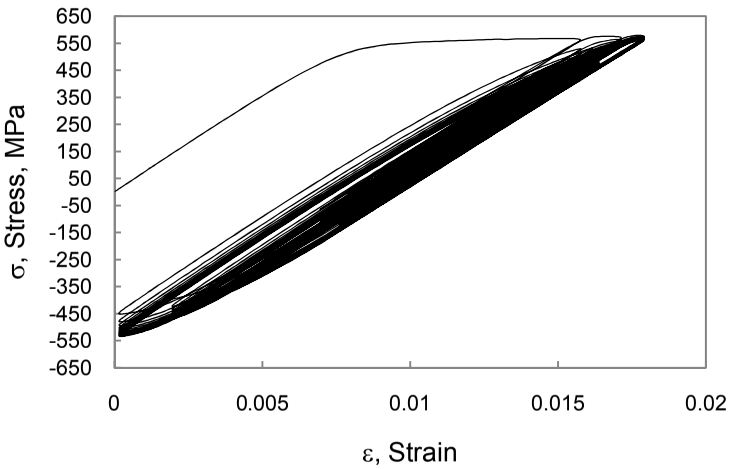
650
550
450
350
250
150
50
-50
-150
-250
-350
-450
-550
-650
σ, Stress, MPa
0
0.005
0.01
0.015
0.02
ε, Strain

Appendix D

Variable amplitude loading fitting results with Wetzel and Jiang model

D.1

7075-T6511

Wetzel and Jiang simulations of test B75-26

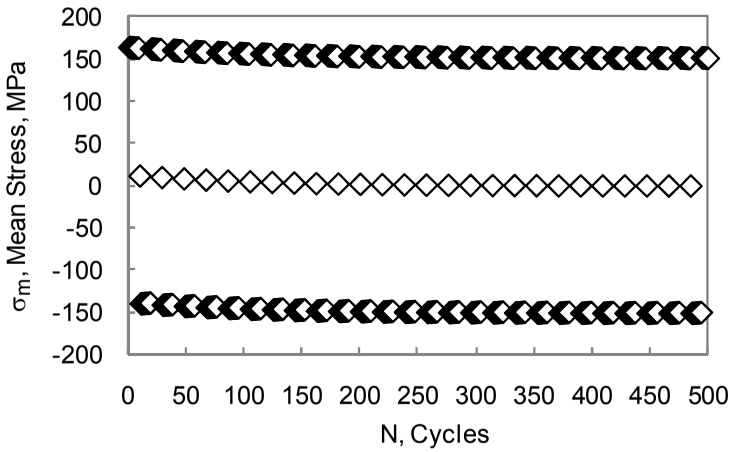

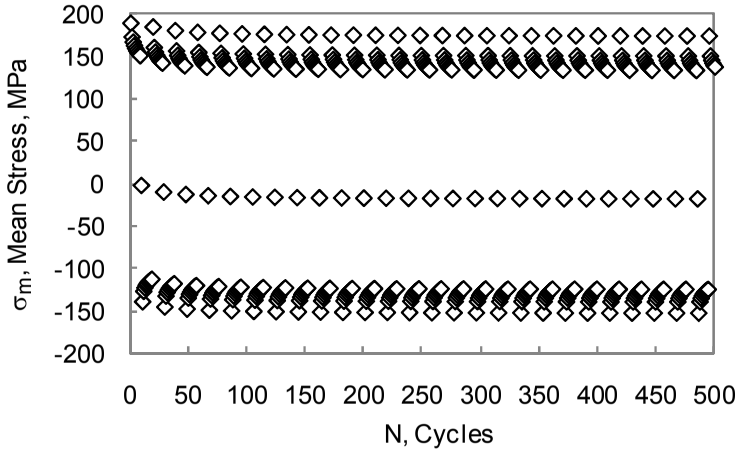

Wetzel and Jiang simulations of test B75-49

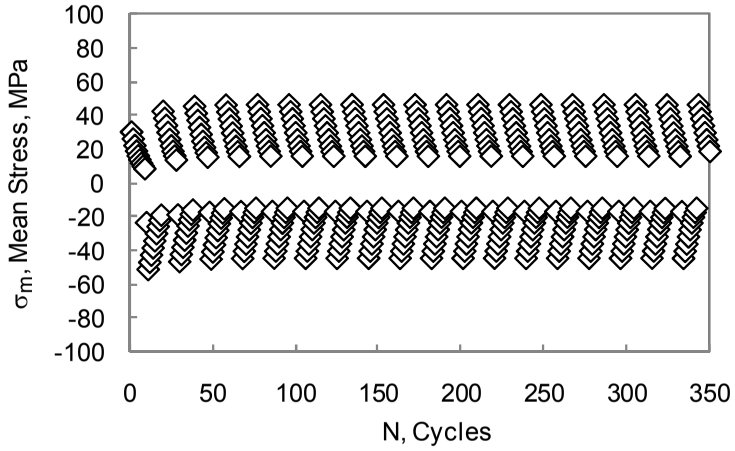

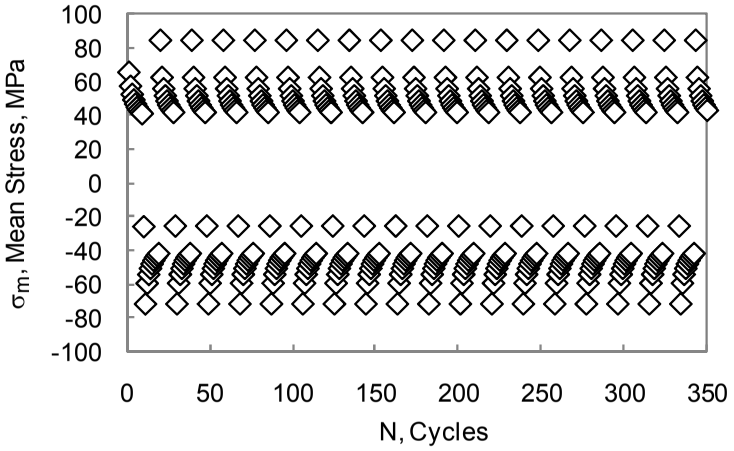

Wetzel and Jiang simulations of test B75-41

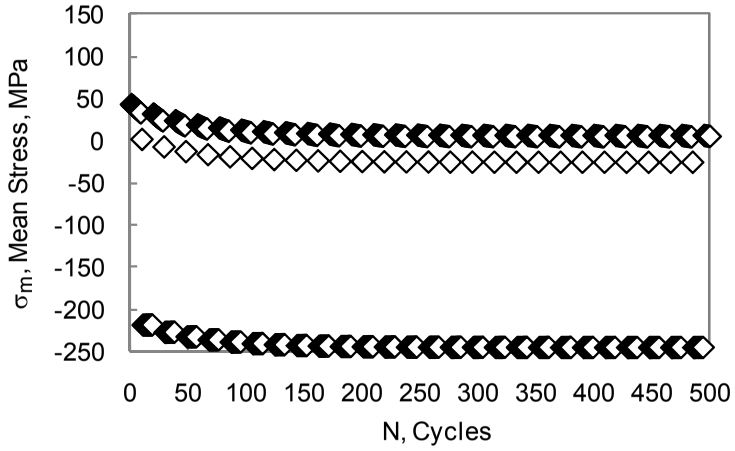

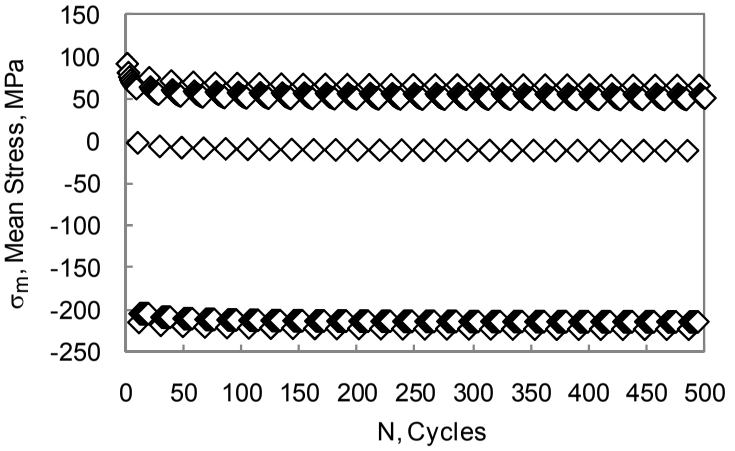

Wetzel and Jiang simulations of test B75-71

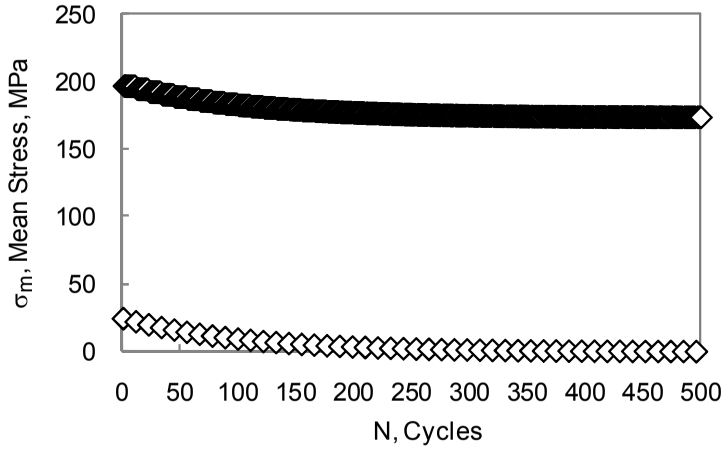

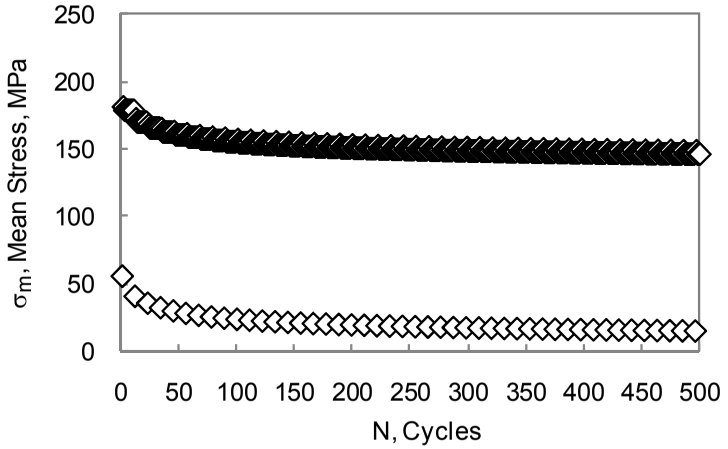

Wetzel and Jiang simulations of test B75-54

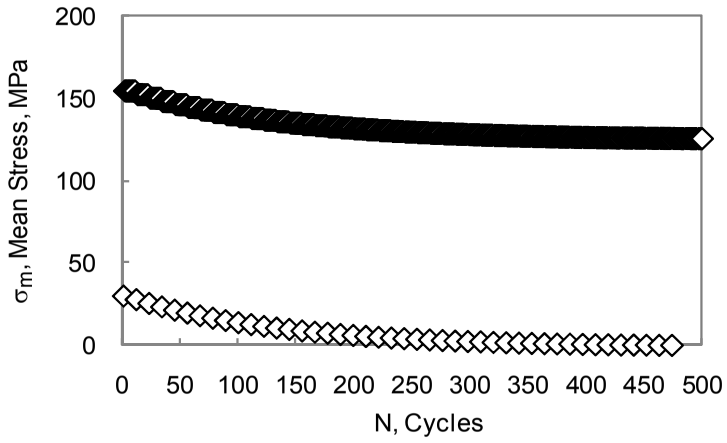

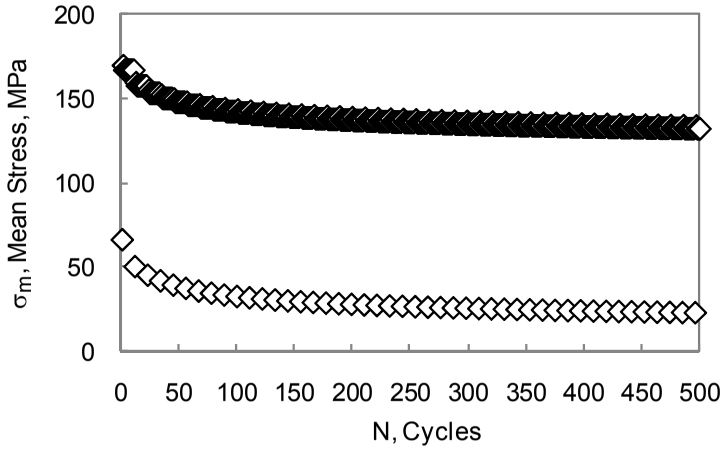

Wetzel and Jiang simulations of test B75-44

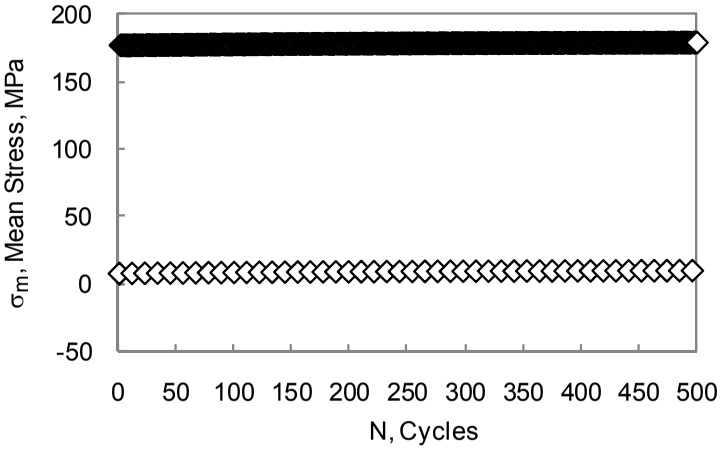

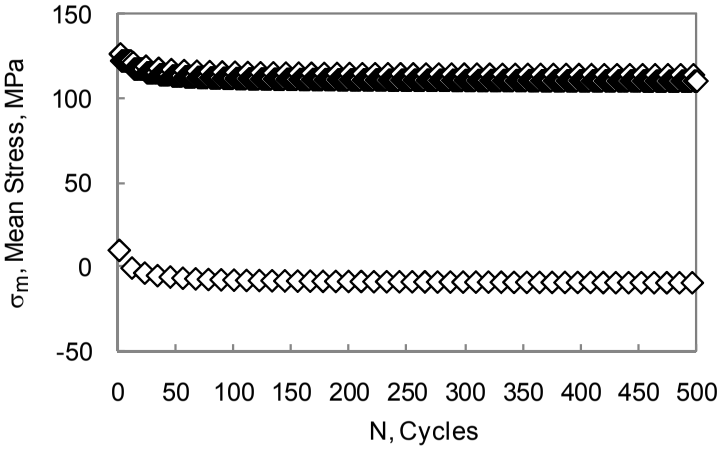

Wetzel and Jiang simulations of test B75-32

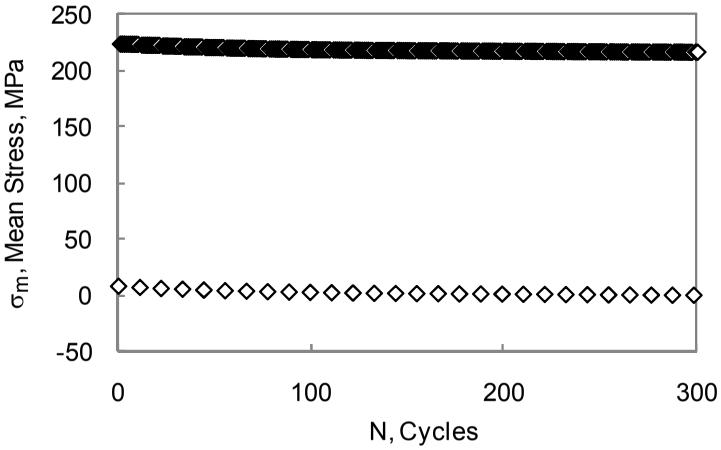

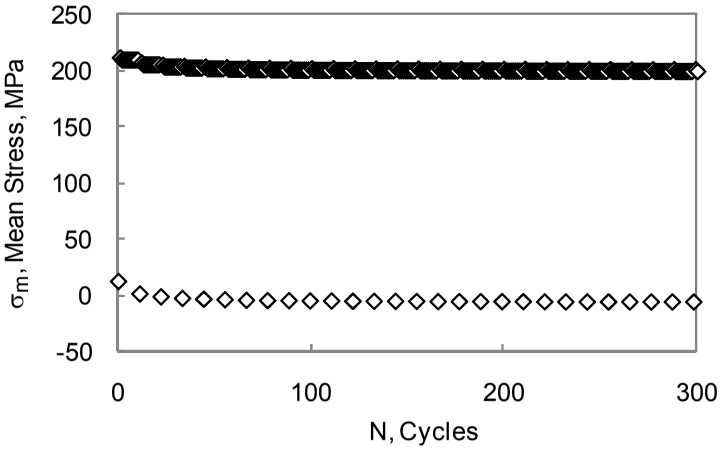

Wetzel and Jiang simulations of test B75-2

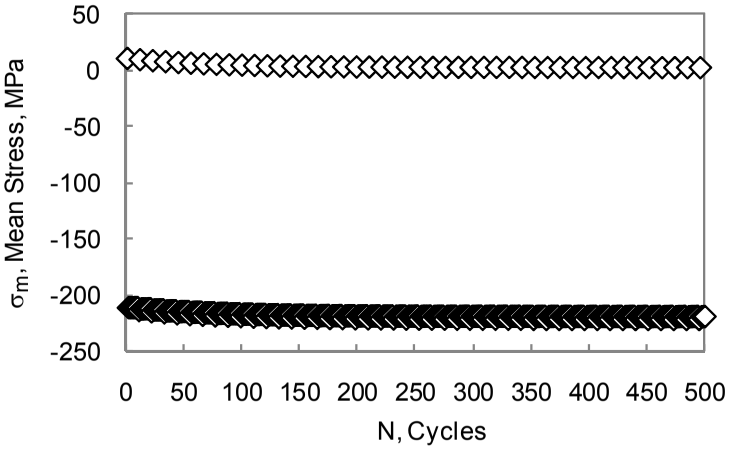

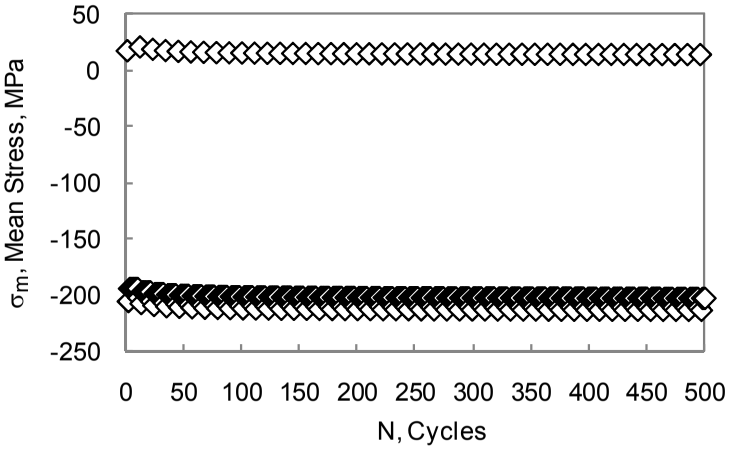

Wetzel and Jiang simulations of test B75-22

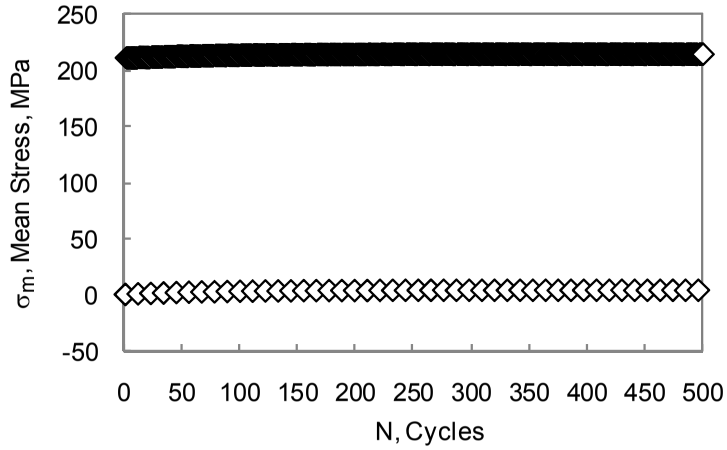

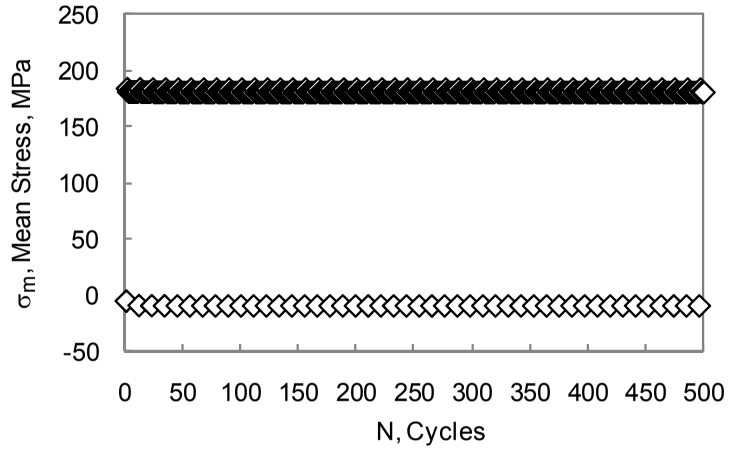

Wetzel and Jiang simulations of test B75-63

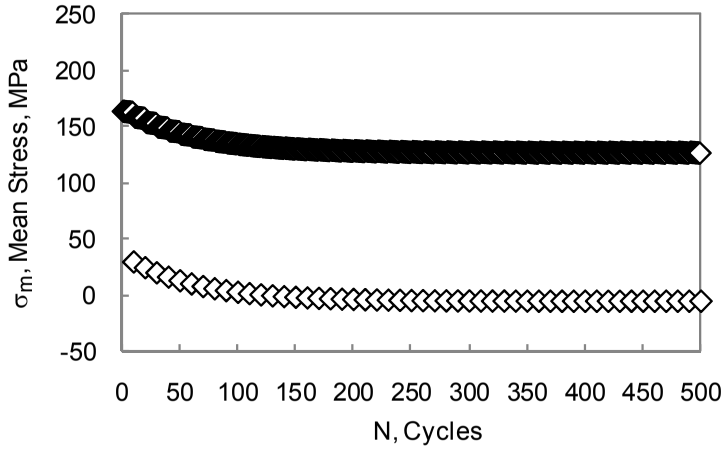

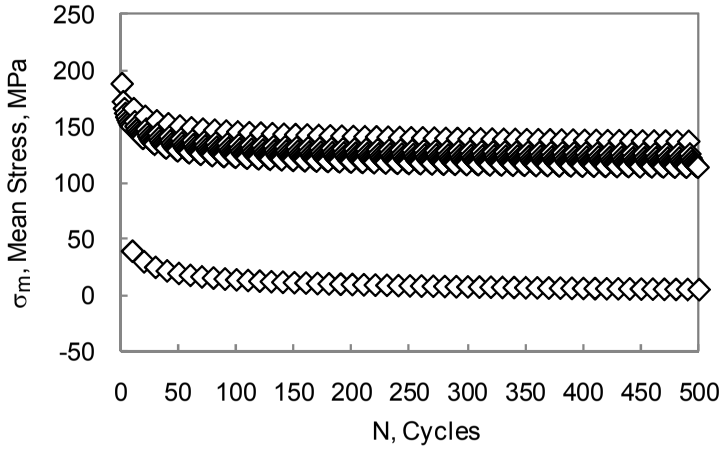

Wetzel and Jiang simulations of test B75-28

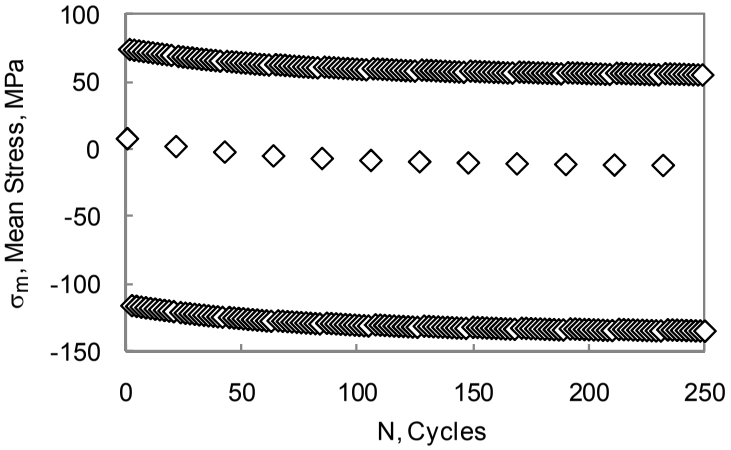

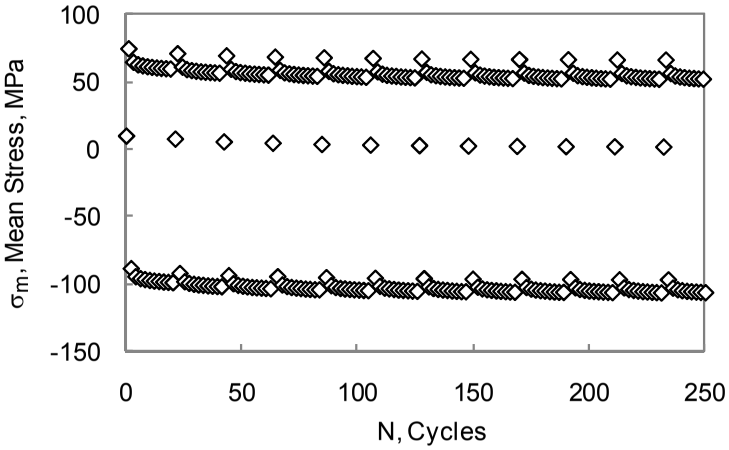

Wetzel and Jiang simulations of test NAV-1-75-15

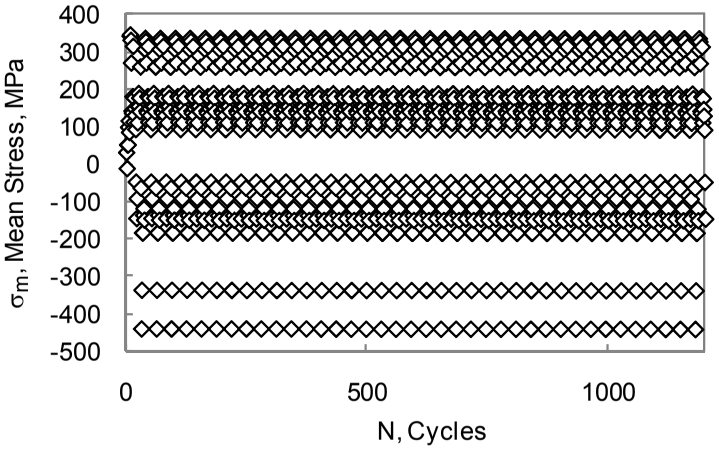

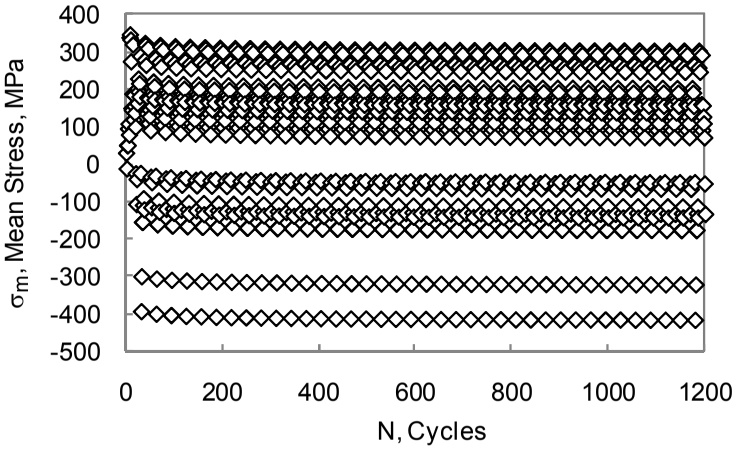

Wetzel and Jiang simulations of test NAV-1-75-12

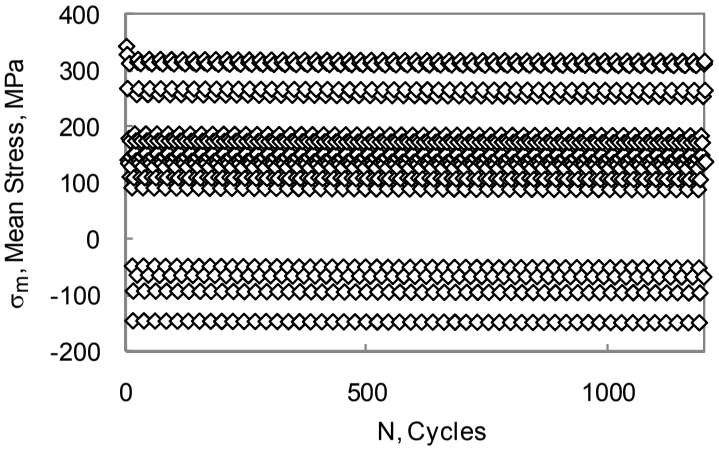

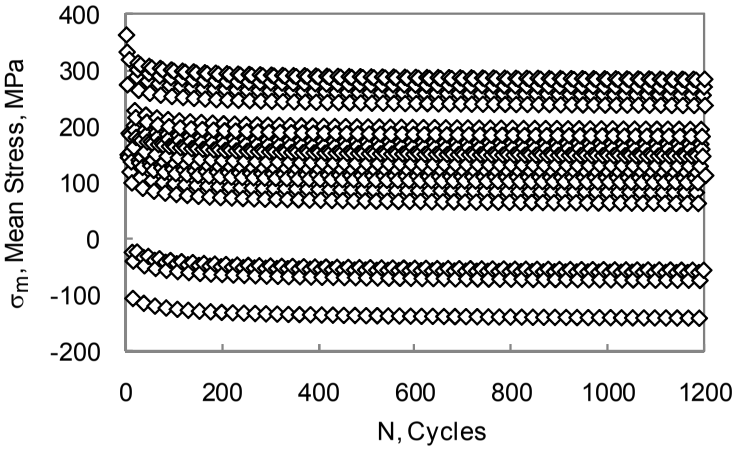

D.1

7249-T76511

Wetzel and Jiang simulations of test B49-44

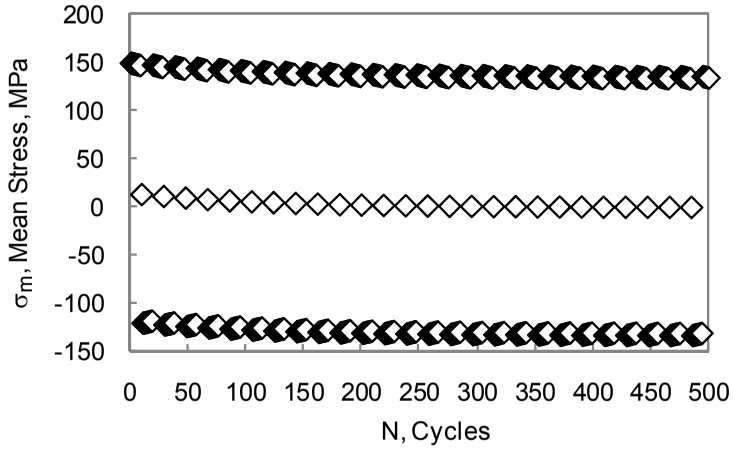

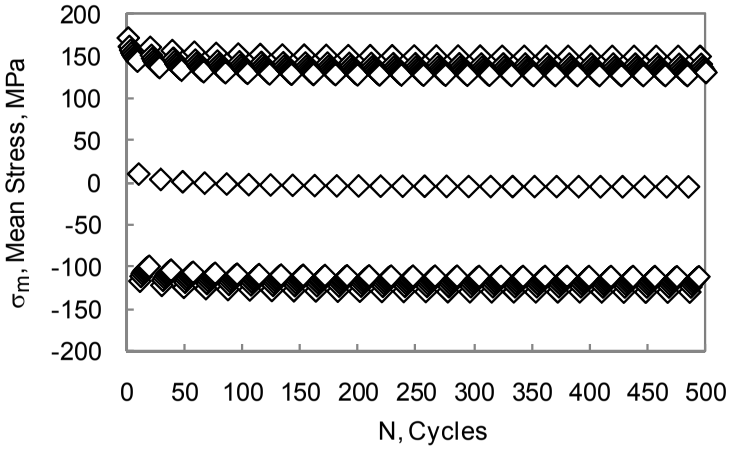

Wetzel and Jiang simulations of test B49-41

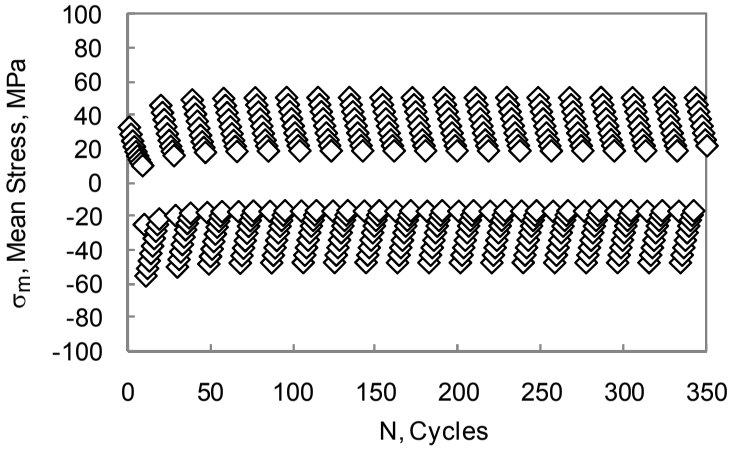

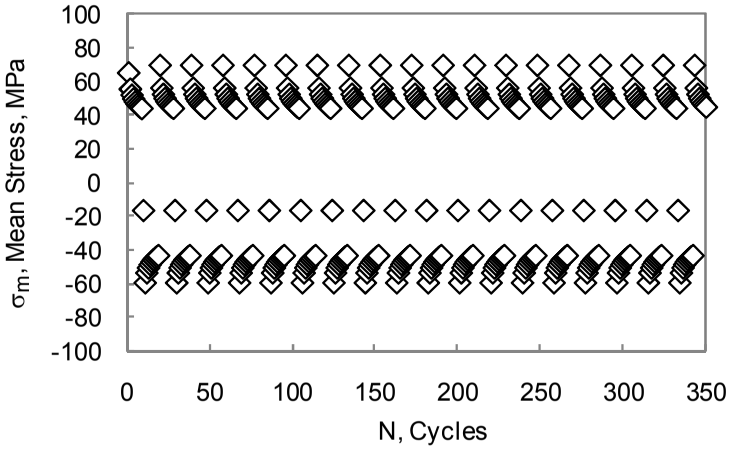

Wetzel and Jiang simulations of test B49-13

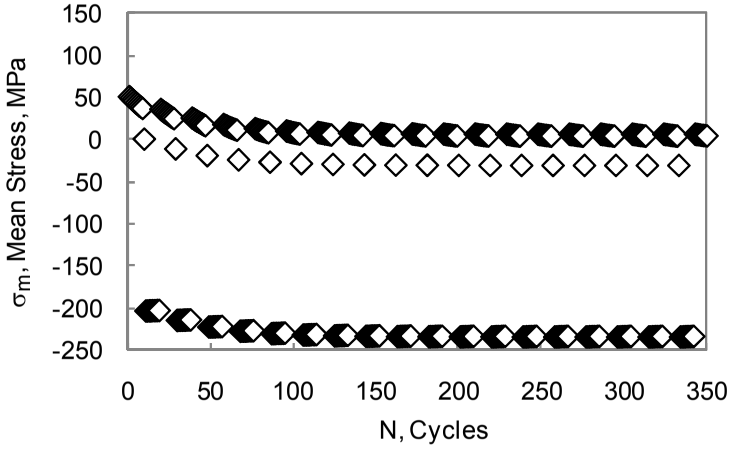

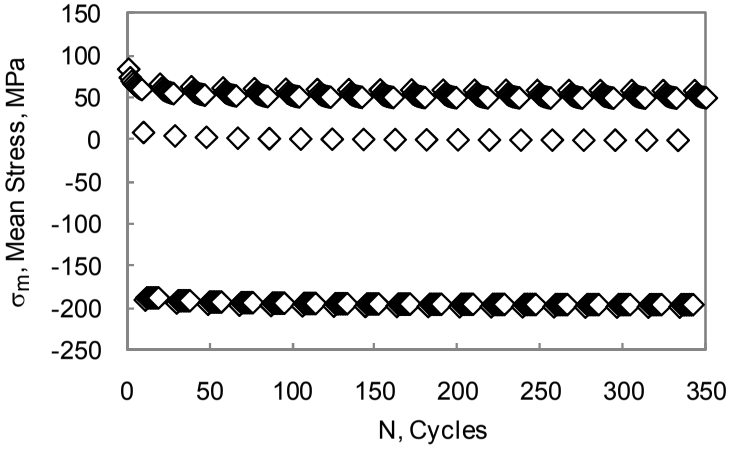

Wetzel and Jiang simulations of test B49-19

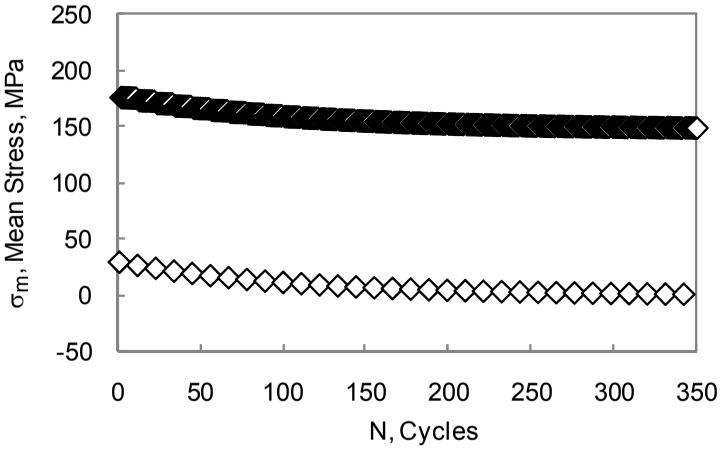

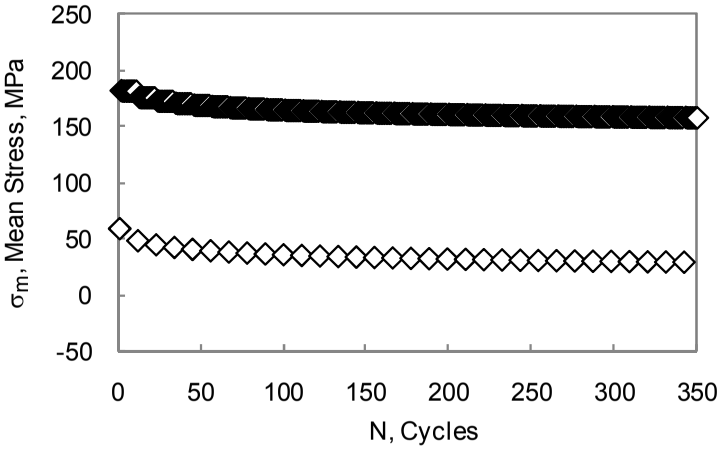

Wetzel and Jiang simulations of test B49-60

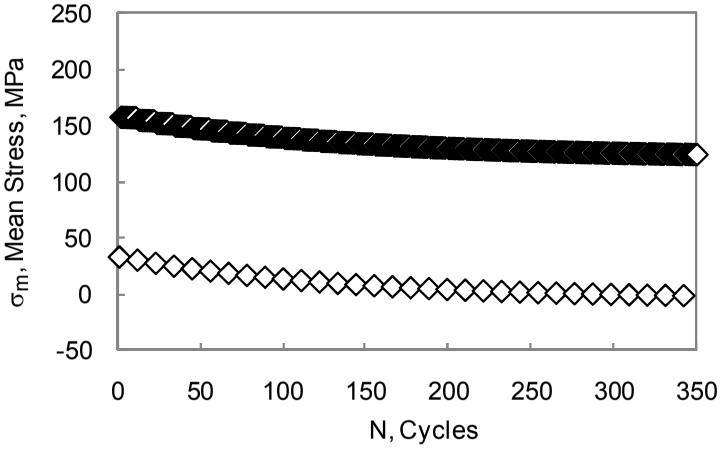

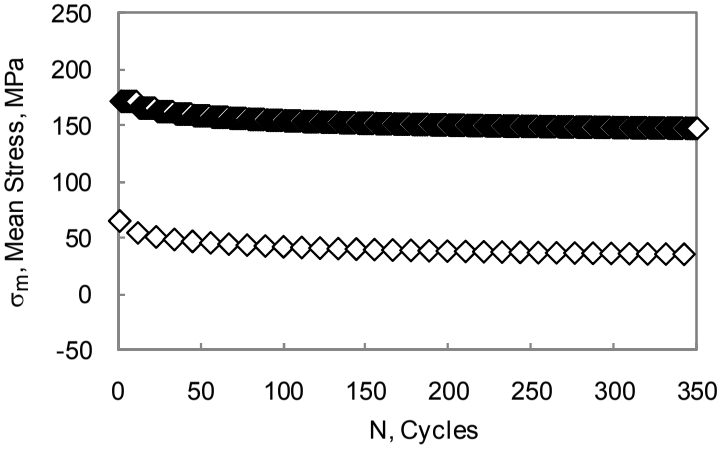

Wetzel and Jiang simulations of test B49-33

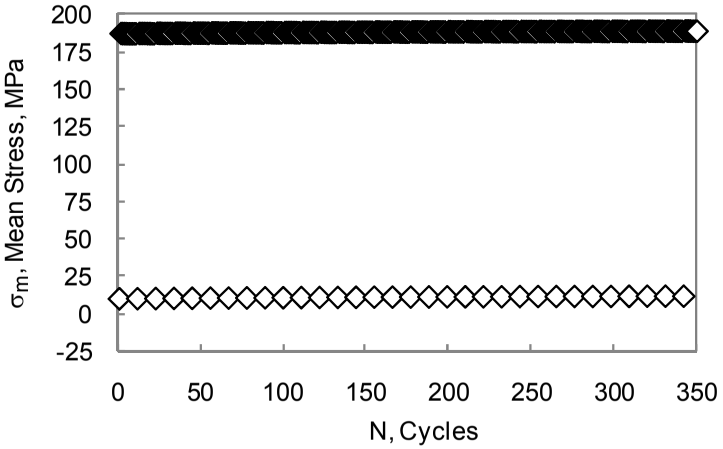

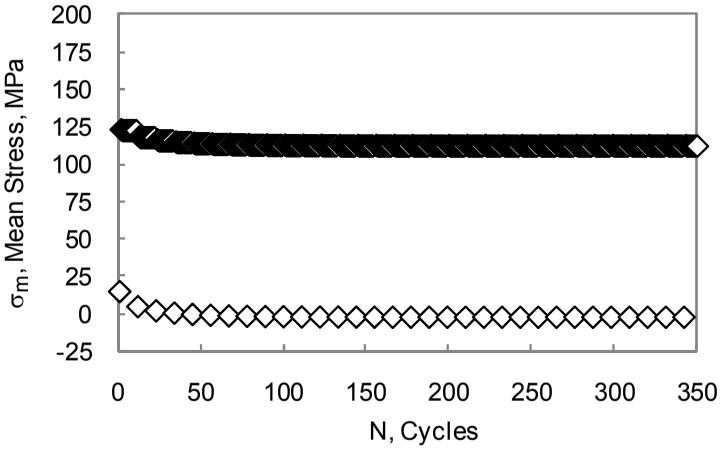

Wetzel and Jiang simulations of test B49-8

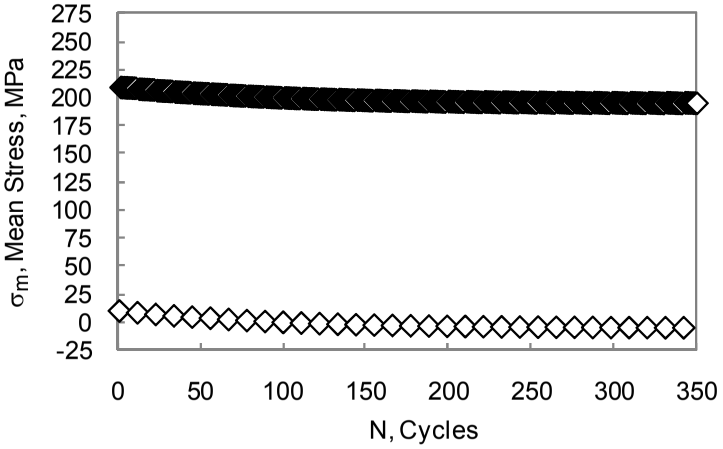

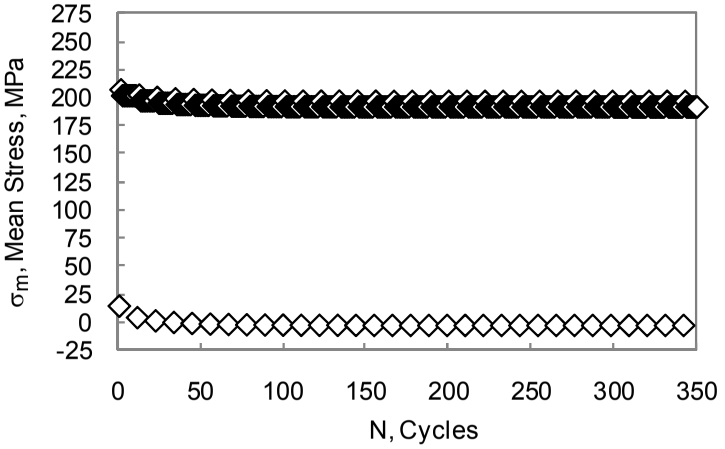

Wetzel and Jiang simulations of test B49-57

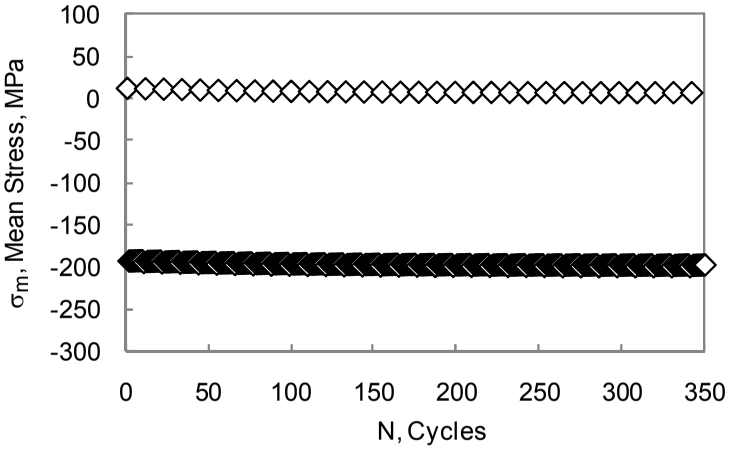

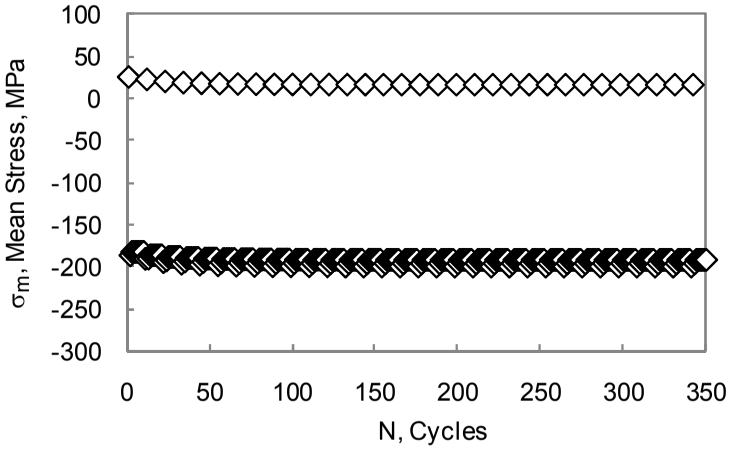

Wetzel and Jiang simulations of test B49-50

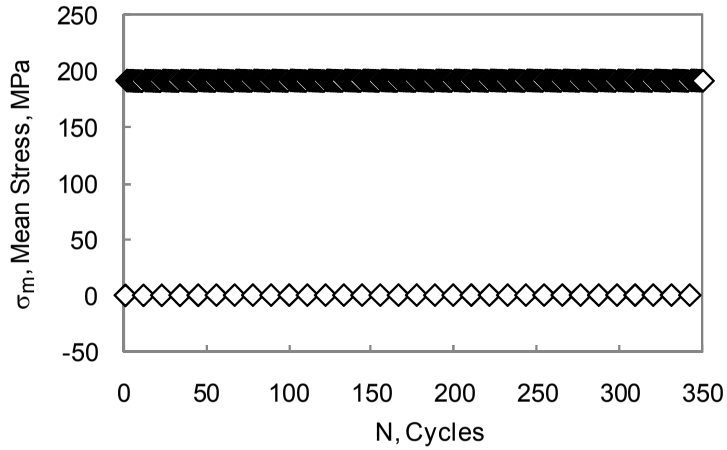

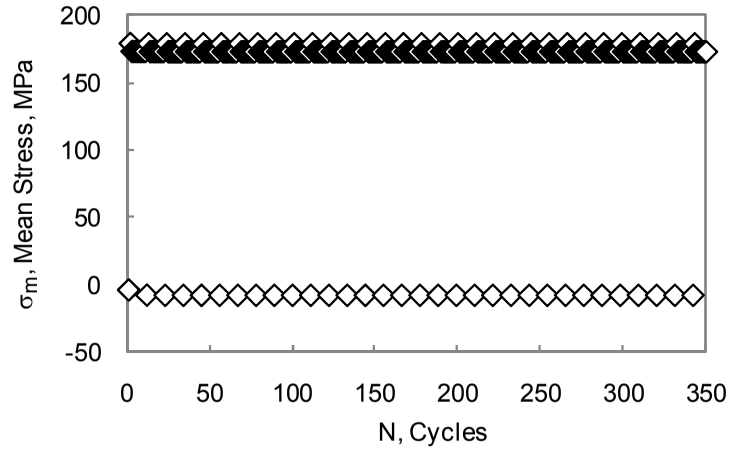

Wetzel and Jiang simulations of test B49-56

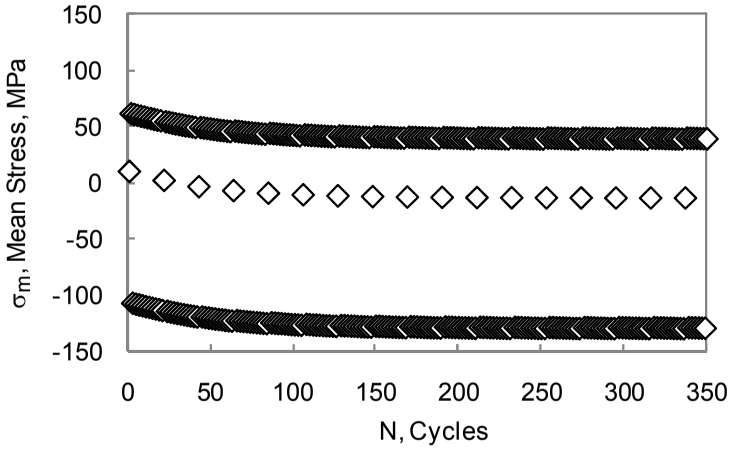

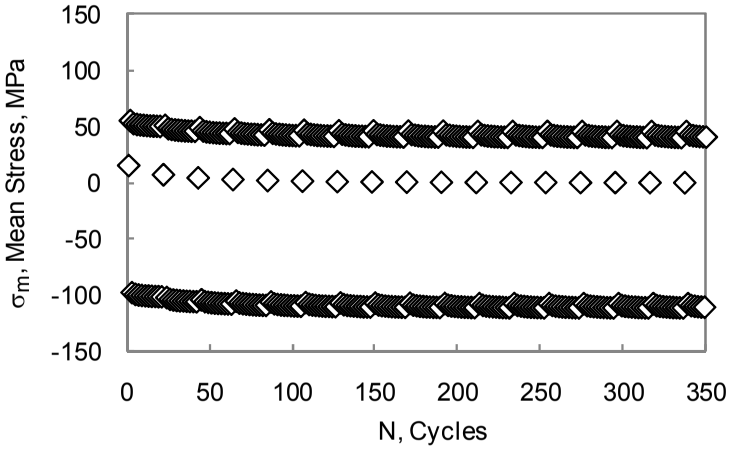

Wetzel and Jiang simulations of test NAV-1-49-1

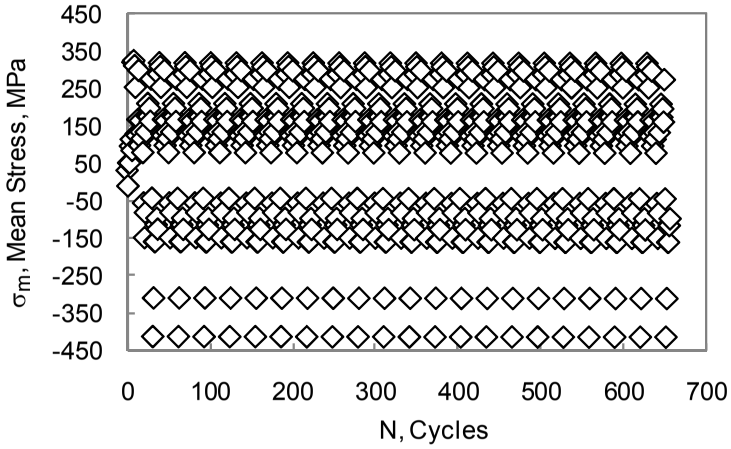

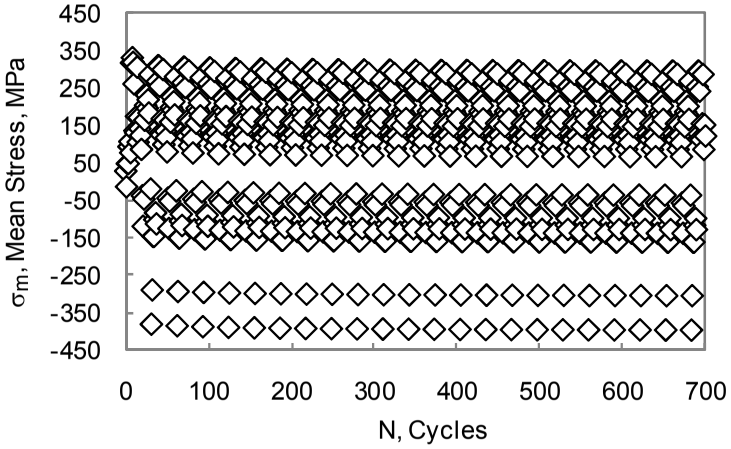
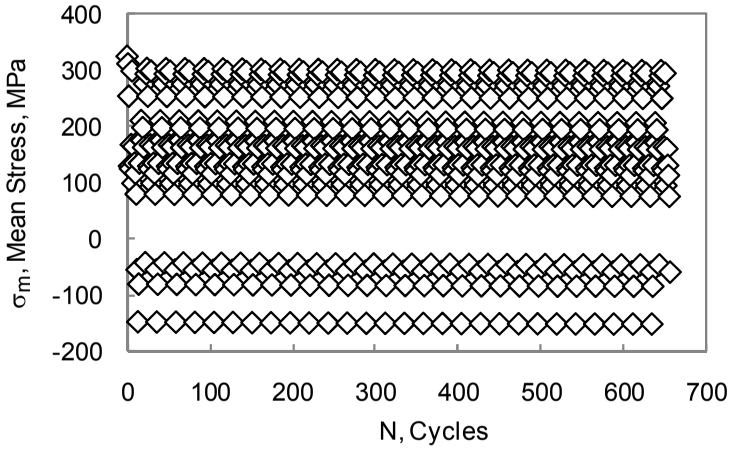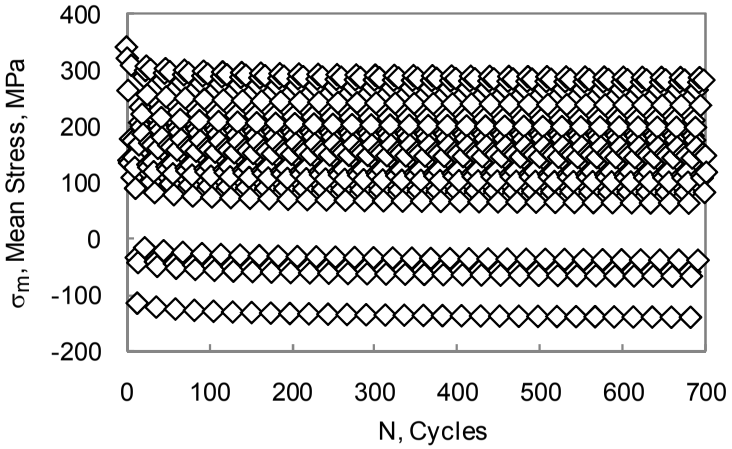
Wetzel and Jiang simulations of test NAV-1-49-16